SKB

TECHNICAL REPORT 89-33

Investigation of flow distribution in a fracture zone at the Stripe mine, using the radar method, results and interpretation

Per Andersson, Peter Andersson, Erik Gustafsson, Olle Olsson
Swedish Geological Co., Uppsala, Sweden

December 1989

SVENSK KÄRNBRÄNSLEHANTERING AB
SWEDISH NUCLEAR FUEL AND WASTE MANAGEMENT CO
BOX 5864 S-102 48 STOCKHOLM
TEL 08-665 28 00 TELEX 13108 SKB S
TELEFAX 08-661 57 19

INVESTIGATION OF FLOW DISTRIBUTION IN A FRACTURE ZONE AT THE STRIPA MINE, USING THE RADAR METHOD, RESULTS AND INTERPRETATION

Per Andersson, Peter Andersson, Erik Gustafsson, Olle Olsson

Swedish Geological Co., Uppsala, Sweden

December 1989

Swedish Geological Co.
Engineering Geology
Uppsala
Sweden

REPORT
ID-no. 89 240
Date: 1990-01-11

INVESTIGATION OF FLOW DISTRIBUTION IN A FRACTURE ZONE AT THE STRIPA MINE, USING THE RADAR METHOD, RESULTS AND INTERPRETATION.

December 1989

PER ANDERSSON

PETER ANDERSSON

ERIK GUSTAFSSON

OLLE OLSSON

Swedish Geological Co., Uppsala, Sweden

December 1989

ABSTRACT

The objective of the current project was to map the steady state flow distribution in a fracture zone when water was injected into the zone from a borehole. The basic idea was to map the flow paths by taking the difference between radar results obtained prior to and after injection of a saline tracer into the fracture zone. The radar experiments were combined with a more conventional migration experiment to provide validation and calibration of the radar results.

The Crosshole Site in the Stripa mine was selected as the experimental site as the geological and the hydrological conditions were well known. The site is located at the 360 m level where seven boreholes were used for this experiment.

Difference tomography using borehole radar was a valuable and successful tool in mapping groundwater flow paths in fractured rock. The data presented were of good quality and sufficiently consistent throughout the investigated rock volume. The interpreted results verified previous findings in the surveyed granite volume as well as contributed to new and unique information about the transport properties of the rock at the site. The inflow data and the tracer breakthrough data has served as a useful aid in the interpretation of the flow distribution within the investigated zone and also within the surrounding rock mass.

From the differential attenuation tomograms the migration of the injected tracer was mapped and presented both in the fracture zone of interest and in the entire investigated granite volume.

From the radar tomographic model, the major tracer migration was found to be concentrated to a few major flow paths. Two additional fracture zones originally detected within this project, were found to transport portions of the injected tracer.

The radar results combined with the tracer breakthrough data were used to estimate the area with tracer transport as well as flow porosity and the wetted surface.

Keywords: Radar, Tomography, Crosshole, Fracture zones, Migration, Saline tracer.

SUMMARY AND CONCLUSIONS

The objective of the current project was to map the steady state flow distribution in a fracture zone when water was injected into the zone from a borehole. The basic idea was to map the flow paths by taking the difference between radar results obtained prior to and after injection of a saline tracer into the fracture zone.

The radar experiments were combined with a more conventional migration experiment where the salt concentration in a number of boreholes was measured as a function of time. These measurements were made to assure that steady state conditions were met at the second round of radar measurements and to provide a calibration of the radar results.

The Crosshole Site in the Stripa mine was selected as the experimental site as the geological and the hydrological conditions were well known. The site is located at the 360 m level where seven boreholes were used for this experiment. All boreholes originate from essentially the same point at the end of a drift. The boreholes outline a tilted pyramid with a height and a base of about 200 m where all boreholes start from the top of the pyramid.

The experimental work was carried out in four phases: The first phase comprised the reference measurement with single hole reflection and crosshole tomography surveys. The second phase included reassessment of the hydraulic conditions at the site and injection of saline tracer at a constant rate in a fracture zone. The inflow rate and concentration of saline water entering the open boreholes was measured as a function of time. When the data indicated steady state conditions the third phase, which comprised a repetition of the radar measurements performed during the first phase, was started. Tomographic inversion has been made of the difference between the radar data collected in phases 1 and 3 to show the location of the saline tracer. The experimental work was concluded with the fourth phase which comprised measurement of salt concentration in the open boreholes in order to check that steady state conditions had prevailed during the radar measurements. Following the completion of the experimental programme an integrated analysis has been made of the collected radar and tracer migration data.

The fracture zone labelled 'C' was chosen as the target for these investigations. It is one of the major zones at the site and it is centrally located within the site and intersects all boreholes at the

site. The injection of saline tracer was performed as a continuous injection with constant flow rate. The tracer, Potassium Bromide (KBr), was injected in a 14.5 m long packed-off interval enclosing Zone C during a period of 905 hours (38 days).

The choice of KBr as tracer was based upon the following considerations:

- easy to detect by measurement of the electrical conductivity
- no sorption on granite
- low background concentration

The initial concentration chosen of KBr was 0.5 %. However, experience from this project has shown that the concentration of the saline tracer could have been higher than the 0.5% used here. A salt concentration of 1% to 2% would have increased the signal to noise ratio and hence simplified the processing of data and increased the quality of radar data. An increased salt concentration would also improve the quality of the tracer breakthrough data especially in boreholes with low inflow rates.

Single hole reflection measurements were made in all boreholes, except F3, with a centre frequency of 60 MHz. The obtained range is approximately 50 m and clear reflections are observed from the fracture zones.

Crosshole tomography measurements has been made in eleven sections outlined by combinations of two of the six available boreholes (F3 not included). All sections have been measured with a centre frequency of 60 MHz. The tomographic measurements were made with a point separation of 4 m in all boreholes. The measurement length for all boreholes was about 100 m in the crosshole tomography surveys.

Tomographic inversions were performed of the residual travel times and the residual amplitudes as well as differential amplitudes between radar data from phases 3 and 1. The inversion was made with the Conjugated Gradient (CG) method described by Ivansson (1984). A new way of introducing damping has been introduced which makes the damping inversely proportional to the ray density in each cell. The ray density dependant damping has been found to give tomograms which better represent the actual information content in the data. It is recommended that this algorithm is used for tomographic work in the future.

The radar reflectograms and tomograms generated within this project are in very good agreement with

the results obtained from previous measurements performed during the Crosshole programme. This implies that the new data, and hence also the interpretation, is in agreement with the previous interpretation (Olsson, Black, Cosma, and Pihl. 1987).

The difference radar data (from phases 3 and 1) are presented both as differential radar reflectograms as well as differential tomograms. The differential reflectograms could be used qualitatively, together with tomographic and salt inflow results, but no quantitative estimates of flow path and volume of salt could be obtained.

From the differential attenuation tomograms the migration of the injected tracer was mapped and presented both in the fracture zone of interest (Zone C) and in the entire investigated granite volume.

The main migration in Zone C section took place in the central parts of the surveyed section. From the differential attenuation tomographic 3-D model the major tracer migration is spreading from the injection point in a few dominating directions. Also, subordinate tracer transport paths were noticed in other directions. There were also portions of the investigated volume with no tracer transport.

Two additional fracture zones originally detected within this project, labelled Zone X and Zone Y, were determined to transport portions of the injected tracer. Both Zone X and Zone Y intersects Zone C, Zone X with an angle of 80°-90°. Zone X has an orientation similar to that of Zone A (a major fracture zone detected in the previous investigations) which indicates that it could be part of the same fracture system as Zone A.

The area interpreted, from the radar results, to include the main and important transport of saline tracer, in Zone C, encompasses 48% of the total area where the saline tracer has been observed from the radar results. This area also includes 78% of all saline tracer in the Zone C section. As about 80% of the flow in Zone C is concentrated to this area there is still about 20% of the mass left in other parts of the zone where interactions between rock surface and water may take place.

The amount of tracer flow path or "preferential flow fraction" was defined as the area with tracer transport divided by the investigated area. The "preferential flow fraction" within Zone C, expressed as percent of surveyed area, in the three studied sections, was in the range 19% to 37%.

The inflow data and the tracer breakthrough data has served as a useful aid in the interpretation of the flow distribution within Zone C and also within the surrounding rock mass. From the breakthrough data determination of transport parameters has been possible to make in several directions and distances within Zone C.

From the tracer breakthrough data the tracer recovery from the boreholes, expressed as mass per time unit, was determined to about 75%. Of the injected tracer 56% was recovered from Zone C.

The integration of the radar method and the conventional tracer migration experiment made it possible to compare the radar interpretation of the groundwater flow paths with the actual breakthrough locations of the tracer. Analysis of tracer breakthrough data has confirmed the radar interpretations both with respect to the flow path distribution within Zone C and with respect to the spreading of tracer to other zones within the surveyed rock volume. In addition, the calculations of tracer mass balance and recovery in the sampling boreholes has made it possible to identify flow paths outside the radar investigated domain. These flow paths caused by the dipole character of the flow field resulted in occasional discrepancies with high recorded inflow of saline tracer together with radar anomalies of moderate magnitudes.

The complexity of the flow distribution within the investigated volume, caused by the presence of the open boreholes, made it difficult to make good quantitative evaluations of flow and transport parameters such as dispersivity and hydraulic fracture conductivity. However, the kinematic porosity could be determined in two different ways and both gave the same value, $2 \cdot 10^{-4}$, which was consistent with values from previous investigations in the Stripa granite.

Based on the combined interpretations of the flow distribution within the investigated rock volume, an attempt was made to give a rough estimate of the wetted surface. The wetted surface is defined as the area of wet rock per volume of rock (m^2/m^3). The estimate was based on the tracer distribution interpreted from the three radar cross-sections of Zone C and resulted in a wetted surface of 1.8 m^2/m^3.

This project has also shown that the presence of several open boreholes may cause a very complicated flow pattern with flow along the boreholes into

adjacent zones. For future investigations of this type it is therefore recommended that the "natural" pressure distribution within the rock mass is maintained by packing off all boreholes within the investigated volume. Such a procedure will also improve the possibility to make good quantitative evaluations of transport parameters. The evaluations would also be improved if 2D or 3D-modelling could be applied, incorporating the radar interpretation of the geometry of the flow paths.

CONTENTS

LIST OF FIGURES

LIST OF TABLES

1 INTRODUCTION

1.1 OBJECTIVES

Most design concepts for high level waste repositories are based on a multiple barrier concept. One of the barriers is the host rock surrounding the repository. The safety added to a future repository by the host rock depends on the groundwater flow rate and transport capacity of radio-nuclides from the repository to the biosphere. In this context parameters such as groundwater gradients, hydraulic properties of the host rock, groundwater flow paths and flow velocity are essential.

Groundwater flow in crystalline rock occurs essentially in fractures which occupy a minor portion of the total rock volume. The development of the borehole radar technique has provided novel possibilities for investigating groundwater flow. Borehole radar is a remote sensing technique and is thus capable of giving high resolution information from observation points located far from the measuring points (boreholes or tunnels). Typical probing ranges are hundreds of meters with resolution on the order of meters. Hence, borehole radar can be used to give a three-dimensional geometric description of fracture zones where groundwater is likely to be concentrated.

The borehole radar technique may also be used to show the actual flow paths through the rock and possibly also flow velocity. The basic idea behind experiments where borehole radar is used to show groundwater flow paths is to use a difference technique. First a reference measurement is made which gives a description of the fracture system and other geological structures at the experimental site. Then saline tracer is injected from a borehole and the measurement is repeated. Saline water increases the attenuation of radar waves and the difference between the measurements will give information on the location of the saline tracer at the time of measurement. If measurements are repeated at regular intervals it should be possible to describe the spread of tracer with time and hence flow velocity.

The objective of the current project is to map the steady state flow distribution in a fracture zone when water is injected into the zone from a borehole. The basic idea is to map the flow paths by taking the difference between radar results obtained prior to and after injection of a saline tracer into the fracture zone. This is expected to give a map of

the tracer distribution in the fracture plane which will give an idea of the geometry of the transport channels. The radar experiments are combined with a more conventional migration experiment where the salt concentration in a number of boreholes is measured as a function of time. These measurements were made to assure that steady state conditions were met at the second round of radar measurements and to provide a calibration of the radar results.

The Crosshole Site in the Stripa mine was selected as the experimental site as the geological and the hydrological conditions were well known. The site had been drilled and comprehensively investigated during the Crosshole Programme carried out in Phase 2 of the International Stripa Project (Olsson, Black, Cosma, and Pihl, 1987). Seven boreholes were available at the site and difference tomography was carried out between a large number of boreholes to obtain a three-dimensional image of the flow paths.

1.2 BACKGROUND

A substantial development of the borehole radar technique and its application to fracture detection in crystalline rock has been made within the Crosshole Programme of the International Stripa Project. The work has been performed by a research group at the Swedish Geological Co. (SGAB). The development efforts have comprised the construction of a new radar system (RAMAC), a comprehensive field testing program, and interpretation technique of the data collected (Olsson, Falk, Forslund, Lundmark, and Sandberg, 1987). The RAMAC system can be applied both for single hole and crosshole measurements. Reflections are observed in both measurement modes and can be used to identify fracture zones or other inhomogeneities in the rock. The analysis of crosshole data has also included tomographic inversion of travel time and amplitude data.

Following the completion of the Crosshole Programme the RAMAC system has been used comprehensively in radioactive waste related projects in Canada, Finland, Japan, Sweden, and Switzerland. In most of these projects borehole radar has been used for characterization of fractures and fracture zones.

The first combined saline injection and radar experiment with the RAMAC system was carried out at the Grimsel Test Site in Switzerland during 1986 and 1987 (Niva and Olsson, 1988). In this experiment radar tomography was made of a quadratic area with the dimensions 150x150 m. Source and receiver positions were located on three sides of the square.

Two sides of the square were outlined by boreholes and the third side by a tunnel. The separation of measurement points in the boreholes was 2.5 m and in the tunnel it was 5 m. Saline tracer was injected in two different fracture zones at two different occasions. The salinity of the injected fluid was approximately 1% and each injection started 3-5 days before commencement of the radar measurements. The salinity of the fluid was sufficient to cause measurable changes in radar intensity well above the noise level.

The largest concentrations of tracer were observed close to the injection points and the tracer followed fracture zones extending from the injection points. Some transport paths did not leave a continuous trace in the difference tomograms. This was considered to indicate transport paths not confined to the plane of measurement. The results obtained at the Grimsel Test Site clearly demonstrated the capabilites of the radar method to map tracer transport through fractured rock.

The experiments at the Crosshole Site described in this report are based on the experiences gained from the work at the Grimsel Test Site but they represent a further step in experimental sophistication. For example, the hydrologic conditions at the Crosshole Site are better known, the borehole configuration allows a mapping of the tracer transport in three dimensions, and the radar surveys are combined with a conventional migration experiment which will facilitate a calibration of the radar results.

1.3 SCOPE OF WORK

The experimental work in the investigation of the flow distribution in a fracture zone has been carried out in four phases: The first phase comprised the reference measurement with single hole reflection and crosshole tomography surveys. The second phase included reassessment of the hydraulic conditions at the site and injection of saline tracer at a constant rate in a fracture zone. The inflow rate and concentration of saline water entering the open boreholes was measured as a function of time. When the data indicated steady state conditions the third phase, which comprised a repetition of the radar measurements performed during the first phase, was started. Tomographic inversion has been made of the difference between the radar data collected in phases 1 and 3 to show the location of the saline tracer. The experimental work was concluded with the fourth phase which comprised measurement of salt concentration in the open boreholes in order to check

that steady state conditions had prevailed during the radar measurements. Following the completion of the experimental programme an integrated analysis has been made of the collected radar and tracer migration data.

This report describes the results from all phases and tries to summarize the experience and know-how gained from the project. A description is given of equipment used, experimental procedures, data processing, and the implication of the results for our understanding of flow through fractured rock.

2 EXPERIMENTAL SETUP

2.1 EXPERIMENTAL SITE

This experiment has been carried out at the Crosshole site situated at the 360 m level in the Stripa Mine (Figure 2.1). At this site seven boreholes were drilled during phases 1 and 2 of the Stripa Project. All boreholes originate from essentially the same point at the end of a drift. The boreholes outline a tilted pyramid with a height and a base of about 200 m where all boreholes start from the top of the pyramid. Data on the boreholes at the Crosshole Site are listed in Table 2.1.

Table 2.1 Position of boreholes E1 and F1-F6, in the local mine coordinates. Bearing from mine north (in degrees), plunge below horizontal plane (in degrees), length (m).

	E1	F1	F2	F3	F4	F5	F6
Collar position:							
X	338.4	337.5	337.4	336.5	336.5	335.5	335.6
Y	1199.7	1199.3	1199.2	1199.1	1199.1	1199.1	1199.1
Z	355.7	355.4	355.9	355.4	356.0	355.4	355.7
Collar direction:							
Bearing	91.70	96.28	95.86	106.19	106.23	122.14	121.92
Plunge	5.20	10.20	20.57	10.14	30.96	10.14	40.16
Length	300	200	250	200	250	200	250

A comprehensive investigation of the geological, geophysical, and hydraulic properties at the site was made as a part of the Crosshole Programme (Carlsten, Magnusson, and Olsson, 1985, Olsson, Black, Cosma, and Pihl, 1987, Black, Holmes, and Brightman, 1987). The rock at the site consists of fine to medium grained granite. The average frequency of fractures is approximately 4.6 fractures per metre where the most intense fracturing is concentrated into zones. The undeformed granite between the zones is massive, fine to medium grained, and grey to pale red in color. The zones with more intensive fracturing generally show a number of signs of deformation such as brecciation, mylonitization, alteration, and red colouring.

The borehole radar and crosshole seismic investigations gave data on the existence, location, and orientation of a number of fracture zones. In

total 9 zones were identified. Four of these zones were considered to be more significant in terms of extent and hydraulic transmissivity. These zones were referred to as the "basic model" and their location in relation to the boreholes are shown in Figure 2.2. The hydraulic investigations showed that the bulk of the groundwater flow at the site was confined to the identified zones. However, high hydraulic transmissivities did not occur at all intersections of the zones with the boreholes. This was taken to indicate that the flow within the zones was channeled.

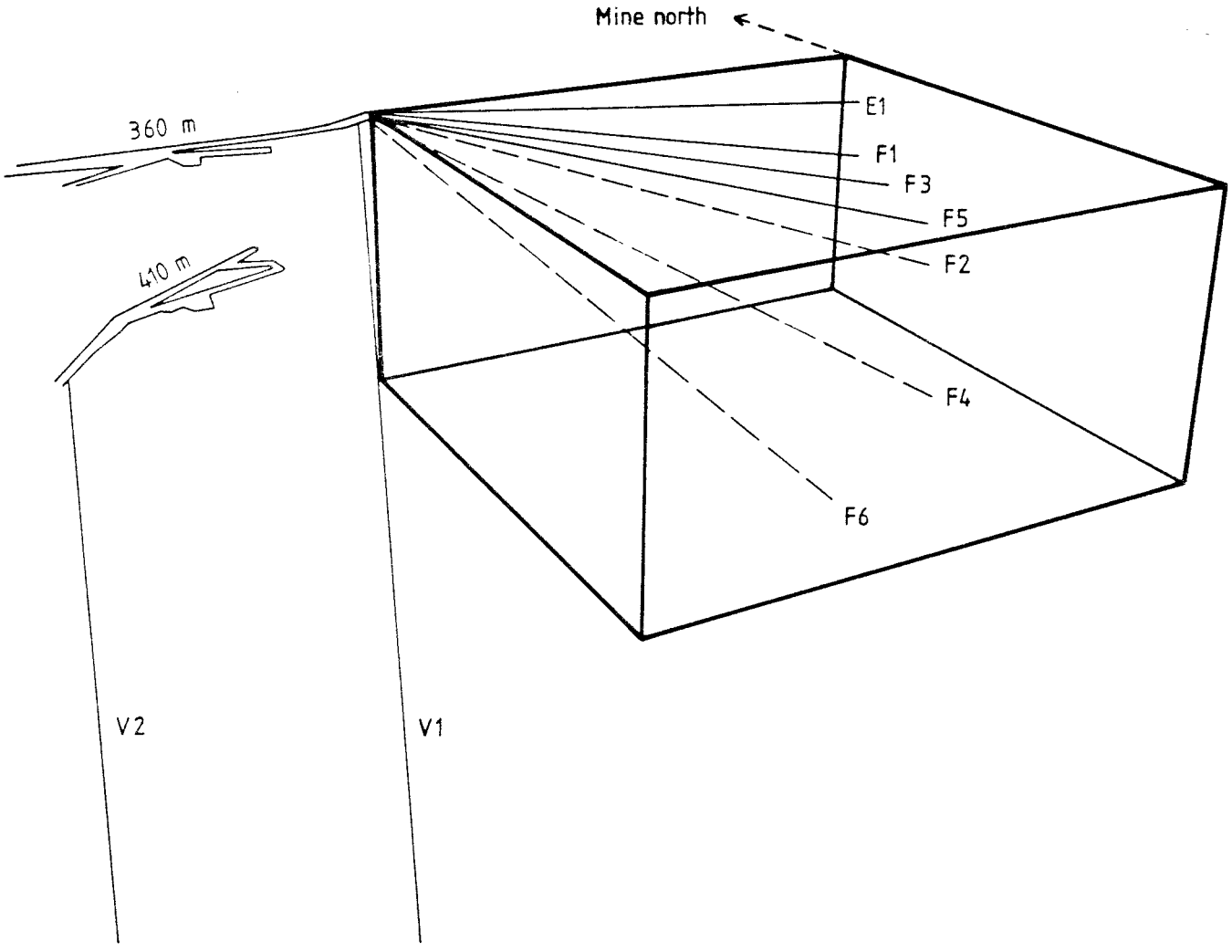

Figure 2.1 Plan view of the Stripa Mine at the 360 m and 410 m levels showing the position of the Crosshole Site and its boreholes.

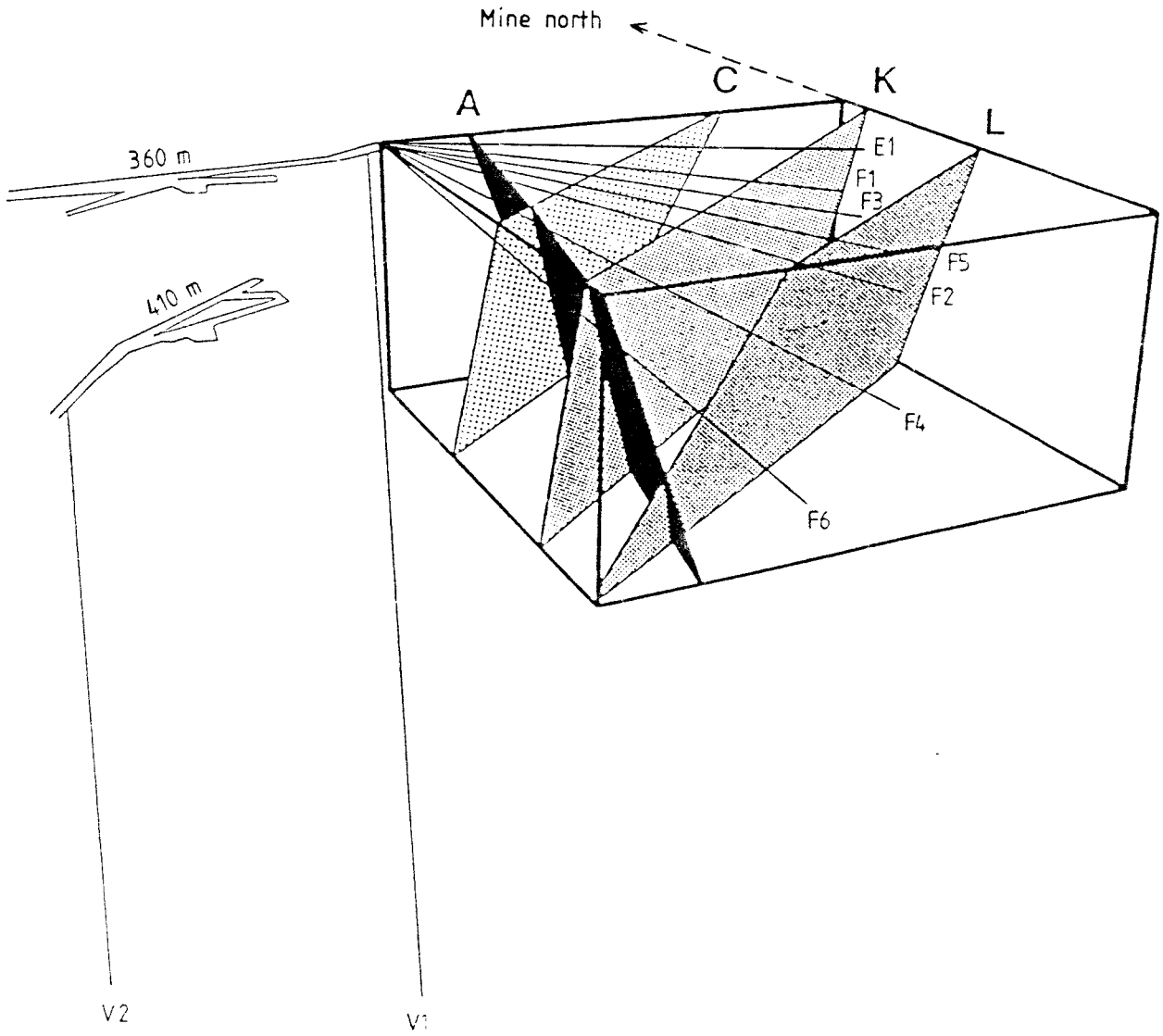

Figure 2.2 Block diagram showing the interpreted extension of the major units which have been identified based on the investigations carried out at the Crosshole Site.

The fracture zone labelled 'C' was chosen as the target for these investigations. It is one of the major zones at the site and it is centrally located within the site. Crosshole hydraulic testing had shown that good hydraulic connections exist from borehole F3 to F2 and F5. Other tested combinations between the boreholes showed no responses except for F5 to F6 (Black, Holmes, and Brightman, 1987). Zone 'C' intersects all boreholes at the site and the radar intersections with the boreholes are tabulated in Table 2.2.

Table 2.2 Radar intersection between zone C and the seven boreholes at the crosshole site in the Stripa mine, as observed in the previous singlehole radar measurements (Olsson, Falk, Forslund, Lundmark, and Sandberg, 1987).

Borehole	Radar intersection with zone C (m)
E1	130-145
F1	118-124
F2	115-119
F3	105-109
F4	93-109
F5	93- 96
F6	103-111

The interval 103.0-118.5 m in F3 was selected as the injection point for the saline tracer. F3 is centrally located and it was considered that measurements in the surrounding boreholes would give a good image of the spreading of the tracer from the injection point.

Fracture zone 'C' is nearly perpendicular to the boreholes which intersect the plane. Figure 2.3 shows the plane of fracture zone 'C' and the relative position of the boreholes where they intersect zone 'C'.

Within this project single hole reflection and crosshole tomographic radar measurements have been made. The tomographic measurements give information on the distribution of saline tracer within the zone along lines connecting the pair of boreholes in which measurements are made. In single hole reflection data the properties of a zone are obtained along a line which is the projection of the borehole onto the plane. In this project single hole reflection measurements have been made in 6 boreholes and crosshole tomographic surveys in 11 sections. The lines across the plane of zone 'C' where information will be obtained are indicated in Figure 2.3. As can be seen from the figure a fairly good coverage of the plane will be obtained.

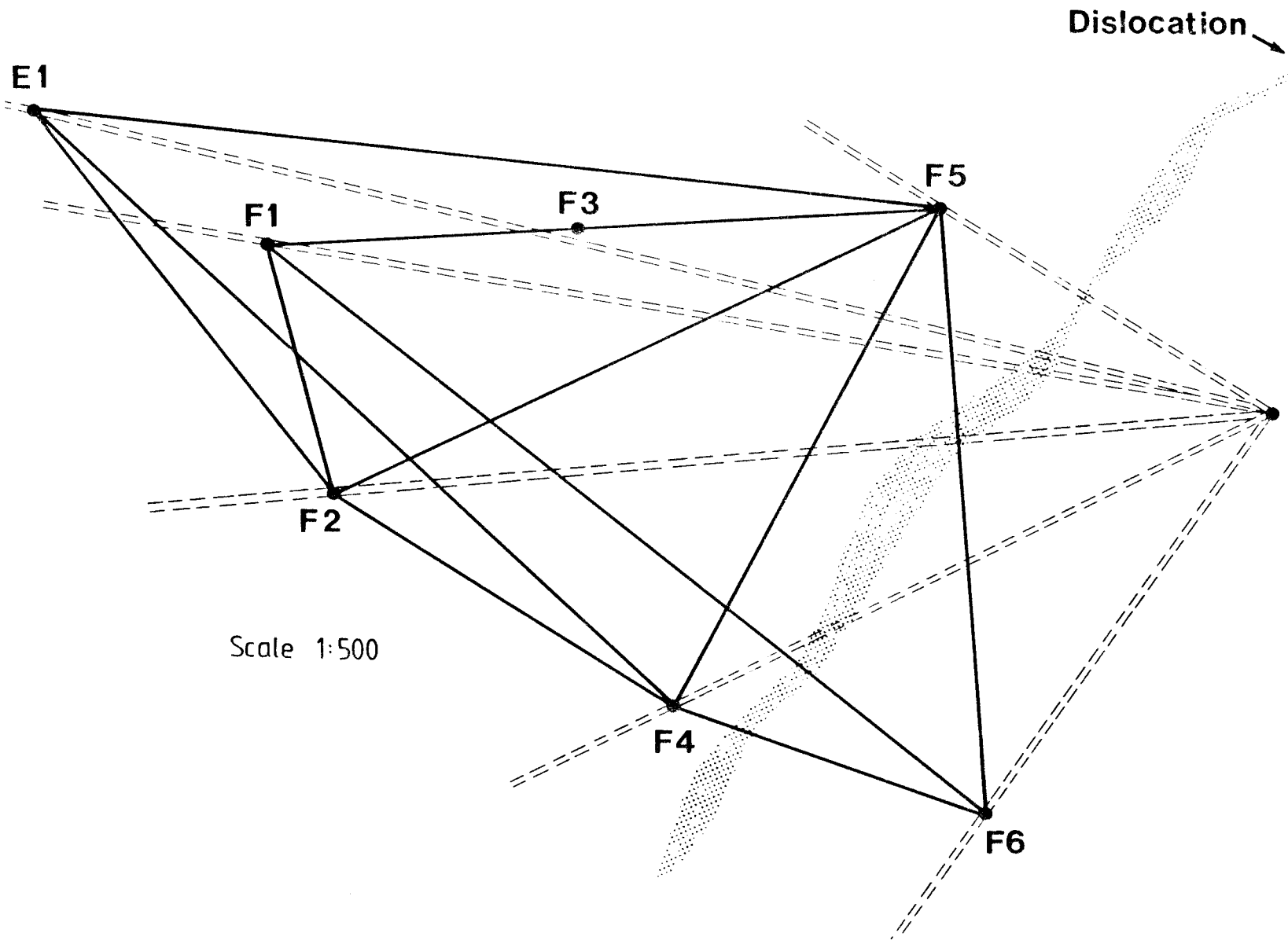

Figure 2.3 Map of the plane of fracture zone 'C'. The solid lines indicate where data on the distribution of saline tracer in the plane will be obtained from the tomographic measurements. The dashed lines indicate where information is obtained from single hole reflection surveys. The depicted dislocation is discussed in chapter 6.3.

2.2 MEASUREMENT PROGRAM

The main tasks of the experimental work has been to make a radar reference measurement, inject saline water into a fracture zone, and to repeat the radar measurements with the saline tracer present in the fracture zone. This section gives a brief outline of the experimental program while details about the radar and migration experiments are given in the following sections.

The measurement program was divided into four phases which are described below.

The first phase comprised the reference measurements with radar. Crosshole tomography measurements were made of 11 borehole sections. For each section a borehole length of approximately 100 m was measured with a point spacing of 4 m. This resulted in approximately 700 rays per section. Single hole reflection measurements were made in the six available boreholes (the borehole used for injection of tracer was not measured). The centre frequency 60 MHz has been used both for the single hole and the crosshole measurements. The measured data have been processed and presented in a preliminary report (Andersson and Olsson, 1988a).

The second phase started with measurements of the natural hydraulic head and water inflow into packed off intervals of all seven boreholes. Then followed injection of unlabelled water into the fracture zone and measurement of inflows in the six detection boreholes. Saline water (KBr) with a concentration of approximately 0.5% was injected in the fracture zone and measurements made of inflow and electrical conductivity in suitable sections as indicated by the tests with unlabelled water (Andersson and Gustafsson, 1988). Tracer concentration was measured as a function of time in the selected sections. Thus, phase 2 was effectively a conventional tracer migration experiment.

The third phase comprised a repetition of the radar measurements made in phase 1 while the salt injection was still going on (Andersson and Olsson, 1988b). The radar measurements were started after 560 hours of tracer injection. At this time steady state conditions had been obtained in the borehole intervals nearest to the injection point. The saline tracer increases the electrical conductivity of the groundwater and hence the attenuation of radar waves. The difference in received radar amplitudes between phase 3 and phase 1 gives information on the location of the saline tracer in space.

The fourth phase comprised measurements of the electrical conductivity (salt concentration) in all open boreholes after the completion of the radar measurements. This was made to provide a check on whether steady state conditions had prevailed during the radar measurements. The injection of saline tracer was terminated after the completion of these measurements and the equipment used removed from the site. The duration of the tracer injection was 905 hours (38 days).

2.3 RADAR MEASUREMENTS

2.3.1 Crosshole tomography

In a crosshole measurement the transmitter and receiver are placed in separate boreholes. One of the probes is kept in a fixed position in one of the boreholes while the other probe is moved in the other hole where measurements are made with fixed intervals. A set of measurements where one probe is fixed in the first borehole and the other probe is moved along the length of the other borehole is termed a borehole scan. According to the reciprocity theorem the transmitter and receiver are interchangeable and it is irrelevant in which of the boreholes each probe is placed.

In this case crosshole tomography measurements have been made in eleven sections outlined by combinations of two of the six available boreholes (F3 not included). The eleven borehole sections, of interest, were measured both before and after injection of the saline tracer. All sections have been measured with a centre frequency of 60 MHz. The tomographic measurements were made with a point separation of 4 m in all boreholes. The measurement length for all boreholes was about 100 m in the crosshole tomography surveys. Tomographic analysis has been made of both travel times, amplitudes, and the amplitude differences between phases 3 and 1. Data on the crosshole tomography measurements are listed in Table 2.3.

Table 2.3 Data on crosshole tomography measurements performed as a part of the project "Investigation of flow distribution in a fracture zone".

Centre frequency:	60 MHz
Sampling frequency:	510 MHz
Number of samples:	512
Number of stacks:	256

Bore-hole 1	Logged depth (m)	Point sep. (m)	Bore-hole 2	Logged depth (m)	Point sep. (m)	No. of rays
F2	71.4-171.4	4	F4	61.4-161.4	4	676
F5	51.4-151.4	4	F4	61.4-161.4	4	676
E1	81.4-197.4	4	F4	61.4-161.4	4	780
F5	51.4-151.4	4	E1	81.4-197.4	4	780
F2	71.4-171.4	4	E1	81.4-197.4	4	780
F5	51.4-151.4	4	F2	71.4-171.4	4	676
F1	71.4-171.4	4	F2	71.4-171.4	4	676
F5	51.4-151.4	4	F1	71.4-171.4	4	676
F1	71.4-171.4	4	F6	51.4-151.4	4	676
F4	61.4-161.4	4	F6	51.4-151.4	4	676
F5	51.4-151.4	4	F6	51.4-151.4	4	676
			Total number of rays :			7748

2.3.2 Single hole reflection

In single hole measurements the transmitter and receiver are located in the same borehole. The transmitter and receiver are kept at a fixed separation by glassfiber rods. The transmitter-receiver array is moved along the borehole and measurements are made at fixed intervals. The measurement at each position takes about 30 seconds including the movement to the next measuring position. Measurements have been performed at a centre frequency of 60 MHz. The six available boreholes, see Table 2.4, were measured both before and after injection of the saline tracer.

The reflection measurements performed as a part of the project are listed in Table 2.4. Included in the table is a list of the system parameters that can be varied during a survey.

Table 2.4 Data on single hole reflection measurements performed as a part of the project "Investigation of flow distribution in a fracture zone".

Centre frequency:	60 MHz
Sampling frequency:	510 MHz
Number of samples:	512

Bore-hole	Logged depth (m)	Point sep. (m)	Tr-Re sep. (m)	No. of stacks
E1	15.1-190.6*	0.5	7.4	256
F1	15.1-193.1	0.5	7.4	256
F2	15.1-205.1	0.5	7.4	256
F4	15.1-205.1	0.5	7.4	256
F5	15.1-192.6*	0.5	7.4	256
F6	15.1-205.1	0.5	7.4	256

* the measured length of the borehole was shorter in phase 3 due to blocking of these boreholes. Termination depth for phase 3; E1: 183.1 m, F5: 147.6 m.

2.3.3 Calibrations

Difference tomography puts heavy demands on both short term and long term stability of the radar system. Both the reference measurement and the identical repetition measurement consist of a sequence of measurements which extend over a relatively long time. In this case 11 tomographic sections were measured in each phase. The time required to complete the measurements in each phase was approximately 10 days. The phase 3 measurements were made 3 months after the completion of phase 1. Hence, the radar measurements within this project are spread out over a considerable time period. In difference tomography the difference in data between the two phases are analyzed and this requires that the system is stable between the measurement period or that any drift can be quantified.

Tomographic analysis of a borehole section involves inversion of the amplitudes or travel times of all rays belonging to the section. This puts a requirement on the short term stability of the radar system. To get a sensible result from the tomographic inversion the system has to be stable during the time it takes to measure the tomographic section.

The stability requirement also applies to the bedrock conditions. In this case it implies that the distribution and concentration of saline tracer should not change during the time it takes to measure one section, i.e. about 8 hours. In addition, the saline tracer distribution should not change significantly during the time required to measure all 11 sections in order to make the sections comparable. The stability of the saline tracer distribution has been checked by measurements of saline tracer concentrations in the boreholes prior to and after the second round of radar measurements. The results indicated only small variations in salinity (see Chapter 8).

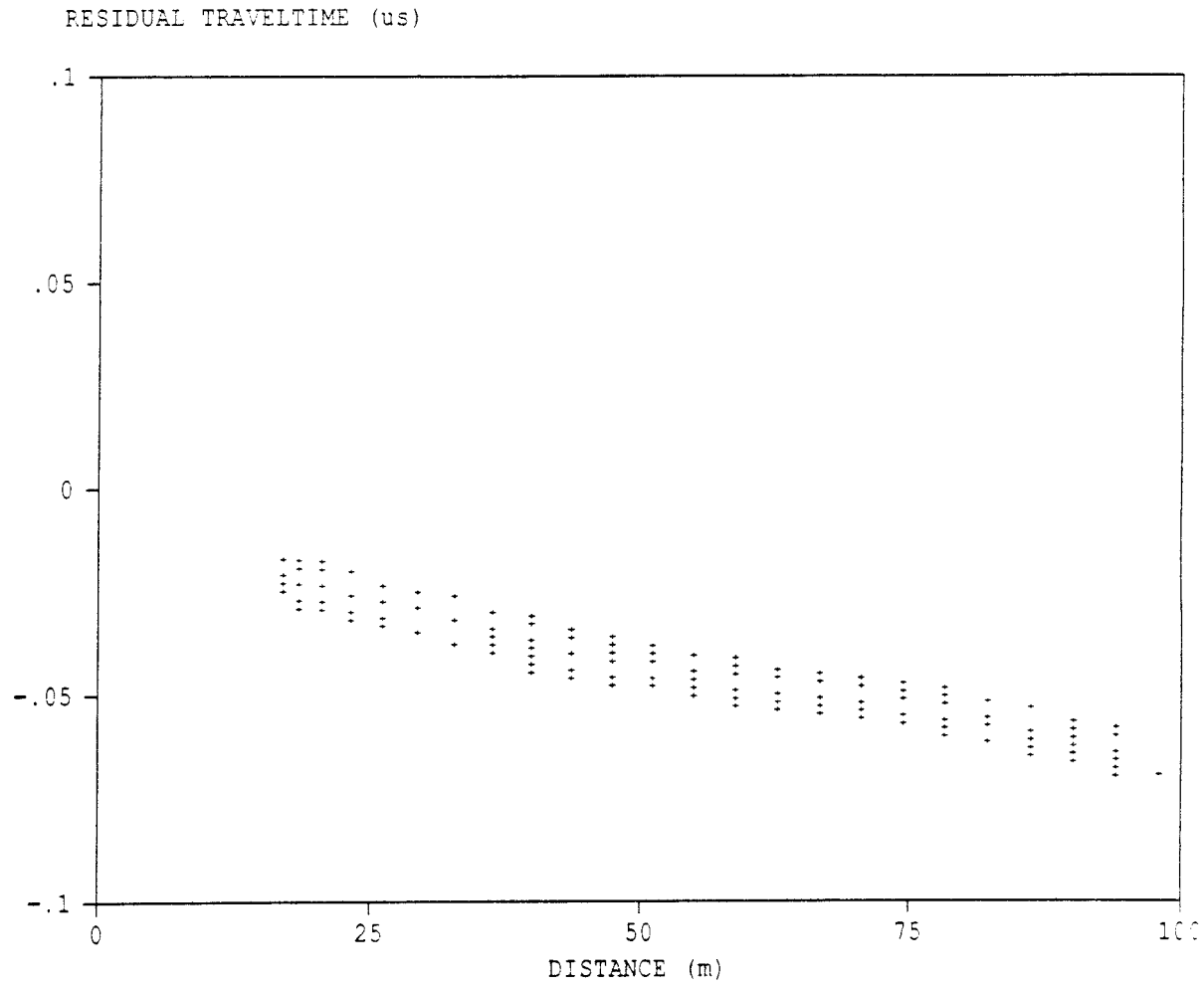

Figure 2.4 Residual travel times from a set of calibration scans (borehole section F2F5) measured during phase 3.

The stability of the radar system was checked through calibration measurements which in principle were made at the start and the completion of every measurement day. The calibration measurements consisted of the recording of a borehole scan. The receiver was fixed at a depth of 31.4 m in borehole F2 while the transmitter was moved in F5. Readings were taken every 4 m for the interval 31.4 to 119.4 m in borehole F5. The calibration measurements mainly revealed drifts due to battery failure and in some instances also equipment breakdowns. Observation of errors in the calibration measurements have where necessary led to remeasurement of the corresponding erratic section.

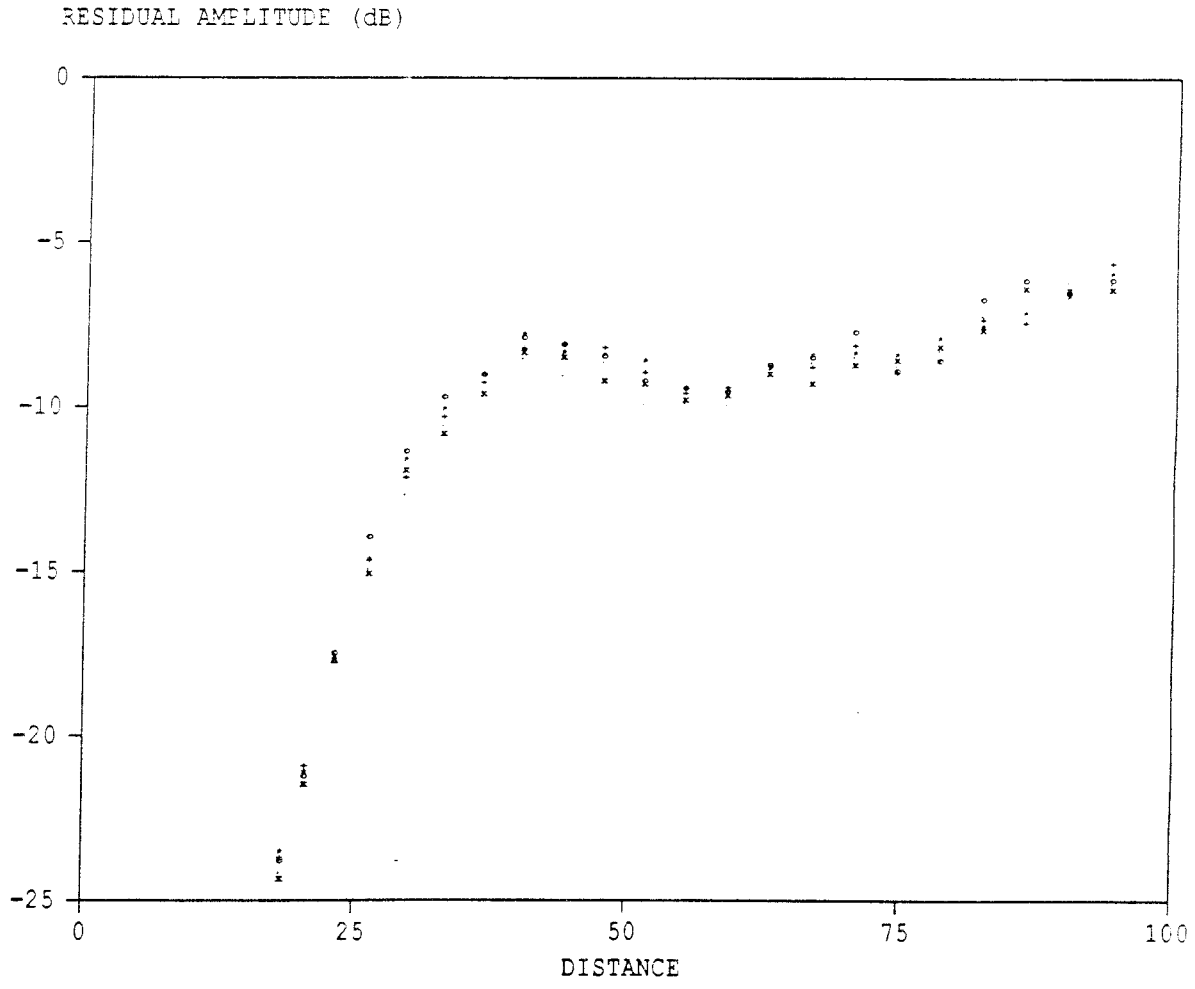

Figure 2.5 Residual amplitudes from a set of calibration scans (borehole section F2F5) measured during phase 1.

Figure 2.4 shows the drift in arrival time observed in a set of calibration measurements made during phase 3 of the project. The spread in the data indicates drift in zero time during the measurement period. The magnitude of the short time drift is about 12 ns. The consistent slope of all calibration curves indicate that the sampling frequency (which is determined by the time base of the system) has been stable.

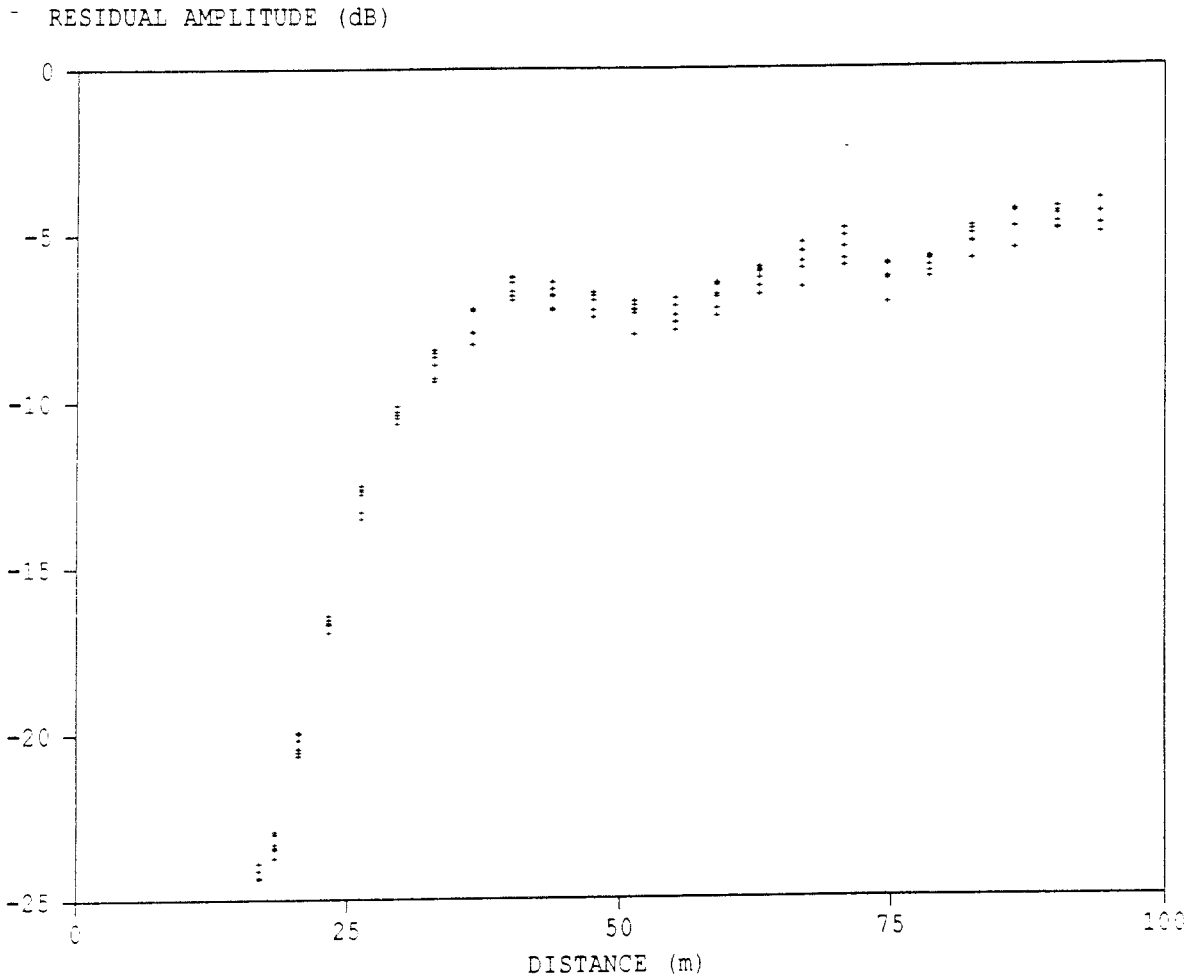

Figure 2.6 Residual amplitudes from a set of calibration scans (borehole section F2F5) measured during phase 3.

Figures 2.5 and 2.6 show residual amplitudes recorded from calibration scans during phases 1 and 3, respectively. The spread in amplitude values are a combined effect of system drifts and quantization errors and other imperfections of the algorithm used for obtaining the amplitude values (cf. Chapter 4). The variations appear to be random and can be treated as noise with a magnitude of approximately 1 dB.

A comparison of Figures 2.5 and 2.6 shows a shift in the average amplitude level of the calibration scans between phases 1 and 3, the amplitudes from phase 3 being about 2 dB larger than from phase 1. This change in gain level was caused by a modification of the receiver amplifier between the measurement phases. Corrections have been made to compensate for this shift in gain. Two sections were measured with a different receiver compared to the rest and the magnitude of the corrections have been different for these two sections. Other sources of error and how they are accounted for are discussed in Section 4.3.

2.3.4 Equipment used

A short pulse borehole radar system (RAMAC) has been used for these measurements. The system was originally developed by the Swedish Geological Co. (SGAB) as a part of the International Stripa Project. A continued development to make the system adapted for field work on a production basis has later been funded by SKB.

The radar system (RAMAC) consists of four different parts;

- IBM-compatible microcomputer with one 5 inch floppy disc units for control of measurements, data storage, data presentation and signal analysis.
- a control unit for timing control, storage and stacking of single radar measurements.
- a borehole transmitter for generation of short radar pulses.
- a borehole receiver for detection and digitization of radar pulses.

The RAMAC system works in principle in the following manner: A short current pulse is fed to the transmitter antenna, which generates a radar pulse that propagates through the rock. The pulse is made as short as possible to obtain high resolution. The pulse is received by the same type of antenna,

amplified, and registered as a function of time. The receiver may be located in the same borehole as the transmitter or in any other borehole. From the full wave record of the signal the distance (travel time) to a reflector, the strength of the reflection, and the attenuation and delay of the direct wave between transmitter and receiver may be deduced.

The recording of the signal is similar to that of a sampling oscilloscope, i.e. for each pulse from the transmitter only one sample of the received electric signal is taken at a specific time. When the next pulse is generated a new sample is taken which is displaced slightly in time. Thus, after a number of samples a replica of the entire signal is recorded. The sampling frequency and the length and position of the sampled time interval can be set by the operator.

Optical fibers are used for transmission of the trigger signals from the computer to the borehole probes and for transmission of data from the receiver to the control unit. The optical fibers have no electrical conductivity and will not support waves propagating along the borehole. Another advantage of optical fibers is that they can not pick up electrical noise and as the signal is digitized down-hole there will be no deterioration of the signal along the cable. The quality of the results will thus be independent of cable length.

There is no direct connection between the transmitter and the receiver. Both probes are instead connected directly to the control unit and the transmitter and the receiver can be put into the same as well as into separate holes. In other words, the radar may be used both for single hole and crosshole measurements. The system also provides absolute timing of the transmitted pulses and a calibrated gain in the receiver which makes it possible to measure travel time and amplitude of the radar pulses in a crosshole measurement and hence provide data for a tomographic analysis. The absolute time depends on the length of the optical fibers and is hence a quantity which has to be obtained through calibration for a given set of optical fibers. The block diagram of the control unit, transmitter, and receiver is shown in Figure 2.7 and the technical specifications of the system are given in Table 2.5.

Table 2.5 Technical specifications of the borehole radar system.

General	
Frequency range	20-80 MHz
Total dynamic range	150 dB
Sampling time accuracy	1 ns
Maximum optical fiber length	1000 m
Maximum operating pressure	100 Bar
Outer diameter of transmitter/receiver	48 mm
Minimum borehole diameter	56 mm
Transmitter	
Peak power	500 W
Operating time	10 h
Length	4.8 m
Weight	16 kg
Receiver	
Bandwidth	10-200 MHz
A/D converter	16 bit
Least significant bit at antenna terminals	1 μV
Data transmission rate	1.2 MB
Operating time	10 h
Length	5.4 m
Weight	18 kg
Control unit	
Microprocessor	RCA 1806
Clock frequency	5 MHz
Pulse repetition frequency	43.1 kHz
Sampling frequency	30-1000 MHz
No of samples	256-4096
No of stacks	1-32767
Time window	0-11 μs

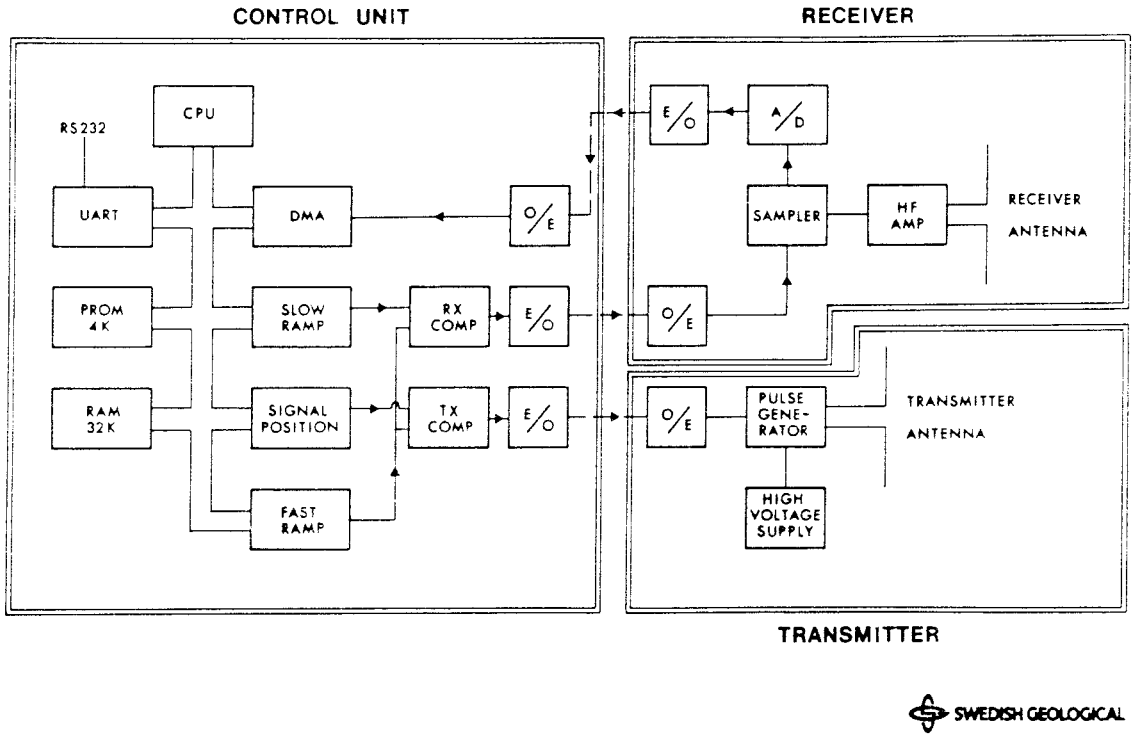

Figure 2.7 Block diagram of the borehole radar system.

2.4 INJECTION OF SALINE TRACER

2.4.1 Injection of tracer

The injection of saline tracer in borehole F3 was performed as a continuous injection with constant flow rate. The tracer, Potassium Bromide (KBr), was injected in a 14.5 m long packed-off interval enclosing Zone C during a period of 905 hours (38 days). The injection data are summarized in Table 2.6 below. The length and location of the injection interval in borehole F3 was decided from hydraulic test data (Black, Holmes, and Brightman, 1987).

Table 2.6 Injection data (mean values).

Injection borehole: F3
Injection interval: 103 - 117.5 m borehole length, (Zone C).
Injection flow rate: 800 ml/min.
Injection pressure: 682 kPa.
Background pressure: 18 kPa.
Tracer concentration: 3357 ppm Br^-.
Electrical conductivity of tracer solution: 530 mS/m

According to the interpretation from previously performed single hole radar measurements (Olsson, Falk, Forslund, Lundmark, and Sandberg, 1987), the extension of Zone C, in borehole F3, is limited to the interval 105-109 m. However, high hydraulic conductivities were also found in the interval 110-123 m (Black, Holmes, and Brightman, 1987). Also, during the inflow measurements, preceding the tracer injection, natural inflow of water was observed in the interval 108-113 m (Andersson and Gustafsson, 1988). Therefore it was decided to include this interval for the injection in attempt to avoid leakage around the lower packer through interconnecting fractures.

The water flowing out of borehole F3, both above and below the injection interval 103-117.5 m, was continuously sampled for tracer analysis in order to detect any potential leakage of tracer solution around the packers. The flow rate measurements indicated only a minor leakage around the lower packer, 7 ml/min (Andersson and Gustafsson, 1988). The measurement of the water flowing out of borehole F3 from the interval 0 - 102 m indicated no leakage around the upper packer.

The choice of KBr as tracer was based upon the following considerations:

- easy to detect by measurement of the electrical conductivity
- no sorption on granite
- low background concentration

The initial concentration chosen of KBr was 0.5 % giving an electrical conductivity of approximately 530 mS/m. This figure, compared to the background conductivity of the Stripa water, 20-30 mS/m, gave a contrast large enough to allow a quantitative evaluation of the breakthrough curves.

The Bromide ion has been reported as a conservative tracer by several authors (e.g. Gustafsson and Klockars, 1981). The low background concentration (0.1 - 0.6 ppm) implies that an even more accurate analysis than the electrical conductivity can be made by utilizing an ion-selective electrode.

2.4.2 Measurements performed

The measurements of the flow distribution within Zone C and the breakthrough of saline tracer are referred to as Phases 2 and 4 of the project. Phase 2 started with measurements of inflow rates in order to decide the detailed measurement programme for Phase 2. These measurements are called the calibration measurements.

Phase 2

Calibration measurements

- Measurements of **natural** inflows to open boreholes and to packed-off intervals (1.0 m) in all seven boreholes (F1-F6 and E1) prior to the start of injection.

- Injection of unlabelled water in borehole F3 (borehole interval, pressure and flow rate as given in Table 2.6) and measurements of inflow rates to the open boreholes and the packed off intervals in the six detection boreholes (F1, F2, F4, F5, F6 and E1).

Salt injection measurements

- Injection of saline tracer (KBr) in borehole F3, according to the data given in Table 2.6, and measurements of inflow rates, electrical conductivity and Bromide concentration in flowing boreholes and in intervals of boreholes chosen from the calibration measurements (Table 2.8).

Phase 4

- Measurements of the electrical conductivity, in all detection boreholes within Zone C and in adjacent highly conductive intervals of the boreholes. The measurements were made immediately after completion of the radar measurements in Phase 3.

The purpose of the natural flow and head measurements was to indicate the location of the potentially water conducting fractures within and adjacent to Zone C and comparing this with the measurements during the

following injection of unlabelled water. Based on this, the final design of the measurement programme for the tracer injection in Phase 2, could be made.

Based on geological data (Carlsten, Magnusson, and Olsson, 1985) and hydraulic data (Carlsson and Olsson, 1985; Black, Holmes, and Brightman, 1987), a total of 139 intervals, with a length of 1.0 m, were selected for the calibration measurements.

Studies of the hydraulic head distribution in Zone C (Black, Holmes, and Brightman, 1987) indicated hydraulic heads on the order of 10-50 metres of water, relative to the instrument drift, except for borehole F6 where the hydraulic head was -4 m, i.e. below the drift level. However, the hydraulic heads during this investigation were found to be considerably lower. Before the start of this investigation, the boreholes had been open for about one month thus lowering the hydraulic head in the rock mass considerably. Heavy pumping at the 410 m-level for the Stripa Project Phase 3 works may also have affected the hydraulic head in the rock mass.

The lower hydraulic head together with the relatively low conductive rock ($K = 10^{-8} - 10^{-11}$ m/s, 10 m intervals) implied a very slow pressure buildup in most of the intervals, so therefore it was decided to measure only the inflow rates in the 139 chosen intervals. Each interval was measured for 30 minutes. A summary of the results (Andersson and Gustafsson, 1988) is presented in Table 2.7.

Table 2.7 Inflow rates to boreholes E1 and F1-F6 during the calibration measurements, natural flow, Q(n) and induced flow, Q(ind).

Bh	Interval (m)	No of intervals	Q(n) (ml/min)	Flowing intervals	Q(ind) (ml/min)	Flowing intervals
E1	119-148	21	0.7	4	152.7	6
F1	92-139	21	3.3	12	14.7	18
F2	86-126	21	3.0	1	295.7	5
F3	93-116	23	26.6	6	INJECTION	
F4	100-139	18	-	-	-	-
F5	89-108	19	0	0	110.0	9
F6	67-133	16	-	-	-	-
TOTAL		139	33.6	23	573.1	38

The results from the calibration measurements indicated good hydraulic connections between the injection interval in F3 and, in particular, boreholes E1, F2, and F5. This is also in agreement with the results from the crosshole hydraulic testing performed within Phase 2 of the Stripa Project (Black, Holmes, and Brightman, 1987). The injection of water also increased the number of flowing intervals from 23 to 38 and the total inflow to all boreholes from 33.6 to 573 ml/min. The flow distribution during injection of water is shown in Figure 2.8. It should be noted that boreholes F4 and F6 could not be measured due to the low hydraulic head in these boreholes.

The original plan for Phase 2 of the project, was to log all the boreholes with a specially designed conductivity probe, see also Section 2.4.3. The logging should be performed more or less continuously, moving the probe between the boreholes. However, the flow distribution pattern shown in Figure 2.8 indicated that the inflow was concentrated to very few spots in some of the boreholes. It was therefore decided to install packers which could be inflated for sampling. The packers should only be inflated for shorter times as the idea was to maintain the same hydraulic conditions during the sampling as later during the radar measurement. This procedure would also improve the quality of the tracer breakthrough data and thereby improve the possibilities to make quantitative interpretations regarding transport parameters.

The detailed inflow measurements between packers were made 30 minutes after packer inflation. In the highly conductive intervals, the flow stabilized rapidly at a constant rate but in some of the intervals with very low flow rates, 0.1-0.5 ml/min, the flow rate decreased versus time as a result of the initial pressure buildup from the packer inflation. Some of these low inflow rates registered may therefore be too high or perhaps even non-flowing. However, in most of the low conductive intervals, zero flow was obtained within 15-20 minutes.

All the electrical conductivity measurements were made in situ and the bromide analyses were made at the SGAB Laboratory in Uppsala with an ion-selective electrode.

The accuracy of the injection equipment, the conductivity probes and the bromide analyses are listed below. The accuracy of the borehole conductivity probes are only estimates based on comparisons and intercalibrations with the fixed conductivity

probe used for the in situ measurements of the samples taken from the packed-off intervals.

- injection pump capacity: 1%
- injection pressure : 0.5%
- fixed conductivity probe: 1%
- borehole conductivity probe with packers: 1%
- borehole conductivity probe without packers: 5%
- bromide analysis: 1%

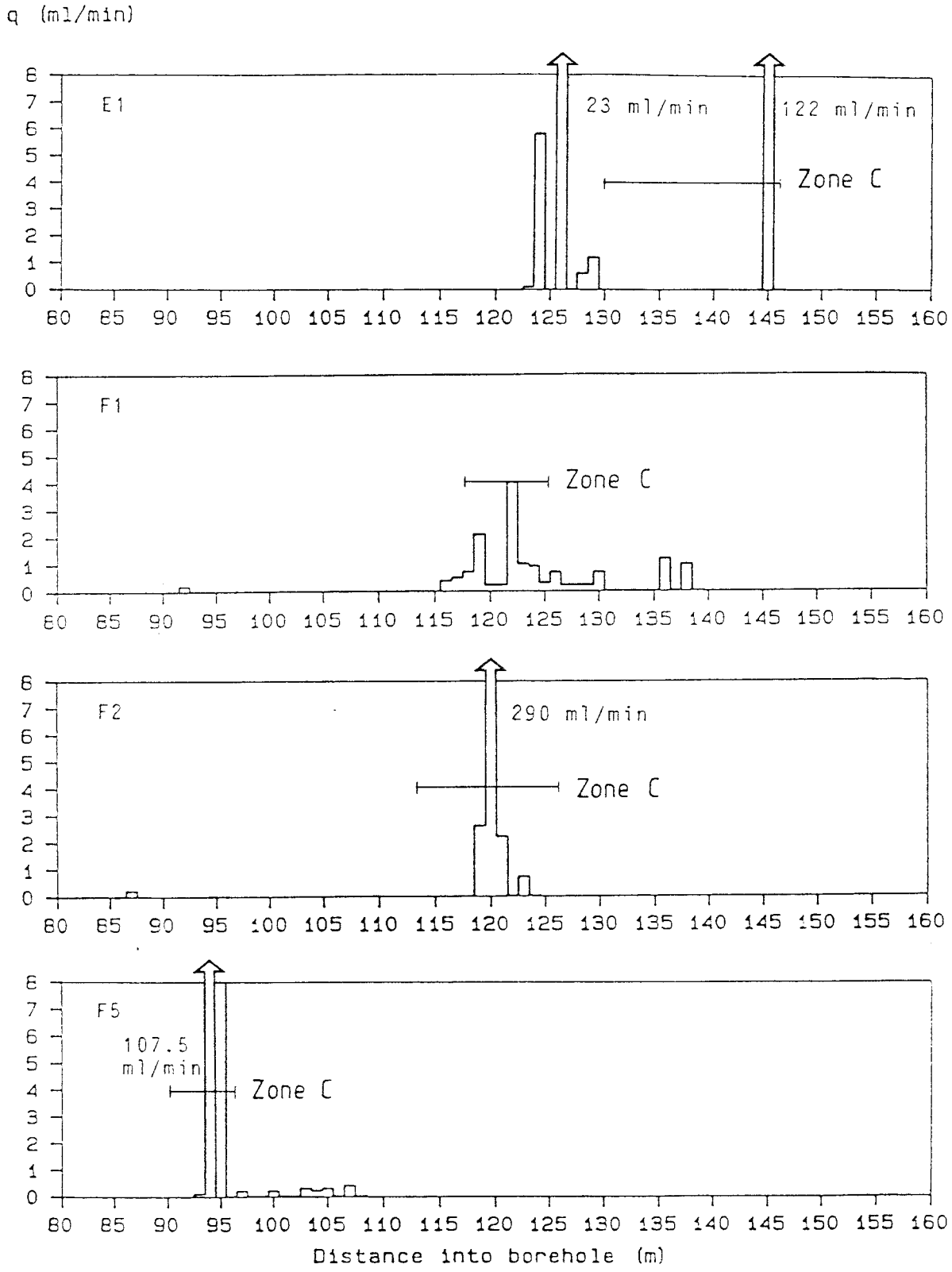

Figure 2.8 **Distribution of inflow rates in boreholes E1, F1, F2 and F5 during injection of unlabelled water in F3. Geological interpretation of Zone C is marked.**

Selection of intervals for tracer detection during Phase 2.

Comments and decisions regarding the sampling during the subsequent tracer injection are presented below and summarized in Table 2.7. The final selection of sampling intervals are summarized in Table 2.8.

Borehole E1: Zone C is interpreted to intersect E1 in the interval 130-145 m, (Olsson, Falk, Forslund, Lundmark, and Sandberg, 1987). During injection in Zone C in borehole F3, the total inflow rate increases from 250 to 450 ml/min from which the interval 145-146 m contributes with 27 % of the total inflow. From the results, it was decided to monitor the intervals 126-127 m and 145-146 m borehole length, using inflatable packers to be intermittently inflated for sampling and subsequent conductivity measurements.

Borehole F1: Zone C is interpreted from single hole radar measurements to the interval 118 - 124 m (Olsson, Falk, Forslund, Lundmark, and Sandberg, 1987). Hydraulic testing of the borehole indicated that Zone C is low conductive in the borehole ($K = 8 \cdot 10^{-11}$ m/s, 116-126 m) (Black, Holmes, and Brightman, 1987). The natural inflow to the borehole is low, with a total inflow from Zone C of 3.4 ml/min, increasing to 14.7 ml/min during injection in F3. Zone C contributes with 31 % of the total natural inflow, increasing to 50 % during injection in F3. From the results, it was decided to log the borehole with the conductivity probe from 108-140 m borehole length without packer inflation, due to the low inflow rates.

Borehole F2: Zone C is interpreted to intersect F2 in the interval 115-119 m. The hydraulic conductivity is $4 \cdot 10^{-9}$ m/s for the interval 116-126 m. However, the interval 118-122 m was found to be somewhat more conductive, $K = 4.5 \cdot 10^{-8}$ m/s and this is also the only interval of the borehole which is naturally flowing and having a good response to the injection in F3. It should also be noted that the open borehole (0-250 m) is not flowing under natural conditions having a hydraulic head of -3 m relative to the instrument drift. However, during injection in F3, the hydraulic head is increased and the open borehole is flowing with 150 ml/min. From the results it was decided to install inflatable packers in the interval 120-121 m, to be intermittently inflated for sampling.

Borehole F3: According to the single hole radar measurements, Zone C intersects the borehole in the interval 103-109 m. Also the hydraulic testing shows

high conductivity values in the interval 102-109 m (K = $8 \cdot 10^{-8}$ m/s). This is also indicated by the natural inflow which is highest in the interval 106-107 m (22.9 ml/min). However, the interval 110-123 m is also relatively high conductive (K = $2.4 \cdot 10^{-8}$ m/s) and having some minor inflows. It was therefore decided to include the conductive part of this interval when performing the tracer injection in Zone C in order to prevent leakage around the packer. Thus, injection was made in the interval 103-117.5 m.

Borehole F4: Zone C is interpreted from the radar measurements to the interval 93-109 m and having a relatively low hydraulic conductivity of $7 \cdot 10^{-11}$ m/s. There is also more highly conductive interval between 118 and 128 m ($9 \cdot 10^{-9}$ m/s). The hydraulic head is -9 m relative to the instrument drift increasing to -7 m during injection in F3. The low hydraulic head made inflow measurements impossible. However, in the three 1m-intervals, 124-127 m borehole length, the water level in the sampling tube was emptied very quickly indicating higher hydraulic conductivity. From the results it was decided to log the interval 90-140 m with the conductivity probe without inflating the packers.

Borehole F5: Zone C is interpreted to intersect F5 in the interval 93-96 m, according to the single hole radar measurements, and having a conductivity of $5 \cdot 10^{-9}$ m/s (91-101 m). No natural inflow was found from Zone C but during injection, a major inflow of 107.5 ml/min was found in the interval 94-95 m. From the results it was decided to install inflatable packers in the interval 94-95 m, to be intermittently inflated for sampling.

Borehole F6: Zone C intersects the borehole at 103-111 m according to the single hole radar measurements and having a low conductivity of $5 \cdot 10^{-11}$ m/s (96-106 m). This borehole has a very low hydraulic head (-35 m) which made the inflow measurements impossible. Some indications of higher conductive intervals were found by filling up the sampling tube, as in borehole F4. Sections 96-97 and 97-98 m were found to be somewhat more conductive. From the results, it was decided to log the borehole in the interval 95-140 m with the conductivity probe without inflating the packers.

Table 2.8 Measurement set-up for the injection of saline tracer.

Bore-hole	Packed-off intervals	Logging interval	Sampled intervals
E1	126-127, 145-146	-	0-300, 126-127, 145-146
F1	-	108-140	0-200
F2	120-121		0-250, 120-121
F3 (inj)	103-117.5		0-102, 118.5-200
F4	-	90-140	-
F5	94- 95		0-200, 94- 95
F6	-	95-140	-

The results of the measurements in Phases 2 and 4 are presented in Section 8.

2.4.3 Equipment used

The injection system, see figure 2.9, consisted of the following components;

1. Tracer tanks, 3 + 2 m^3 volume, could be used separately or together.
2. Filters to avoid pump damage caused by particles
3. Injection pump giving constant flow rate up to 7 bars
4. Electrical mass-flow meter
5. Pressure transducer to register the injection pressure
6. Packer system with perforated injection tube
7. Circulation pump used to dissolve and homogenize the tracer solution.
8. Strip chart recorder recording flow rate, injection pressure, barometric pressure and electrical conductivity.

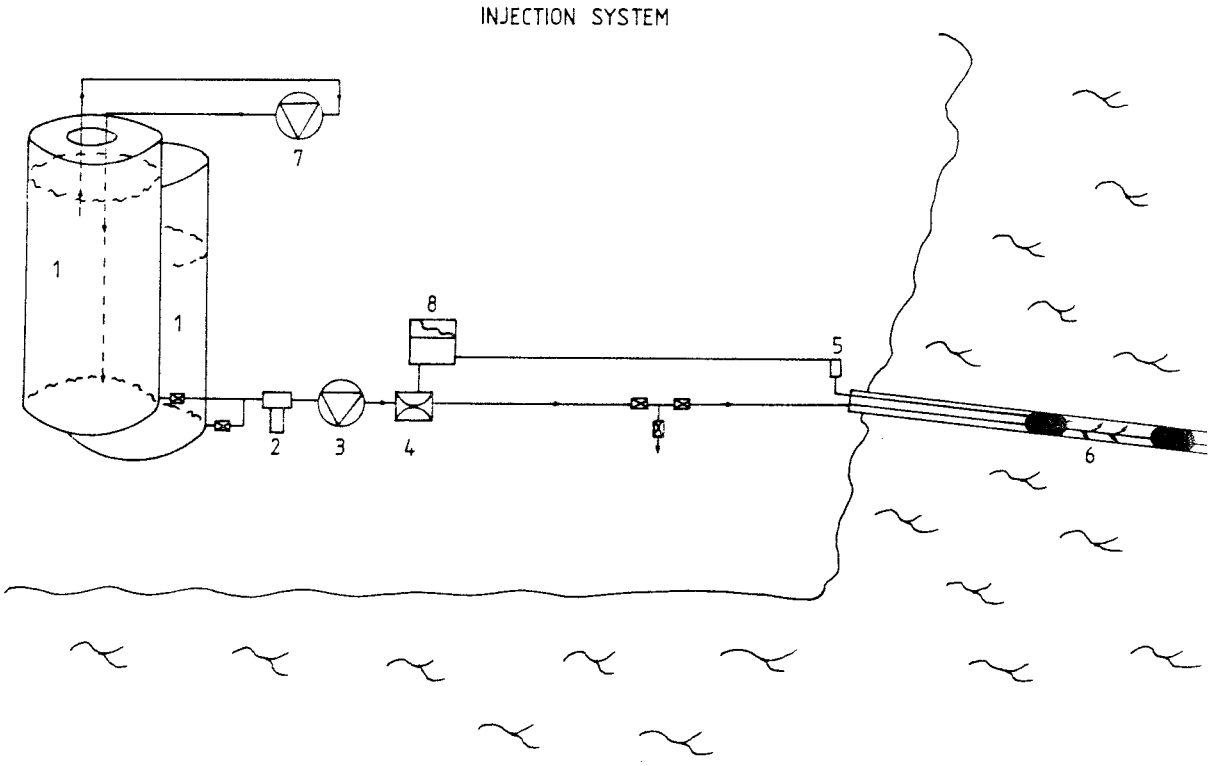

Figure 2.9 Tracer injection system.

The injection was started with unlabelled water and when steady-state conditions were obtained the tracer salt, Potassium bromide (KBr), was poured into one of the tanks. The water was heavily circulated for about 30-60 minutes until the salt was completely dissolved and homogeneously distributed in the tank. The injection of tracer was then started by switching the outlet valves of the tanks. The two-tank system made it possible to refill tracer without stopping the injection. The tanks could also be coupled together in order to achieve longer periods between refillment.

The detection of tracer in the sampling/detection boreholes was made in two ways, with a moveable conductivity probe and by packing off selected intervals of the boreholes and sampling the water flowing into the packed-off intervals.

The specially constructed conductivity probe, Figure 2.10, which was lowered into the boreholes with glassfibre rods, measures the electrical conductivity of the borehole fluid. Inflating the packers gives an interval length of 1.0 metre. The dummy decreases the volume of the interval to approximately 0.8 litre thus decreasing the water residence time and allowing for shorter logging times.

In addition to the conductivity probe, fixed straddle packers were installed in boreholes with only one or two flowing intervals. The packers were inflated only for shorter time intervals at the sampling events in order to avoid disturbances in the flow pattern.

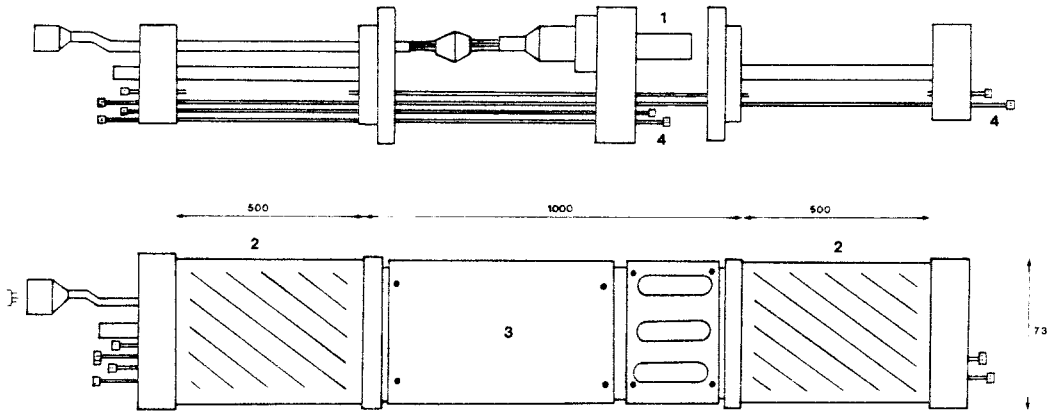

1. 4-electrode conductivity sensor
2. inflatable packers
3. dummy
4. tubing for water sampling

Figure 2.10 Electrical conductivity probe.

2.5 CONCLUSIONS AND RECOMMENDATIONS

During the progress of the project results have shown that the planning and performance, on the whole, was executed in an competent and professional manner. Both the radar measurements and the tracer breakthrough measurements were performed without any major problems. The planning and design of the measurement program and time schedule based on earlier data from the site and predictions of the saline tracer breakthrough was shown to be satisfactory.

Experiences from this project has shown that the concentration of the saline tracer could have been higher than the 0.5% used here. A salt concentration of 1% to 2% would have increased the anomalies of interest, thus simplifying the processing of data and increasing the quality of radar data. An increased salt concentration would also improve the quality of the tracer breakthrough data especially in boreholes with low inflow rates.

As the boreholes in the investigated volumes were open during the survey, hydraulic connection between major fracture zones, through the open holes, possibly exists. During this investigation, these interconnections could only be interpreted from the electrical conductivity logging together with earlier data on hydraulic head and conductivity distribution. For future surveys, of this kind, it is advisable to hinder the hydraulic connection along the boreholes with packers around the pre-known fracture zones, of interest.

The calibration routines where stability of the radar system was checked, showed to be invaluable as it revealed system drifts due to battery failure and in some instances also equipment breakdowns. Observations of errors in the calibration measurements have where necessary led to remeasurement of the corresponding erratic section. The only detail that should be changed to oncoming similar projects is that the calibration measurements, executed as a borehole scan, should be performed in a rock mass which is unaffected by the injected tracer.

The inflow measurements showed to be very valuable for both the design as well as the interpretation of the saline tracer breakthrough. For future projects it is recommended that inflow measurements are made not only within the investigated zone but also in adjacent zones or highly conductive fractures. In order not to make this procedure too time consuming, the measurement interval could be increased from 1 m to 2 m or even

longer intervals depending on the experimental geometry.

The electrical conductivity logging, performed towards the end of the experiment, was also shown to improve the interpretations and add some information about the interconnections between different zones, caused by the presence of the open boreholes. Within this project the logging was performed down to a distance of 40-80 m beyond the investigated zone. However, the experience from this project showed that the logging should be performed throughout the entire length of the boreholes in order to be able to determine more exactly the inflow and outflow positions and the flow distribution within the boreholes.

3 PRINCIPLES OF TOMOGRAPHIC INVERSION

3.1 DEFINITION OF THE PROBLEM

The general idea behind tomographic reconstruction is that information about the properties of the interior of a region can be obtained through measurements at the boundary. In general the transmitter and receiver probes are located at the boundary of the area and each ray connecting transmitter and receiver can in principle be considered to represent the average of a measured property of the rock along the ray path. In order to obtain an estimate of this property at a given point it is necessary that several rays pass close to the same point and that the rays have different directions and hence different information content. The requirement that several rays should intersect the same point puts some severe constraints on the borehole geometry. The main one being that the source and receiver positions and hence the boreholes have to be confined to the same plane.

In mathematical terms the tomographic problem can be formulated in the following way

$$d_i = \int_{T_i(m)} m(x) \cdot ds \qquad (3.1)$$

where d_i is the measured data for ray number i. The objective of the tomographic inversion is to estimate the spatial distribution of some property, $m(x)$, characteristic of the medium (x denotes the spatial coordinates). The data is thought of as being a sum (line integral) of this property along the ray path, $T_i(m)$, from the transmitter to the receiver. The actual ray path is dependant on the properties of the medium, $m(x)$, and is normally the curve which gives the least possible travel time. The complex dependance of the ray paths, T_i, on the properties of the medium, $m(x)$, makes the problem nonlinear. The problem can be linearized by replacing the curves T_i with straight line segments, L_i, connecting sources and receivers.

In a borehole radar crosshole measurement data on the travel time and the amplitude of the direct wave between transmitter and receiver, i.e. the first arrival, can be extracted. It is assumed that the travel time can be constructed as the line integral of the slowness, $s(x)$, along each ray, i.e.

$$d_i = \int_{L_i} (1/v(x)) \cdot ds = \int_{L_i} s(x) \cdot ds \qquad (3.2)$$

The ray paths have been assumed to be straight lines

in order to make the equations linear and in this way simplify the inversion problem.

The amplitudes can not be obtained from a line integral directly. The logarithm has to be taken of the data in order to linearize the problem and to allow tomographic inversion. The amplitude of the electric field sent out by the transmitter decays with distance according to

$$E = c_t \, a(\theta) \, \exp(-\alpha r)/r \tag{3.3}$$

where $a(\theta)$ is the antenna radiation pattern and c_t some constant which gives a measure of the radiated power. The received signal amplitude is also dependant on the directionality of the receiver antenna gain. The received amplitude is thus obtained by multiplying (3.3) with the directional antenna gain pattern of the receiver antenna. This directional gain is identical to that of the transmitter if the same type of antennas are used. Hence the received amplitude is

$$E_m = c \, \frac{\exp(-\alpha r)}{r} \, a(\theta_1) a(\theta_2) \tag{3.4}$$

Taking the logarithm and rearranging terms we obtain

$$\alpha r = \int_{L_i} \alpha(x) \cdot ds = \ln \frac{c \, a(\theta_1) a(\theta_2)}{r \, E_m} \tag{3.5}$$

Here it has been assumed that the product αr can be constructed as a line integral of the attenuation along each ray. Thus, an inversion of the logarithm of the received amplitudes should give an estimate of the distribution of attenuation in the investigated plane. In equation (3.5) 'c' represents a normalization constant describing the combined effects of transmitted power and receiver gain and 'E_m' is the amplitude of the received electric field.
The next problem is to devise a procedure for inverting the data to obtain the distribution of slowness or attenuation in the plane between the boreholes. First a discretization is made of the problem. The plane between the boreholes is divided into a number of cells and the line integral is calculated as a sum where the contribution from each cell is considered in proportion to the length of the ray within each cell, cf. Figure 3.1. A discretization of (3.1) assuming straight ray paths transforms the equation into the following form

$$d_i = \sum_{j=1}^{M} G_{ij}\, b_j \qquad (3.6)$$

where G_{ij} represents the length of ray 'i' in cell 'j' and b_j the attenuation or slowness of cell 'j'.

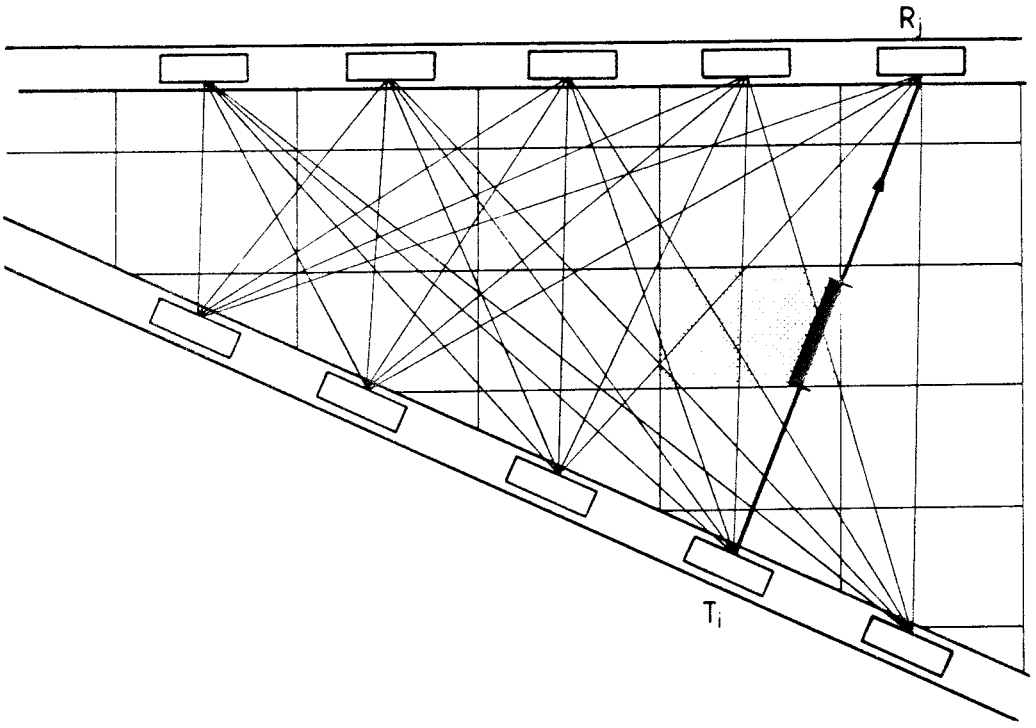

Figure 3.1 Generalized crosshole tomography geometry with a decomposition into cells and an example of a ray pattern.

The problem has now been transformed into a system of linear equations, where the number of equations correspond to the number of rays, N, and the number of unknowns, b_j, to the number of cells, M. Hence, we may write

$$\mathbf{d} = \underline{\mathbf{G}} \cdot \mathbf{b} \qquad (3.7)$$

This equation system can be both overdetermined and underdetermined at the same time and errors in the data may cause some equations to be in conflict. The

most common solution concept for this type of equation is through minimization of the functional $|\mathbf{d}-\underline{\mathbf{G}}\cdot\mathbf{b}|^2$.

Experience shows that the equation system is often unstable and it is necessary to introduce some form of damping. An effective and natural way of introducing damping is to assume that the slowness (or attenuation) of adjacent cells are equal. Introducing equations constraining the solution in this way gives that a minimization should be made of the functional

$$|\mathbf{d} - \underline{\mathbf{G}}\cdot\mathbf{b}|^2 + \lambda^2 \, |\underline{\mathbf{C}}\cdot\mathbf{b}|^2 \qquad (3.8)$$

where the parameter λ is a measure of the strength of the damping and $\underline{\mathbf{C}}$ is a matrix containing the equations for equal slowness (or attenuation) in adjacent cells. λ determines the weight of the constraining equations and the practical consequence is that the differences in slowness between adjacent cells are limited to a certain extent. This type of damping gives a smoothed tomographic image without creating serious artifacts.

The solution to (3.8) has the following form

$$\mathbf{b}=(\underline{\mathbf{G}}^T\cdot\underline{\mathbf{G}}+\lambda^2\cdot\underline{\mathbf{C}}^T\cdot\underline{\mathbf{C}})^{-1}\cdot\underline{\mathbf{G}}^T\cdot\mathbf{d} \qquad (3.9)$$

Here $\underline{\mathbf{G}}$ and $\underline{\mathbf{C}}$ are known and depend on the ray pattern and the division of the investigated area into cells. In other words they contain the geometrical information about the measurement setup. The term in the parenthesis is a square matrix which may be inverted through standard procedures and when this has been done a least squares estimate of $\mathbf{b}$ is obtained through matrix multiplication. However, the direct inversion of the matrix has its practical limitations as the matrix is large. The number of elements of $\underline{\mathbf{G}}^T\cdot\underline{\mathbf{G}}$ is M^2, i.e. the number of cells squared, and this is for most problems a very large number which prohibits direct inversion of the matrix due to the enormous computing times involved. Note that the computing time required for inversion of a matrix is proportional to M^3.

Normally the number of unknowns in the equation system is too large for direct inversion and iterative procedures will have to be used to obtain the solution. The conjugate gradient (CG) method which was developed as a part of the Stripa Project, Phase 2, is considered to be an efficient inversion procedure. The convergence is fast and hence few iterations are needed to arrive at the final solution. The CG-method has been shown to give smaller computing times and better reconstructions of model examples than the other iterative methods (Ivansson, 1984). Hence, the CG-method has been used

for all tomographic inversions presented in this report.

A comprehensive description of the theory behind tomographic inversion and details about the CG-method can be found in Ivansson (1984).

3.2 RESIDUAL ATTENUATION AND VELOCITY

The radar velocity (or slowness) has small variations around a certain average value. We have found it useful to put the crosshole data in such a form that these variations are studied rather than the absolute values of these properties. The concept has also been adopted for the amplitude data. In this context we define the terms 'residual travel time' and 'residual amplitude'. These residual data correspond to the measured data after subtraction of the expected data value which would have been obtained in a homogeneous medium with properties close to those of the investigated rock.

The residual travel time, t_r, is defined as the measured travel time, t_m, minus the estimated travel time for a homogeneous medium with a constant velocity, v_0. The residual travel time then becomes

$$t_r = t_m - r/v_0 \qquad (3.10)$$

where r is the distance between transmitter and receiver.

The residual amplitude is defined as the quotient (expressed in dB) of the received amplitude, E_m, and the estimated amplitude in a homogeneous medium with constant attenuation α_0. The residual amplitude, d_r, thus becomes

$$d_r = -20 \log_{10} \frac{E_0}{E_m} \frac{\exp(-\alpha_0 r)\ a(\theta_1)\ a(\theta_2)}{r} \qquad (3.11)$$

where E_0 represents a reference level corresponding to the ratio of transmitted power to receiver sensitivity. Through the use of the base 10 logarithm and the multiplication by 20, the residual amplitudes become represented in dB.

With this conversion into residual data it is possible to look at small variations from large average values. The residual data are also suitable for detecting systematic errors in the data and can be used for calibration of some system parameters.

3.3 THE EFFECT OF SALINE TRACER ON RADAR WAVE PROPAGATION

A number of theories have been put forth which describe the electric bulk properties of a material based on the properties of the constituent materials. Most commonly rock is considered as a two component mixture where one component is the mineral grains and the other component is the fluid occupying the voids between the grains. The volume fraction occupied by the fluid is defined as the porosity.

An empirical relation for low frequencies (steady state) relating bulk conductivity to pore fluid conductivity and porosity was established by Archie (1942):

$$\sigma_r = a\ \sigma_w \Phi^m \qquad (3.12)$$

where

σ_r = bulk conductivity of the rock
σ_w = pore fluid conductivity
Φ = porosity
m = cementation factor (approximately 1.5)
a = dimensionless parameter (approximately 1)

In low porosity rocks like granite it has been shown that surface conduction along grain boundaries plays a significant role and a surface conduction term should be added to the right hand side of Archies equation above (Brace, Orange, and Madden, 1965, Magnusson, Carlsten, and Olsson, 1987).

$$\sigma = \sigma_s + \sigma_w \Phi^m \qquad (3.13)$$

where

σ_s = surface conductivity

Hence, surface conduction will give a higher bulk conductivity than if conductivity was only attributed to the pore fluid.

An equation describing the bulk electric properties at higher frequencies was derived by Sen, Scala, and Cohen (1981). This equation has been named the Bruggeman-Hanai-Sen equation and reads as follows:

$$\left(\frac{\varepsilon^*_c-\varepsilon^*_m}{e^*_w-\varepsilon^*_m}\right)\left(\frac{\varepsilon^*_w}{\varepsilon^*_c}\right)^L=\Phi \qquad (3.14)$$

where

$\varepsilon^*=\varepsilon_r+i\ \sigma/\omega\varepsilon_0$ = relative complex dielectric constant

ε^*_c=bulk dielectric constant

ε^*_m=matrix dielectric constant

ε^*_w=pore fluid dielectric constant

L=dipolarization constant (1/3 for anisotropic media)

It has been shown that this equation gives Archies law (3.12) in the low frequency limit. There are also a few papers which report good agreement between the BHS formula and electric properties measured on core samples (e.g. Sen, Scala, and Cohen, 1981, Shen, Savre, Price, and Athavale, 1985).

Within this project a study has been made of the fit between electric properties measured on core samples from Stripa and the BHS formula. Data on electrical properties of core samples in the frequency range 25 kHz to 70 MHz have been obtained during previous work at Stripa (Magnusson, Carlsten, and Olsson, 1987, Olsson, Eriksson, Falk, and Sandberg, 1988).

The BHS formula (3.14) is relatively complex and to study the dependance of the bulk property on the properties of the constituents an approximation has been made which is valid in the frequency range of interest and for low porosity values. For small porosity values we can use the following approximation

$$\varepsilon^*_c\approx\varepsilon^*_m+\Phi(\varepsilon^*_w-\varepsilon^*_m)(\varepsilon^*_m/\varepsilon^*_w)^{1/3} \qquad (3.15)$$

of the BHS formula (Sihvola, 1989).

The ratio of the real to the imaginary part, $Q=\varepsilon_0\varepsilon_r\omega/\sigma$, of the complex dielectric constant is an important parameter as it determines whether wave propagation or diffusion effects will dominate in the medium. If $Q\gg1$ then the complex dielectric constant, ε^*, may be approximated with ε_r and if $Q\ll1$ then $\varepsilon^*\approx i\sigma/\omega\varepsilon_0$. In a limited frequency range, which roughly agrees with the range of interest, i.e. from about 10 MHz to 70 MHz we have a situation where the value of Q is greater than

one for the rock matrix while it is less than one for the pore fluid. Hence, we make the following assumptions concerning the complex dielectric constants

$$\varepsilon^*_m \approx \varepsilon_r$$

$$\varepsilon^*_w \approx i\sigma_w/\omega\varepsilon_0$$

If these approximations are inserted in (3.15) we get the following expression for the bulk relative dielectric constant

$$\varepsilon_c = \varepsilon_r + \frac{\Phi\ \varepsilon r^{1/3}\sigma_w^{2/3}}{2\ \varepsilon_0^{2/3}\omega^{2/3}} \qquad (3.16)$$

and the expression for the bulk attenuation becomes

$$\alpha = \frac{\sqrt{3}}{4} Z_0\varepsilon_0^{1/3}\omega^{1/3}\Phi\sigma_w^{2/3}\varepsilon_r^{-1/6} \qquad (3.17)$$

where Z_0 is the free space wave impedance (377 Ω).

If this equation is compared to experimental data we find good agreement. Equations (3.16 and 3.17) predicts the following general characteristics of the bulk properties:

- The bulk dielectric constant will be roughly constant for frequencies above a few MHz and will increase for lower frequencies. Insertion of relevant data into (3.16) yields values in good agreement with data on core samples.

- The radar attenuation is proportional to porosity (i.e. m=1). This is in rough agreement with results from core sample measurements which have given a cementation factor of about 0.7 (Magnusson, Carlsten, and Olsson, 1987).

- The radar attenuation is proportional to frequency raised to the power 1/3. This is in good agreement with core sample data and in situ data which show that attenuation increases with frequency according to $f^{0.38}$. Olsson, Falk, Forslund, Lundmark, and Sandberg (1987) found that the agreement between attenuation data from core samples and in situ measurements was very good.

- Insertion of relevant data into (3.17) gives values of attenuation in good agreement with values obtained from measurements on core

samples and in situ. On the average calculated values are 10-30% lower than measured values.

- The radar attenuation is proportional to the conductivity of the pore fluid raised to the power 2/3 if matrix conductivity is assumed to be zero.

The generally good agreement between equations (3.16 and 3.17) and measured values indicate that the approximate BHS formula is a relevant approximation for predictions of the bulk electric properties for the porosity and frequency range studied in this project.

The last point above warrants a special discussion as it has significant implications for a saline tracer experiment like this one where the natural pore fluid is replaced by a more conductive fluid. At the Crosshole Site the conductivity of the borehole fluid was in the range 20-30 mS/m prior to the injection of saline tracer, while the conductivity of the injected fluid was 520 mS/m, i.e. approximately 20 times higher than the original pore fluid. This corresponds to an expected increase in attenuation by a factor of about 7. Due to the potentially large increase in conductivity and hence radar attenuation the salinity of the injected fluid was kept at a low value.

As shown in Chapter 7 the increase in attenuation caused by the saline tracer was at most 15 % of the background value and from the measurements of saline tracer concentration (Chapter 8) in the boreholes we know that the tracer has passed with little dilution through portions of the rock mass. If we assume the approximate BHS formula (3.16 and 3.17) to be valid this implies that only a small portion of the original pore fluid has been replaced with the injected conductive fluid.

4 PROCESSING OF RADAR DATA FOR TOMOGRAPHIC ANALYSIS

4.1 TRAVEL TIME AND AMPLITUDE PICKING

A typical example of a radar signal recorded from a crosshole measurement is shown in Figure 4.1. From this signal trace we want to obtain the time of first arrival and the magnitude of the signal.

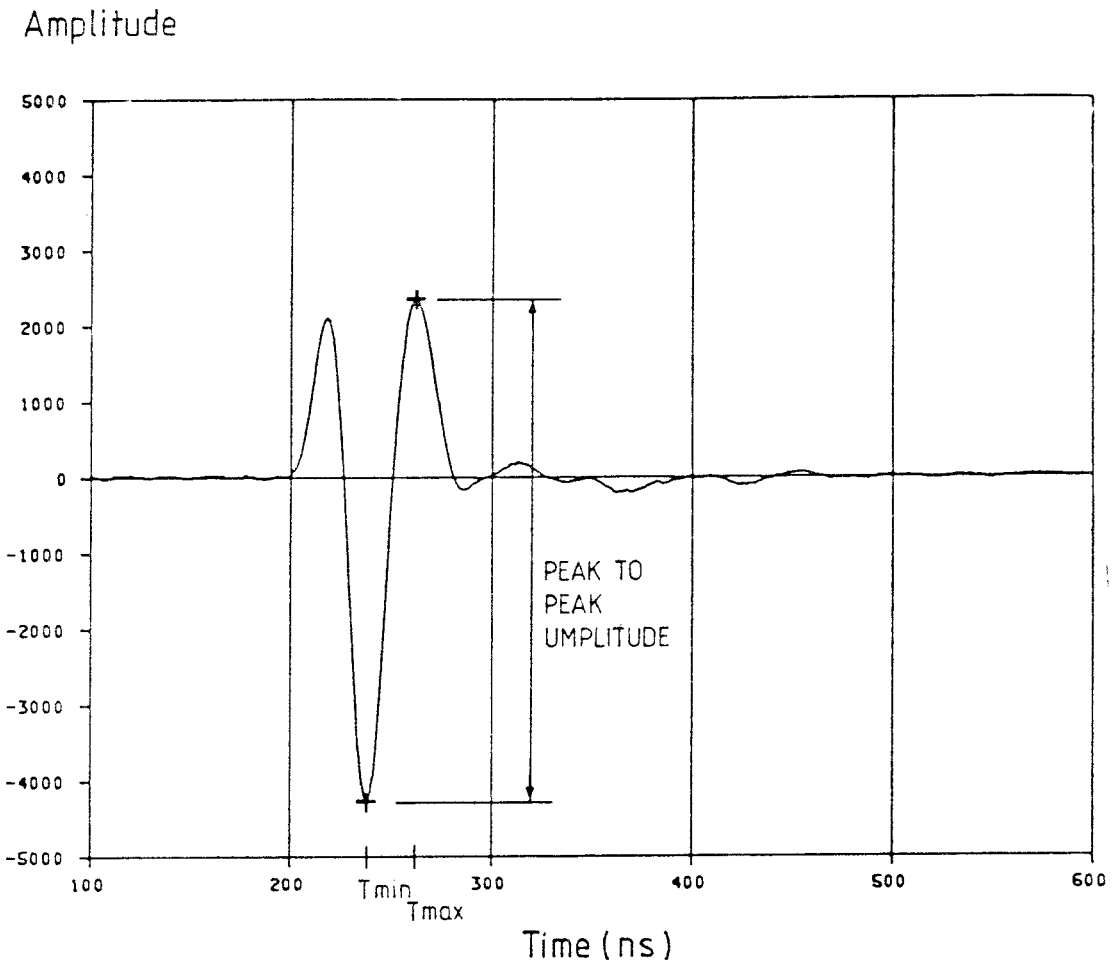

Figure 4.1 Radar signal obtained from a crosshole measurement. The data identified by the automatic routine for extraction of travel times and amplitudes are indicated.

A tomographic survey normally includes a large number of rays (in this case about 15 000 rays). It is therefore of utmost importance to arrive at some automatic procedure which can pick the data from the recorded traces, especially as a manual treatment of each ray would be extremely time consuming and hence costly. For the radar data we have adopted a simple approach which in a number of cases has proven to be reasonably efficient. An algorithm has been devised which picks out the maximum and the minimum for each trace and the time instances at which these events occur. The travel time is then defined as the time to the maximum or minimum of the pulse and the amplitude is defined as the difference between the maximum and the minimum, i.e. peak-to-peak amplitude.

This scheme is useful for radar signals where the first pulse in most cases also is the largest one. The procedure is normally not useful for seismic crosshole investigations as the maximum signal in that case is normally not obtained within the first pulse cycle. The first arrival has one significant maximum and two minima of almost equal magnitude. As there is some dispersion of the pulse the relative magnitude of the two minima will vary somewhat and the minimum time will be picked from either of these two minima. The minimum travel times are thus sensitive to small changes in the pulse form which is not the case for the maximum times. The minimum travel times will normally be picked inconsistently between different rays while the maximum times are picked consistently and have consequently been used for the analysis. The peak-to-peak amplitudes have been shown to provide a satisfactory data set even if they also are affected by the dispersion of the pulse.

4.2 ATTACHMENT OF COORDINATES TO DATA

The basic step in preparing data for tomographic inversion is the attachment of coordinates to the picked travel times and amplitudes. The accuracy required in source and receiver coordinates is of the same order as the propagation distance during a sampling interval. In these measurements the sampling interval corresponds to approximately 0.3 m. Borehole coordinates were measured as a part of the Crosshole Programme.

After the travel time and amplitude data have been combined with the coordinates of the source and receiver points the residual data are calculated according to (3.10) and (3.11).

The tomographic inversion software requires the source and receiver points to be in the X-Z plane and in order

to accomplish this the coordinate system is rotated. In this case the coordinate system is rotated around a point a few metres behind the start of E1. This point is the approximate intersection point of the lines defined by the 7 boreholes at the site. Each tomographic section is rotated individually to make the two boreholes which belong to the section to lie in the X-Z plane.

4.3 DATA QUALITY CHECKS AND CORRECTIONS

The tomographic data is subject to a number of errors such as; errors in time and amplitude picking, quantization errors, constant offset errors in time and gain, and coordinate errors. It is essential to get a grasp of both the stochastic and systematic errors which may exist in the data set. The errors must be understood, quantified and corrected before a tomographic inversion is attempted. A good way to reveal errors is to plot the residual data as a function of the length of the rays. From these plots an offset and a slowness or attenuation correction is determined. A grey scale plot (or ray check plot) is then made of the average slowness or attenuation for all rays. In this plot individual rays containing errors (e.g. due to errors in time and amplitude picking) can be identified. Rays containing errors are then removed from the data set before the tomographic inversion. Below follows a discussion on the most common types of errors included in the data and how they can be corrected for.

The main sources of stochastic errors are noise on the recorded traces and digitization errors. Digitization errors are due to the finite sampling frequency and the limited (16-bit) resolution of the A/D-converter in the receiver. Digitization errors are notable in the travel time data and limits the resolution of the slowness tomograms. Digitization errors and noise affect amplitude data only for traces with very low amplitudes (i.e. the longest rays).

The main errors in the residual travel time are due to imprecise knowledge of the zero time, i.e. the start time of the pulse, and the assumed velocity of the medium. Let us denote the picked travel time by, t_m, where we assumed the pulse to have been sent at a time, t_0. Now, assume there is an error in the start time, Δt_0, and in the velocity used for calculation of the residual travel time. The assumed velocity, v_0, is related to the real velocity, v, in the following way

$$v = v_0 \ (1+\delta v) \qquad (4.1)$$

If these assumptions are inserted in (3.10) we obtain

$$\begin{aligned} t'_r &= t_m - t_0 - \Delta t_0 - r/(v_0(1+\delta v)) \\ &\approx t_m - t_0 - r/v_0 - \Delta t_0 + r\delta v/v_0 \\ &= t_r - \Delta t_0 + r\delta v/v_0 \end{aligned} \qquad (4.2)$$

In this equation we can see t_r as the real residual travel time while t'_r is the residual time including the errors caused by the last two terms. In the case of a homogeneous medium the real data, t_r, would be zero and $t'_r = -\Delta t_0 + r\delta v/v_0$ would be a straight line in a t_r versus r diagram. The offset, $-\Delta t_0$, and the error in the estimated velocity (slope) can directly be read from such a plot.

If we divide equation (4.2) by the length of the ray we get the residual slowness for the ray, s'_r;

$$s'_r = s_r - \Delta t_0/r + \delta v/v_0 \qquad (4.3)$$

Again we let the unprimed quantity define the error free value. Here it is important to note that an error in the assumed velocity will pose no problems as this will only lead to a constant offset in the residual slowness values and the error in the slowness estimate will be the same for all rays. Errors in the pulse transmission time will cause errors in the slowness estimate which are dependant on the length of the rays and hence different for different rays. Offset errors of this type normally generate artifacts in the resulting tomograms. A typical artifact caused by offset errors is a diagonal cross in the tomogram. This is consistent with the different size of error for the longest (i.e. diagonal) rays compared to the shorter ones.

The amplitude data can be analyzed in a similar fashion. Here we assume an average attenuation, α_0, with an error, $\Delta\alpha_0$, such that

$$\alpha = \alpha_0 + \Delta\alpha_0 \qquad (4.4)$$

We also assume that we have a percentage error, δE_0, in the reference level, E'_0, such that

$$E_0 = E'_0 \ \delta E_0 \qquad (4.5)$$

In an analogue fashion to the error analysis of the residual travel times we obtain

$$d'_r = d_r - 20 \log_{10} \delta E_0 + 20\Delta\alpha_0 r/\ln(10) \qquad (4.6)$$

for the residual amplitudes. Again the offset error in the received amplitude levels is the error which will

most severely affect the tomographic inversion as it gives rise to a systematic error which is different for rays of differing lengths.

The corrections to apply can generally be deduced from plots of the residual data as a function of the distance between the source and receiver points. The residual data will in most cases form a cluster centered along a line. The slope of this line will then give the error in the estimated velocity or attenuation and the intersection with the Y-axis (i.e. the value for zero distance) will give the offset error in time or power.

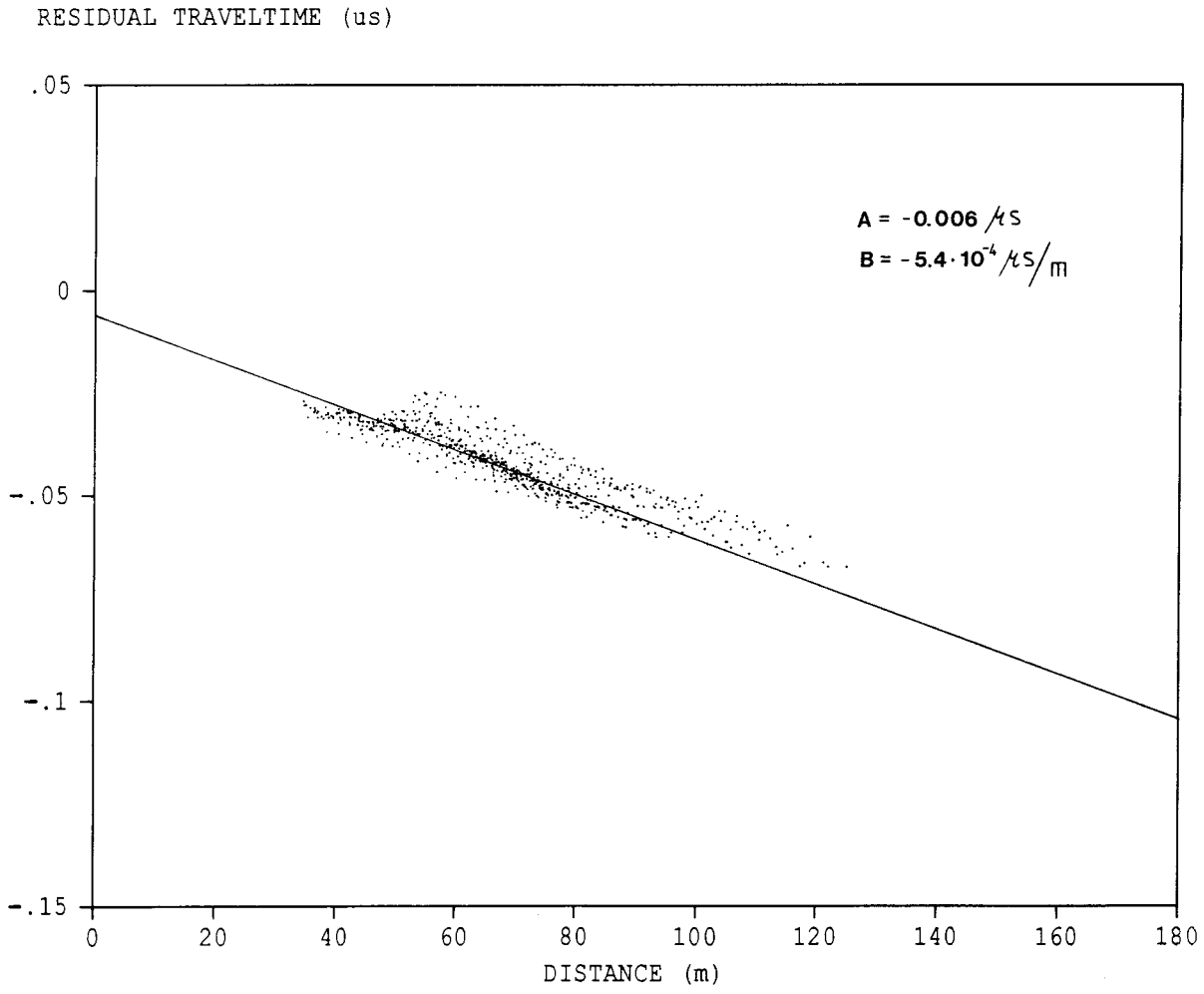

Figure 4.2 Residual travel times as a function of ray length. Data shown are from the borehole section F5F2 measured during Phase 1.

An example of a plot of residual travel times versus distance is given in Figure 4.2. The residual travel times were calculated using an assumed velocity of 120 m/μs. The actual velocity is evidently larger than the assumed value as long rays have shorter residual travel times than longer rays. The travel times form a cluster along a line with a negative slope of $\delta v/v_0$=0.00054 μs/m which gives an actual average velocity of 128 m/μs. From this plot the offset error is estimated to -0.006 ns.

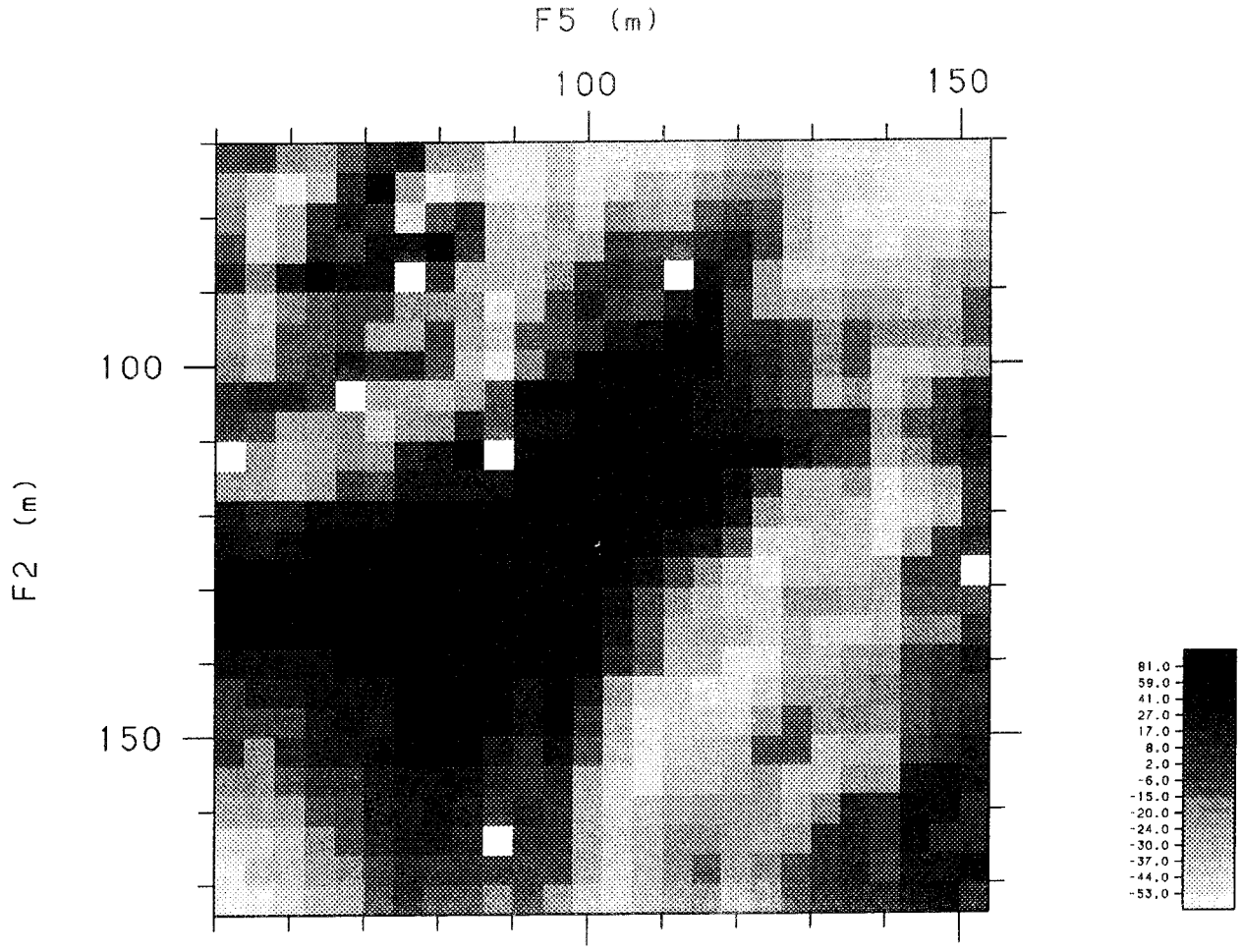

Figure 4.3 Map of residual attenuation for each ray from the boreholes section F5F2. Data are from Phase 1.

There will also be a number of cases where the algorithm for getting the travel time and amplitude data has failed. Such erroneous data have to be identified and removed from the data set. It is normally not cost efficient, but sometimes necessary, to go back to the original recorded traces and to perform a manual retrieval of the travel times and amplitudes. Instead such data is removed from the data set used for tomographic inversion.

In this project we have encountered a considerable amount of removed traveltime and amplitude data from rays with short ray-lengths (transmitter-distances less than 20 m). The short ray-length is causing a saturation of the receiver amplifier resulting in erroneous picking of traveltime and amplitude data. Three sections; F1F2, F2F4, and F4F6 were excluded in the final interpretation due to the large number of excluded rays (>31%) caused by the saturated signals. Two sections; F5F1 and F5F6, had more than 25% of excluded rays but this was due to malfunctioning of the radar system during a few successive survey scans.

Identification of erroneous rays is made by means of ray check plots which display the average slowness or attenuation for each individual ray. Erroneous rays normally have significantly larger or smaller average slowness compared to neighboring rays and stand out as either white or black pixels in the ray check plot. An example of a ray check plot is given in Figure 4.3.

4.4 DIFFERENCE TOMOGRAMS

Difference tomography is based on the principle that there are two nearly identical sets of measurements available and by studying the difference between these two sets we can obtain information on changes in the investigated regions between the two measurements. In this case we have studied changes caused by injection of saline water in borehole F3. The measurements made during Phase 1 serves as a reference measurements to which the Phase 3 measurements are compared. The introduction of a saline tracer into the rock causes an increase in the attenuation of radar waves and difference tomography has been made of amplitude data. As major changes in dielectric constant, and therefore radar wave velocity, were not expected in this case no efforts have been made in using the travel time data for difference tomography. Although, tests were performed in producing difference tomograms, based on traveltime data for a few sections, just confirming the above mentioned assumption of no detectable changes on dielectric constant.

There are two possibilities for making radar difference tomography. One possibility is to construct the difference of the residual amplitudes corrected for any changes in offset levels. The difference data

$$\mathbf{d}_{diff}=\mathbf{d}_2-\mathbf{d}_1 \qquad (4.7)$$

are then used as input to the tomographic inversion algorithm (cf. equation 3.9) which yields an estimate of the changes in attenuation, $\mathbf{b}_{diff}$, between the two measurements. The other possibility is to construct the tomograms from each measurement in order to obtain two attenuation distributions, $\mathbf{b}_1$ and $\mathbf{b}_2$, and then take the difference of these two results to get the distribution of attenuation change

$$\mathbf{b}_{diff}=\mathbf{b}_2-\mathbf{b}_1. \qquad (4.8)$$

The two procedures should in principle give the same result as equation (3.9) is linear. The problem is that the data sets contain errors and these errors are not necessarily the same for the two data sets. Errors will generate artifacts in the tomograms and these are likely to be different for the two data sets.

The details as to how errors propagate through the tomographic inversion procedure are not clear and an analysis is not easy to perform.

Experience from the analysis of the data from the Grimsel Test Site (Niva and Olsson, 1988) showed that better and more stable results were obtained by taking the difference of the amplitudes for each ray according to equation (4.7) followed by a tomographic inversion of the difference data. This procedure was used for all results shown in this report. In this case rays which had been identified as containing errors in either of the two phases were removed before calculation of the difference tomograms.

There were changes in transmitter output power and receiver gain between the different phases which appear as offset errors in the data. The difference in offset between the different phases was estimated from crossplots of the residual amplitudes obtained for each ray in the two phases (Figure 4.4) and from calibration data (cf. Section 2.3.3). Most of the data points fall along a straight line in the figure. This line represents a best fit of the Phase 1 and Phase 3 results for rays not affected by the saline tracer. The lines indicate an offset of 2 dB between the Phase 1 and Phase 3 data.

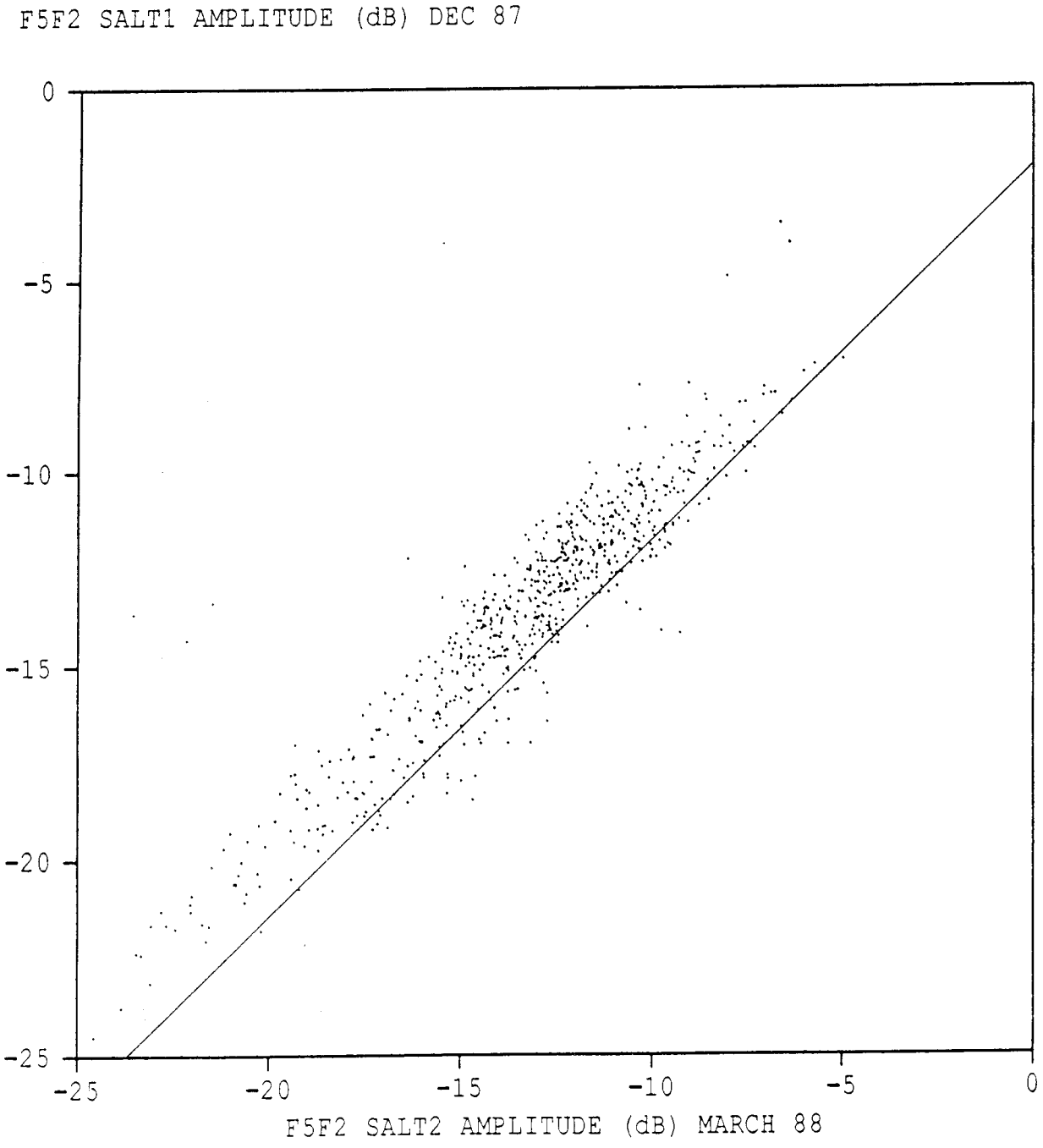

Figure 4.4 Crossplot of residual amplitude of hole to hole rays for the borehole section F5F2 obtained from Phase 1 and Phase 3 measurements.

The data points above the line indicate points where the amplitude is smaller in the Phase 3 data set and points below the line correspond to rays where the amplitude has increased. The spread of the points around the lines give an indication of the errors (noise) in the raw data. The errors can be estimated to approximately ±1 dB. It can be noted that most of the points which do not fall along the line are located above it, i.e. the amplitude is smaller for the Phase 2 data. This indicates that the saline tracer has caused a measurable reduction in amplitude which is larger than the noise in the data.
After the difference for each ray of the residual amplitudes from each phase has been calculated, ray check plots are produced in the same manner as for the ordinary tomographic analysis. As an example the ray check plot corresponding to the data shown in Figure 4.4 is shown in Figure 4.5. An area with higher attenuation is distinguished close to borehole F2 at about 120 metres depth.

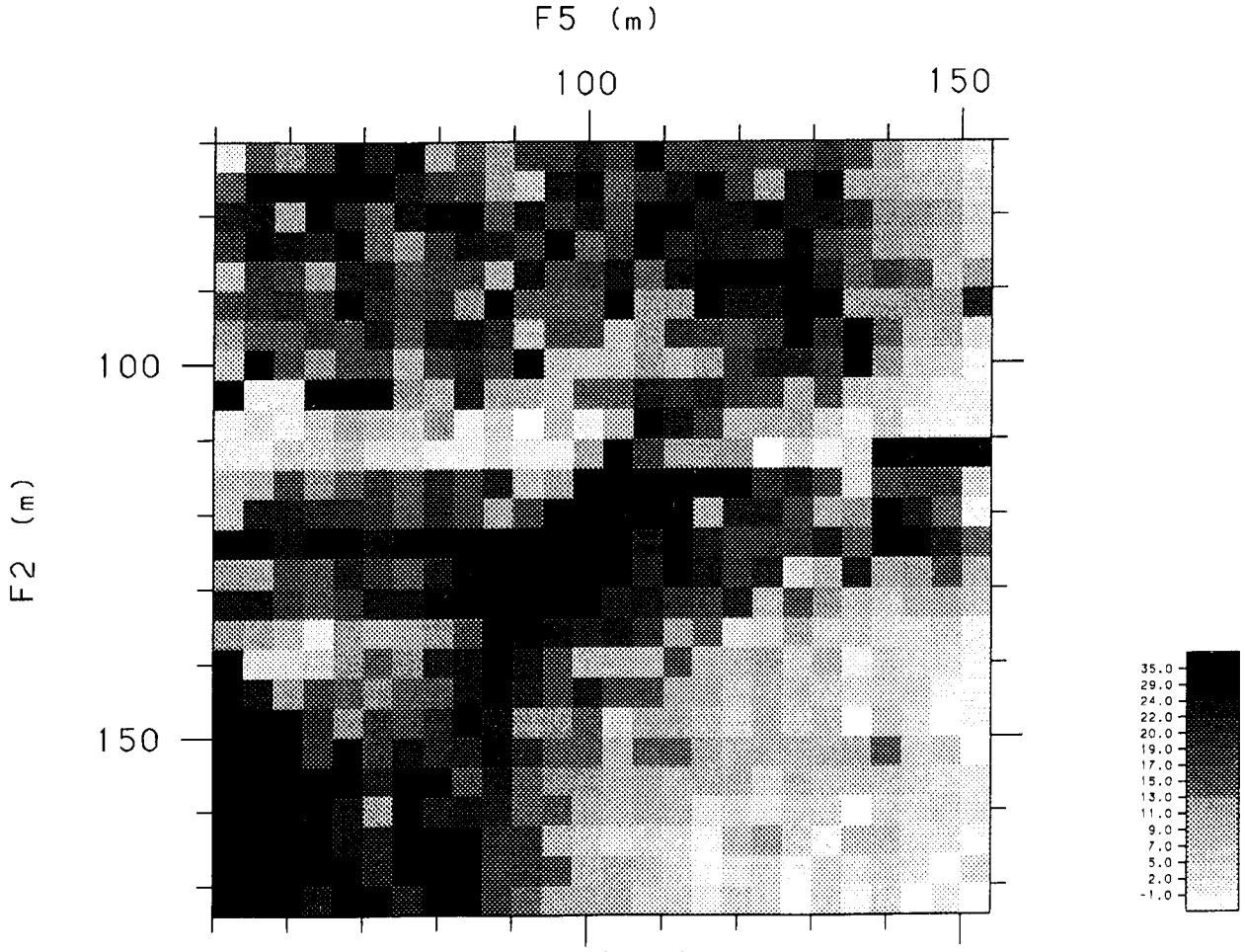

Figure 4.5 Map of attenuation increase for each ray between Phase 1 and Phase 3 measurements of the borehole section F5F2. Borehole to borehole data after offset correction of 1.5 dB.

4.5 TOMOGRAPHIC INVERSION PROCEDURE

Tomographic inversions were performed of the residual travel times and the residual amplitudes after corrections and removal of erroneous rays as described in the previous section. The inversion was made with the Conjugated Gradient (CG) method described by Ivansson (1984).

The inversion was made with rectangular basis functions, i.e. the velocity of each cell is assumed to be constant within that cell. This means that no interpolation is made of the values between adjacent cells. In the tomographic inversion of a data set the following parameters may be varied:

- the cell size
- the number of iterations
- the damping constant (λ).

For this project cell sizes of approximately 3 meter were used. The damping constant is a measure of the length over which the slowness or attenuation is averaged.

The tomographic inversion of the slowness and attenuation data from Phases 1 and 3 was carried out in three steps. The first step consisted of inversion of the data sets where rays assumed to contain errors had been removed manually. The rays to be removed were identified on the ray check plots.

The general strategy of the three step inversion procedure is first to make a tomographic inversion with a large damping constant in order to identify any remaining rays containing errors. The large damping constant will give a smoothed solution and rays inconsistent with this solution will be identified and removed. The criteria for removal of rays has been that the error should be greater than 2 times the RMS-error of all rays compared to the solution obtained by the tomographic inversion. Inversions with a large damping constant are made twice (steps 1 and 2) and erratic rays are successively removed. In the third step a smaller damping constant is used to obtain a high resolution image. The cell size is the same for all three inversions.

The damping constant used during the first two inversions has had a value of 50. Previous experience has shown that it is essential to have a large damping constant during the first inversions in order to assure that the correct rays are removed (Niva and Olsson, 1988). If the damping constant is too small it may well happen that a ray containing a large error will distort the solution with the consequence that rays adjacent to

the erratic one are removed incorrectly. The number of iterations used in all inversions has been 11.

During the inversion of the amplitude difference data some problems were encountered. The salt injected into the rock caused relatively small changes in the radar amplitudes. For several sections the changes were close to the noise level. The small amplitude differences made the tomographic solutions very sensitive to any systematic errors such as shifts in the gain level. This resulted in typical artifacts in the tomograms, such as nearly circular high attenuation anomalies between the boreholes close to the edge of the tomographic section (Figure 4.6). Ivansson, Hammarström, and Pihl (1987) has shown that the conjugated gradient method tends to concentrate errors into regions of low ray density when the number of iterations is large. They also showed that the CG-method converges to the solution given by (3.9), i.e. the correct solution. If the iterative process is interrupted after a small number of iterations the least square solution to (3.8) has not been obtained, but in practice this means that errors are more evenly distributed over the tomographic section.

After studying these results we concluded that accumulation of errors in certain parts of the section must be due to the applied damping procedure. The damping is defined by the matrix $\underline{C}$ which contains equations for equal attenuation or slowness in adjacent cells. In the original algorithm $\underline{C}$ only included equations for adjacent cells along the same row or column (a quadratic cell mesh is used). Hence, no equations constrained the velocities of diagonally located cells. This at times generated anomalies along the cell diagonals, especially when low damping constants were used. In the attempt to improve the tomographic inversion algorithm constraining equations for diagonal cells were added to the matrix $\underline{C}$.

Another feature of the old damping algorithm was that the weight (λ) of all constraining equations was the same. This actually means that the relative damping is less for cells intersected by few rays compared to cells with many rays. A consequence of this is that anomalies appear in parts of the tomograms where there actually is no information to define the location of the anomalies. The most common example are circular type anomalies at the edges of the tomographic sections (Figure 4.6) where essentially only parallel rays are existing. If a region is traversed only by parallel rays it is not possible to define the location of the anomaly and a proper representation of the data should give an anomaly of roughly the equal magnitude along the rays which extends all the way between the boreholes. To accomplish this we introduced a weight on

the constraining equations which was dependant on the ray density in each cell. The weights were defined by the following equation

$$\lambda_j = \frac{\lambda_0}{1 + \rho_j/\rho_0} \tag{4.9}$$

where λ_j is the damping constant for cell j
ρ_j the ray density for cell j
λ_0 a parameter defining the magnitude of the damping
ρ_0 a parameter determining the sensitivity of the damping constant to the ray density.

Several test runs were made with different values for the parameters λ_0 and ρ_0. The best results were obtained with small values for the parameter ρ_0, i.e. a strong dependance on the ray density. For the difference tomograms presented in this report the following values have been used; λ_0=60 m, ρ_0=1. The average ray density for the sections measured at the Crosshole Site has been in the range 25 to 30, this implies that the damping effectively has been inversely proportional to the ray density. The effect of the new way of introducing damping into the tomographic inversion algorithm is demonstrated in Figure 4.7. Compared to the tomogram shown in Figure 4.6 the shape of the anomalies have changed mainly in the regions of low ray density. The anomalies in these parts have become smeared out reflecting the low information content in the data.

We also found that the applied algorithm for removing erratic rays sometimes tended to remove rays not containing errors passing through anomalous regions. Hence, the applied algorithm removed too many rays and this tended to give distorted [illegible] of the tomograms.

The ray density dependent damping algorithm and two step inversion has been used for all difference tomograms. The Phase 1 and phase 3 tomograms were made with old damping algorithm.

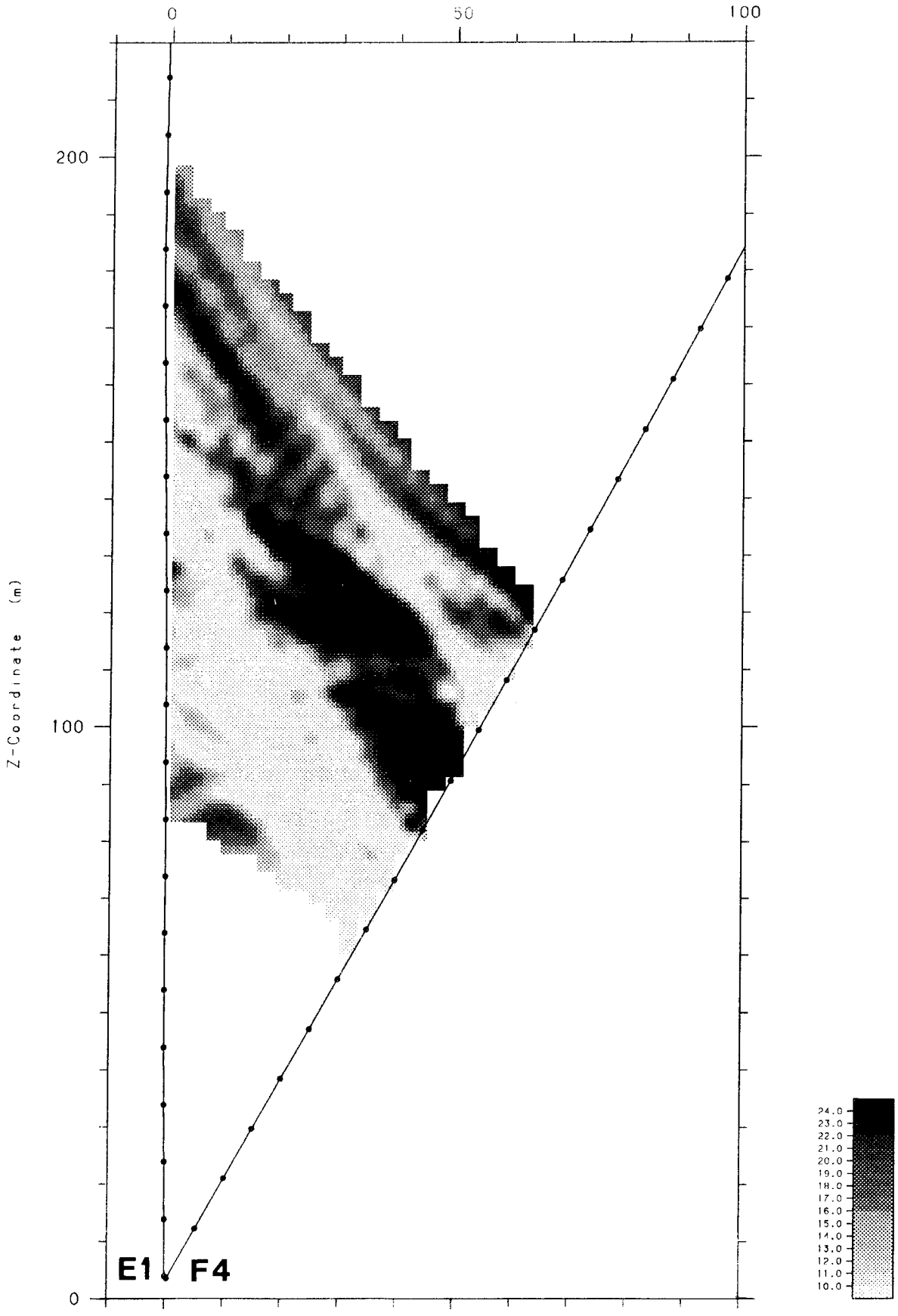

Figure 4.6 Tomographic map of amplitude differences between Phases 3 and 1 for the section E1F4 obtained with the old damping algorithm.

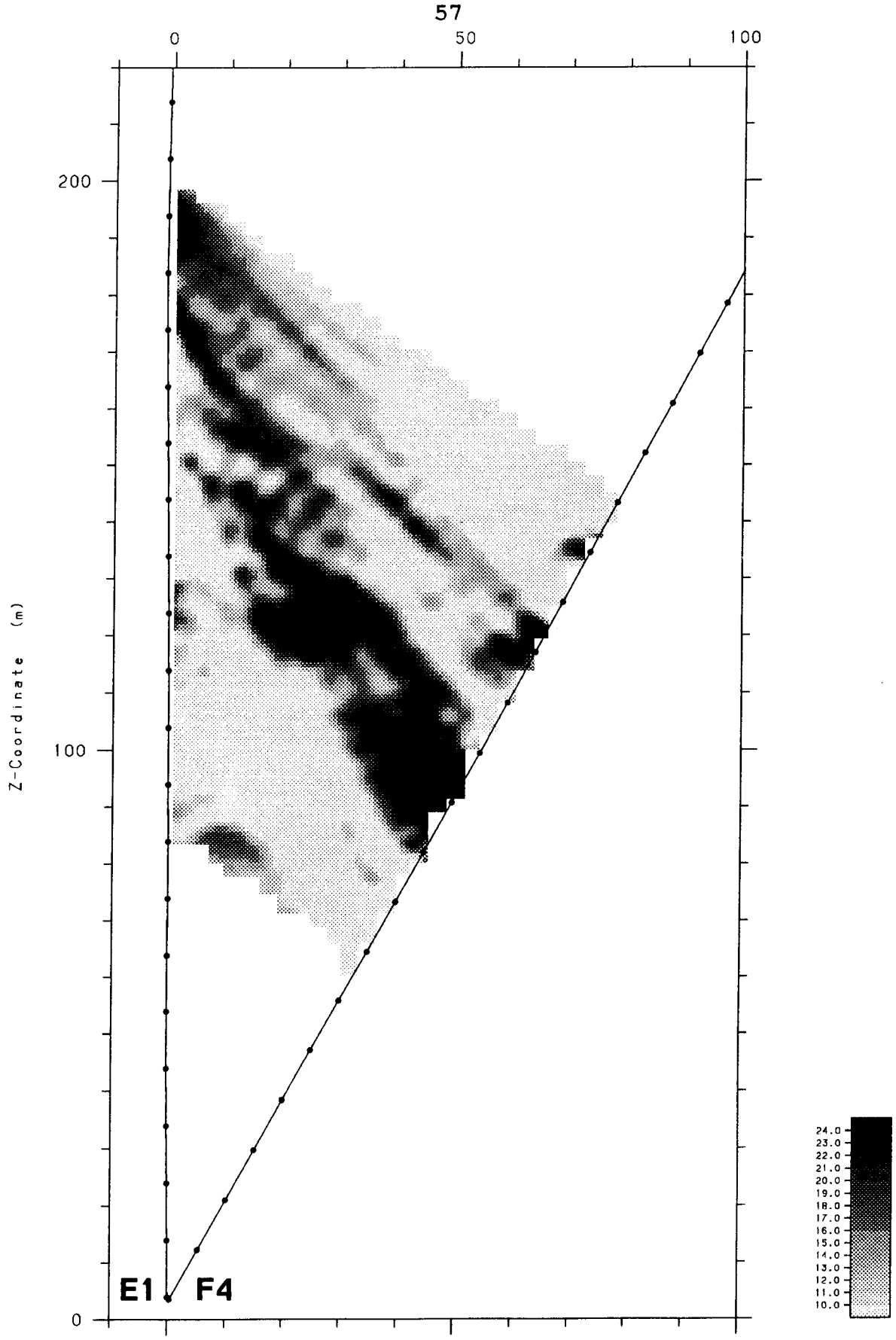

Figure 4.7 Tomographic map of amplitude differences between Phases 3 and 1 for the section E1F4 obtained with a damping approximately inversely proportional to the ray density of each cell.

4.6 RESOLUTION AND SOURCES OF ERROR

Resolution is defined as the ability to define two nearby objects as two separate entities. The resolution in a tomogram is limited by the used wavelength. In this case a wavelength of approximately 3 meter has been used and the theoretically achievable resolution is thus about 1.5 meter. For a tomographic survey the resolution also depends on the ray density, the directional ray coverage for each cell, the damping constant, and the size of the cells. Smaller damping constant and smaller cell size will give better resolution but the tomographic image will become more noisy.

In these surveys quadratic cells with a size of approximately 3 m have been used. The ray density dependant damping constant has been made as small as possible not to make the noise in the tomographic image dominant. The resolution in the central portions of the tomograms, where the ray density is high, is estimated to about 3 m, i.e. equal to the cell size. The resolution in portions of the sections with low ray density is poorer and can be estimated to about 10 meters.

Data errors which affect a tomographic image and how they are corrected for have been discussed in Section 4.3. Noise in the input data will to some extent cause noise in the resulting image. The extent to which noise propagates through the inversion procedure depends on the damping constant. The noise is estimated to approximately 5-10 dB/km for the attenuation tomograms and about 10 ps/m for the slowness tomograms.

The uneven ray distribution and the lack of source and receiver points at parts of the boundary of the tomographic section will generate artifacts. The existence and properties of artifacts in tomograms is a complicated matter which will not be discussed here. The reader is referred to a comprehensive discussion by Ivansson (1984) on this matter.

4.7 CONCLUSIONS AND RECOMMENDATIONS

The procedures adopted for travel time and amplitude picking have been shown to be reasonably efficient. The algorithm used, worked properly except for a small proportion of the rays. The corresponding rays have been identified and removed from the data set. The exclusion of these rays have not had a significant effect on the resulting tomograms. The used procedure is considered satisfactory but other procedures for extracting travel time and amplitude could of course be discussed. The procedure used for checking the data set

and correcting for errors is considered to be reasonably efficient.

The originally used procedure for constraining the tomographic solution, i.e. the damping equations, was found to produce artifacts in the tomograms, especially in regions with low ray density. A new way of introducing damping has been introduced which makes the damping inversely proportional to the ray density in each cell. The ray density dependant damping has been found to give tomograms which better represent the actual information content in the data. It is recommended that this algorithm is used for tomographic work in the future.

It was also found that the originally applied automatic procedure used for removing remaining erratic rays tended to remove too many rays. The number of inversion steps made with the objective to find erratic rays should be reduced to one otherwise the shape of anomalous regions might be distorted. Also, the introduction of additional constraining equations for diagonal cells improved the tomographic images.

5 TRACER TRANSPORT IN CRYSTALLINE ROCK

5.1 PRINCIPLES

Groundwater flow through crystalline rock is mainly governed by the fracture zones. The rate at which radionuclides can migrate through the rock is dependent on the hydraulic properties and the sorption capacity of the matrix and the fracture zones. It is therefore essential to understand the flow distribution within fractures and fracture zones in different scales.

In this project, the main objective is to map the steady-state flow distribution in a fracture zone using the borehole radar, through injection of saline water into the zone from a borehole. In addition, the injection of saline water was used as a conventional tracer experiment. In this section, the principles for the evaluation and interpretation of the tracer migration is described.

5.1.1 Hydraulic conductivity

The most common way to express the hydraulic properties of the bedrock and the fractures is the hydraulic conductivity, K (m/s). The hydraulic conductivity may be determined both from different kinds of hydraulic tests (injection, pumping, interference) and from tracer tests. In this project, the hydraulic conductivity of the injection interval in F3 was determined from the steady-state solution of the general flow equation for a homogeneous and isotropic aquifer (Moye, 1967):

$$K = \frac{Q}{H_o \cdot L} \cdot \frac{1 + \ln(L/2 \cdot r_w)}{2\pi} \qquad (5.1)$$

where Q (m^3/s) is the injection flow rate, H_o (m) is the injection excess head, L (m) is the length of the injection interval and r_w (m) is the borehole radius.

The hydraulic conductivity determined from a tracer test, the equivalent single fracture conductivity, K_{esf} (m/s), can be determined in different ways depending on the assumptions made. The flow pattern may be regarded as radially diverging, linear or as a dipole flow field. In the present evaluation of the test, the radial and the linear flow assumptions were used. The equivalent single fracture conductivity was determined using two different concepts, the volumetric flow and the flow between two smooth parallel plates. The equations for the **radial flow** assumption given

below (Andersson and Klockars, 1985), are both based on Darcy's law:

$$K_{esf}^{t} = \frac{\ln(r/r_w)\cdot(r^2-r_w^2)}{2\cdot t_o\cdot\Delta h} \qquad (5.2)$$

where r (m) is the distance between injection and sampling intervals, t_o (s) is the mean residence time, and Δh (m) is the hydraulic head difference between injection and sampling intervals. Equation (5.2) gives K_{esf} based on the mean transport time, t_o, thus representing the volumetric flow in the fracture. Equation (5.3) is based on the flow into the injection interval, Q, and is given by:

$$K_{esf}^{Q} = \left[\frac{Q\cdot\ln(r/r_w)\cdot\sqrt{g}}{2\pi\cdot\Delta h\cdot\sqrt{12\,\nu}}\right]^{2/3} \qquad (5.3)$$

where g (m/s^2) is the acceleration due to gravity and ν (m^2/s) is the kinematic viscosity of the water.

Equation (5.2) for the **linear flow** assumption can be written:

$$K_{esf}^{t} = \frac{L^2}{t_o\cdot\Delta h} \qquad (5.4)$$

5.1.2 Equivalent fracture aperture

The equivalent single fracture aperture, e_{esf} (m), can be determined by using equation (5.5) (Snow, 1968) for laminar flow between two smooth parallel plates and inserting the different values of K_{esf} determined from equations (5.2-5.4). The different fracture apertures will be denoted by e_{esf}^{t} and e_{esf}^{Q}, respectively.

$$e_{esf}^{t,Q} = \left[\frac{K_{esf}\cdot 12\,\nu}{g}\right]^{1/2} \qquad (5.5)$$

The equivalent single fracture aperture is not an actual geometric property as the fracture aperture may vary considerably across a fracture plane. Furthermore, the transport in a fracture zone as Zone C involves several fractures with different fracture apertures implying the use of the term **equivalent** fracture aperture.

Another way to calculate the equivalent fracture aperture is to divide the volume of the fracture by the area of the fracture plane. This is called the

mass balance fracture aperture and is here denoted e_m (m).

$$e_m = \frac{Q \cdot t_o}{\pi \cdot (r^2 - r_w^2)} \qquad (5.6)$$

5.1.3 Dispersion

The spreading in time and space of a water soluble substance which is transported with the groundwater is called dispersion. The dispersion is dependent upon two factors; the velocity distribution in the medium and the molecular diffusion. However, in most cases the molecular diffusion can be neglected.

The portion of the dispersion that is dependent upon the velocity distribution in the fracture system is commonly termed mechanical dispersion and is given by the general dispersion equation for one-dimensional flow of non-reactive substances:

$$\frac{\delta C}{\delta t} = D_l \cdot \frac{\delta^2 C}{\delta x^2} - v \cdot \frac{\delta C}{\delta x} \qquad (5.7)$$

where D_l (m^2/s) is the longitudinal dispersion coefficient and v (m/s) is the average transport velocity of the groundwater in the x-direction.

In the case of continuous injection with constant flow and tracer concentration C_o, Equation (5.7) has the following solution (Ogata and Banks, 1961):

$$\frac{C}{C_o} = \frac{1}{2} \cdot \left[\operatorname{erfc} \frac{1 - t/t_o}{2\sqrt{n \cdot t/t_o}} + e^{1/n} \cdot \operatorname{erfc} \frac{1 + t/t_o}{2\sqrt{n \cdot t/t_o}} \right] \qquad (5.8)$$

where $n = D_l / v \cdot x$ is the dimensionless dispersion parameter which more commonly is expressed as the Peclet Number, Pe = 1/n. Equation (5.8) is valid only for purely mechanical dispersion where n can be assumed to be constant and molecular diffusion can be neglected (Zuber, 1974)

5.1.4 Mass balance and recovery

The recovery ratio of a tracer is a very important parameter to determine in a tracer experiment. The recovery can be regarded as a measure of the degree of control of the experiment. Low recoveries implies that there is little control of where the tracer has been transported or that the tracer has been sorbed or chemically decomposed in the groundwater. Hence, in order to determine the recovery, mass balance calculations have to be made.

The mass balance calculations were performed with two different objectives;

1) to determine the flow distribution in the sampling boreholes resulting from the injection, and

2) to determine the total recovery of tracer.

The flow distribution was determined as the mass recovery, R_f, per time unit in each borehole:

$$R_f = \frac{q \cdot C_s}{Q \cdot C_o} \qquad (5.9)$$

where q and C_s are the inflow rate and the concentration of tracer at steady-state in the sampling borehole, respectively, and Q and C_o are the injection flow rate and the initial concentration in the injection interval, respectively.

The total recovery, R, was determined by integrating the breakthrough curves and calculating the total recovered mass including the tracer left in the boreholes at the end of injection. However in boreholes F4 and F6 only estimates based on measurement with the electrical conductivity probe and hydraulic data (Black, Holmes, and Brightman, 1987) could be made.

Mass balance calculations were also made based on the electrical conductivity logging versus depth (Phase 4) in order to determine the flow distribution within the sampling boreholes.

5.1.5 Flow porosity

The porosity of the rock can be represented by the formula (Norton and Knapp, 1977):

$$\Phi_T = \Phi_k + \Phi_d + \Phi_r \qquad (5.10)$$

where Φ_T (dimensionless) is the total porosity, Φ_k the flow porosity, Φ_d the diffusion porosity and Φ_r is the residual porosity.

The total porosity includes all fracture openings and pores within the rock mass. However, the property of interest for the groundwater transport is the flow porosity or kinematic porosity. There are also discontinuous fractures or fractures of such small width that the water cannot move under the prevailing hydraulic conditions. These fractures, where the transport of aqueous components is governed by diffusion, makes up the diffusion porosity. The last term of equation (5.10), the residual porosity includes all remaining pore volumes and makes up more than 90 % of the total porosity (Norton and Knapp, 1977).

The flow porosity, Φ_k can be calculated as the ratio between the volume of moving water in the rock mass and the total volume of the rock mass providing Darcy's law is valid and that the gradient in the rock mass is equally large as the gradient in the fractures.

$$\Phi_k = \frac{Q \cdot t_o}{\pi \cdot r^2 \cdot L} \qquad (5.11)$$

where t_o (s) is the mean residence time for the groundwater to move a distance r (m) from the injection point.

The values calculated from equation (5.11) are dependent on the length of the injection interval. This is essential to have in mind when comparing different porosity values.

5.2 PROCESSING OF MEASURED DATA

The measured data during the injection of saline tracer as described in section 2.4 were:

1. Inflow rate and electrical conductivity in packed-off highly conductive intervals of the 6 sampling boreholes.

2. Total inflow rate and electrical conductivity in the boreholes drained to the instrument drift, E1, F1, F2, and F5.

3. Bromide concentration of samples taken in the packed-off intervals and in the water drained to the instrument drift from boreholes E1, F1, F2, and F5.

4. Electrical conductivity logs of boreholes with low and diffuse inflows, F1, F4, and F6.

5. Electrical conductivity logs versus depth in all 6 boreholes at the end of the injection (Phase 4).

6. Injection flow rate and pressure in the injection interval in borehole F3.

The electrical conductivity was measured with 3 different probes as described in section 2.4.2. The fixed probe used to measure the samples taken for Bromide analysis, was used as reference. This probe was calibrated at the SGAB Laboratory prior to the experiment. The two borehole probes used for conductivity logging were calibrated against the fixed probe and the measured data were corrected. The movable probe used for Phase 4 was a 2-electrode type with a manual temperature compensation control. During the measurements the temperature compensation was fixed, implying a small positive drift of the electrical conductivity versus depth due to increasing temperature versus depth. However, the temperature increase versus depth was only in the order of 0.5 - 1°C/100 m thus making the corrections very small. Nevertheless, all the data were corrected for the temperature drift.

The electrical conductivity data were also used in the mass balance calculations of the saline tracer. Corrections were then made also for the background level (25-30 mS/m).

6 RADAR RESULTS FROM THE REFERENCE MEASUREMENT

6.1 TOMOGRAMS

The radar measurements, performed after tracer injection, have been processed following the procedures described in Chapter 4 to yield the slowness tomograms shown in Appendix 3 and the attenuation tomograms in Appendix 4. These measurements were originally processed with the tomographic inversion algorithm which did not include a ray density dependant damping. Following the development of the new inversion algorithm the data were reprocessed. The reference values (0-level) used for the residual slowness and amplitude data were 127.8 m/μs and 0.415 dB/m, respectively.

A few borehole sections, namely F1-F2, F2-F4, and F4-F6, contained a large portion of short rays. For these rays very high signal amplitudes were obtained which caused saturation of the receiver. Both travel time and amplitude data for these rays were in error and the corresponding rays were consequently excluded from the data set. Hence, these sections where a significant portion of the rays have been removed contain artifacts and should be given less weight in the interpretation.

6.2 RADAR REFLECTION RESULTS

Single hole reflection measurements were made in all boreholes, except F3, with a centre frequency of 60 MHz. Deconvolved reflection reflectograms from the boreholes are shown in Appendix 1. The obtained range is approximately 50 m and clear reflections are observed from the fracture zones. The drift passing across the site at a borehole length of about 170 m is also clearly seen.

6.3 GEOPHYSICAL INTERPRETATION

The Crosshole Site was thoroughly investigated as a part of the Crosshole Programme carried out within the framework of the International Stripa Project. A combined analysis was made of both radar, seismic, hydraulic, and geological data and the results are presented by Olsson, Falk, Forslund, Lundmark, and Sandberg (1987) and Olsson, Black, Cosma, and Pihl (1987).

A number of fracture zones were found to intersect the site. These zones had an extension at least comparable to the dimensions of the site, i.e. about 200 m, and were considered to be roughly planar. The fracture

zones were divided into two sets; a "basic model" which contained the largest zones and an "extended model" which also included some minor zones. The zones could also be divided into two groups based on their orientation: one with a northeasterly strike dipping about 70^{o} to northwest and one with a northerly strike dipping about 70^{o} towards east. The zones contained in the "basic" model are shown in Figure 2.2 where it can be seen that zone 'C' belongs to the northeast striking set and zone 'A' to the set with a northerly strike.

The radar tomograms and reflectograms generated within this project are in very good agreement with the results obtained from the measurements made during the Crosshole programme. This implies that the new data, and hence also the interpretation, is in agreement with the previous interpretation which is summarized above and in Chapter 2. For a detailed description please refer to Olsson, Black, Cosma, and Pihl (1987).

In this experiment we have concentrated the investigations on zone 'C' and some additional characteristics on this zone may be noted. The data from eight of the eleven tomographic sections have been used to create maps of the variation of residual slowness and attenuation in the plane of zone 'C'. From the tomograms information on the properties of zone 'C' is obtained along the lines indicated in Figure 2.3. Data along these lines have been put into an interpolation routine to generate a map of the properties in the plane of zone 'C'. The resulting residual attenuation and slowness maps are shown in Figures 6.1 and 6.2, respectively. We can note an area of increased attenuation and slowness close to borehole F1. High attenuation values are also observed in the vicinity of F2 while the region of increased slowness extends from F1 towards F4 and F6.

Figures 6.1 and 6.2 show the variation in properties of zone 'C' as defined by the tomographic data obtained along the lines shown in Figure 2.3. However, the tomograms also indicate that zone 'C' has variations in thickness. The boundaries of zone 'C' as defined by the tomographic sections have been used as input data to a three-dimensional CAD-system (Intergraph Engineering Modelling System) to generate images showing the three-dimensional extent of zone 'C'. Two perspective views of zone 'C' are shown in Figure 6.3, one from above and one from below. The total set of seven CAD-generated views, showing the mapped Zone C model are presented in Appendix 7.1.

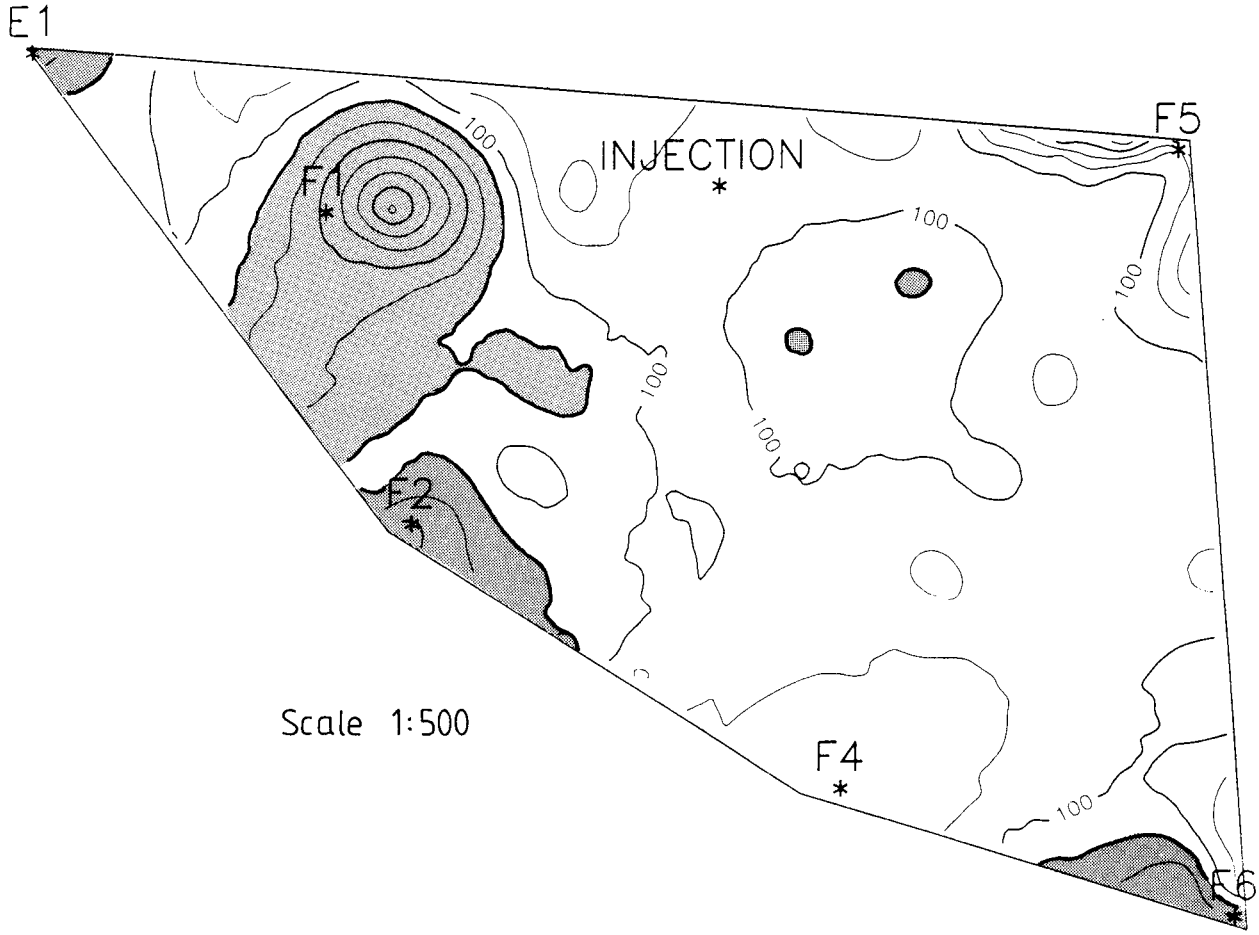

Figure 6.1 Residual attenuation (dB/km) in the plane of zone 'C' obtained from the reference measurement. Distance between the iso-lines are 50 dB/km.

The large width of zone 'C' close to borehole E1 is caused by the splitting of zone 'C' into two parts. The separation into two parts was discovered already during the Crosshole Programme (Olsson, Black, Cosma, and Pihl, 1987) and the parts were identified as zones 'C1' and 'C2'. It is also evident that the fracture zone has a rough surface and that there are significant variations in thickness.

The large width of zone 'C' between borehole F2 and F6 in the view from below is an artifact caused by linear interpolation between tomographic sections and truncation.

In the reflection data from most of the boreholes a dislocation of zone 'C' can be observed. The dislocations occur at relatively large distances from the boreholes and are only observed in the 22 MHz reflection measurements collected during the Crosshole

Programme due to their larger range compared to the 60 MHz data collected during this experiment. By combining the reflection data from all measurements the location of the fault can be determined. The line of dislocation in the plane of zone 'C' is shown in Figure 2.3. The line is found to be nearly parallel to the F4-F5 plane. The magnitude of the displacement is estimated to a couple of metres where the northern part (where all holes except F6 intersect) is closer to the site from where the boreholes have been drilled. The dislocation most likely corresponds to a fault which extends in a direction nearly parallel to boreholes F4 and F5. A zone parallel to the boreholes is not likely to be observed in the tomograms and this is the reason the fault is not observed in the F4-F6 and F5-F6 tomographic sections which it intersects. However, indications of the fault can be seen in the reflection data from F4 and F5 where a discontinuous reflector nearly parallel to the boreholes can be observed at distances of 10-20 m from the boreholes.

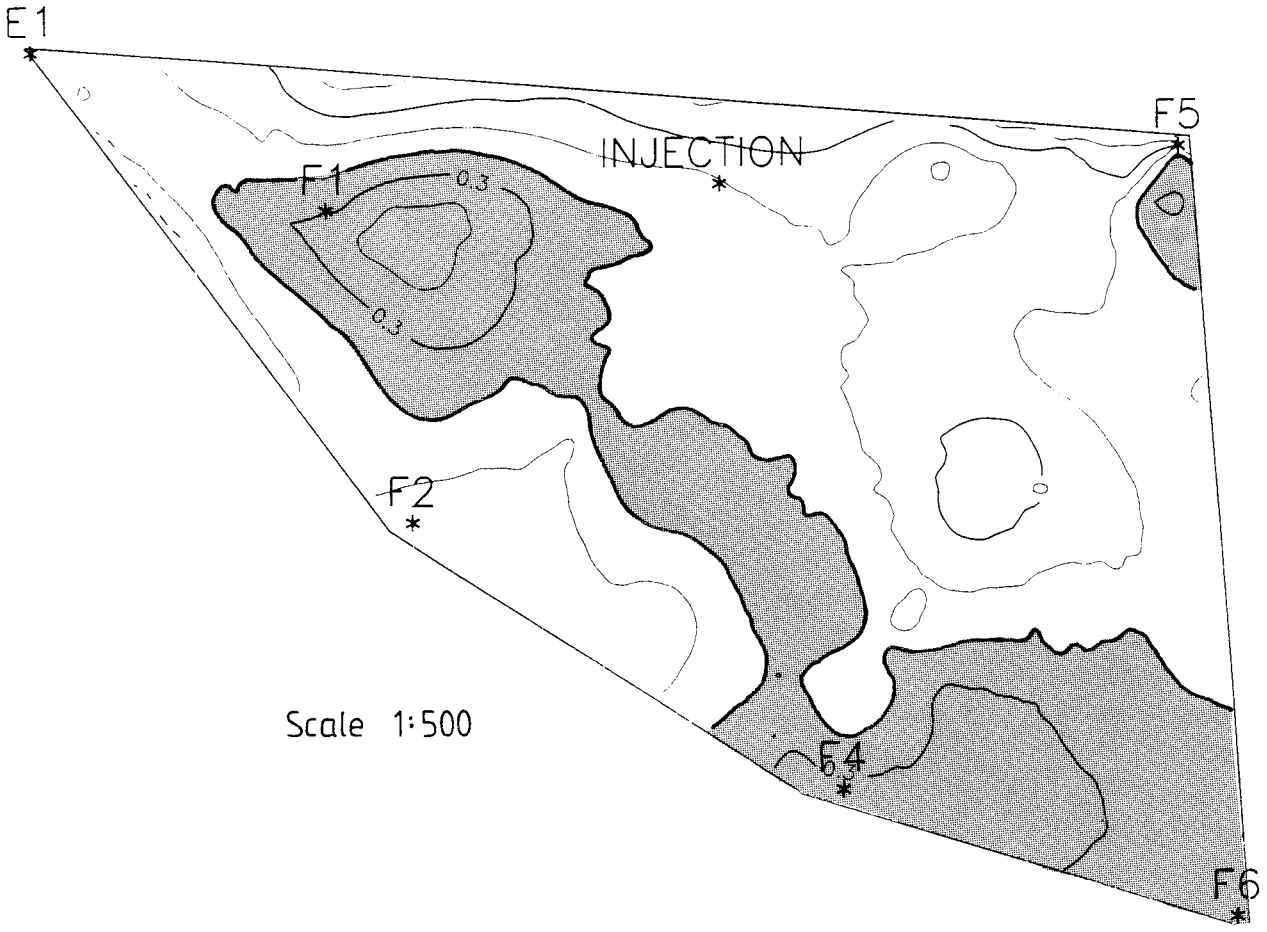

Figure 6.2 Residual slowness (ns/m) in the plane of zone 'C' obtained from the reference measurement. The distance between the iso-lines are 0.1 ns/m.

It should be noted that the different orientations of 'C' and 'A' will make these zones intersect along a line extending below the site (cf. Figure 2.2).

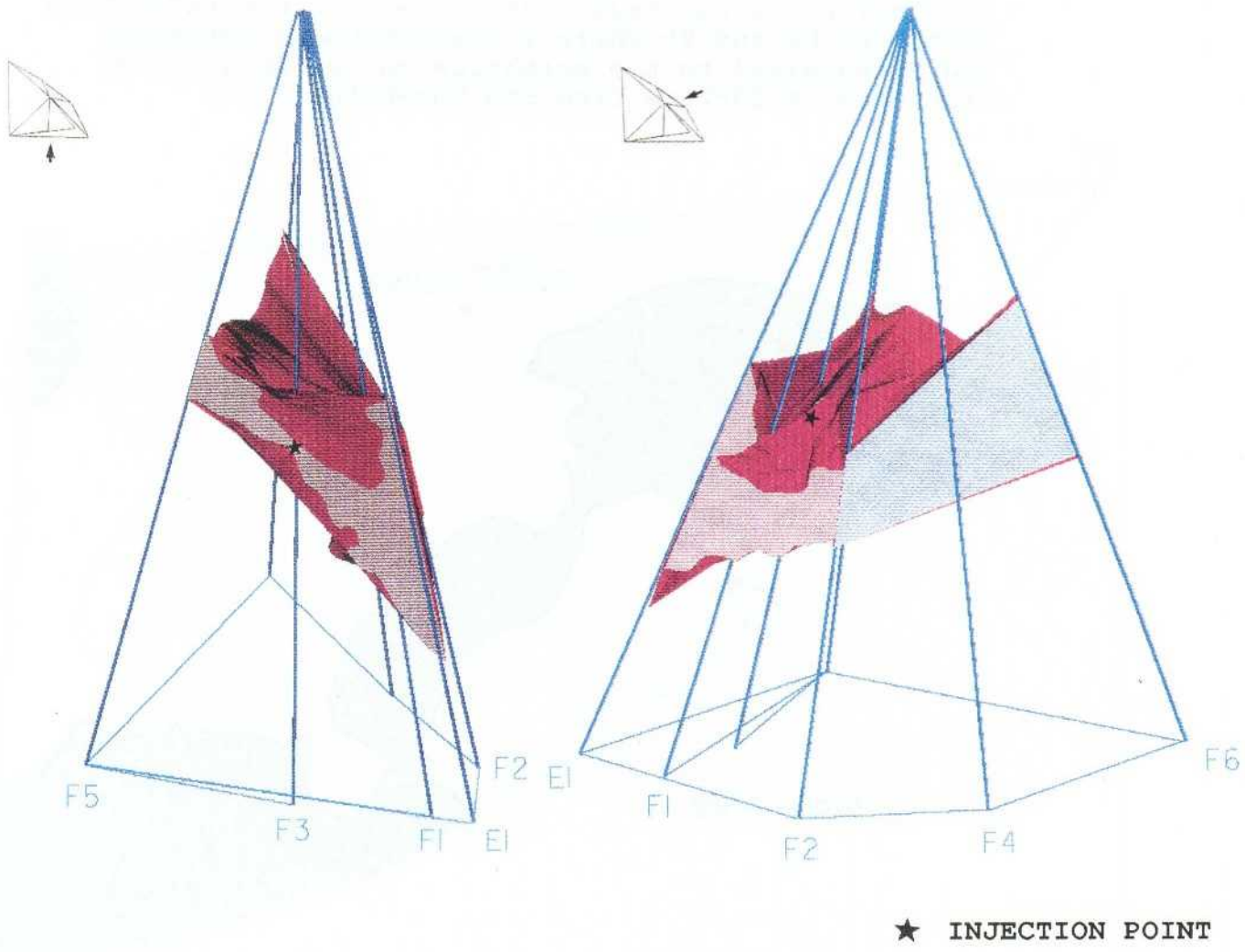

Figure 6.3 Perspective view of zone 'C' where the Crosshole site is viewed from above and below, respectively.

7 RADAR RESPONSES DUE TO SALINE TRACER

7.1 DIFFERENCE TOMOGRAMS

This project is based on the principle that the difference between two essentially identical sets of radar data will give information on changes in the investigated volume between the two separate measurements. In this project changes are caused by injection of saline water which cause an increase in radar wave attenuation.

The difference tomograms are produced by taking the difference of the residual amplitudes after correction for changes in offset levels. The difference data are then used as input to the tomographic inversion algorithm which gives an estimate of the changes in attenuation between the two measurements.

During the tomographic processing of the residual attenuation data some problems were encountered. The injected salt tracer caused relatively small changes in the radar amplitudes. For several sections the changes were close to the noise level and hence very sensitive to systematic errors such as shifts in the gain level which caused offset errors in the data. The difference in offset between the two phases was estimated to 2 dB. The offset was determined from crossplots of residual amplitudes from the two phases and from calibration data. The random errors (noise) in the radar data was estimated to approximately ±1 dB (cf. Section 4.4).

Generation of the difference tomograms comprised an iterative, and hence time-consuming, procedure which included offset corrections and removal of erroneous rays. The relevance and presence of artifacts was checked by comparing tomograms from adjacent sections and tomograms intersecting along a line.

It was found necessary to modify the tomographic algorithm which resulted in significant improvement on the results (cf. Section 4.5).

The cell-size used in the tomographic inversion was approximately 3 x 3 metres. The tomographic inversion of the difference data was carried out with two inversions (11 iterations each) using damping constants of 60 and 5, respectively (cf. Section 4.5).

Figures 7.1 and 7.2 show two difference tomograms where the attenuation increase caused by the saline tracer appear as regions of darker colour. These two tomograms are examples of obtained results. The complete set, which consists of 11 difference tomograms

combined with tracer injection data, are presented in Appendix 5.

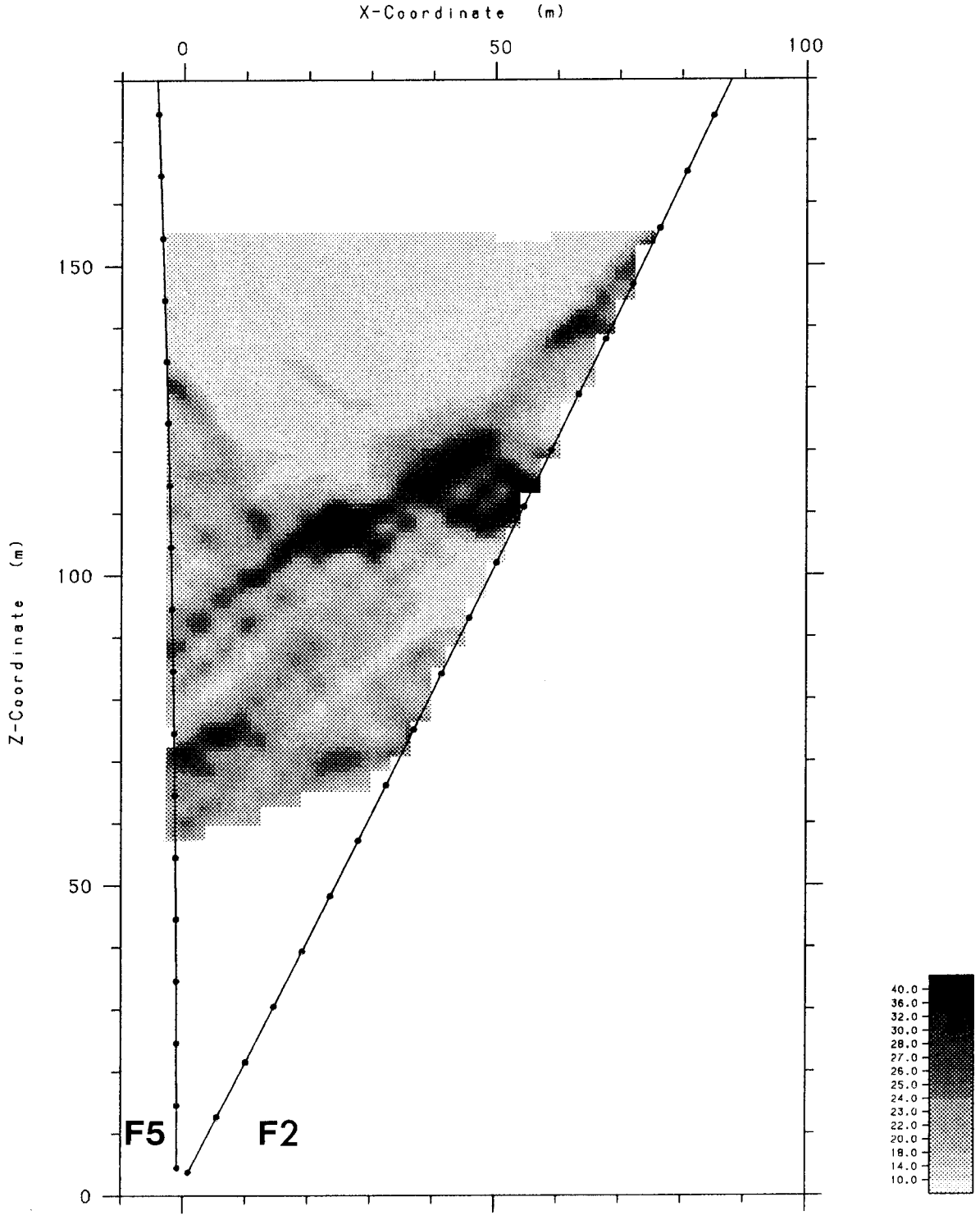

Figure 7.1 Difference tomogram for section F5F2 showing residual attenuation (dB/km) in the rock formation, due to injection of saline tracer.

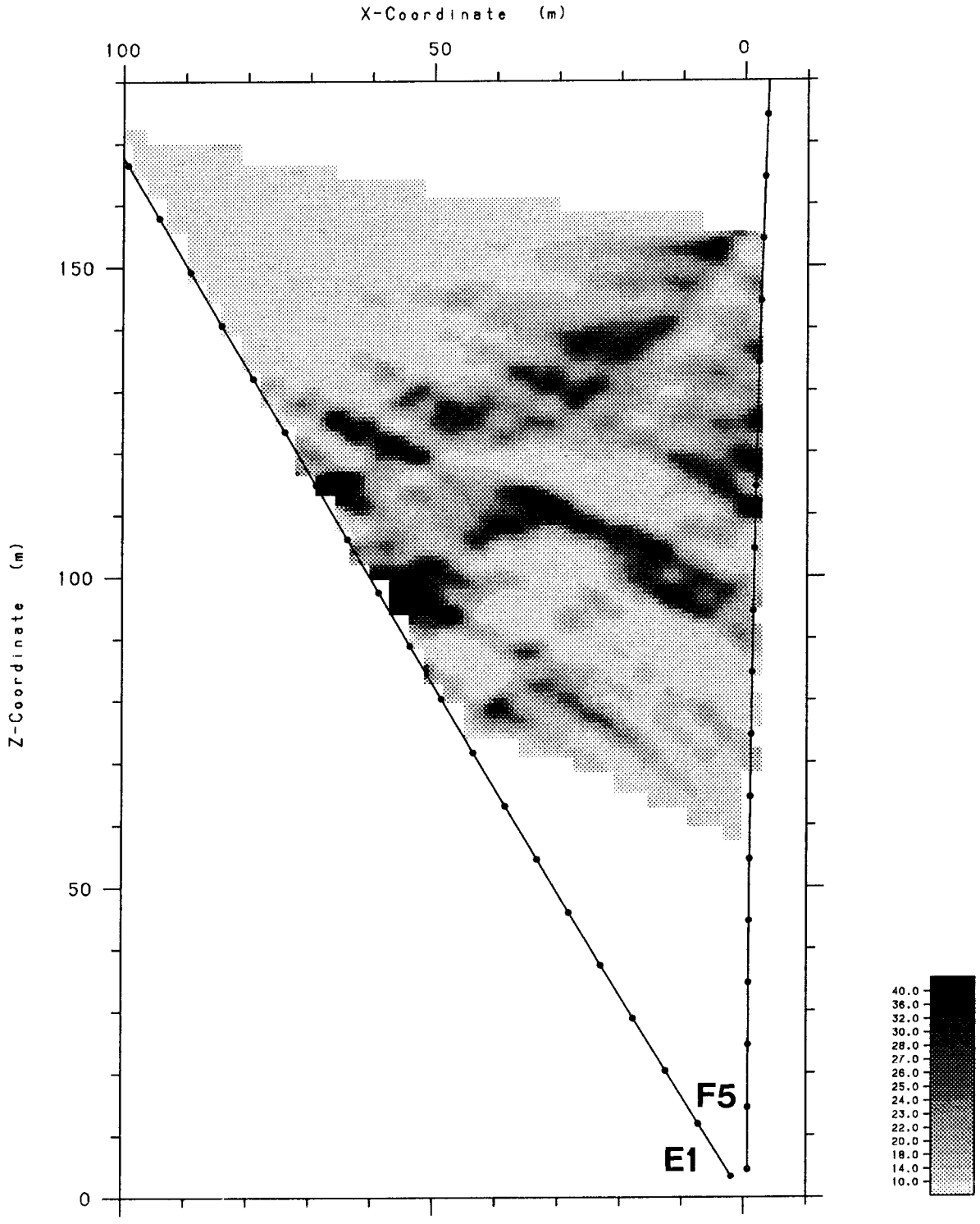

Figure 7.2 Difference tomogram for section F5E1 showing residual attenuation (dB/km) in the rock formation, due to injection of saline tracer.

As can be seen in Figures 7.1 and 7.2 the tomograms show well-defined areas/regions of increased attenuation caused by the injected saline tracer. The identified areas with increased attenuation can also, in many cases, be observed and followed in bisecting and adjacent tomographic sections.

7.2 DIFFERENTIAL RADAR REFLECTOGRAMS

In the early stages of this project it was anticipated that differential radar reflectograms would reveal qualitative as well as quantitative information on changes caused by the saline tracer.

On subtracting the radar singlehole reflection data, measured during and before the salt injection, serious problems were encountered. Originally a subtraction was made on a sample by sample basis. This made the results very sensitive to timing instabilities and position differences between the two measurements. To reduce the sensitivity to timing instability a low frequency signal was created by calculating the envelope of the traces. The difference of the envelopes were then calculated. This resulted in considerable improvement of the difference reflectograms as shown in Appendix 2. Figures 7.3 and 7.4 are included here to exemplify the results which show the residual changes caused by the saline tracer.

As can be seen in Figures 7.3, 7.4 and in Appendix 2, the differential radar reflectograms generally contain little useful information, which was a negative finding. The most distinct features in all difference reflectograms is the responses from saline-filled boreholes and the injection pipe in borehole F3. Also, the adjacent drift located in the inner part of the investigated rock formation is clearly visible in the differential plots, which probably is caused by saline tracer in the vicinity of the drift, transported from the injection point. Another cause, for seeing the drift, can be seasonal variations in the groundwater flow in the surroundings of the drift.

In some boreholes there are indications of increased reflectivity from some of the fracture zones. The information obtained from the difference reflectograms indicate tracer migration in Zone C mainly in the vicinity of boreholes E1, F1 and F2. In the neighborhood of boreholes F4, F5 and F6 no, or hardly any, evidence of tracer migration could be detected in the difference reflectograms.

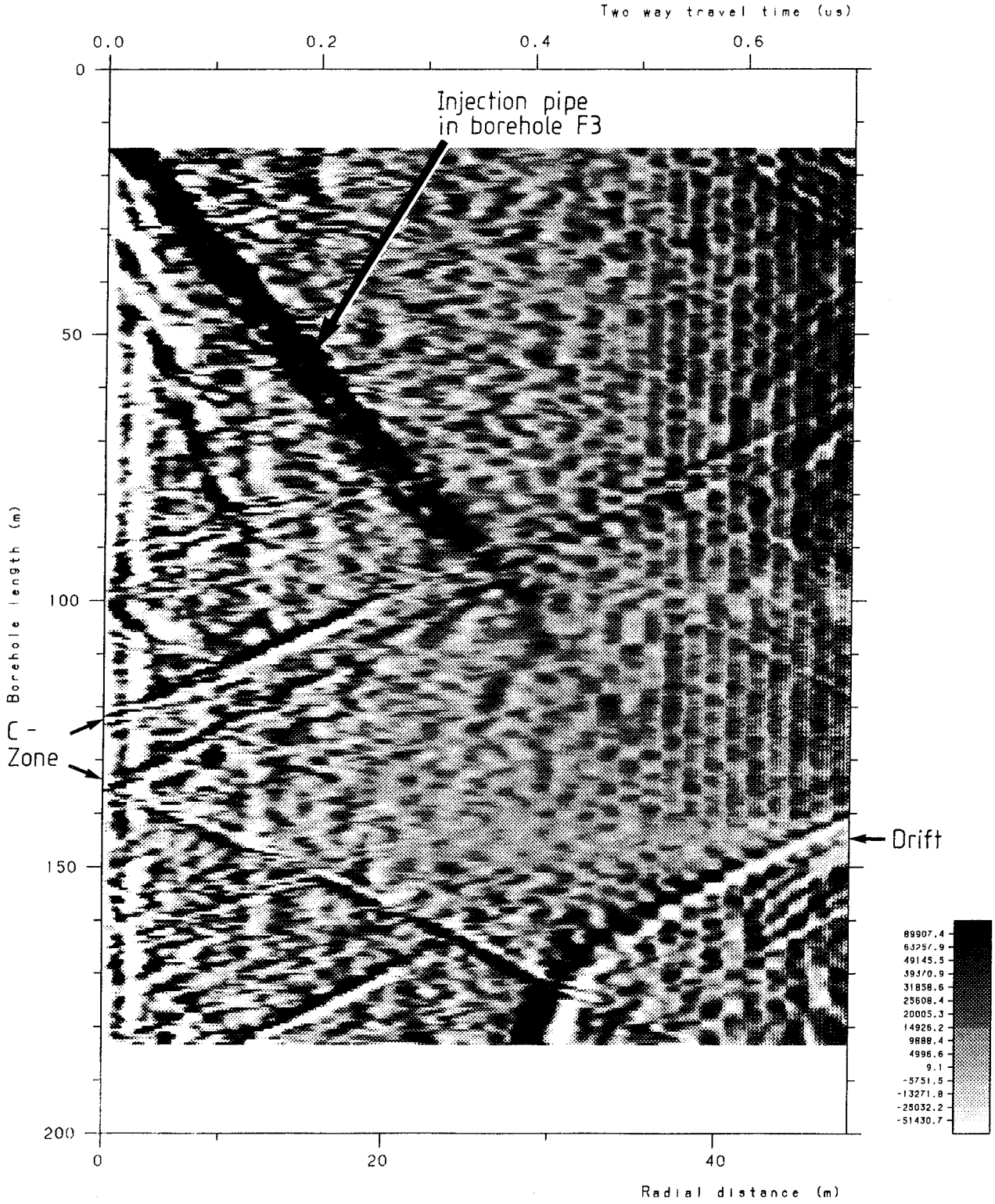

Figure 7.3 Difference radar reflectogram from two separate surveys in borehole E1, showing changes in the rock formation, due to injection of saline tracer. 60 MHz antenna, envelope filtered data.

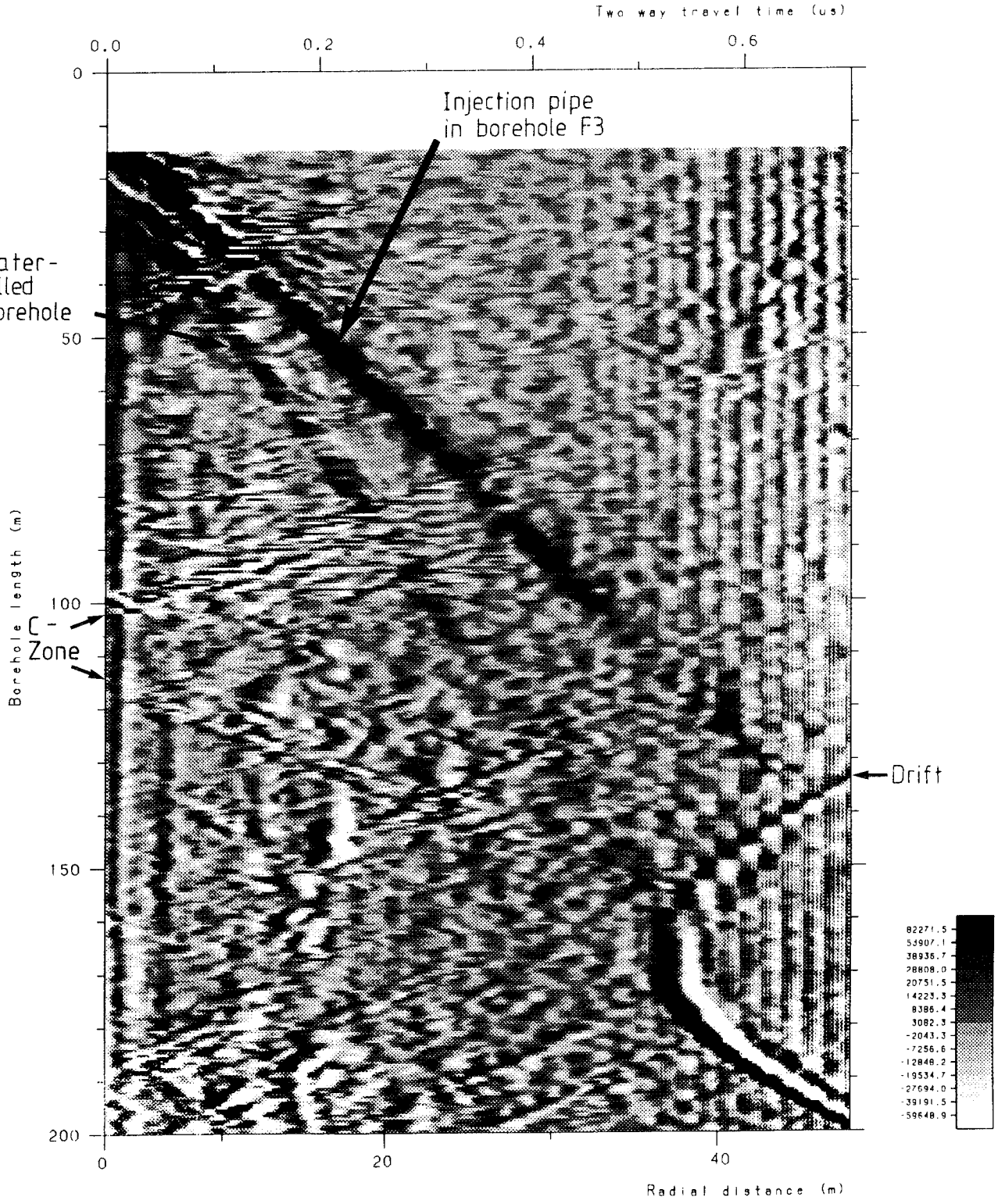

Figure 7.4 Difference radar reflectogram from two separate surveys in borehole F4, showing changes in the rock formation, due to injection of saline tracer. 60 MHz antenna, envelope filtered data.

7.3 RADAR MODEL OF TRANSPORT PATHS

7.3.1 Transport paths in Zone C

In order to determine the tracer migration paths in Zone C from the radar measurements, a differential tomographic map in the plane of Zone C, as shown in Figure 2.3, was produced. In Figure 7.5 the data points available, for such a differential tomogram of Zone C, are shown. The exact location of the midpoint, of Zone C, used for these calculations are presented in Table 7.1. The position of Zone C was defined as a plane with intersections in boreholes F1, F5 and F6 based on the radar reflection measurements performed as a part of this project. This definition of Zone C as a plane will result in slightly different intersections in the other boreholes than the radar intersections presented in Table 2.2.

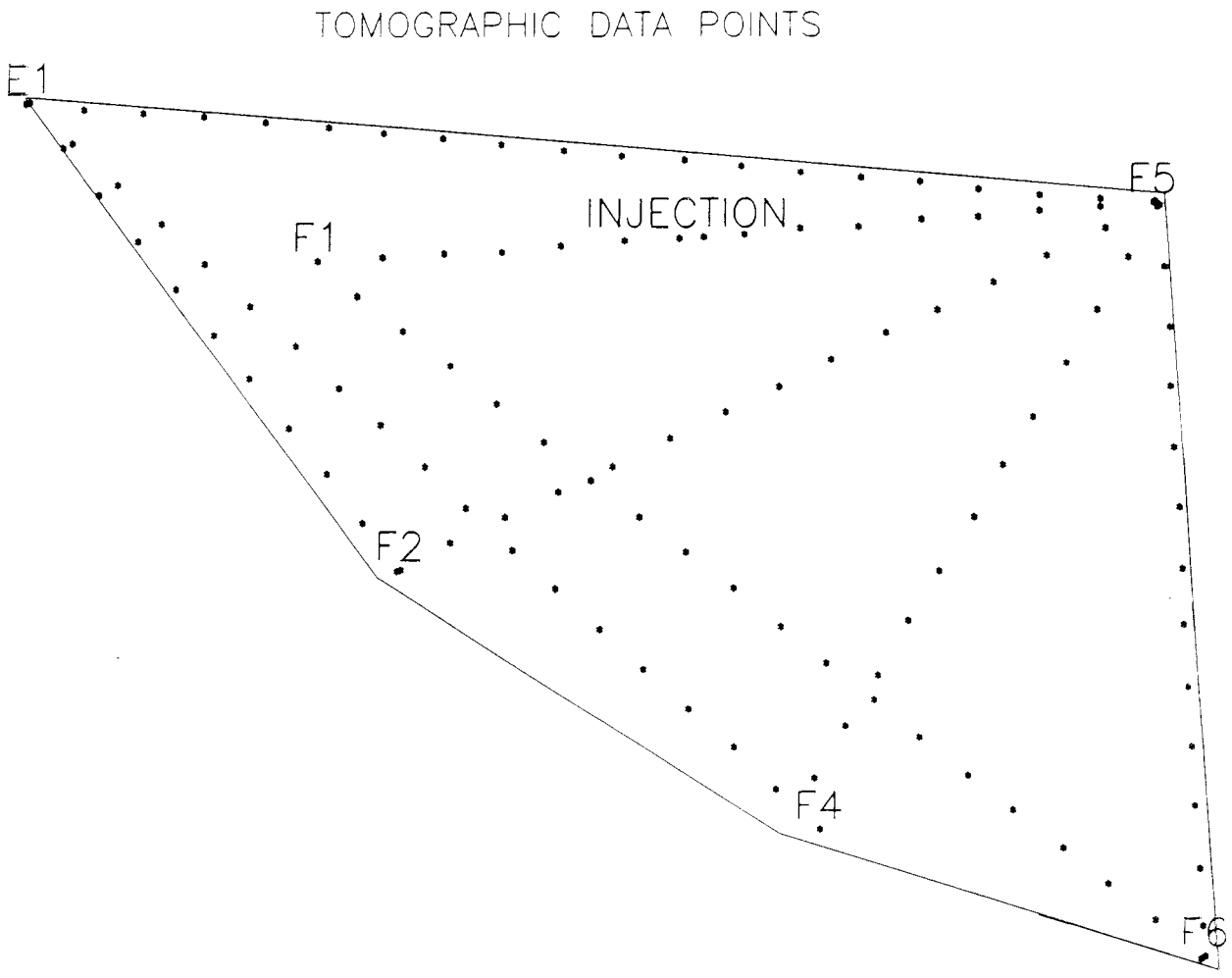

Figure 7.5 Data points available, in the Zone C location, for a differential tomographic analysis.

Table 7.1 Defined position of the plane for tomographic analysis in Zone C.

Borehole	Intersection with zone C (m)
E1	144
F1	122
F2	122
F3	107
F4	111
F5	95
F6	106

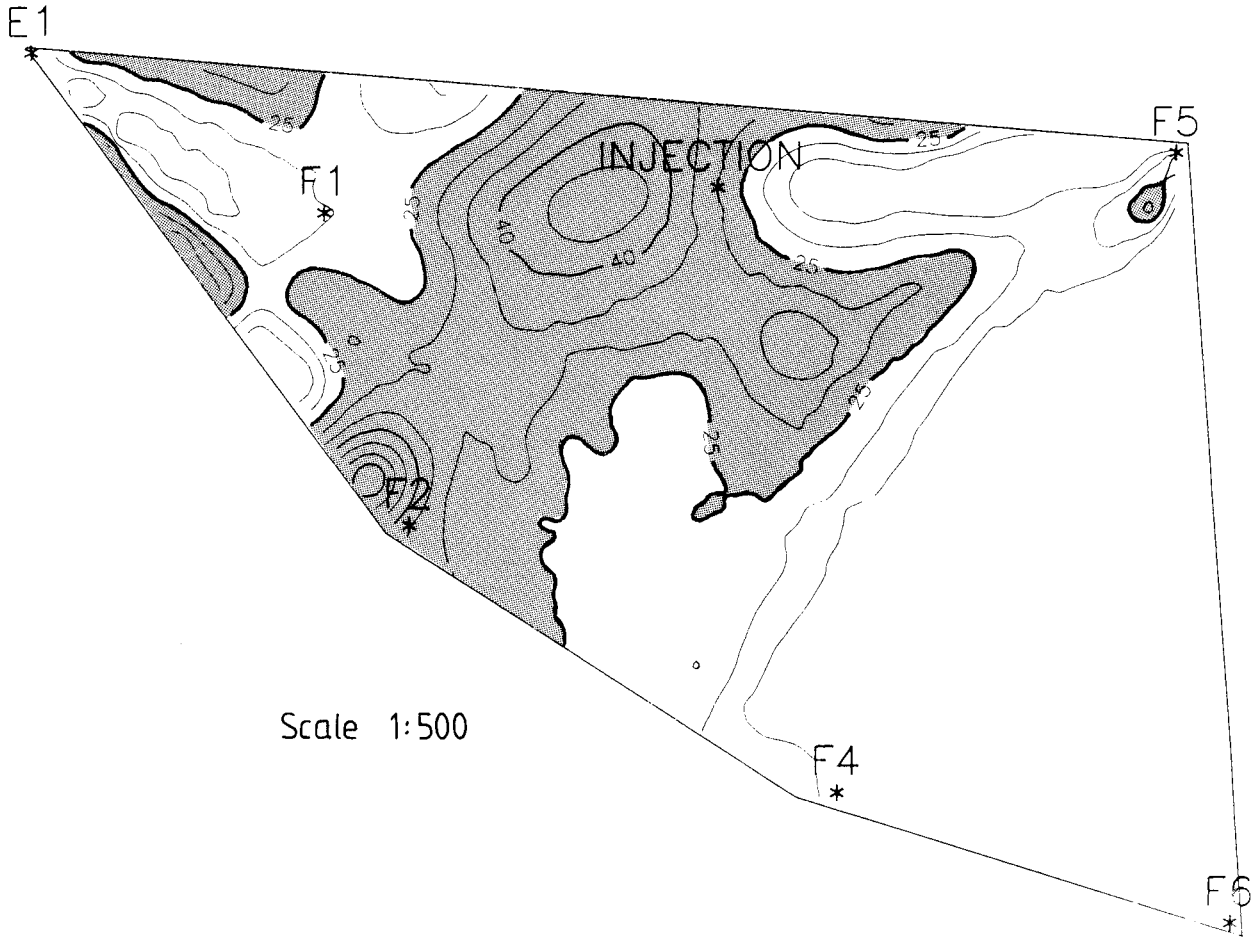

Figure 7.6 Difference tomogram for the middle section of Zone C, showing residual attenuation (dB/km) in the rock formation, due to injection of saline tracer. Borehole F3 is injection point.

In order to obtain an estimate of the effective migration width in Zone C, two analogous differential tomographic sections were produced, parallel to the one defined above and located 4 metres to each side.

The three differential tomographic sections, using residual attenuation data are presented in Figure 7.6 to 7.8. Figure 7.6 corresponds to Zone C as defined above and the other two corresponds to sections, parallel to and located **plus** 4 metres (Figure 7.7) respectively **minus** 4 metres (Figure 7.8) from the defined Zone C location.

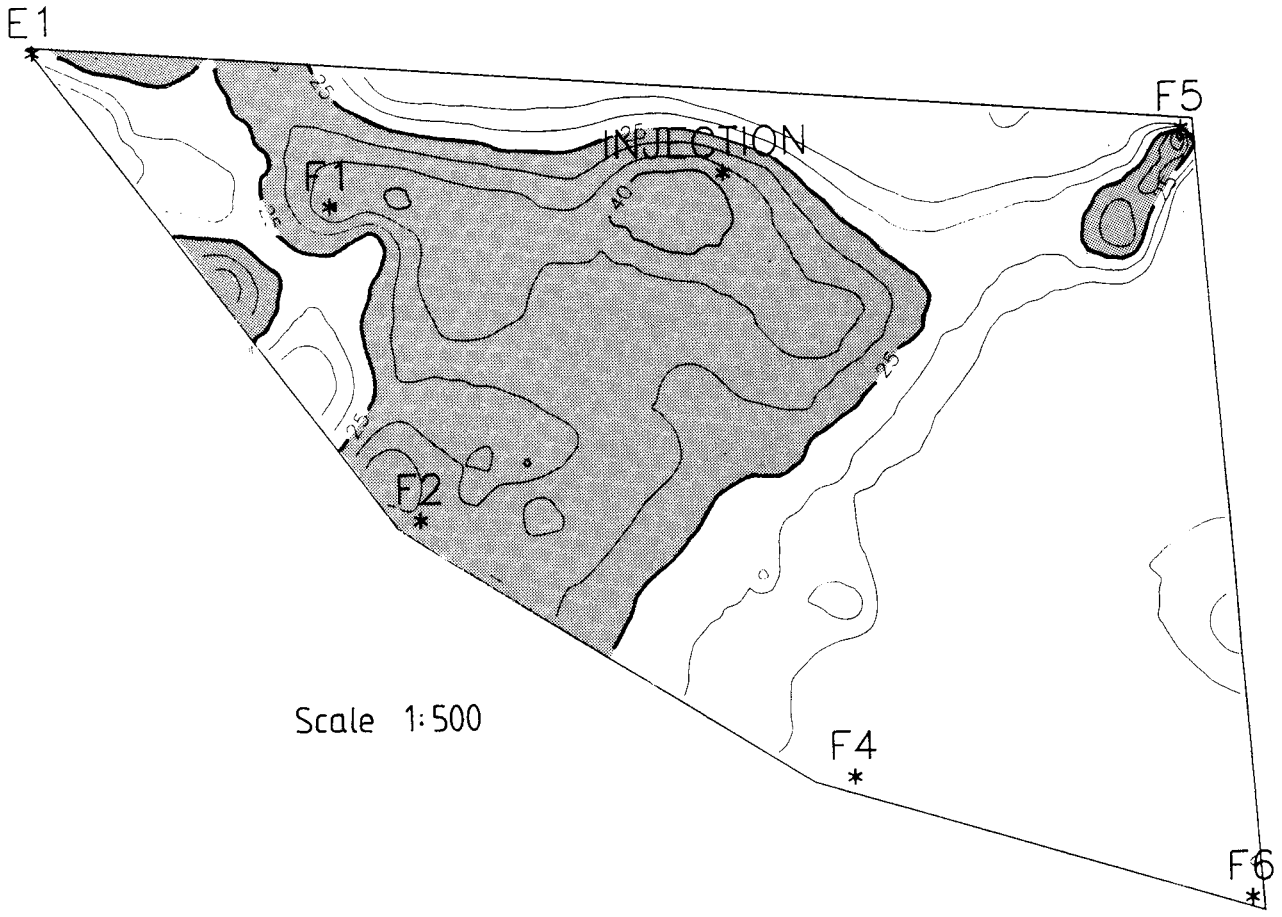

Figure 7.7 Difference tomogram for the lower part of Zone C (**plus** 4 meter into the rock), showing residual attenuation (dB/km) in the rock formation, due to injection of saline tracer. Borehole F3 is injection point.

The three differential tomographic results are also visualized as surface maps in Figures 7.9 to 7.12 (the differential tomographic results in Zone C are presented in two surface maps showing two alternative views). The vertical axis, in these surface maps, corresponds to the increase in calculated differential attenuation in the three individual sections.

The migration of the saline tracer in Zone C (i.e. the differential tomographic results referring to Zone C) can be interpreted from the results presented in Figures 7.6 to 7.8. The hatched areas in Figures 7.6 to 7.8 is interpreted as regions where most of the injected tracer is transported.

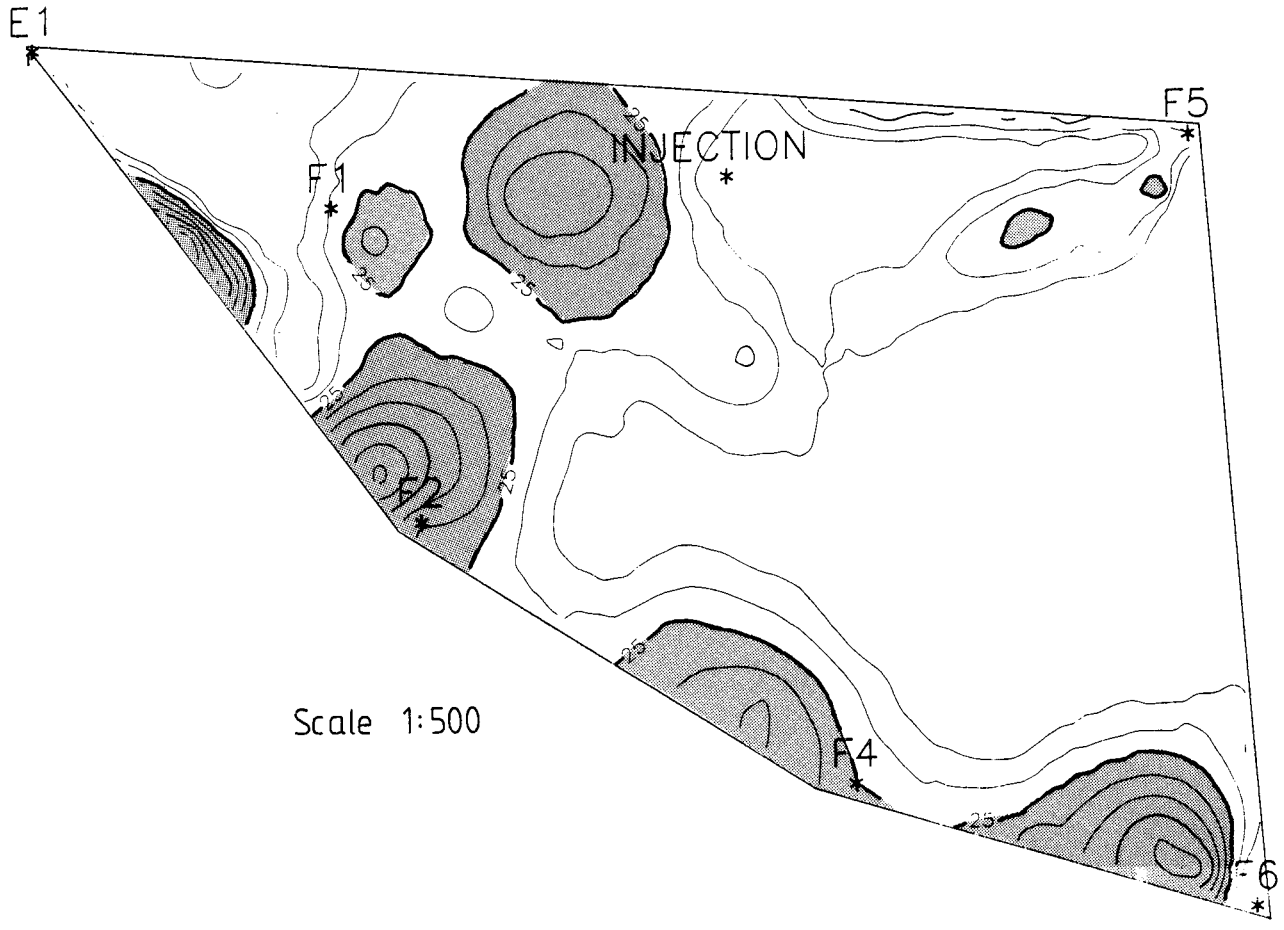

Figure 7.8 Difference tomogram for the upper part of Zone C (**minus** 4 meter), showing residual attenuation (dB/km) in the rock formation, due to injection of saline tracer. Borehole F3 is injection point.

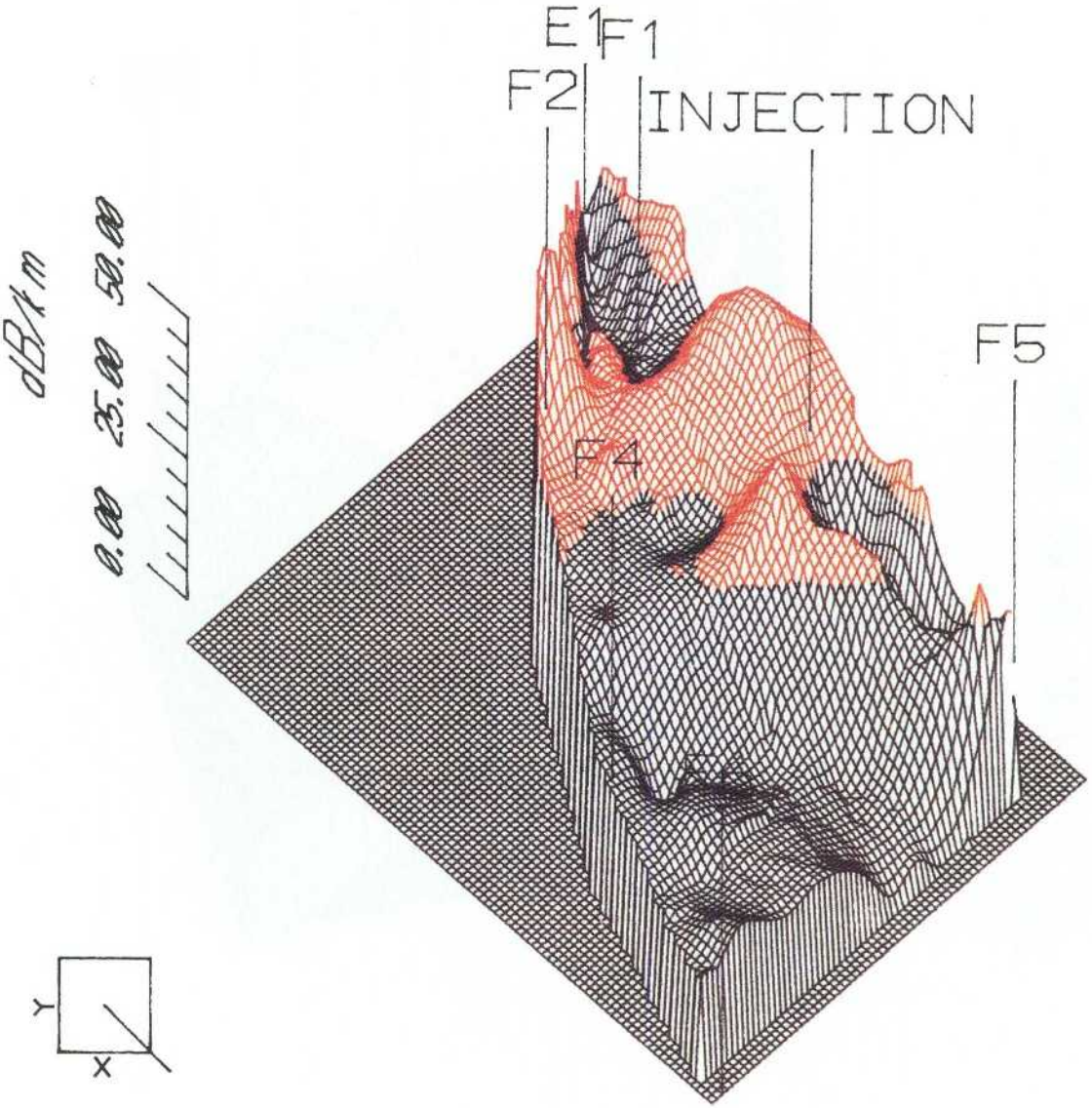

Figure 7.9 Difference tomogram, presented as a surface map, for the middle section of Zone C, showing residual attenuation (dB/km) in the rock formation, due to injection of saline tracer. Borehole F3 is injection point.

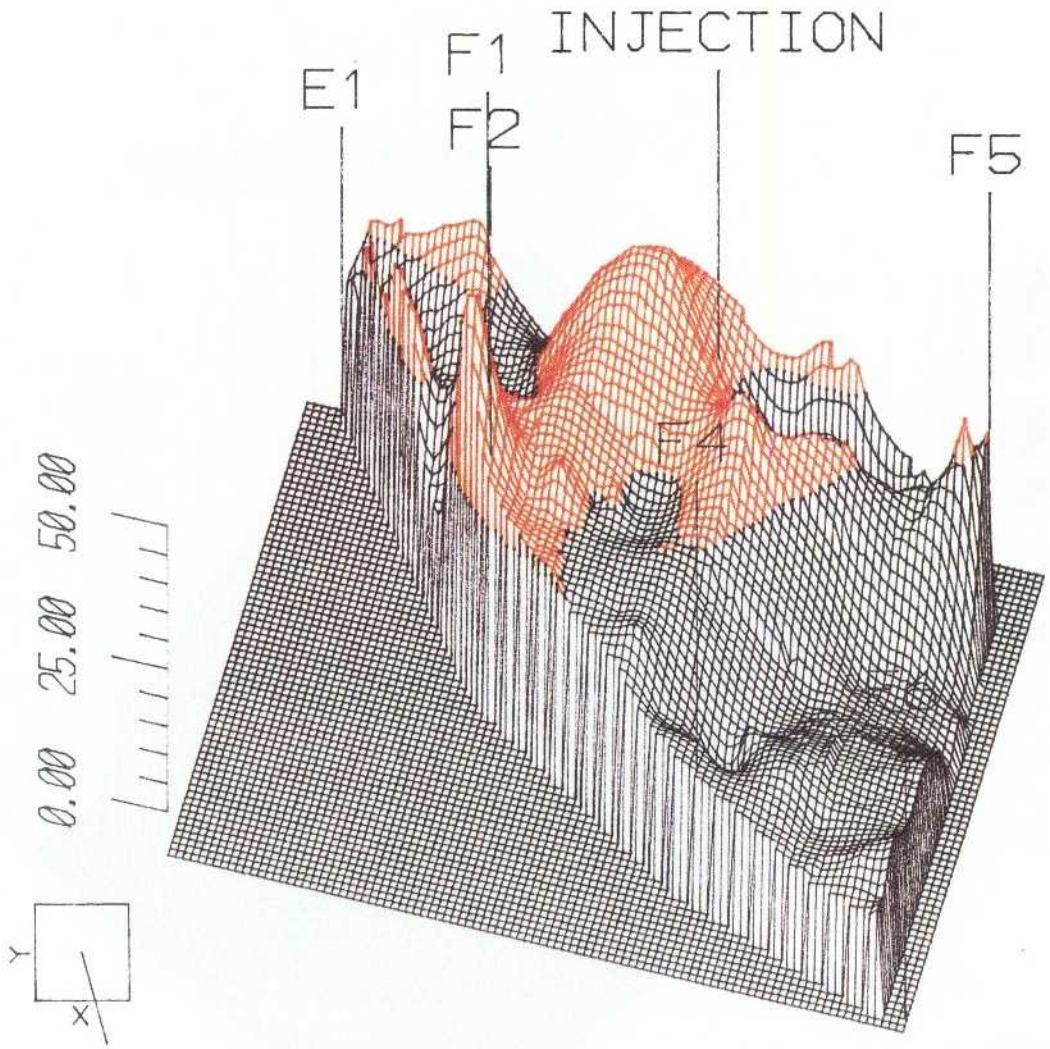

Figure 7.10 Difference tomogram, presented as a surface map, for the middle section of Zone C, showing residual attenuation (dB/km) in the rock formation, due to injection of saline tracer. Same data used as in Figure 7.9 but presented in another view. Borehole F3 is injection point.

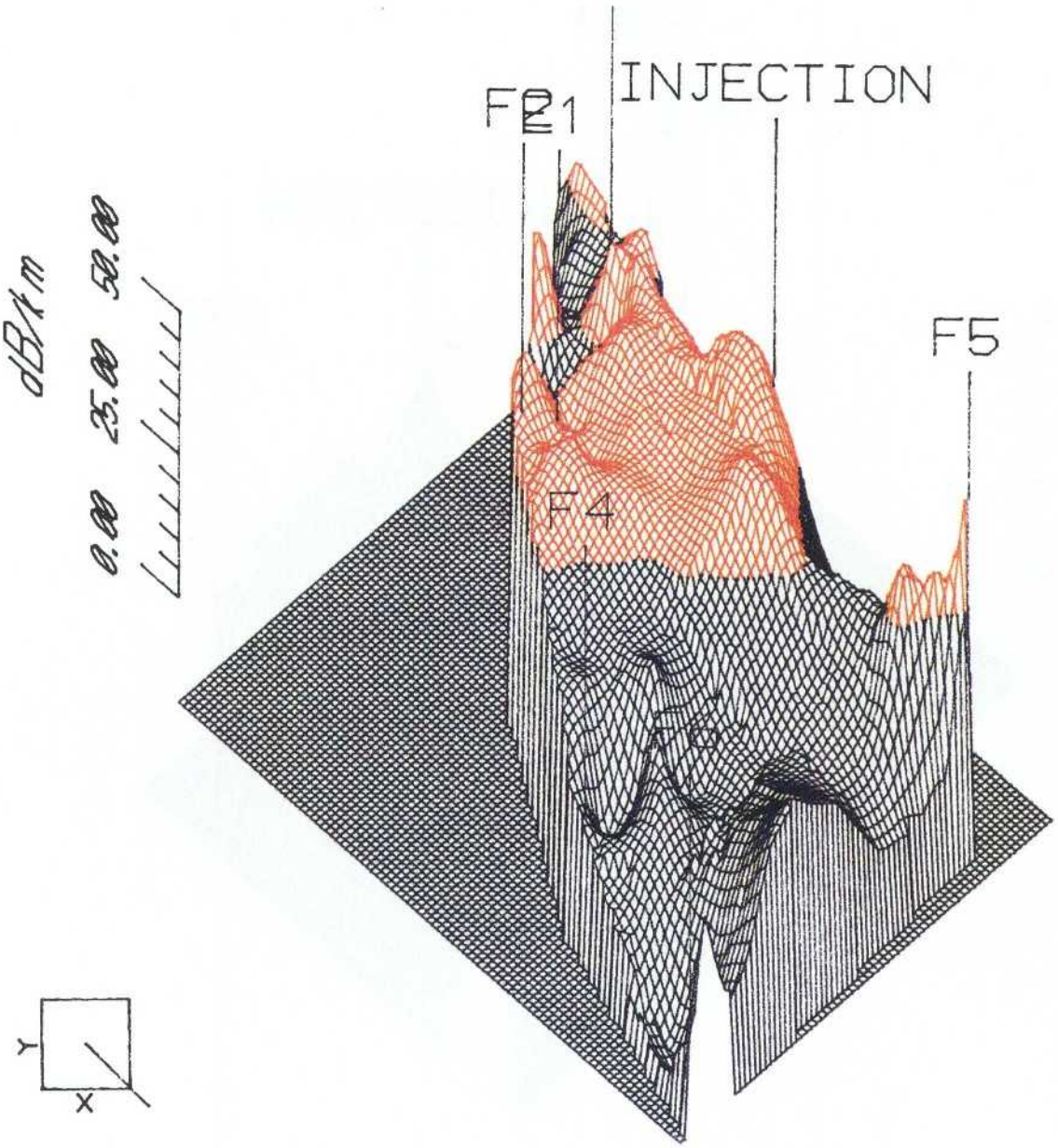

Figure 7.11 Difference tomogram, presented as a surface map, for the lower part of Zone C (**plus** 4 meter into the rock), showing residual attenuation (dB/km) in the rock formation, due to injection of saline tracer. Borehole F3 is injection point.

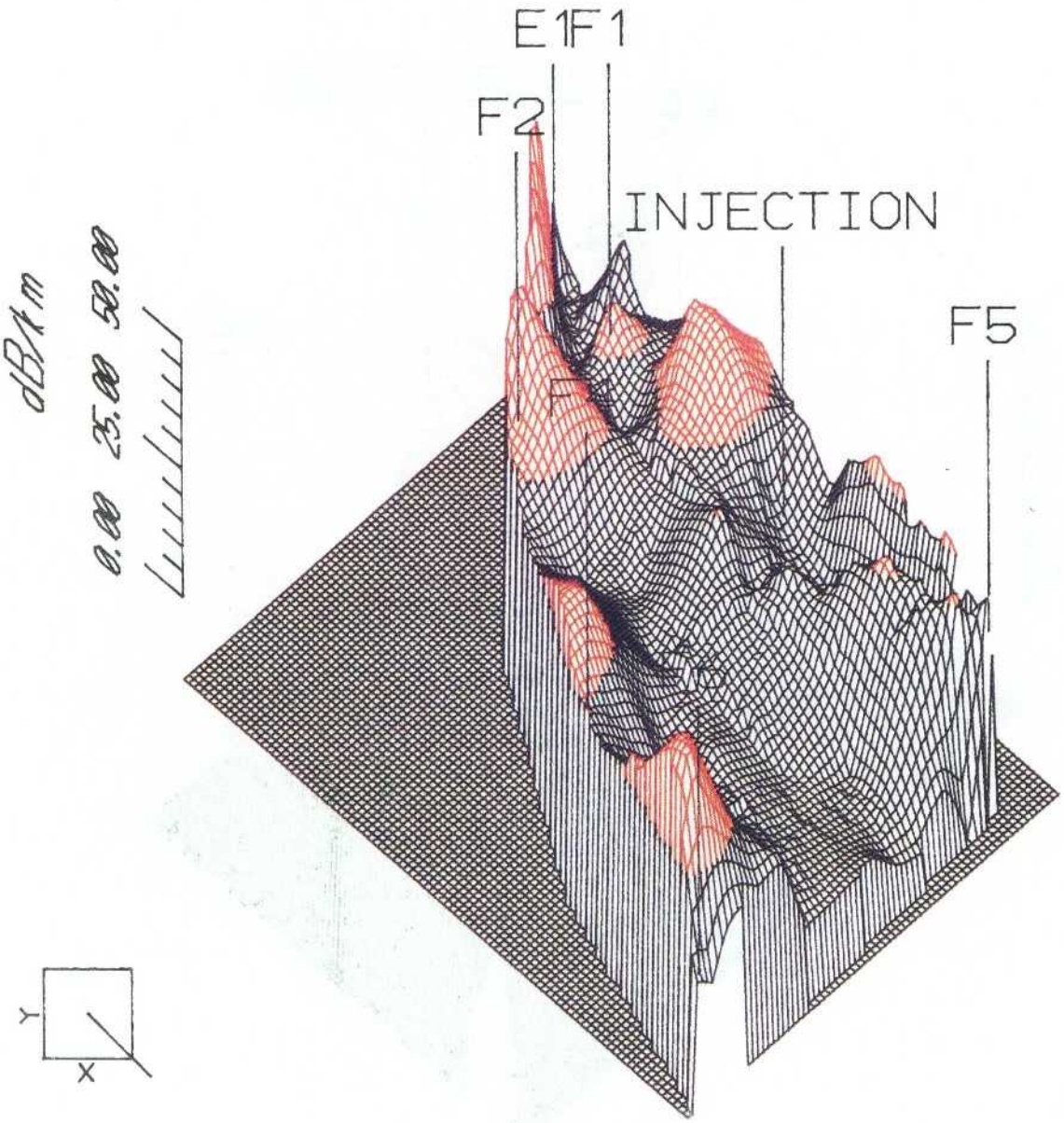

Figure 7.12 Difference tomogram, presented as a surface map, for the upper part of Zone C (**minus** 4 meter) , showing residual attenuation (dB/km) in the rock formation, due to injection of saline tracer. Borehole F3 is injection point.

The noise in these radar measurements is estimated to approximately 10 dB/km and as the mean length of the radar rays are about 100 meter this corresponds to a noise level of about 1 dB (cf. Section 4.6). A cut-off level for significant changes in the residual attenuation, caused by the saline tracer, were consequently chosen to 15 dB/km. The highest level of increase in residual attenuation, in the Zone C plane, was slightly above 45 dB/km. With an interval of attenuation increase, caused by the saline tracer, of 15-45 dB/km, we have taken 45 dB/km to correspond to the initial saline concentration (C_0) and 15 dB/km to zero (C=0). A cut-off level of 15 dB/km for tracer transport is in good agreement with the fact that no or hardly any tracer transport is observed, towards boreholes F4 and F6 and that the recorded residual attenuation in the vicinity of those two boreholes is 15 dB/km and less (Figure 7.6).

The area in the Zone C plane was divided into classes defined by the seven iso-lines plotted in Figure 7.6. The "migration area" for each class was defined as the area with data values included in the respective interval. With the radar attenuation proportional to $\sigma_w^{2/3}$ (cf. Section 3.3) and tracer concentrations as; C0=45 dB/km and C=0 at 15 dB/km, it is possible to determine the tracer concentration (C) within each class. In Figure 7.13 the relative tracer concentration is plotted against the "accumulated migration area" for the defined classes. The area under the graph corresponds to the relative tracer mass in Zone C.

A choice of 25 dB/km as the cut-off level for the main tracer transport within Zone C corresponds to a concentration of $0.2 \cdot C_0$. The area with values higher than 25 dB/km encompasses 48% (hatched area) of the total area where the saline tracer has been observed (assuming a cut-off level of 15 dB/km) and includes 78% of all saline tracer in the Zone C section, see Figure 7.13. Consequently, the area interpreted to include the main and important transport of saline tracer in Zone C (the hatched areas) is the area enclosed by the boundary with a residual attenuation of 25 dB/km and more.

The interpreted migration paths, visualized as hatched areas in these figures, reveal that the major flow path, in Zone C, stretches in the middle and lower parts (larger borehole depths) of the zone, Figures 7.6 and 7.7. In the upper part of Zone C (smaller borehole depths), Figure 7.8, only minor flow passages are encountered. The amount of tracer flow path or "preferential flow fraction" was defined as the area with tracer transport divided by the investigated area. The "preferential flow fraction" within Zone C,

expressed as percent of surveyed area, in the three sections of interest, are presented in Table 7.2. The "preferential flow fraction" in the range 19% to 37%, as presented in this project, is higher than previous indications found in granites and presented by Bourke et.al., 1985 (20%) and Abelin et.al., 1985 (5-20%). However, it should be noted that the previous observations were made in single fractures in the near vicinity of a drift, whereas the values presented in this report represents a much larger scale both regarding distance and number of fractures.

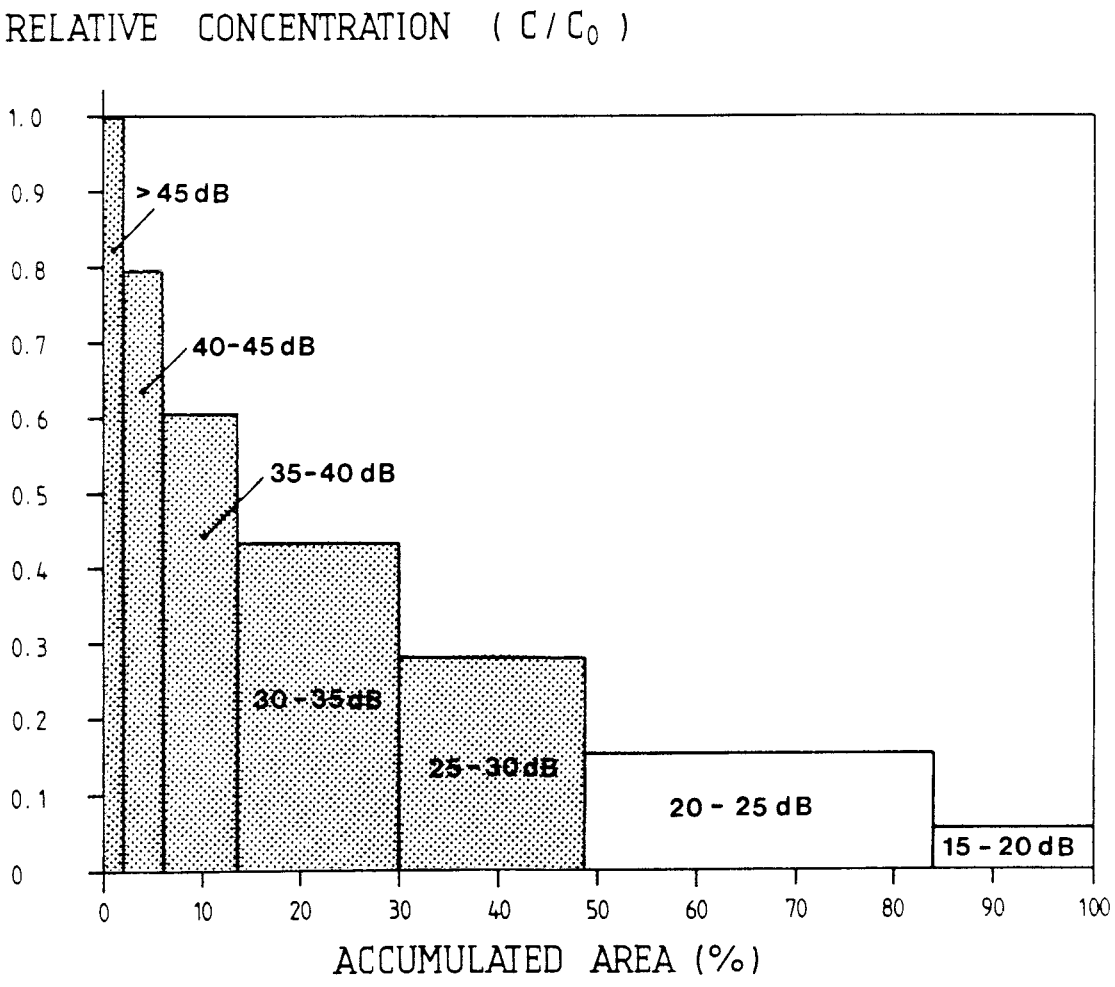

Figure 7.13 The relative tracer concentration, in Zone C, plotted against the accumulated migration area, in Zone C. The area under the graph corresponds to the relative tracer mass in Zone C.

Table 7.2 The amount of tracer flow fraction expressed as percent of surveyed area in Zone C and two sections parallel to and located 4 metres on each side of Zone C.

Section	Preferential flow fraction in Zone C
Zone C	31.7 %
Zone C (+4 m)	37.1 %
Zone C (-4 m)	19.9 %

From the differential tomographic result, in Zone C (Figure 7.6), it is obvious that the main migration path is from borehole F3 to F2. This major flow path, towards borehole F2, is also extending in the opposite direction out of the investigated rock volume, above the E1F5 section. There is also a saline migration path towards borehole F5, as seen by the increased residual attenuation. Anomalous portions with increased attenuation is also noticed on the line between boreholes F2 and E1. These anomalies can be interpreted as a subordinate transport path emerging from F3 and continuing towards F2 and then bending off towards borehole E1. This subordinate migration path towards borehole E1 is partly extending outside the investigated part of Zone C causing the inconsistent pattern of these anomalies. On the other side of Zone C towards boreholes F4, F5 and F6, no or hardly no tracer transport is noticed, except for the transport path towards F5, discussed above.

A comparison between the tracer migration result, in Zone C, as presented in Figure 7.6 and the two tomograms based on attenuation and slowness data from the reference radar measurement was made. The differential tomographic result, in Zone C, show that the saline injection has caused a migration more or less along with the attenuation and slowness anomalies as presented in Figure 6.1 and 6.2, with the exception that no saline tracer has migrated along the major attenuation anomaly surrounding borehole F1.

The migration paths in the lower part of Zone C, Figure 7.7, depicted as hatched areas show that the major flow path extends from borehole F3 out in the middle part of this section, towards boreholes F1 and F2. In this section a smaller part of the tracer transport is observed extending from F3 to borehole F5. As in the middle section of Zone C there is no or hardly no, tracer transport detectable towards boreholes F4 and F6.

The transport of saline tracer in the upper part of Zone C, Figure 7.8, represented as hatched regions, shows a more inconsistent pattern than the two previous sections. Apart from a more or less consistent migration path in the F3/F2 direction there is also a tendency of a saline transport towards boreholes F4 and F6, following the route F2-F4-F6. The tomographic results from Figure 7.8 shows only minor increases in the residual attenuation towards F5. The tracer transport towards borehole F5 is consequently located in the middle and lower parts of Zone C, see Figures 7.6 and 7.7.

It is also interesting to establish the active injection interval in borehole F3. On the basis of Figures 7.6 to 7.8 it is possible to determine the active interval with significant out-flow of saline tracer. The interval with the main out-flow from F3 are interpreted to be located in the lower part of Zone C, between and in the close vicinity of the section 107 to 111 meter.

7.3.2 Transport paths in the investigated rock formation

A differential tomographic three-dimensional model was produced to show the transport paths in the investigated rock volume. A plastic model was made in the scale 1:500 and comprised of the eleven tomographic sections measured within this project. The plastic model also served the purpose to give an understanding of the quality of the produced tomograms. As mentioned above, the only way to determine the quality and the errors of the difference tomograms was to compare equally located data in bisecting tomograms.

In order to visualize and present the migration results, generalized pictures of the saline tracer migration model as well as a model of the mapped Zone C were produced with an advanced three-dimensional CAD-system (Intergraph Engineering Modelling System). The CAD-generated pictures displays the models in eight separate and individual views.

In order to visualize the results in distinct and easy to understand CAD-pictures it was necessary to generalize the migration model as well as the mapped Zone C model. The models were produced as "binary" models where areas with significant increase in attenuation, caused by the saline tracer, were defined as dark coloured areas, whereas regions with no attenuation increase were defined as transparent areas.

The generalization of the two resulting models will cause the CAD-generated models to be less detailed

than the tomograms, regarding both the tracer migration as well as the outline of Zone C. Special considerations must be taken when examining the boundaries of the CAD-generated models. Especially in the volume between the measured borehole sections as the radar attenuation as well as geometrical shape of Zone C between the borehole sections are unknown. The shape of the CAD-generated models between the measured borehole sections are interpolations accomplished interactively with the used CAD-program and can in some cases produce unwanted artifacts.

The CAD-generated pictures are not produced for detailed interpretation of the saline tracer migration. The CAD-generated pictures are composed exclusively for a visualization and (hopefully) an understanding of the general distribution of the saline tracer within the investigated granite volume.

A total of 45 CAD-pictures has been produced displaying the migration model and a model of the mapped Zone C as well as a combination of these two models. A complete set of the CAD-generated pictures are presented in Appendix 7.1-7.6.

The general distribution of the saline tracer within the investigated volume is presented in two CAD-generated views, Figures 7.14 and 7.15. From these figures it is noticed that the injected tracer is transported in three different zones, marked with red, green and yellow colours, respectively. The two views are produced and visualized with 45 degrees rotation between the two views. The total set of eight CAD-generated views, showing the generalized tracer migration within the investigated volume are presented in Appendix 7.2.

During the processing phase it was apparent that three of the eleven recorded tomographic sections contained errors which prohibited their use in the final interpretation. The three excluded sections were F1F2, F2F4 and F4F6 and the reason for the unacceptable results in these sections were the large amount of skipped traces (>31%). The large amount of skipped traces in these sections was due to the small transmitter-receiver distances causing oversaturated radar signals (cf. Section 4.3). Comparing equally located data in the F1F2-, F2F4- and F4F6- tomograms with nearby situated tomograms resulted in poor agreement. The conclusion is that the final interpretation had to be based on the eight remaining differential tomograms. Combinations of these eight tomographic sections are presented in Figures 7.16 to 7.19 and 7.23, demonstrating the sufficiently good agreement between data in corresponding sections.

The amount of tracer flow path or "preferential flow fraction" within the investigated granite volume is not produced in the same straightforward way as for the Zone C plane section, presented above. From the tomograms it is obvious that tracer transport also takes place outside Zone C. To get a measure on the spreading of the tracer we relate the area with significant tracer transport to the total area of Zone C in each of the eight tomographic sections. The "preferential flow fraction" for each section is given in Table 7.3. Note that this definition differs from the "preferential flow fraction" used for Table 7.2 which referred to the area of transportation within the plane of Zone C.

Table 7.3 The "preferential flow fraction in the investigated volume" expressed as migration path compared to Zone C region, in the differential tomographic sections.

Section	Preferential flow fraction in the investigated volume
F5E1	145.8 %
F5F1	116.9 %
F5F2	47.6 %
F5F4	62.3 %
F5F6	5.8 %
F1F6	35.6 %
E1F4	64.0 %
F2E1	95.2 %

The presented values on the "preferential flow fraction"in Table 7.3 are high, the explanation being that portions of the tracer migration takes place outside the outlined Zone C. The high values in sections F5E1, F5F1 and F2E1 are caused by tracer migration in both Zone C and outlying zones.

Figure 7.14 The generalized model of the injected saline tracer distribution within the investigated volume. Yellow colour corresponds with Zone C, red corresponds with Zone X and green to Zone Y.

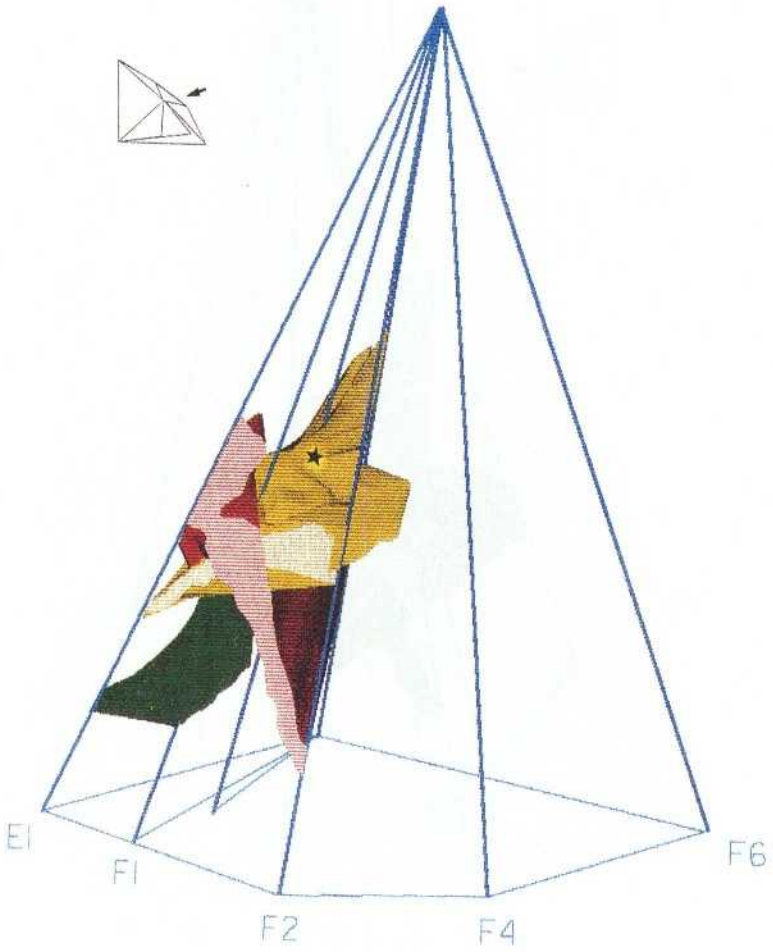

Figure 7.15 The generalized model of the injected saline tracer distribution within the investigated volume. Yellow colour corresponds with Zone C, red corresponds with Zone X and green to Zone Y.

Zone C

The fracture zone labelled 'C' is one of the major zones at the investigation site and it is centrally located within the site. Zone C is clearly observed from the geophysical methods, geological mapping as well as hydraulic testing. Crosshole hydraulic testing had shown that good hydraulic connections exist from borehole F3 to F2 and F5. Zone C intersects all boreholes at the site and the radar intersections with the boreholes are tabulated in Table 2.2. The interval 103.0-118.5 m in borehole F3, incorporating Zone C, was selected as the injection point for the saline tracer.

From the differential attenuation 3-D tomographic model it is apparent that the major tracer migration from the injection point is spreading, in the F5F2 plane and in Zone C, towards borehole F2. This major migration path can be followed in Figures 7.16 to 7.18. In Figure 7.16 the tracer flow from the injection point is observed in the middle of the section F5F2. The main flow path of the injected salt water is extending towards borehole F2 (as marked in Figure 7.16). Anomalies from this flow path are also observed in sections F1F6 and E1F4 , Figures 7.17 and 7.18.

The major flow path, towards borehole F2, is also extending in the opposite direction, as already depicted in the results regarding Zone C (Figure 7.6), traversing and producing anomalies in sections F5F1 and F5E1, Figure 7.19. This tracer spread opposite to the F2-direction is not, as seen in the tomogram sections, intersecting any boreholes in Zone C section. The most striking information following these results is that no tracer transport, in Zone C, is noticed towards borehole F1.

Further transportation, of injected tracer in Zone C, is detected towards borehole E1 but only in the F2E1-section Figure 7.16. In the E1F4-tomogram no sign of saline migration is apparent, as visualized in Figures 7.18. In the F5E1-tomogram only a tendency of a saline transport is visible, Figure 7.19. These features, together with the results from Zone C section (Figure 7.6), reveals that a saline migration path is emerging from Zone C, close to borehole F2 towards borehole E1. This migration path towards borehole E1 is partly extending outside Zone C section, and partly outside the investigated rock volume causing the inconsistent pattern of the recorded anomalies.

The migration of the injected tracer, in Zone C, is mainly concentrated in the paths towards the rock mass located at the F2/E1-side, described above. But there is also paths stretching towards borehole F5 in the F5F2-and F5E1-sections. In Figures 7.16 and 7.18 these

flow paths towards F5 can be seen. Surprisingly, the tomographic section situated between the F5F2- and F5E1-tomograms show no sign of migration towards borehole F5 (Figure 7.19), which indicates a compact bedrock between the injection point(F3) and borehole F5. The interpretation of a compact rock mass between boreholes F3 and F5, is also supported by the migration results, in Zone C, presented in Figure 7.6.

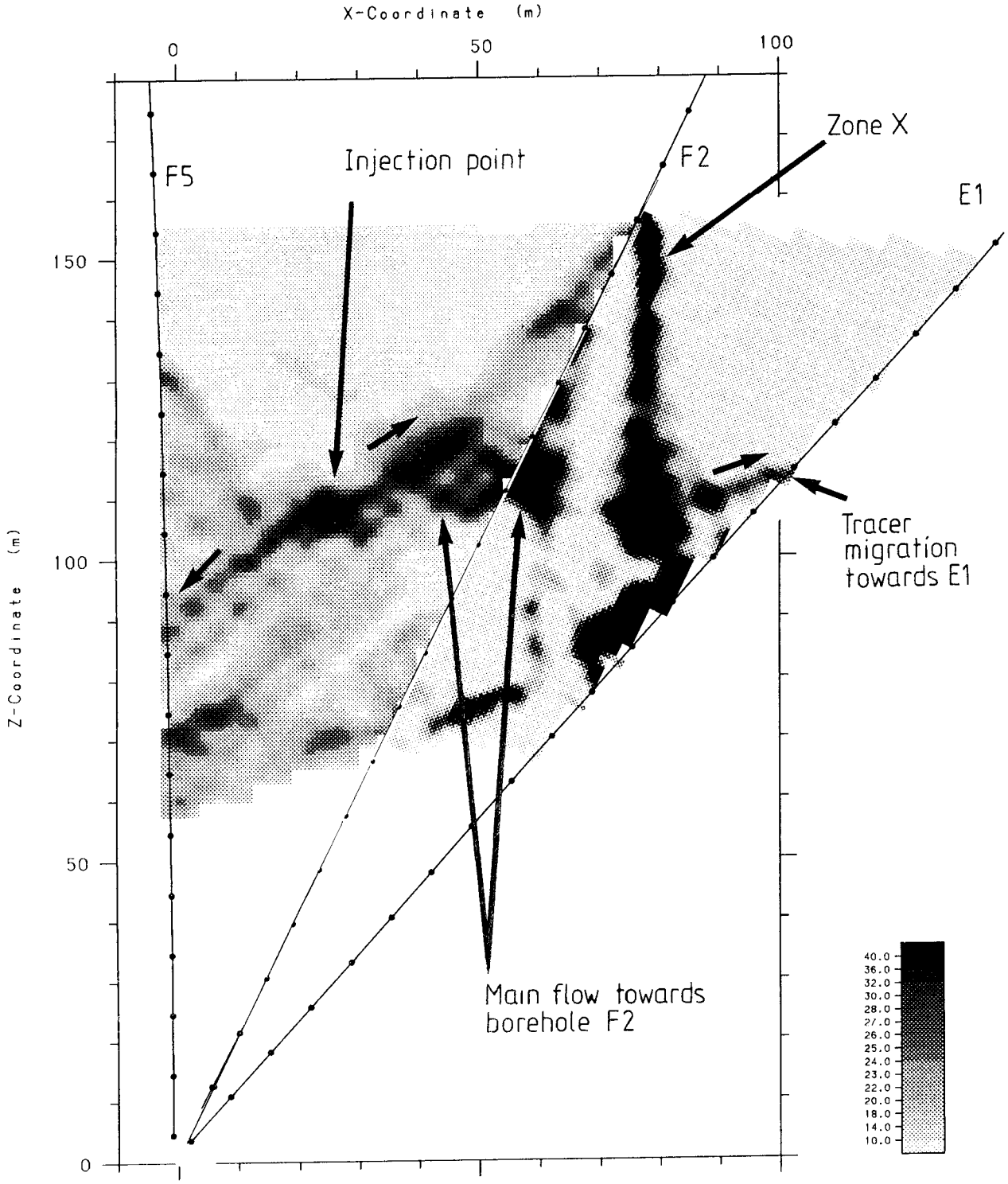

Figure 7.16 Combination of the two difference tomograms, F5F2 and F2E1 , showing the saline migration in the rock formation. Direction of tracer migration is marked with arrows.

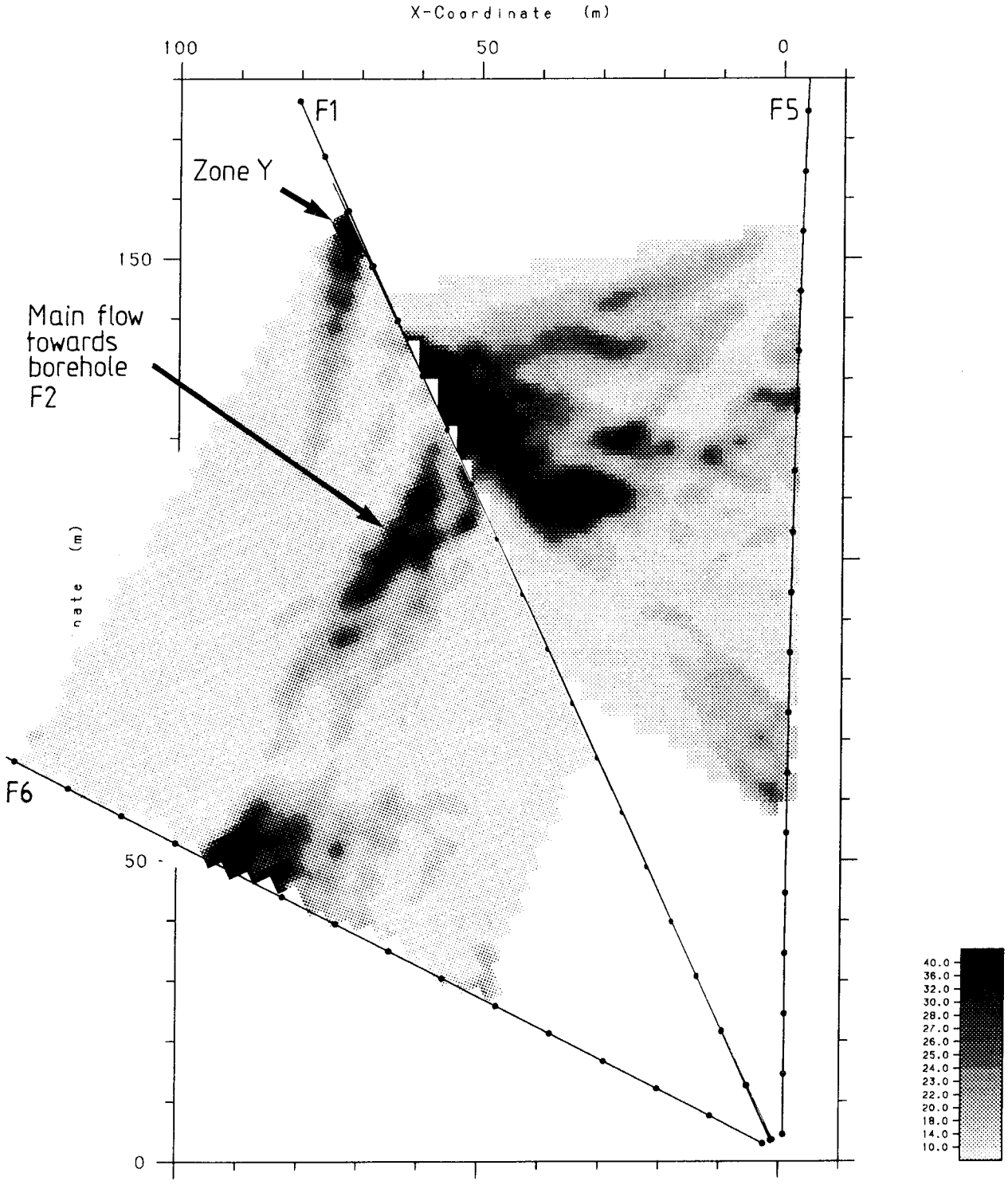

Figure 7.17 Combination of the two difference tomograms, F5F1 and F1F6 , showing the saline migration in the rock formation. Direction of tracer migration is marked with arrows.

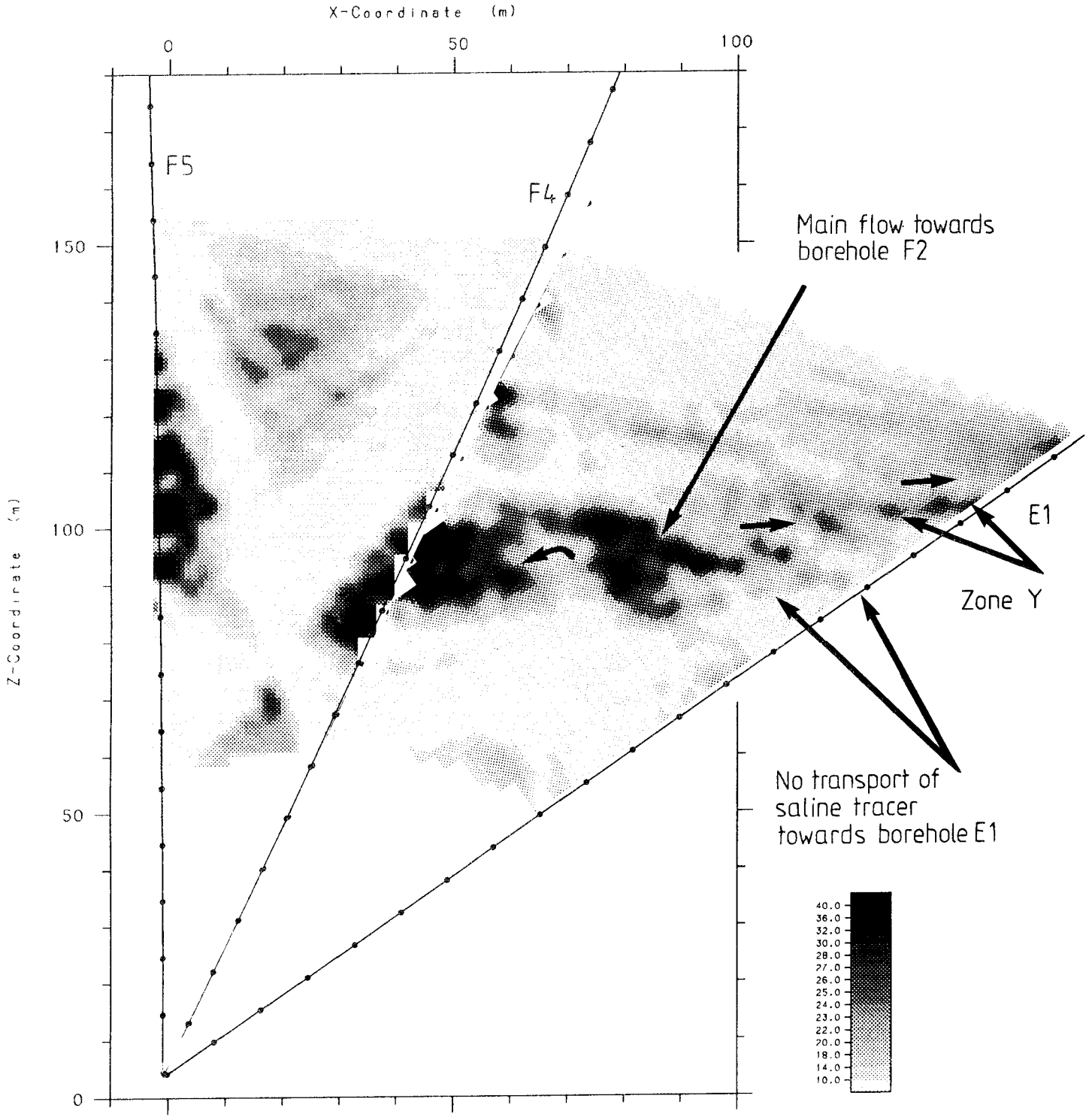

Figure 7.18 Combination of the two difference tomograms, F5F4 and E1F4 , showing the saline migration in the rock formation. Direction of tracer migration is marked with arrows.

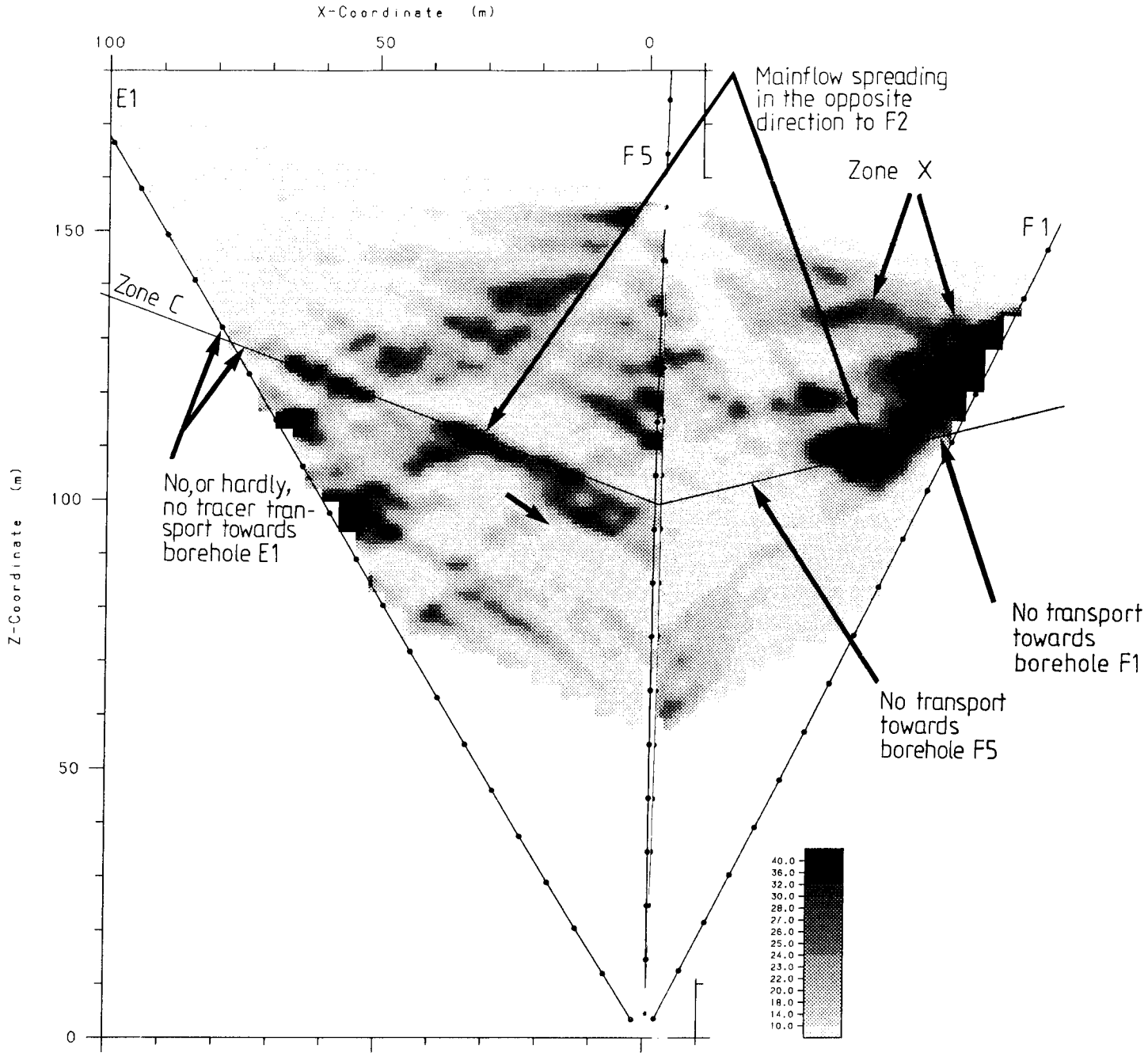

Figure 7.19 Combination of the two difference tomograms, F5E1 and F5F1 , showing the saline migration in the rock formation. Direction of tracer migration is marked with arrows.

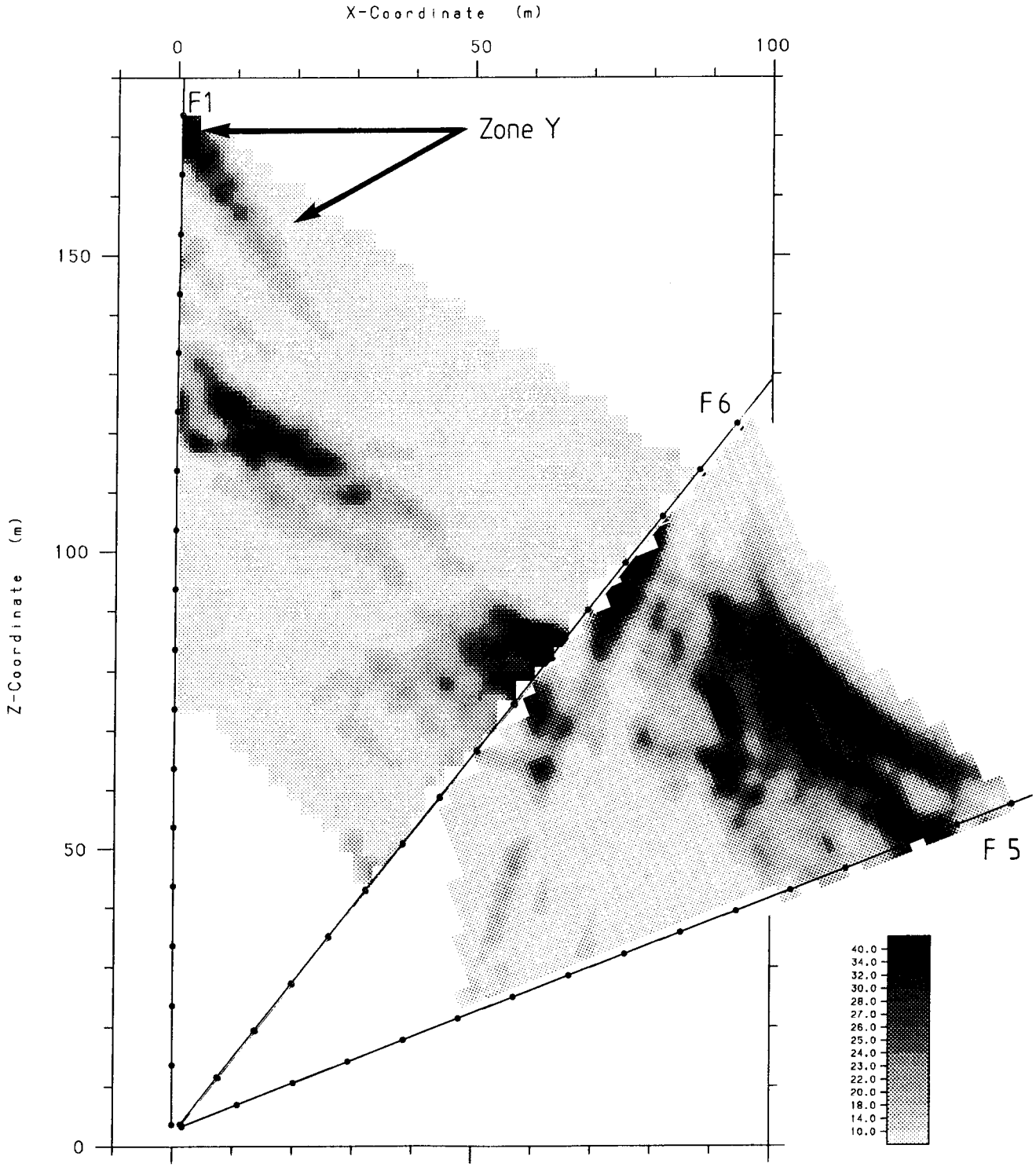

Figure 7.20 Combination of the two difference tomograms, F1F6 and F5F6 , showing the saline migration in the rock formation. Direction of tracer migration is marked with arrows.

Only subordinate tracer transport paths is noticed towards boreholes F4 and F6. The residual attenuation anomaly visible in the vicinity of borehole F4, seen in Figure 7.18 (sections E1F4 and F5F4), is interpreted as caused by a flow of saline tracer, in Zone C and in the E1F4 section. Other minor and unaddressed anomalies, in the F4/F5/F6 area are difficult to understand and are, with one exception, interpreted as insignificant with no importance to the combined migration interpretation. The above-mentioned exception is the anomaly in the lower parts of the F5F6-section, Figure 7.20, which is interpreted as tracer flow, emerging from borehole F5, into the fault shearing the rock mass in the volume outlined by boreholes F4, F5 and F6 (cf. Section 6.3).

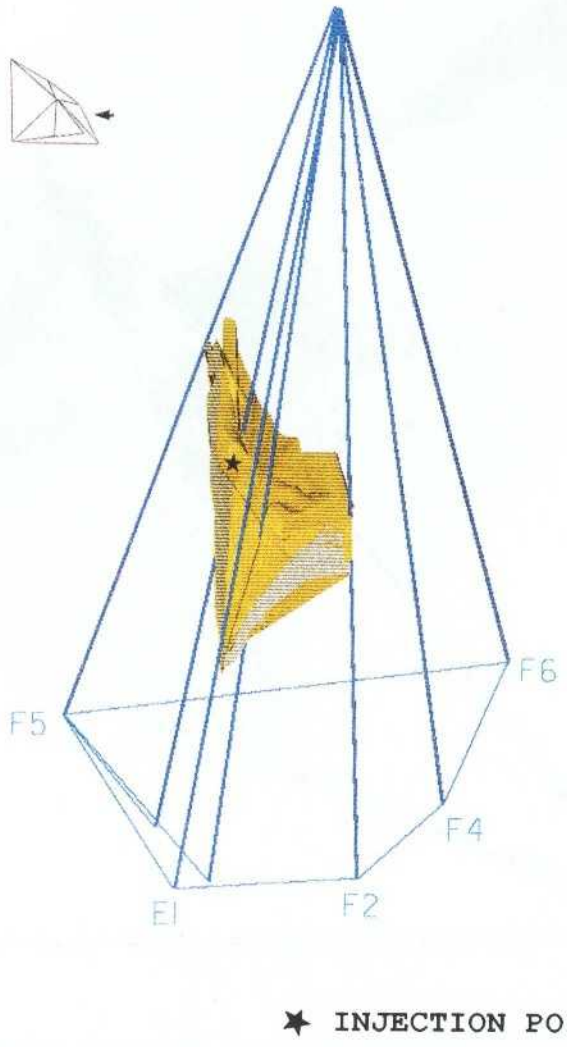

Figure 7.21 The generalized model of the injected saline tracer distribution within Zone C.

The general distribution of the saline tracer within Zone C is presented in two CAD-generated views, Figures 7.21 and 7.22. The two views are produced and visualized with 45 degrees rotation between the two views. The total set of eight CAD-generated views, showing the generalized tracer migration within the investigated volume are presented in Appendix 7.3.

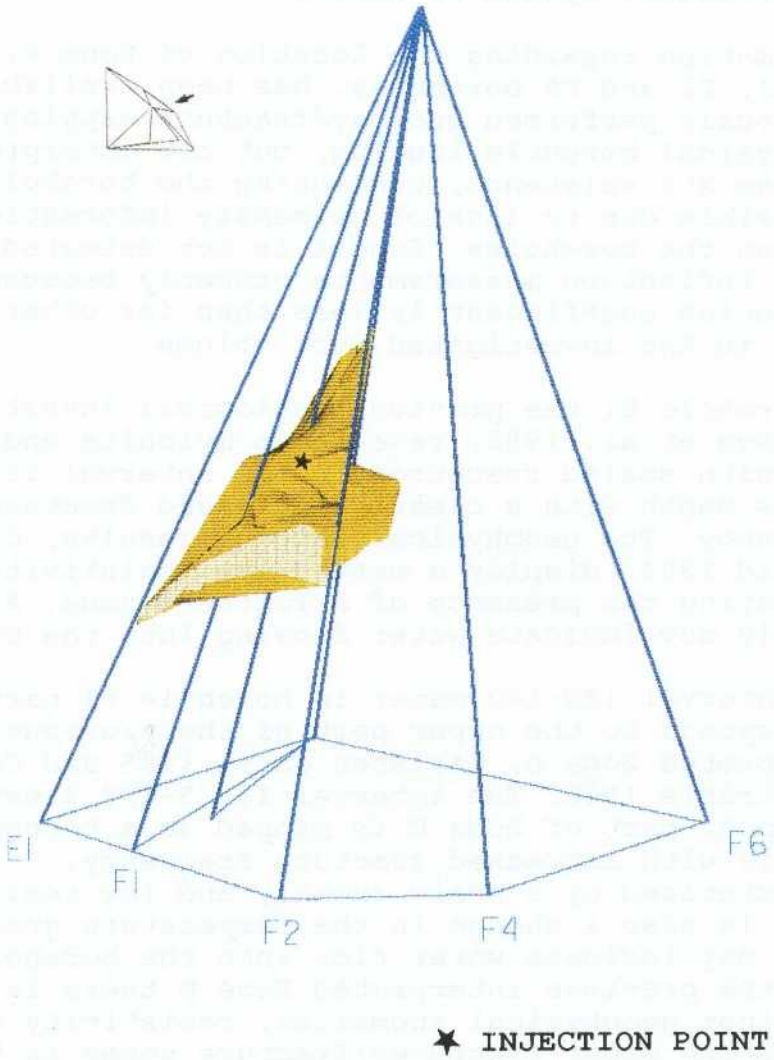

Figure 7.22 The generalized model of the injected saline tracer distribution within Zone C.

Zone X

A fracture zone originally detected within this project, is found to transport portions of the injected tracer. This fracture zone, termed Zone X, is most distinct in borehole sections E1F5 and F2E1, Figure 7.23, but is also seen in section F5F1, Figure 7.19, and is intersecting boreholes E1, F1, F2 and F5 within the investigated granite volume. Zone X, intersecting Zone C with 80°-90° degrees angle, is connecting E1 at about 125-130 meter, F1 at about 130-140 meter, F2 at about 165-175 meter, and F5 at about 155-165 meter borehole depth. This zone has an orientation (dip 55° and strike 10°) similar to that of Zone A which indicates that it could be part of the same fracture system as Zone A.

Information regarding the location of Zone X, in the E1, F1, F2 and F5 boreholes, has been available from previously performed geology/fracture mapping and geophysical borehole logging, but the interpretation of Zone X's existence, connecting the boreholes, was impossible due to lack of necessary information between the boreholes. Zone X is not detected in the radar reflection measurements probably because the reflection coefficient is less than for other fracture zones in the investigated rock volume.

In borehole E1 the previous geological investigations, Carlsson et.al. 1982, revealed a mylonite and breccia zone with sealed fractures in the interval 127-132 meters depth with a clearly increased fracture frequency. The geophysical logging results, Olsson and Jämtlid 1984, display a marked low resistivity anomaly indicating the presence of a fracture zone. A small SP anomaly may indicate water flowing into the borehole.

The interval 130-140 meter in borehole F1 partly corresponds to the upper part of the previous interpreted Zone D, Carlsten et.al.1985 and Carlsten and Stråhle 1985. The interval 138.3-138.9 meter in the upper part of Zone D is mapped as a tectonized breccia with increased fracture frequency, characterized by a sonic anomaly and low resistivity. There is also a change in the temperature gradient which may indicate water flow into the borehole. Apart from the previous interpreted Zone D there is also a few minor geophysical anomalies, resistivity and sonic, indicating minor fractures/fracture zones in the interval 130-140 meter. One of these minor fracture zones can also be observed in the core samples, in the borehole section 135.9-136.2 meter.

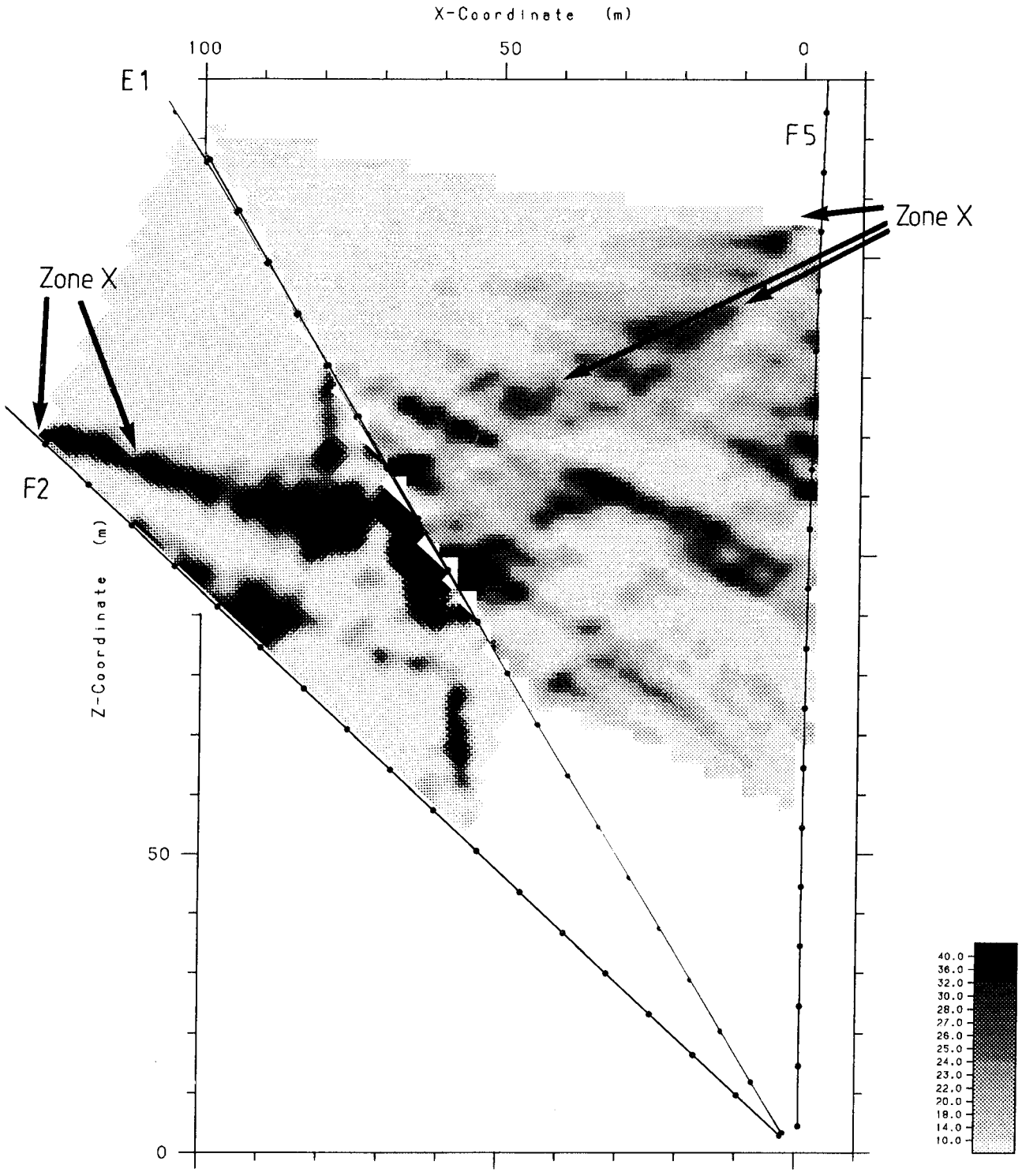

Figure 7.23 Combination of the two difference tomograms, F5E1 and F2E1 , showing the saline migration in the rock formation. Direction of tracer migration is marked with arrows.

In the F2 borehole the previous geological investigations, Carlsten and Stråhle 1985, the borehole section 165-176 meter is interpreted as a partly tectonized granite with several healed fractures. This interpretation is supported by the geophysical logs, Carlsten et.al.1985, where a few relatively small anomalies (resistivity, sonic and neutron) are present in this interval, indicating fractures/minor fracture zones.

The interval 155-165 meter in borehole F5 partly corresponds to the upper part of the previous interpreted Zone F, Carlsten et.al.1985 and Carlsten and Stråhle 1985. The interval 161.5-164.2 meter in the upper part of the Zone F is mapped as a partly tectonized granite with high fracture frequency, featured with a distinct and low resistivity anomaly. There is also a very small change in the temperature gradient which may indicate water flow into the borehole.

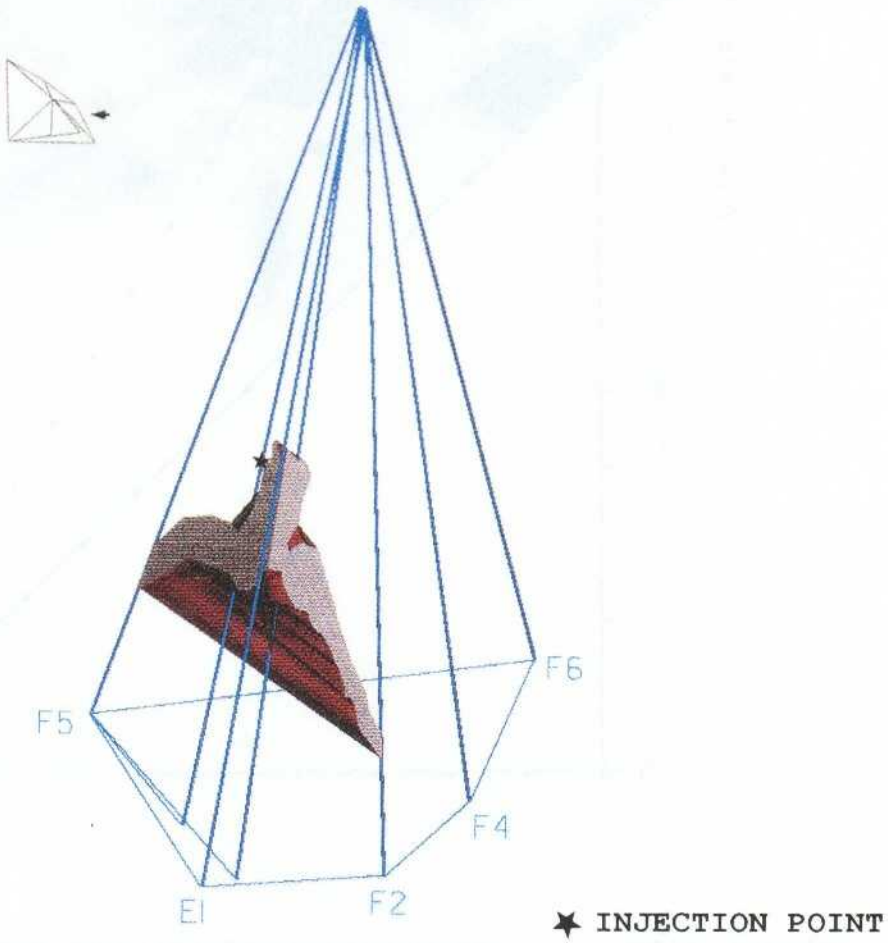

Figure 7.24 The generalized model of the injected saline tracer distribution within Zone X.

The general distribution of the saline tracer within Zone X is presented in two CAD-generated views, Figures 7.24 and 7.25. The two views are produced and visualized with 45 degrees rotation between the two views. The total set of eight CAD-generated views, showing the generalized tracer migration within Zone X, are presented in Appendix 7.4.

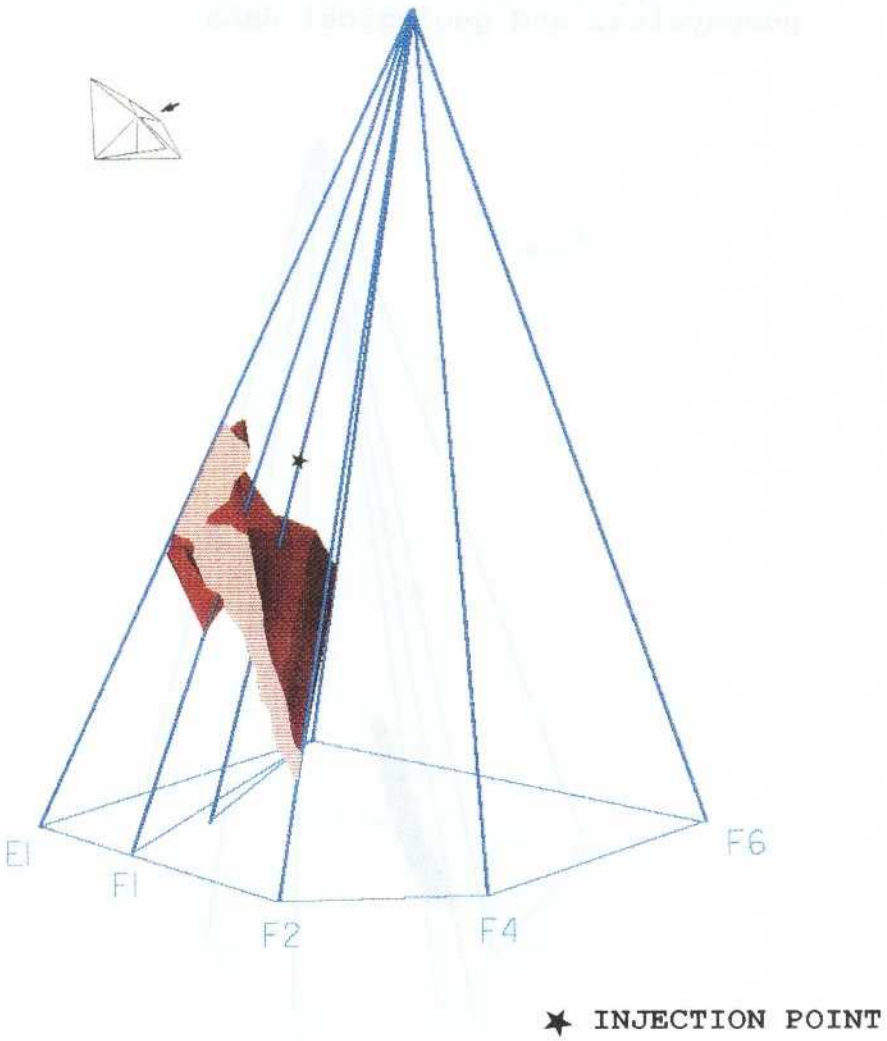

Figure 7.25 The generalized model of the injected saline tracer distribution within Zone X.

Zone Y

There is also a flow path supporting tracer migration from Zone C towards the lower parts of borehole E1. This previously unknown flow path, labelled Zone Y, is extending from Zone C in the E1F4 plane section, Figure 7.18, on the migration path from F3 to borehole F2. Zone Y is extending towards borehole E1, intersecting E1 at about 175-180 meters depth. Zone Y is also partly visible in the F1F6 section, Figure 7.20, intersecting borehole F1 at about 162-170 meter depth.

At about 180 meters depth in borehole E1 there is a distinct change in the salinity and a small change in the temperature gradient indicating a water flow into the borehole (Olsson and Jämtlid, 1984). There is no other supporting information in the other presented geophysical and geological data.

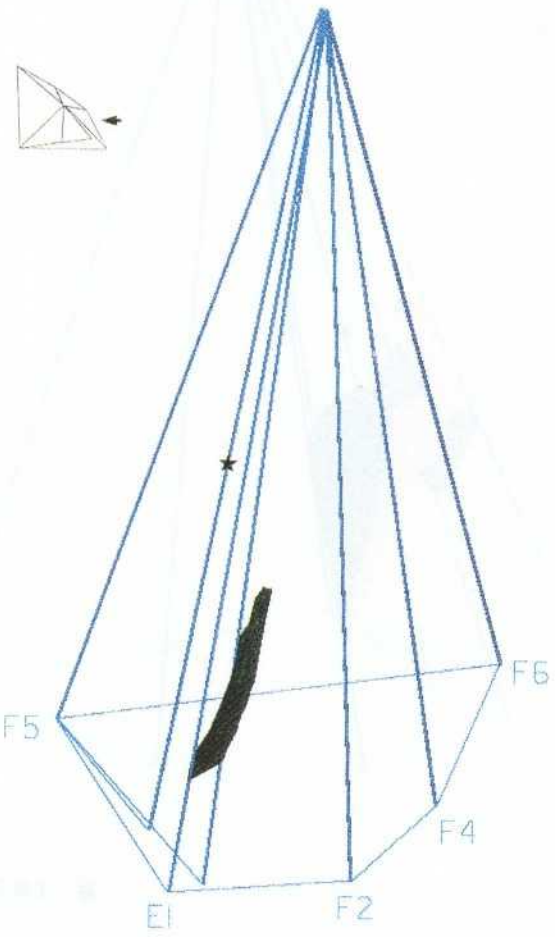

★ INJECTION POINT

Figure 7.26 The generalized model of the injected saline tracer distribution within Zone Y.

For the F1 borehole a fracture zone is interpreted between 163.4-164.2, from the core samples (Carlsten and Stråhle, 1985) followed by a interval (164.25-164.75 meter) with several healed fractures. From the geophysical logs, Carlsten et.al.1985, a distinct change in the temperature gradient was detected in this interval, indicating a water flow into the borehole. As for borehole E1, there is no further supporting information in the other geophysical logs.

The general distribution of the saline tracer within Zone Y is presented in two CAD-generated views, Figures 7.26 and 7.27. The two views are produced and visualized with 45 degrees rotation between the two views. The total set of eight CAD-generated views, showing the generalized tracer migration within Zone Y, are presented in Appendix 7.5.

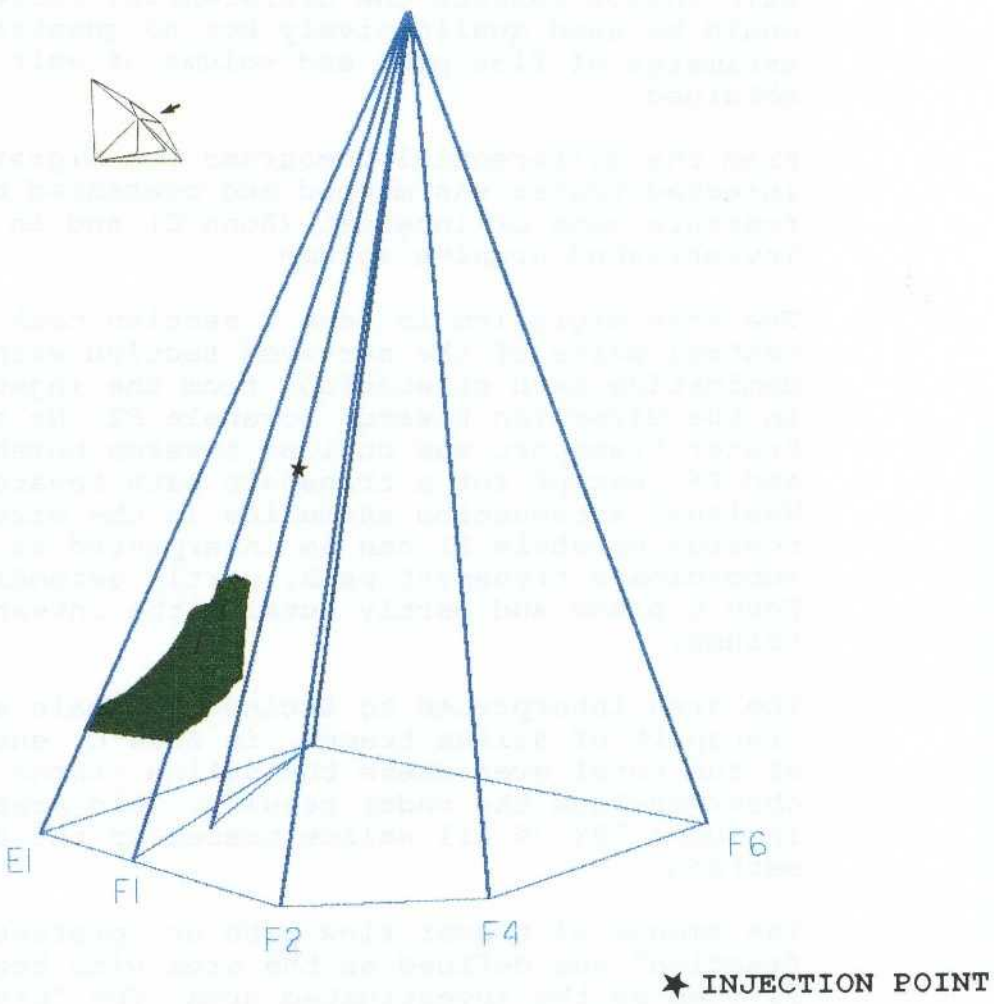

Figure 7.27 The generalized model of the injected saline tracer distribution within Zone Y.

7.4 CONCLUSIONS AND RECOMMENDATIONS

Difference tomography using borehole radar is a valuable and successful method in mapping groundwater flow paths in fractured rock. The presented data are of good quality and sufficiently consistent throughout the investigated rock volume. The interpreted results verified previous findings in the surveyed granite volume as well as contributed to new and unique information.

The radar data is presented both as differential radar reflectograms as well as differential tomograms. The differential radar reflectograms generally do not contain much useful information, which was a negative finding. The most explicit information reveals tracer transport in Zone C mainly in the vicinity of boreholes E1, F1 and F2. In the surroundings of boreholes F4, F5 and F6 no, or hardly no, evidence of tracer migration could be detected. In agreement with tomographic and salt inflow results the differential reflectograms could be used qualitatively but no quantitative estimates of flow path and volume of salt could be obtained.

From the differential tomograms the migration of the injected tracer was mapped and presented both in the fracture zone of interest (Zone C) and in the entire investigated granite volume.

The main migration in Zone C section took place in the central parts of the surveyed section with a dominating path stretching, from the injection point, in the direction towards borehole F2. No or hardly no tracer transport was noticed towards boreholes F4, F5 and F6, except for a transport path towards F5. Residual attenuation anomalies in the direction towards borehole E1 can be interpreted as a subordinate transport path, partly extending outside Zone C plane and partly outside the investigated rock volume.

The area interpreted to include the main and important transport of saline tracer, in Zone C, encompasses 48% of the total area where the saline tracer has been observed from the radar results. This area also includes 78% of all saline tracer in the Zone C section.

The amount of tracer flow path or "preferential flow fraction" was defined as the area with tracer transport divided by the investigated area. The "preferential flow fraction" within Zone C, expressed as percent of surveyed area, in the three studied sections, is in the range 19% to 37%.

From the differential attenuation tomographic 3-D model it is evident that the major tracer migration is spreading from the injection point, in Zone C, towards borehole F2. Only subordinate tracer transport paths were noticed towards boreholes F4, F5 and F6, except for a transport path, within Zone C, towards F5. No or hardly any tracer transport was noticed, in Zone C, towards borehole F1. Two fracture zones originally detected within this project and termed Zone X and Zone Y, were determined to transport portions of the injected tracer.

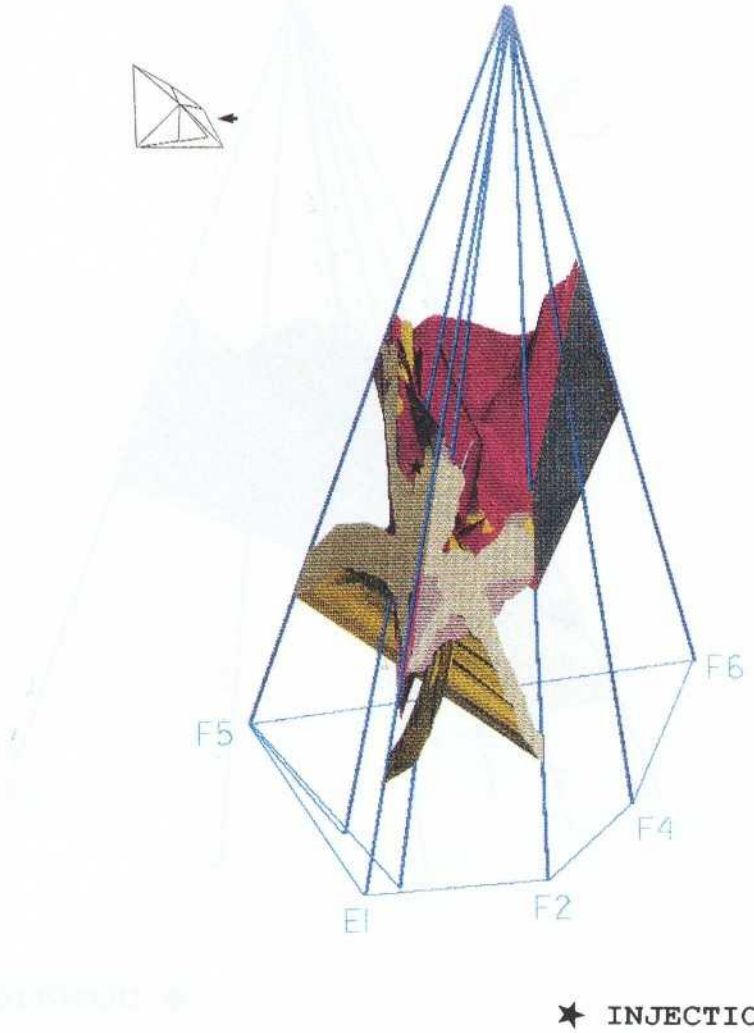

Figure 7.28 The generalized model of the injected saline tracer distribution within the investigated volume in combination with the Zone C model. Yellow colour corresponds to the tracer distribution within the investigated rock volume. Red colour corresponds with the Zone C model.

The model of the general distribution of the saline tracer within the investigated volume is presented in combination with the Zone C model in two CAD-generated views, Figures 7.28 and 7.29. The two views are produced and visualized with 45 degrees rotation between the two views. The total set of six CAD-generated views, showing the generalized tracer migration together with the Zone C model are presented in Appendix 7.6.

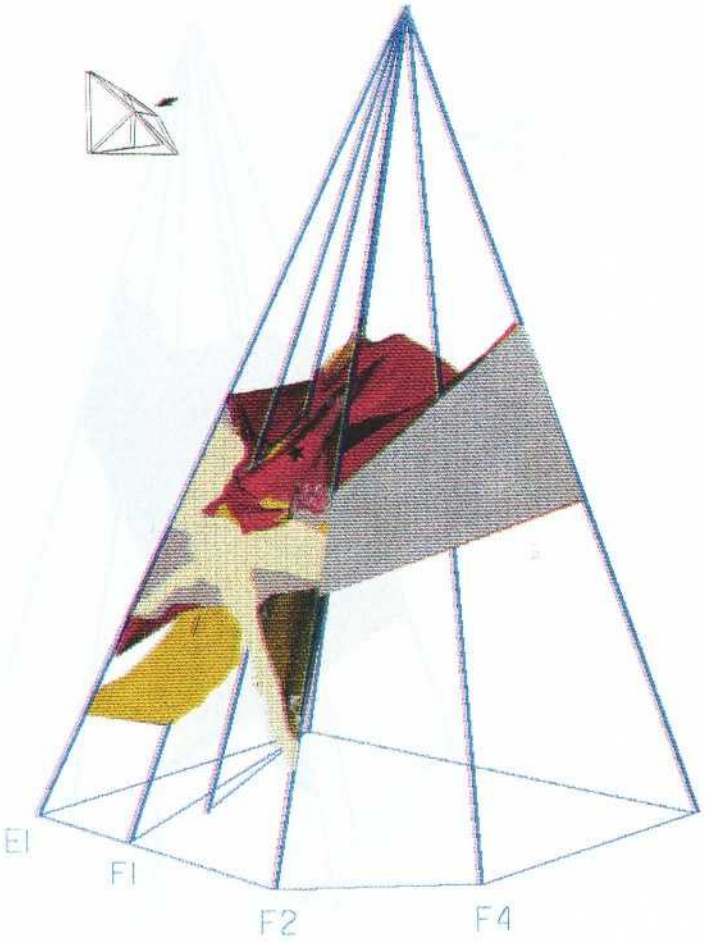

✱ INJECTION POINT

Figure 7.29 The generalized model of the injected saline tracer distribution within the investigated volume in combination with the Zone C model. Yellow colour corresponds to the tracer distribution within the investigated rock volume. Red colour corresponds with the Zone C model.

During the progress of the project results have shown that the planning and performance was, on the whole, executed in an competent and professional manner. Experiences from this project has shown that the concentration of the saline tracer could have been higher than the 0.5% used here. A salt concentration of 1% to 2% would have increased the anomalies of interest, thus simplifying the processing of data and increasing the quality of radar data.

As the boreholes in the investigated volumes were open during the survey the hydraulic connection between major fracture zones, through the open holes, caused complications in the interpretation. For future surveys, of this kind, it is advisable to hinder the hydraulic connection along the boreholes with packers isolating known fracture zones.

8 TRACER MIGRATION

8.1 RESULTS AND INTERPRETATION

8.1.1 Breakthrough curves

The breakthrough of saline tracer was registered in all 6 sampling boreholes. In three of the boreholes, E1, F2, and F5, highly conductive 1-m intervals were isolated with inflatable packers. The breakthrough of saline tracer could therefore be registered with more detail in these intervals and thereby allowing for a better quantitative evaluation of the breakthrough curves. In the remaining three boreholes, F1, F4, and F6, the exact position of the major inflows could not be determined due to the low inflow rates and, in F4 and F6, the low hydraulic head as described in Section 2.4. Consequently, the hydraulic parameters and the transport parameters could only be roughly estimated from the electrical conductivity logging performed in these boreholes.

The breakthrough curves for Bromide in the packed-off intervals of boreholes E1, F2, and F5 are presented in Figure 8.1 as relative concentration C/C_o versus elapsed time. The breakthrough curves seem to reach a steady-state but none of the curves reaches $C/C_o=1$, indicating that dilution with unlabelled water is likely to occur. It should also be noted that the breakthrough in E1 only is registered to 375 hours and in F2 and F5 there is only one measurement point after 375 hours. The straight line between the point at 375 hours and the point at 900 hours is therefore somewhat ambiguous. In addition, the tracer concentration of the water from the whole length of the boreholes flowing out into the drift, after the removal of the packers at 375 hours, was measured (Andersson and Gustafsson, 1988). These breakthrough curves shown in Figure 8.2 indicate that steady-state is reached after about 700 hours of injection.

The breakthrough in boreholes F1, F4, and F6 were registered as electrical conductivity versus time by the intermittent logging with the conductivity probe as described in Section 2.4.2. The resulting breakthrough curves (Figure 8.3) were determined from the measurements of the electrical conductivity by subtracting the background conductivity and dividing with the conductivity of the injected tracer solution, C_o.

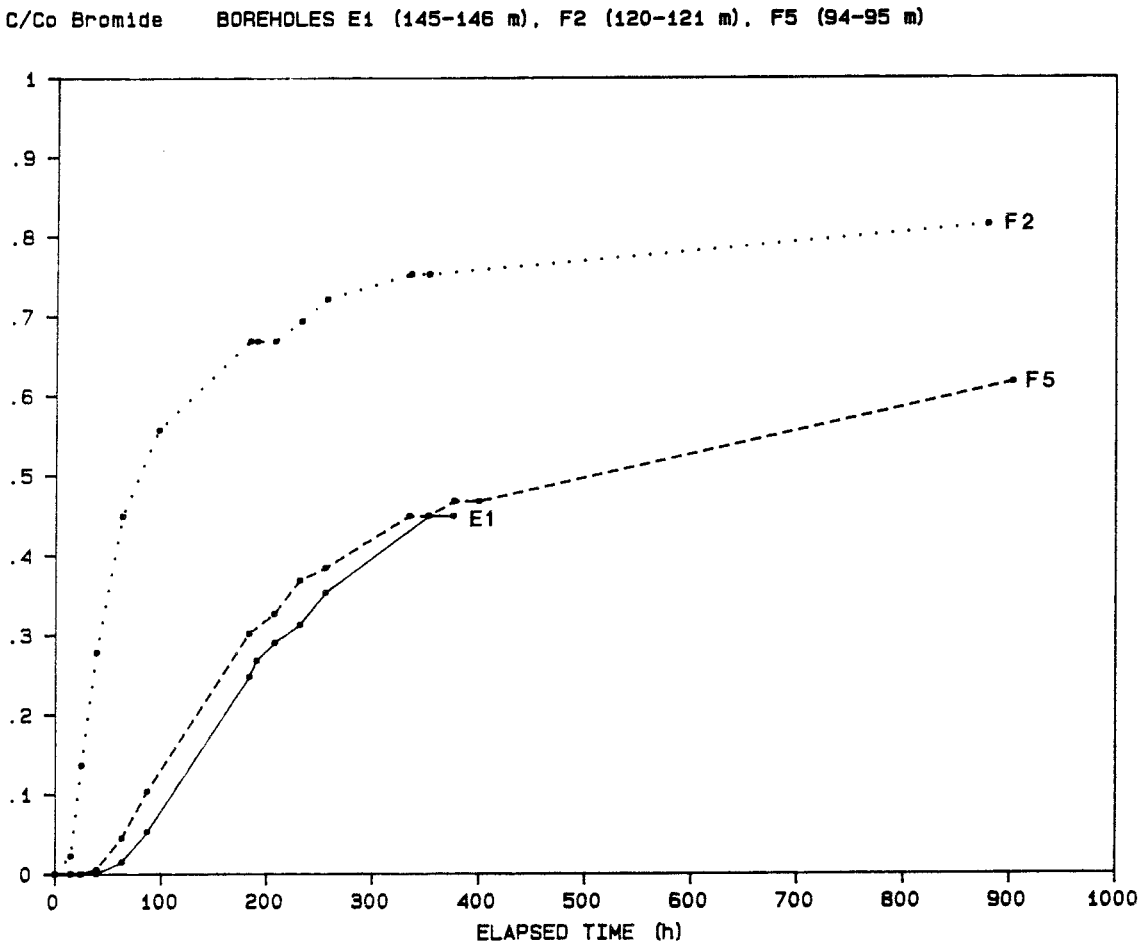

Figure 8.1 Breakthrough curves for Bromide in packed-off intervals of boreholes E1, F2, and F5.

The breakthrough curves show that the tracer reaches all six sampling boreholes with first arrivals, t_a, of less than 200 hours. The fastest breakthrough is recorded in borehole F2 with a first arrival of about 10 hours.

The fast transport to F2 and F5 was expected from earlier hydraulic cross-hole tests in Zone C (Black, Holmes, and Brightman, 1987). Pressure responses were also registered in borehole F4 but no response in F1. In F1, the tracer inflow rate is small and the resulting pressure buildup may therefore have been too low and slow to register.

The results of the evaluation of the breakthrough curves regarding transport parameters and the mass balance calculations are given in Sections 8.2 and 8.3.

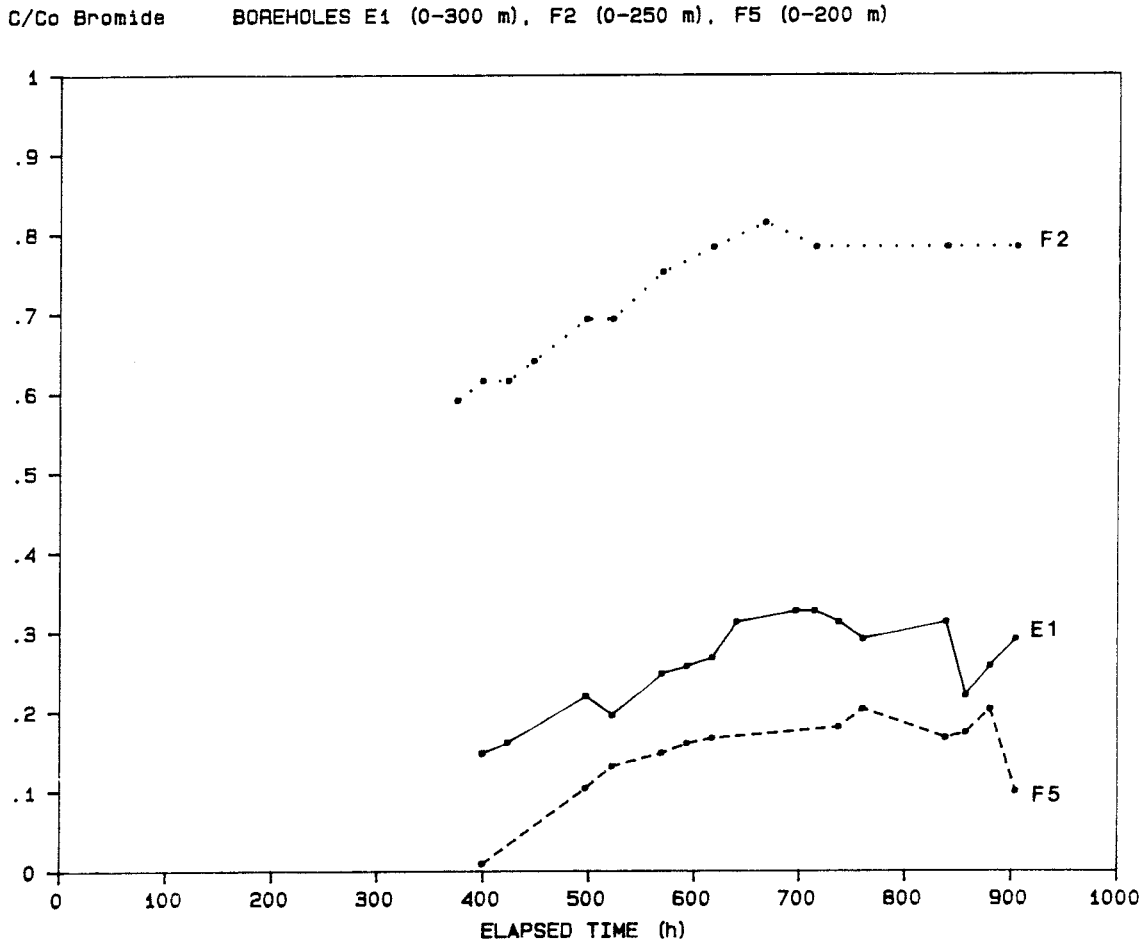

Figure 8.2 Breakthrough curves for Bromide in boreholes E1, F2, and F5

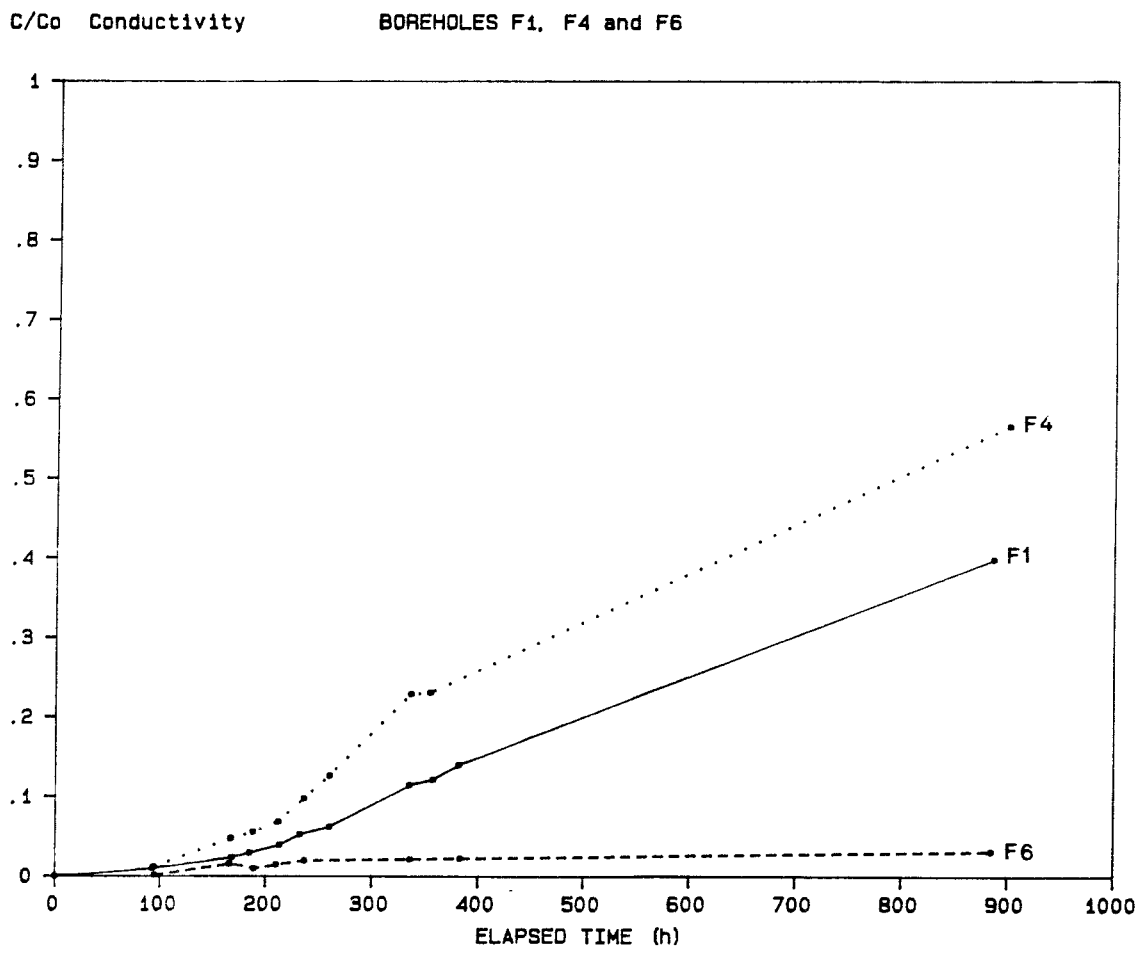

Figure 8.3 Breakthrough curves determined from measurements of the electrical conductivity in boreholes F1, F4, and F6.

The flow distribution within Zone C during the tracer injection was rather complex due to the presence of the open sampling boreholes. The boreholes were kept open in order to perform radar measurements and to maintain the flow distribution during the complete investigation.

The injection of tracer with an excess pressure implies a radially diverging flow, however this flow pattern is heavily disturbed by the presence of the open sampling boreholes. Thus, the flow pattern between the sampling boreholes with high inflow rates and the injection borehole is close to a dipole flow field. In the present evaluation of the experiment, only radial and linear flow assumptions have been used due to this very complex flow pattern with dipole fields overlapping the radially diverging flow field. Figure 8.4 is a schematic illustration of how the flow regime may have looked like during the experiment. Figure 8.4 was made using the SLAEM-code (Strack, 1986) assuming a homogeneous, porous media with a transmissivity of $1.9 \cdot 10^{-7}$ m^2/s and assigning the measured inflow and outflow rates to the boreholes.

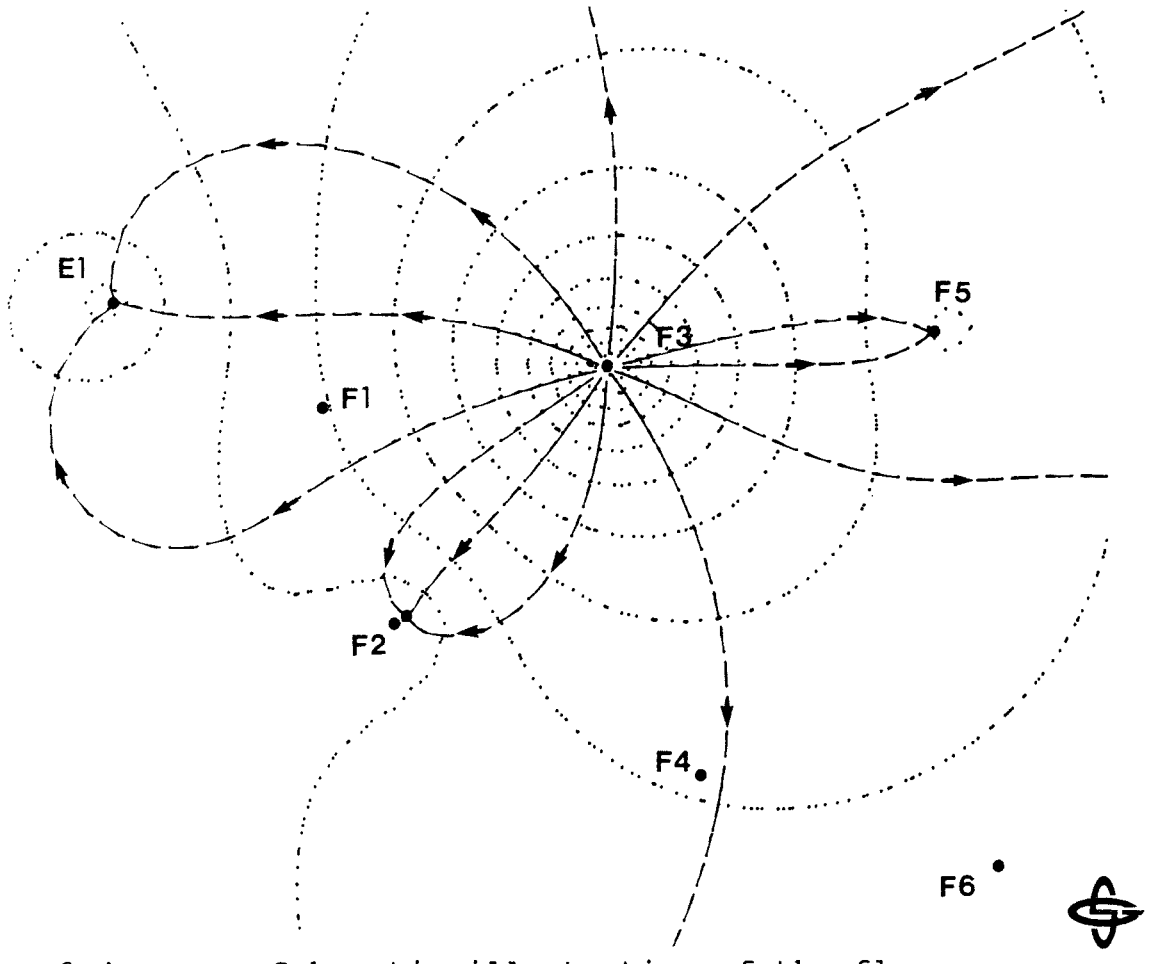

Figure 8.4 Schematic illustration of the flow distribution within Zone C.

The evaluation and interpretation of the breakthrough curves (Figures 8.1, 8.2, and 8.3) was made according to the theories described in section 5.1.

8.1.2 Hydraulic conductivity

The hydraulic conductivity of the injection interval in borehole F3 was calculated according to Equation (5.1) (Moye's formula) to $K=1.3 \cdot 10^{-8}$ m/s or given as Transmissivity, $T=1.9 \cdot 10^{-7}$ m^2/s. This value is somewhat lower compared to the value earlier reported , $T= 7 \cdot 10^{-7}$ m^2/s (Black, Holmes, and Brightman, 1987).

8.1.3 Mean residence times, flow rates, distances and dilution factors

The mean residence times were determined from fits with theoretical solutions to the Advection-Dispersion Equation (5.9) for the three packed-off intervals in boreholes E1, F2, and F5. For the other boreholes, the mean residence time was estimated as the time when C/C_o reaches 50% of the steady-state concentration, C_s. This approach was used as the breakthrough curves never reach $C/C_o = 1$ due to the dilution with water from other water conducting zones and/or from other directions of Zone C. The ratio C_o/C_s is defined as the dilution factor, D and is given in Table 8.1.

The tracer inflow rates, q, were also corrected for the dilution in a similar way. The values of q given below are based on the measured inflow rates except for borehole F4 which is not drained to the drift. The inflow rate was instead calculated from the slope of the breakthrough curve. The mean residence times, inflow rates and the distances between the injection interval and the sampling intervals are given in Table 8.1.

Table 8.1 Mean residence times, t_o, first arrivals, t_a, flow rates, q, injection-sampling distances, r, and dilution factors, D.

Borehole	Interval (m)	t_o (h)	t_a (h)	q (ml/min)	r (m)	D ( )
E1	145-146	370	40	233	53.0	1.44
F1	108-136	500	90	5.2	23.3	2.50
F2	120-121	110	10	211	30.2	1.24
F4	90-140	365	≤100	16	43.3	1.76
F5	94- 95	280	30	74	31.7	1.61
F6	90-140	-	≤150	-	59.4	-

The breakthrough in borehole F6 could not be quantitatively evaluated. However, hydraulic conductivity data (Black, Holmes, and Brightman, 1987) indicates low values for Zone C, which is supported by the low and slow breakthrough of tracer in F6.

8.1.4 Equivalent single fracture conductivity

The equivalent single fracture conductivity, K_{esf} (m/s), was determined in two different ways as described in Section 5.2, using the residence time (K_{esf}^t) and the flow rate (K_{esf}^Q). Both radial and linear flow assumptions were also used to calculate K_{esf}^t (Equations 5.2-5.4).

The equivalent single fracture conductivities are presented in Table 8.2.

Table 8.2 Equivalent single fracture conductivities, K_e^t and K_e^Q (m/s), with radial and linear flow assumptions.

Borehole	Interval (m)	RADIAL K_{esf}^t (m/s)	RADIAL K_{esf}^Q (m/s)	LINEAR K_{esf}^t (m/s)	Remarks
E1	145-146	$1.1 \cdot 10^{-4}$	$3.2 \cdot 10^{-3}$	$3.1 \cdot 10^{-5}$	
F1	108-136	$1.4 \cdot 10^{-5}$	$2.9 \cdot 10^{-3}$	$4.4 \cdot 10^{-6}$	Estimate
F2	120-121	$1.1 \cdot 10^{-4}$	$3.0 \cdot 10^{-3}$	$3.4 \cdot 10^{-5}$	
F4	90-140	$7.4 \cdot 10^{-5}$	$3.1 \cdot 10^{-3}$	$2.1 \cdot 10^{-5}$	Estimate
F5	94- 95	$4.9 \cdot 10^{-5}$	$3.0 \cdot 10^{-3}$	$1.5 \cdot 10^{-5}$	
Mean (E1,F2,F5)		$9.1 \cdot 10^{-5}$	$3.1 \cdot 10^{-3}$	$2.6 \cdot 10^{-5}$	

The mean values in Table 8.2 are only given for the three packed-off intervals in E1, F2, and F5 where good breakthrough data were registered. The values of K_{esf} for F1 and F4 are rough estimates.

There is a difference between the mean values of K_{esf}^{t} and K_{esf}^{Q} with a factor of 30. This difference may be explained by the fact that K_{esf}^{t}, determined from the tracer residence time, represents the volume of the flow paths while K_{esf}^{Q}, determined from the flow rate, represents the narrowest parts of the flow paths. This has earlier been indicated by Andersson and Klockars, 1985, among others. The variation of the K_{esf}^{Q} values is very small which is evident from the definition (Equation 5.3). The only parameter in the expression that varies is the distance between the boreholes. There is also a minor difference (a factor of 3) between the radial and the linear flow assumptions as expected.

Earlier performed cross-hole tests (Black, Holmes, and Brightman, 1987) gave good responses within Zone C in boreholes F2 and F5 when injecting in borehole F3. They also determined the hydraulic diffusivity K/S_s and the apparent "dimension" of the interpretation using the concept of fractal dimensions, see Figure 8.5. In Figure 8.6 are the calculated equivalent single fracture conductivities K_{esf}^{t} presented in a similar way. A comparison between the hydraulic responses and the tracer breakthrough data, here represented by the equivalent single fracture conductivities, indicates that hydraulic cross-hole tests of this kind only can be used to find the fastest flow paths.

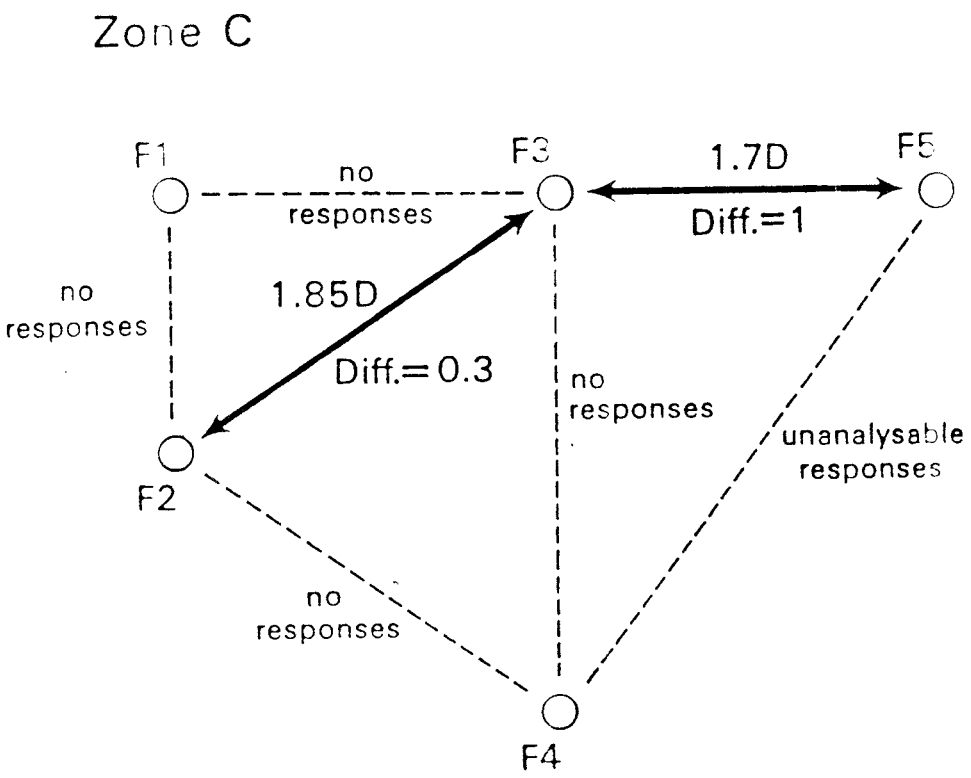

Figure 8.5 Schematic illustration of fractional dimension results shown in relation to borehole layout for Zone C. D is the fractional dimension of the flow and Diff. is the hydraulic diffusivity (m^2/s) (from Black et. al. 1987).

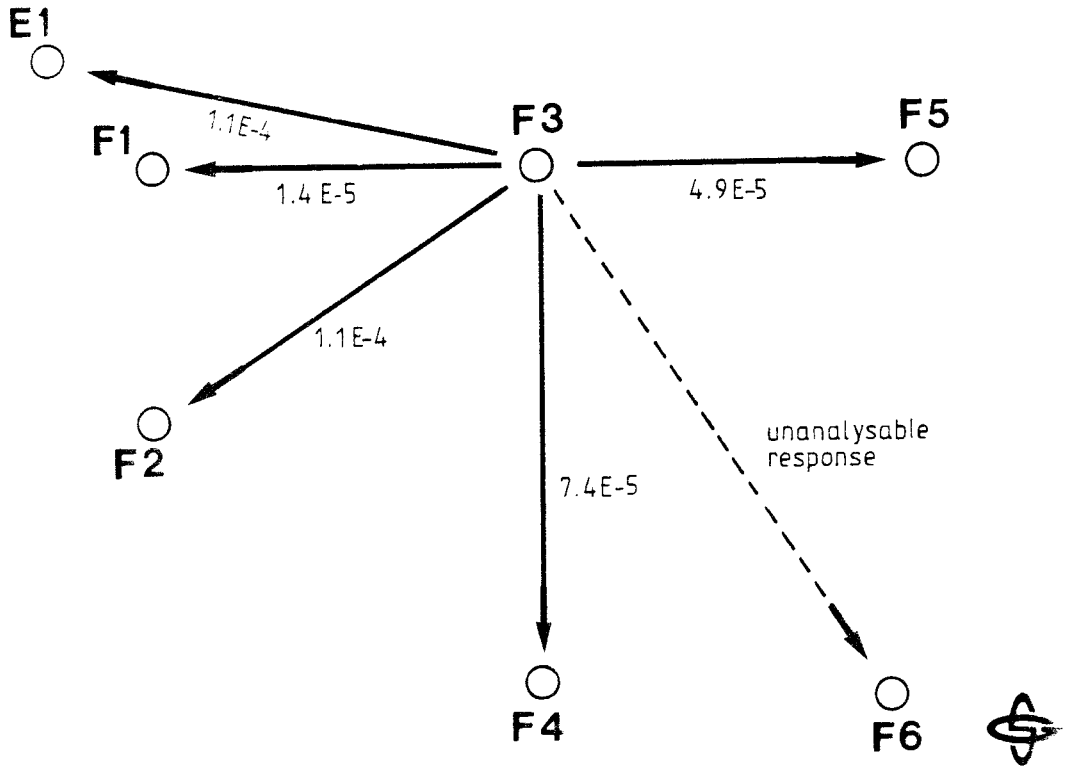

Figure 8.6 Schematic of the equivalent single fracture conductivity distribution (m/s) within Zone C.

8.1.5 Equivalent fracture aperture

The equivalent fracture aperture was calculated using the concept of frictional loss between two parallel plates, e_{esf} (Equation 5.3), with both the residence time (e_{esf}^{t}) and the flow rate (e_{esf}^{Q}) as described in Section 5.1 and also by using the mass balance, e_m (Equation 5.6). The results regarding the transport within Zone C between the injection borehole F3 and the sampling boreholes, presented in Table 8.3, show very large values for the mass balance fracture aperture, e_m, as compared to e_{esf}. This is an effect of the definitions of e_{esf} (Equation 5.5) and e_m (Equation 5.6) assuming a radial and homogeneous flow distribution over the whole fracture surface which definitely not is true in this case.

Table 8.3 Equivalent fracture apertures.

Borehole	Interval (m)	RADIAL e_{esf}^{t} (μm)	RADIAL e_{esf}^{Q} (μm)	RADIAL e_m (μm)	LINEAR e_{esf}^{t} (μm)
E1	145-146	13	71	2010	7
F1	108-136	5	68	14070	3
F2	120-121	13	69	1840	7
F4	90-140	11	71	2970	6
F5	94- 95	9	69	4260	5
Mean values (E1,F2,F5)		12	70	2700	6

8.1.6 Dispersivity

The dispersivity was determined from the fitting procedure of the Advection-Dispersion (AD) model to the experimental data. Only the three packed-off intervals in boreholes E1, F2, and F5 were fitted with theoretical curves (Figure 8.7). The rest of the breakthroughs were not evaluated regarding dispersivity. The results are given both as dispersivity, D/v (m), and Peclet Number, Pe (dimensionless), in Table 8.4 below.

Table 8.4 Dispersivities, D/v, and Peclet Numbers, Pe.

Borehole	Interval (m)	D/v (m)	Pe ( )
E1	145-146	26.5	2.0
F2	120-121	33.2	0.9
F5	94- 95	12.7	2.5
Mean value (E1, F2, F5)		24.1	1.8

The low Peclet numbers are most likely a result of the dipole character of the flow distribution, see Figure 8.4, including a number of different flow paths with different residence times. Rough estimates of the Peclet Number for the transport to F4 was also made using analytical expressions (Gelhar, 1987) resulting in Pe = 17 which, at the distances involved, is a more realistic value of the dispersivity in a radially diverging flow field.

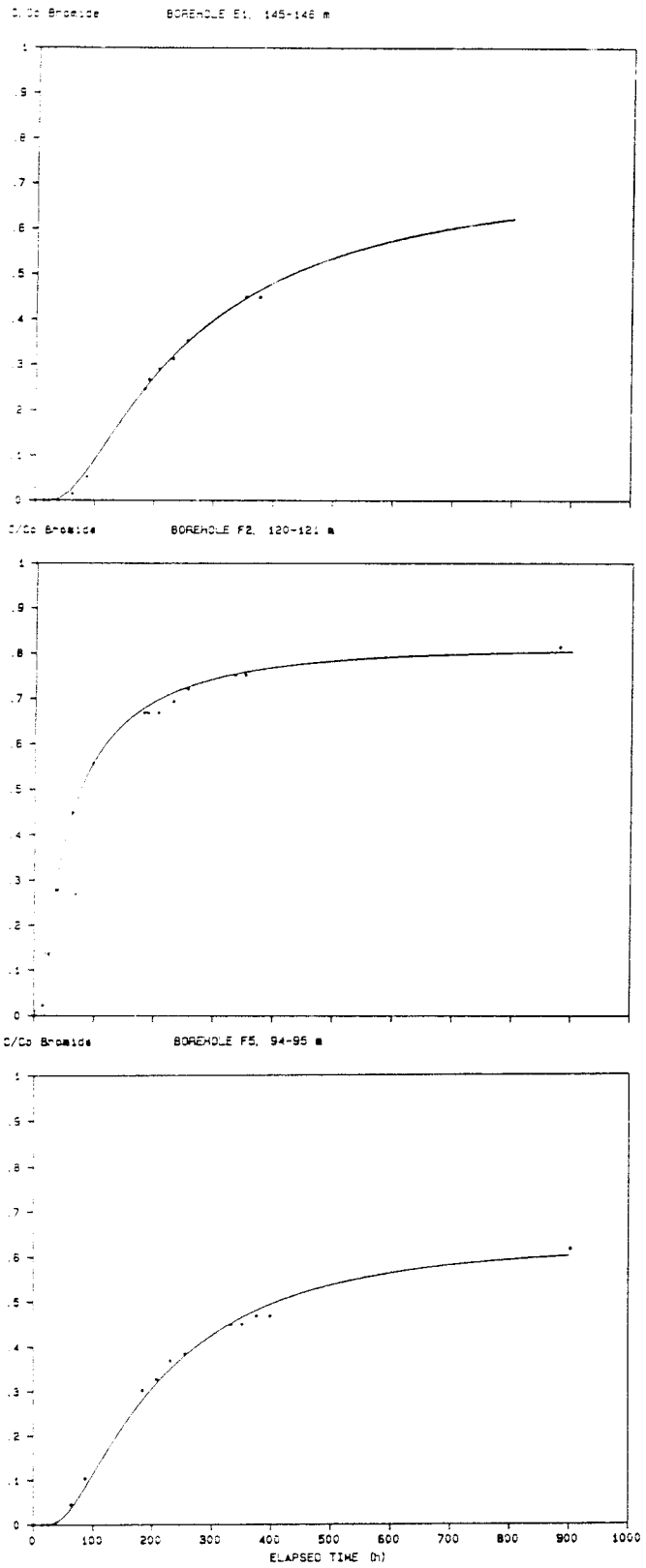

Figure 8.7 Theoretical fits with the AD-model to the experimental data.

8.1.7 Mass balance and recovery

The mass-balance of the injected tracer was determined by means of several different methods. The first approach was to calculate the mass recovery per time unit, R_f from Equation (5.9). This was accomplished in different ways described below depending on the varying kinds of input data available. The second approach was to calculate the total mass recovery at the end of the injection, R. Assuming that steady-state conditions were prevailing, the volume of tracer left in the rock mass may be used to estimate the flow porosity as described in Section 8.2.7.

In boreholes **E1**, **F2**, and **F5**, flow rates and concentrations were measured both in the packed-off intervals and in the water flowing out of the open boreholes. This information together with the logging of the electrical conductivity, which was performed towards the end of the injection (Phase 4), made it possible to estimate the mass balance within these boreholes. The electrical conductivity log also indicated possible tracer inflow locations to the boreholes.

In borehole **F1**, the mass balance was determined from the flow rate and concentration measured in the water flowing out of the borehole together with the inflow measurements performed prior to the injection of saline tracer.

In the non-flowing borehole **F4**, R_f was determined from the calculated inflow rate in combination with the electrical conductivity log. Finally, in borehole **F6**, no quantitative calculations could be made due to the low inflow rates in combination with the low hydraulic head.

In Table 8.5 the mass-balance calculations are summarized for all the boreholes. The calculations presented are based on the measured electrical conductivity. The same calculations were also performed based on the Bromide data showing no significant differences. The total mass recovery per time unit (R_f) was 74.1 % for the conductivity data and 77.6 % for the Bromide data. Values without brackets are measured values and values within brackets are calculated values. All values are given as % of the total injected mass per time unit ($Q \cdot C_o$).

An example of the electrical conductivity log versus depth for borehole F4 is presented in Figure 8.8. The interpretations of tracer inflow positions and flow directions within the borehole are also given. The logs for all boreholes are presented in Appendix 6.

Table 8.5 Summary of the mass recovery per time unit, R_f (%), and the indications of tracer inflows in the sampling boreholes.

Borehole	Interval (m)	Geophys. unit	R_f (%)
E1	115-120		*
	126-129	C	*
	145-146	C	16.4
	185		(8.5)
	0-300		24.9
F1	116-139	C,D	(0.5)
	190	E	*
	0-200		0.5
F2	44- 48	A	(-13.4)
	120-121	C	28.0
	200-220	E,F	(8.5)
	0-250		23.1
F3	103.5-117.5	C	100.0 (INJ.)
	118.5-200		0.9
F4	50	A	
	103	C	
	130		(2.0)
	200	D	
	50-250		(2.0)
F5	94- 95	C	9.3
	104	D	*
	138-146	E	*
	0-200		9.3
F6	65	A	*
	105	C	*
	200-220		*

* = Indication from the conductivity log.
( ) Values calculated from the mass-balance of each borehole.

Comments regarding the interpretations are given for each borehole below.

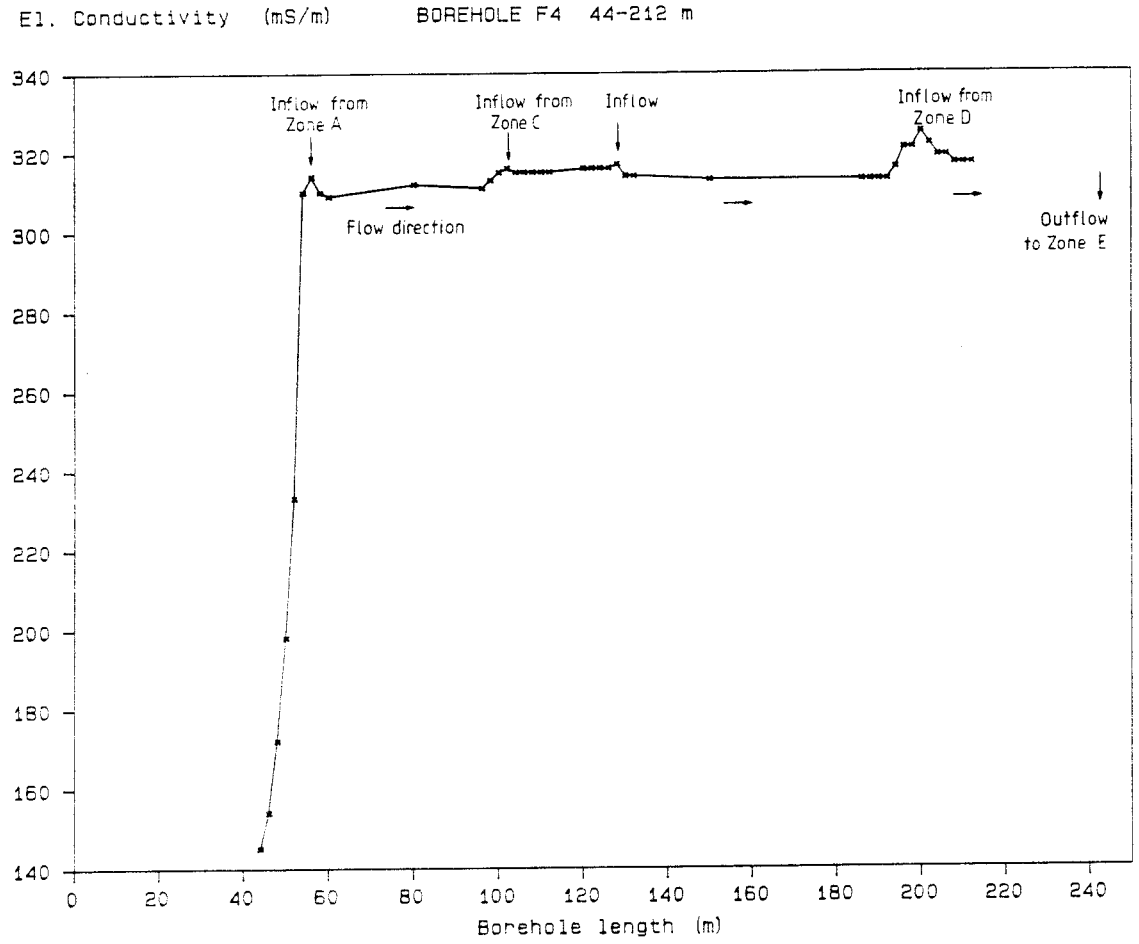

Figure 8.8 Electrical conductivity log versus depth for borehole F4 (after 900 hours of injection).

Borehole E1: The major inflow is located to the packed-off interval, 145-146 m in Zone C, but this inflow does not account for the total inflow to the borehole. The electrical conductivity log (Appendix 6) indicates an increased conductivity around 180-185 m corresponding to a highly conductive structure also indicated by geophysical measurements (Carlsson and Olsson, 1985; Olsson and Jämtlid, 1984). This structure most likely accounts for the rest of the tracer inflow to E1. Minor inflows are also indicated by the electrical conductivity log at 115-120 m and 126-129 m. The interval 126-127 m was also found to be flowing during the calibration measurements (see Section 2.4.2) but when both this interval and the major inflow at 145-146 m was simultaneously packed-off for sampling, no inflow could be registered after a couple of minutes. This indicates that there is a good hydraulic connection between these flow paths.

Borehole F1: The inflow measurements indicated several small inflows (totally 0.5 % of the injected mass per time unit) distributed within the interval 116-139 m corresponding to Zones C and D. There is also an indication from the conductivity log of inflow from Zone E, at about 190 m depth.

Borehole F2: The mass-balance of F2 is more complex due to the highly conductive Zone A at 44-48 m depth. The mass per time unit entering the borehole in the packed-off interval at 120-121 m is larger than the mass flowing out of the open borehole. Thus, a part of the tracer mass is most likely flowing from the open borehole into Zone A. This is also strongly supported by the conductivity log (Appendix 6). The log also indicates tracer inflow at the highly conductive Zones E and F at about 200-220 m depth. An estimate of the mass entering F2 at 200-220 m was made from the transmissivity value of the interval and the electrical conductivity values from the conductivity log (Appendix 6). From this, also the mass per time unit entering Zone A could be estimated to 13.4 % of the total mass injected.

Borehole F3: In the interval behind the inner packer, a small portion, 0.9 %, of the injected mass per time unit was recovered. This figure is a maximum figure assuming that all of the water leaking from this interval is undiluted tracer solution. No leakage was registered around the upper packer.

Borehole F4: The mass-balance of F4 was determined from the calculated inflow to the borehole and the conductivity log, see Figure 8.8. There are indications of tracer inflow at about 50 m corresponding to Zone A which could be the tracer entering Zone A in borehole F2. The hydraulic connection in Zone A between F2 and F4 has earlier been found to be very strong (Black, Holmes, and Brightman, 1987) and the hydraulic head is higher in F2 than in F4 which supports the indication of tracer transport. There are also indications of tracer inflow at 103, 130, and 200 m corresponding to Zones C and D. The hydraulic head and conductivity distribution within the borehole suggests that there is a transport towards the highly conductive Zone E at the end of the borehole.

Borehole F5: The main tracer inflow to this borehole is in the packed-off interval at 94-95 m accounting for 9.3 % of the total injected mass per time unit. There are indications of minor inflows at 104 m (Zone D) and 138-146 m (Zone E).

Borehole F6: No quantitative evaluation of the mass recovery could be made but the low conductivity values measured during the logging indicate that very small

amounts of tracer reaches the borehole. The transport within the borehole is most likely directed towards the highly conductive interval at 205-231 m which also has a very low hydraulic head (Black, Holmes, and Brightman, 1987). In this interval there is also a peak in the electrical conductivity indicating tracer inflow. There are also minor indications at 65 m (Zone A) and 105 m (Zone C).

The total mass recovery was calculated using the Bromide breakthrough data in combination with the electrical conductivity data for the non-flowing boreholes (F4 and F6). The recovery presented in Table 8.6 as % of the total mass injected also includes the mass remaining in the borehole volumes.

Table 8.6 Total recovery of tracer in the sampling boreholes.

Borehole	Recovery (%)	
E1	14.5	
F1	1.0	
F2	41.0	(of which 12.3% is lost into Zone A)
F4	2.0	
F5	7.4	
F6	-	(estimated to less than 1%)
Total Recovery:	65.9%	

The total mass recovery of 65.9 % given above implies that 34 % of the totally 139.5 kg of Bromide is remaining within Zone C and in flow paths connected to other zones, or given as volume of C_o, 14.7 m^3.

8.1.8 Flow porosity

The flow porosity was calculated as the ratio of the volume of moving water and the total volume of the rock mass according to Equation (5.11) The porosity values presented in Table 8.7 were calculated using L = 14.5 m, i.e over the whole thickness of Zone C.

Table 8.7 Flow porosities, Φ_k, in Zone C (14.5 m thickness)

Borehole	Φ_k	
E1	$1.4 \cdot 10^{-4}$	
F1	$9.7 \cdot 10^{-4}$	
F2	$1.3 \cdot 10^{-4}$	
F4	$2.1 \cdot 10^{-4}$	
F5	$2.9 \cdot 10^{-4}$	
Mean value	$1.9 \cdot 10^{-4}$	(E1, F2, and F5)

A comparison with flow porosities determined from other tracer experiments in the Stripa mine show that the values presented in Table 8.7 are somewhat higher. Porosity values determined in the Stripa 3-D experiment (Abelin, Birgersson, Gidlund, Moreno, Neretnieks, Widén, and Ågren, 1987) were ranging between 0.2-$1.5 \cdot 10^{-4}$ with a mean value of $0.6 \cdot 10^{-4}$ and in the small-scale experiments at the SGAB tracer test site (Andersson and Klockars, 1985) it was $0.7 \cdot 10^{-4}$ (mean value). However, both previous experiments were made in low conductive parts of the Stripa granite whereas this experiment was performed in a defined fracture zone with 1-2 orders of magnitude higher transmissivity values.

An estimate of the flow porosity can also be made based on the volume of the tracer solution remaining in the fractures at injection stop:

$$\Phi_k = V_w / V_r \qquad (8.1)$$

where V_w is the measured volume of tracer solution remaining in the fractures and V_r is the volume of rock where the tracer has been injected.

According to the calculations of the recovery (Section 8.2.6) a total amount of 14.7 m^3 (as volume of C_o) is remaining within Zone C and in flow paths connected to other zones. If only the recovery from flow paths within Zone C is considered (see Table 8.5), a total amount of 7.9 m^3 remains in the zone after injection stop. Assuming that the rock volume is a circular slice around the injection interval with a radius of 60 metres and a thickness of 14.5 meters, which is the length of the injection interval, then $\Phi_k = 1.9 \cdot 10^{-4}$. The choice of 60 metres is based on the mean transport times to the different boreholes. This flow porosity based on the recovery of tracer compares very well with

the values determined from Equation (5.11) (see Table (8.7).

8.2 CONCLUSIONS AND RECOMMENDATIONS

8.2.1 Flow distribution

The flow distribution within Zone C, based on the tracer breakthrough, is strongly governed by the open boreholes. The very high recovery of about 75 % (as mass per time unit) implies that the open boreholes are draining Zone C effectively. This should be compared to the mantle area which the boreholes cover in relation to the total mantle area of the injection, which is only 0.2 %. Thus, in a closed, homogeneous and isotropic system the recovery should have been within this order of magnitude.

However, the flow is not homogeneously distributed within Zone C. There seems to be three very distinct and fast flow paths between the injection interval in F3 and narrow, less than 1 metre thick, intervals in boreholes E1, F2, and F5, Figure 8.1. These three flow paths together have a recovery of 54 % (as mass per time unit). Tracer breakthroughs were also registered in the remaining three boreholes, F1, F4 and F6, Figure 8.2, but with lower inflow rates and later first arrivals. In these boreholes, no distinct and well defined inflow interval could be detected, in the case of F4 and F6 partly because of the low hydraulic head in these boreholes.

Most of the transport takes place within Zone C but there are also clear indications of transport to adjacent zones. Especially in the previously interpreted D, E and F-zones (Carlsten, Magnusson, and Olsson, 1985) and in the X and Y-zones interpreted in this investigation (see Section 7.3.2). The recovery of tracer within the borehole intervals outside Zone C was calculated from the mass balance of each borehole to a total amount of 18 % (as mass per time unit).

The transport of saline water along the boreholes are also important to consider in the evaluation of possible flow paths. The open boreholes acts as short-circuits between different zones and may allow tracer transport between the zones depending on the distribution of hydraulic heads and hydraulic conductivities along the boreholes. From the logging of the electrical conductivity, the mass-balance and the hydraulic conductivity and head distribution, the flow pattern along the boreholes could be determined, see section 8.2 and Appendix 6. The results indicate that tracer is transported to the previously

interpreted A-zone through borehole F2 and then through the A-zone to boreholes F4 and F6 whereas there are no indications of transport from Zone C to Zone A within the rock mass, based on the radar measurements. There are also indications of transport along boreholes F4 and F6 towards the highly conductive and low head zones E and F.

8.2.2 Flow and transport parameters of Zone C

The complexity of the flow distribution prevailing within Zone C, see Section 8.2, makes it difficult to perform an unambiguous evaluation of the transport parameters of the zone. Within the frames of this project, only a simplified analytical evaluation, stating a radially diverging or linear flow field in a homogeneous and isotropic aquifer, has been applied.

For the three dominating flow paths, from F3 to E1, F2, and F5 respectively, high inflow rates were measured in the sampling intervals. These boreholes are obviously located within highly conductive parts of Zone C. The tracer concentration in the highly conductive intervals never reaches the injection concentration during the injection/sampling period of 900 hours. However, the breakthrough curves (Figures 8.1 and 8.2) seems to reach a steady state after about 700 hours indicating mixing with unlabelled water from Zone C.

The mean residence times determined from fits with a one-dimensional Advection-Dispersion model (t_o = 110-500 hours) are affected by the dipole character of the flow distribution, e.g. the mean residence time of 110 hours for F2, 120-121 m, while the tracer first arrival corresponding to the major flow path is only 10 hours. The mean residence times are then used in the calculations of equivalent single fracture conductivities, K_{esf}^t and apertures, e_{esf}^t, thus probably underestimating these parameters. This dipole character will also result in unrealistically high dispersivity values (D/v = 13-27 m) caused by the transport in many flow paths.

The two ways of determining the flow porosity of Zone C gave very similar values; $1.9 \cdot 10^{-4}$ from the calculations of tracer volume left in the bedrock, and the same mean value calculated from the injected volume of tracer, assuming a thickness of 14.5 m for Zone C.

8.3.3 Recommendations

The major problem regarding the evaluation of the tracer migration experiment is the effects of the open boreholes earlier discussed. At the time of the experiment the borehole radar could not be operated in packed-off boreholes. However, developments of the method are in progress which makes it possible to perform radar measurements in packed-off boreholes. For future investigations of this kind it is therefore recommended to pack-off the sampling boreholes in order to maintain "natural" head and flow conditions. The tracer breakthrough then has to be registered in situ, i.e. without removing any samples from the boreholes.

The complexity of the flow distribution within the investigated rock volume makes it difficult to evaluate transport parameters with simple one-dimensional models. It is therefore recommended that two- or three dimensional modelling is used, incorporating all hydraulic parameters, boundaries etc. known.

9 INTEGRATED INTERPRETATION

9.1 COMPARISON OF RADAR AND TRACER MIGRATION RESULTS

The combination of the radar method and the conventional tracer migration experiment made it possible to compare the radar interpretation of the groundwater flow paths with the actual breakthrough locations of the tracer. Analysis of tracer breakthrough data has confirmed the radar interpretations both regarding the flow path distribution within Zone C and regarding the spreading of tracer to other zones within the surveyed rock volume. In addition, the calculations of tracer mass balance and recovery in the sampling boreholes have made it possible to identify flow paths outside the radar investigated domain.

The interpretation of the data was complicated by the transport of salt tracer along borehole F2. The salt tracer was transported from zone C along borehole F2 and into Zone A. As Zone A was not included in the radar investigated volume, the transport within zone A could only be detected from analysis of the tracer breakthrough data. Tracer breakthrough data (Table 8.5) also show that saline tracer enters boreholes F1 and F2 through zones E and F which are outside of the radar investigated volume where they intersect these boreholes.

Presented below is an analysis of the agreement (and disagreement) between radar interpretation and tracer breakthrough data within the investigated rock volume. The comparisons have been made for the three zones, C, X and Y where both radar measurements and tracer breakthrough measurements has been performed. Tracer breakthrough outside the rock volume investigated by radar is discussed in section 8.2. The combined interpretations are presented in Figures 9.1 to 9.2 and Appendix 5 combining radar difference attenuation tomograms with the tracer breakthrough data.

Zone C

The main tracer migration in Zone C, as seen from the radar results, is in the central parts of Zone C with a dominating path extending, from the injection point, in borehole F3, in the direction towards borehole F2. The radar measurements showed that the main migration path intersected borehole F2 at a depth of 120-125 meter, see Figure 9.1. The radar interpretation is in agreement with the fast tracer breakthrough results (t_o=110 h, t_a=10 h) and the high mass recovery (R_f=28%) recorded in the 120-121 meter interval in F2.

The major flow path, towards borehole F2, also extends in the opposite direction through the E1F5 plane out of the investigated volume. This outflow of tracer from the investigated part of Zone C is interpreted to migrate back into the measured rock volume towards boreholes F5 and E1, as discussed below.

The radar results show two migration paths extending from the injection point in borehole F3 towards borehole F5. These paths are seen in the F5F2 and F5E1 tomographic sections, Figures 9.1 and 9.2, while the tomographic section F5F1, situated between these two sections, show no evidence of transport towards borehole F5. This indicates that there is a region between boreholes F5 and F3 which is impermeable.

The tracer inflow data show that there is a relatively large inflow in the interval 94-95 meter in borehole F5 with a high mass recovery (R_f=9.3%). The radar data show two migration paths towards F5 but the magnitude of these anomalies is moderate, and hence the volume of salt tracer, which would lead us to expect a smaller mass recovery in F5 than was actually observed. However, the differential radar maps of Zone C (Figures 7.6-7.8) indicate that only a minor portion is seen of the transport path from borehole F3 to borehole F5 which roughly follows the E1F5 plane. It is therefore likely that a substantial part of the flow towards F5 takes place outside of the investigated part of Zone C. Transport out of the investigated volume and back to borehole F5 is also to be expected from the dipole character of the hydraulic potentials as illustrated by Figure 8.4.

Another possible explanation of high recovery rates and radar anomalies of moderate magnitude is that the tracer between the injection point and borehole F5 is transported through a very thin high-conductive single fracture. The amount of saline tracer in a thin high-conductive fracture will cause only small increases in attenuation of the radar rays traversing the fracture. In comparison, a major fracture zone comprised of numerous single fractures will contain sufficient quantities of saline tracer to cause large attenuation of the traversing radar rays. To explain the high mass recovery in borehole F5 (R_f=9.3%), the tracer flow in a thin single fracture must be exceptionally high and rapid. A comparison of the tracer breakthrough data from borehole F5 and borehole F2 (the major migration path) reveals roughly the same transport velocities indicating that the tracer migration towards borehole F5 is not supported through a thin single fracture.

Hence, the conclusion is that the tracer transport to borehole F5 follows the two migration paths indicated by the radar data and that a large portion of the

transport follows the transport path that goes out of the investigated volume.

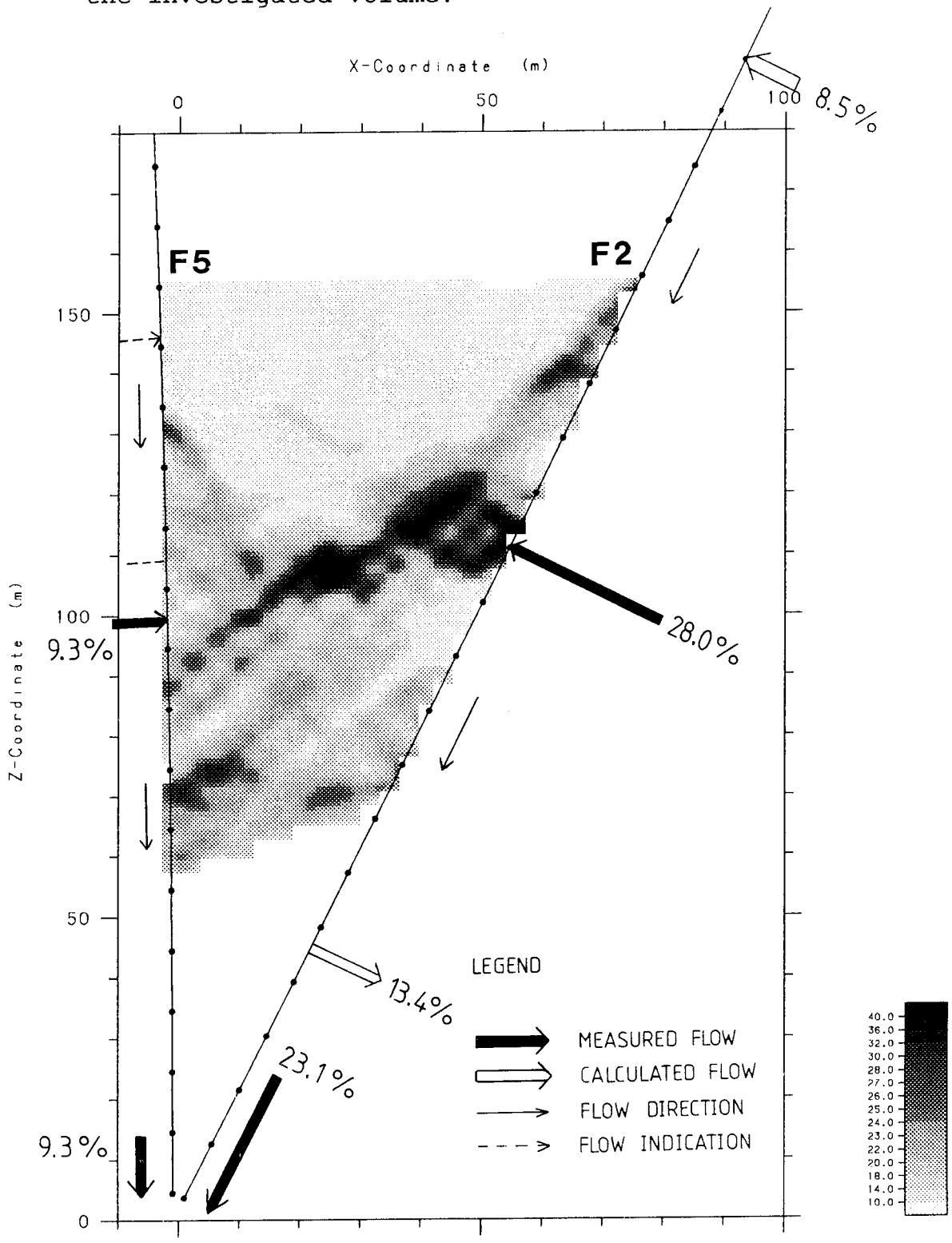

Figure 9.1 Radar difference attenuation tomogram for section F5F2 combined with tracer breakthrough data. Location of tracer breakthrough and flow direction are marked with arrows. Numbers are referring to the recovery, R_f (%).

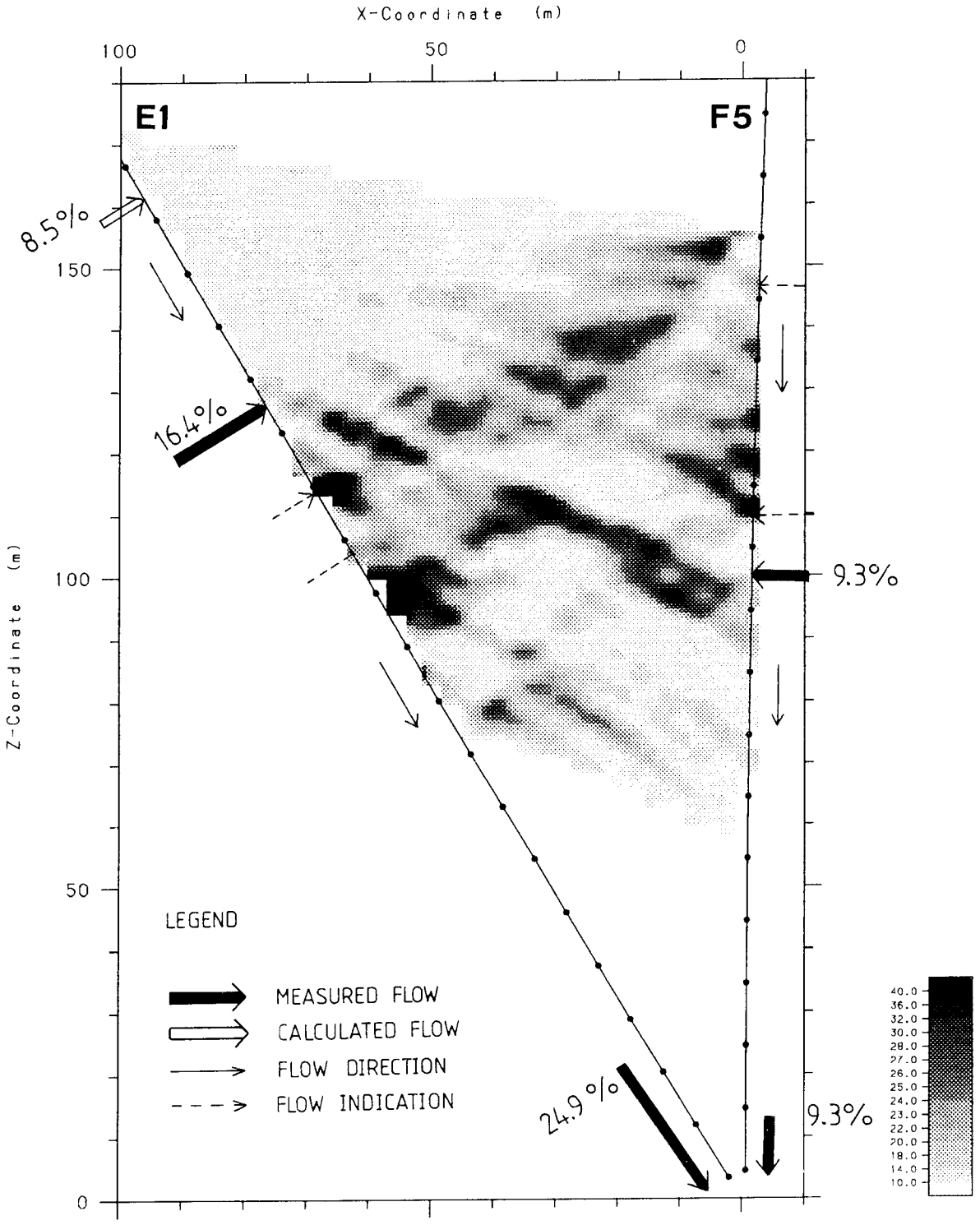

Figure 9.2 Radar difference attenuation tomogram for section F5E1 combined with tracer breakthrough data. Location of tracer breakthrough and flow direction are marked with arrows. Numbers are referring to the recovery, R_f (%).

From the radar results a tracer migration path towards borehole E1 is seen in the F2E1-section. In the E1F4-tomogram there is no sign of saline migration and in the F5E1-tomogram only a weak indication of a saline transport path is visible. Also, the radar results from the Zone C plane (Figure 7.6), shows no obvious and consistent migration path between boreholes F3 and E1. Tracer inflow data show a relatively large inflow at the interval 145-146 meter in borehole E1, with a high mass recovery (R_f=16.4%).

The discrepancy in the recorded high inflow of saline tracer in borehole E1 and the radar results which only indicate a minor migration path towards borehole E1 (see Figure 9.2) can, as for borehole F5, be explained in two ways; migration through a thin high-conductive single fracture or migration from the injection point towards borehole E1 traversing partly outside the measured rock volume. Also in this case tracer transport through a very thin high-conductive single fracture is interpreted to be unrealistic in the same way as for borehole F5. A comparison of the tracer breakthrough data from borehole E1 and borehole F2 (the major migration path), as well as borehole F5, reveals roughly the same transport velocities. This indicates that the tracer migration towards borehole E1 follows the flow pattern roughly outlined in Figure 8.4, caused by the dipole character of the hydraulic conditions and that transport is partly outside the measured rock volume.

A consequence of the dipole flow pattern is that one migration path extends from the injection point, close to borehole F2 towards borehole E1. This migration path towards borehole E1 extends partly outside the investigated rock volume and causes the inconsistent pattern of the recorded radar anomalies, see Figure 7.6. Also, the major flow path extending in the opposite direction of borehole F2 out of the investigated volume is migrating back into the measured rock volume partly towards borehole E1. This migration path towards borehole E1, partly outside the measured volume, is to some extent supported by the radar results in borehole section E1F5 (Figure 7.6).

An important result from the radar data is that no tracer migration in Zone C is observed in the vicinity of borehole F1. This is in agreement with the tracer inflow data which show an exceptionally low tracer inflow to borehole F1 and a very low mass recovery (R_f=0.5%) The flow rate was established to 5.2 ml/min which was the lowest of all the measured boreholes. These findings, with no tracer migration in Zone C towards borehole F1 is also in agreement with previous findings by Black, Holmes, and Brightman, 1987.

The radar results show only a minor transport path towards boreholes F4 and F6 which appears to be located in the upper part of Zone C (i.e. it is only seen in Figure 7.8). This is in agreement with the inflow and breakthrough results which show low mass recovery and relatively long mean residence times.

The active injection interval in borehole F3, i.e. the interval with significant out-flow of saline tracer was interpreted to be between 107-111 m from the radar measurements. Inflow measurements performed during the calibration phase supports this interpretation. The major "natural inflows" were found in the interval 106-108 m and minor inflows were registered in the interval 108-113 m. The radar interpretation is further supported by cross-hole hydraulic tests performed by Black, Holmes, and Brightman, 1987. They monitored hydraulic responses in boreholes F2 and F5 during injection of water in the intervals 103-106 m, 107-109 m and 110-116 m in borehole F3, the latter interval only gave a very weak response in borehole F5, see also Figure 8.5.

Zone X

A new fracture zone was detected within this project and was found to transport portions of the injected tracer. This fracture zone, termed Zone X, intersects boreholes E1, F1, F2 and F5 within the investigated granite volume. Zone X, which intersects Zone C with an angle of 80°-90°, intersects E1 at about 125-130 meter, F1 at about 130-140 meter, F2 at about 165-175 meter, and F5 at about 155-165 meter borehole depth, see Section 7.3.2. Zone X has an orientation (dip 55° and strike 10°) similar to that of Zone A which indicates that it could be part of the same fracture system as Zone A.

The radar interpretation of tracer transport within Zone X is strongly supported by the inflow measurements performed during the calibration phase. In borehole E1, the interval 126-127 m borehole depth was found to be flowing with 23 ml/min which was the fourth largest inflow rate registered of the 139 intervals measured. This interval together with the major inflow at 145-146 m (Zone C) was then simultaneously packed off during the tracer injection (Phase 2) resulting in no flow at 126-127 m. These observations indicate that Zone X (126-127 m) has a good hydraulic connection with Zone C (145-146 m) and thus supports the interpretation that tracer is transported through Zone X.

In borehole F1 there are indications of tracer inflow in the interval 130-140 m (Table 8.6 and Appendix 6).

This interval is also the most highly conductive in the borehole according to Black et al., 1987. These facts also support the radar interpretation of transport within Zone X.

No inflow measurements were made at the intersections of Zone X with boreholes F2 and F5, However, the conductivity logging (Phase 4) indicates a slight increase in the salinity between 160-180 m in borehole F2 and in borehole F5 there is a distinct drop in the salinity at 154 m, see Appendix 6, which is an indication of water movement. No measurements could be made beyond this depth as the borehole was blocked, most likely by a piece of rock which had fallen out from the geologically interpreted (Carlsten and Stråhle, 1985) fracture zone at about 156 m depth.

In summary, the tracer breakthrough measurements and inflow measurements supports the radar interpretation of tracer transport within Zone X. The measurements also indicate that Zone X has a good hydraulic connection with Zone C.

Zone Y

This previously unknown flow path is extending from Zone C in the E1F4 plane, Figure 7.15, from the main migration path between boreholes F3 and F2. Zone Y extends towards borehole E1, which it intersects at a depth of about 175-180 meters. Zone Y is also partly visible in the F1F6 section where it is seen to intersect borehole F1 at a depth of about 162-170 meters.

The radar interpretation, which indicates transport of tracer towards borehole E1, to the interval 175-180 m, is strongly supported by the electrical conductivity log (Appendix 6) which shows a significant increase in borehole fluid conductivity from 257 to 270 mS/m in the depth interval 170-178 m. The interpretation is also supported by hydraulic conductivity measurements and geophysical measurements (Carlsson and Olsson, 1985; Olsson and Jämtlid, 1984). No inflow measurements were performed within this interval.

In borehole F1 there were no inflow measurements performed at the intersection with Zone Y. The borehole is altogether low conductive and there are no significant indications of tracer inflow at the intersection with Zone Y based on the electrical conductivity logging of F1. However, head measurements reported by Black, Holmes, and Brightman, 1987 gave a very low hydraulic head (-15 m relative to the Crosshole drift) in the interval 166-176 m. This suggests that the interval is hydraulically connected

with the old drift at the 410 m level. It is therefore possible that some of the saline tracer which enters borehole F1 is transported from the borehole into the radar interpreted Zone Y at 162-170 m depth.

9.2 FLOW AND TRANSPORT PROPERTIES OF ZONE C

The amount of tracer flow paths or "preferential flow fraction" was estimated from the radar measurements based on three differential tomographic sections (Figures 7.6-7.8) as described in section 7.3.1. The results, presented as a percentage of the surveyed area, indicate a "preferential flow fraction" of 20-37% for the surveyed area of Zone C, i.e. the part of the area with significant tracer transport. These figures are higher than values obtained from previous investigations in granite which were in the range 5-20% (Bourke, Durrance, Heath, and Hodgkinson, 1985; Abelin, Nerentieks, Tunbrandt, and Moreno, 1985). However, it should be noted that the previous observations were made in single fractures in the near vicinity of drifts, whereas the values presented in this report represents a much larger scale both with respect to distance and number of fractures. The interpretation is surely not unambiguous but considering the effects of two main sources of error, the choice of cutoff level for the attenuation data and the choice of the size of the surveyed area, the results should not be too far from reality. In this case an increase in residual attenuation excess of 25 dB/km was assumed to represent the main flow paths. This level of attenuation increase represents 78% of the mass of saline tracer following the theory outlined in Section 3.3 and the discussion in Section 7.3.1. The surveyed area is another property which might be difficult to define especially in a radially diverging flow field. In this investigation the area was defined by the borehole locations, but the tracer migration may also have taken place outside the area surveyed by the radar. The high recovery of tracer (74-78%) within the boreholes indicate that there are no major flow paths stretching outside the investigated volume, except part of the flow paths to E1 and F5 as discussed above, and thus the area defined by the borehole locations seems to be a reasonable estimate of the total area.

The "preferential flow fraction" was also calculated using the eight tomographic sections (Appendix 4) as the percentage of flow path related to the surveyed area of Zone C. These tomographic sections are not related to any particular fracture zone as in the case of the plane section of Zone C discussed above and the reference area is different in the two cases. The values presented in Table 7.3 give a measure of the distribution of the saline tracer within the

investigated rock volume. The very high values for the sections F5E1 and F5F1 (117-146%) may be explained by their short distance from the injection point and also due to the transport within Zone X which intersects these two sections. Zone X also intersects the E1F2 section, thus giving a high value also for this section.

The flow porosity of the investigated rock volume was calculated from the tracer breakthrough data assuming that the transport took place within a 14.5 m thick cylindrical slice with the injection interval in the centre. The radius of the slice was set to 60 meters, which is the distance to the most distant detection boreholes. The radar interpretation indicates that the main transport within Zone C is concentrated to only about 20-37% of the zone, based on the "preferential flow fraction" data presented in Table 7.2. This indication from the radar data is of great importance for the transport properties and also for the interaction between rock and water, e.g. the rock surface available for sorption and matrix diffusion.

Based on the combined interpretations of the flow distribution within the investigated rock volume, an attempt was made to give a rough estimate of the wetted surface. The wetted surface, defined as the area of wet rock per volume of rock (m^2/m^3) is an important parameter regarding the sorption capacity of the rock and hence for the safety analysis.

The estimate is based on the tracer distribution interpreted from the three radar cross-sections of Zone C (Figures 7.6 to 7.8). The area covered by saline tracer is about 200 m^2 (mean value of the three cross-sections). The following assumptions were made to determine the wetted surface;

1. Zone C consists of 25 fractures which is the mean value of the number of TV-logged fractures found within the geologically interpreted Zone C (Carlsten, Magnusson, and Olsson, 1985).

2. Each fracture has the same distribution of tracer as the cross-sections in Figures 7.6 to 7.8.

3. Zone C has a thickness of 8 meters which is the thickness of the three radar cross-sections available, Figures 7.6 to 7.8.

The above assumptions gives a total surface of about 10 000 m^2 and a total investigated volume of 5 600 m^3. Hence, the wetted surface is 1.8 m^2/m^3. This value is in the same order of magnitude as estimates made by

Abelin, Birgersson, Gidlund, Moreno, Neretnieks, Widen, and Ågren, 1987. They estimated the wetted surface or specific surface, to 0.7-4 m^2/m^3 based on values of porosity combined with recovery data for the tracers.

The calculations above were made by making several assumptions that might be questioned. The number of fractures conducting water is probably much lower than 25 as assumed above thus decreasing the wetted surface. The number of fractures covered by each cross-sections (Figures 7.6 to 7.8) is another uncertain parameter.

Two extreme cases for the wetted surface were also considered to illustrate the span of the wetted surface; firstly that Zone C consists of only one fracture and secondly that Zone C consists of 25 fractures which were totally filled with tracer solution. The first case will give a wetted surface of $0.07 m^2/m^3$ and the second case, a wetted surface of 6.3 m^2/m^3.

10 CONCLUSIONS AND RECOMMENDATIONS

Difference tomography using borehole radar is a valuable and successful tool in mapping groundwater flow paths in fractured rock. The data presented in this report are of good quality and sufficiently consistent throughout the investigated rock volume. The interpreted results verified previous findings in the surveyed granite volume as well as contributed to new and unique information about the transport properties of the rock at the site.

The radar tomograms and reflectograms generated within this project are in very good agreement with the results obtained from previous measurements performed during the Crosshole programme. This implies that the new data, and hence also the interpretation, is in agreement with the previous interpretation (Olsson, Black, Cosma, and Pihl. 1987). In this experiment we have concentrated the investigations on zone 'C' and some additional characteristics on this zone may be noted.

The radar data is presented both as differential radar reflectograms as well as differential tomograms. The differential reflectograms could be used qualitatively, together with tomographic and salt inflow results, but no quantitative estimates of flow path and volume of salt could be obtained.

From the differential attenuation tomograms the migration of the injected tracer was mapped and presented both in the fracture zone of interest (Zone C) and in the entire investigated granite volume.

The main migration in Zone C section took place in the central parts of the surveyed section with a dominating path stretching, from the injection point in borehole F3, in the direction towards borehole F2.

From the differential attenuation tomographic 3-D model the major tracer migration is spreading from the injection point, in Zone C, towards borehole F2. Only subordinate tracer transport paths were noticed towards boreholes F4, F5 and F6, except for a transport path, within Zone C, towards F5. No tracer transport was noticed, in Zone C, towards borehole F1.

A fracture zone originally detected within this project, was determined to transport portions of the injected tracer. This fracture zone, termed Zone X, is most distinct in borehole sections E1F5 and F2E1 and intersects boreholes E1, F1, F2 and F5 within the investigated granite volume. Zone X intersects Zone C with an angle of 80°-90°. Zone X has an orientation (dip 55° and strike 10°) similar to that of Zone A

which indicates that it could be part of the same fracture system as Zone A.

There is also a tracer flow path from Zone C towards the lower parts of borehole E1. This previously unknown flow path, labelled Zone Y, is spreading from Zone C in the E1F4 plane section, on the migration path from F3 to borehole F2.

The inflow data and the tracer breakthrough data has served as a useful aid in the interpretation of the flow distribution within Zone C and also within the surrounding rock mass. From the breakthrough data determination of transport parameters has been possible to make in several directions and distances within Zone C.

The integration of the radar method and the conventional tracer migration experiment made it possible to compare the radar interpretation of the groundwater flow paths with the actual breakthrough locations of the tracer. Analysis of tracer breakthrough data has confirmed the radar interpretations both with respect to the flow path distribution within Zone C and with respect to the spreading of tracer to other zones within the surveyed rock volume. In addition, the calculations of tracer mass balance and recovery in the sampling boreholes has made it possible to identify flow paths outside the radar investigated domain.

The complexity of the flow distribution within the investigated volume, caused by the presence of the open boreholes, made it difficult to make good quantitative evaluations of flow and transport parameters such as dispersivity and hydraulic fracture conductivity. However, the flow porosity or kinematic porosity could be determined in two different ways and both gave the same value. The value is also consistent with values from earlier investigations in the Stripa granite.

The radar measurements indicate that the "preferential flow fraction" is about 20-37% for Zone C. This observation is of great importance for the transport and retardation mechanisms as discussed above. However, although about 80% of the flow is concentrated to this "preferential flow fraction" there is still about 20% of the mass left in other parts of the zone where interactions between rock surface and water may take place.

Experience from this project has shown that the concentration of the saline tracer could have been higher than the 0.5% used here. A salt concentration of 1% to 2% would have increased the anomalies of interest and give a better signal to noise ratio and

hence simplified the processing of data and increased the quality of radar data. An increased salt concentration would also improve the quality of the tracer breakthrough data especially in boreholes with low inflow rates.

This project has also shown that the presence of several open boreholes may cause a very complicated flow pattern with flow along the boreholes into adjacent zones. For future investigations of this type it is therefore recommended that the "natural" pressure distribution within the rock mass is maintained by packing off all boreholes within the investigated volume. Such a procedure will also improve the possibility to make good quantitative evaluations of transport parameters. The evaluations would also be improved if 2D or 3D-modelling could be applied, incorporating the radar interpretation of the geometry of the flow paths.

REFERENCES

Abelin, H., Neretnieks, I., Tunbrant, S., Moreno, L., 1985. Final report of the migration in a single fracture - Experimental results and evaluation. Stripa Project TR 85-03, SKB, Stockholm, Sweden.

Abelin, H., Birgersson, L., Gidlund, J., Moreno, L., Neretnieks, I., Widén, H., Ågren, T., 1987. 3-D migration experiment - Report 3 Part 1. Performed experiments, results and evaluation. Stripa Project TR 87-21, SKB, Stockholm, Sweden.

Andersson, Per, Olsson, O.,1988a. Investigation of a fracture zone, using the radar method. Phase 1, reference measurements with the radar equipment. SKB Progress Report AR 88-25, SKB, Stockholm, Sweden.

Andersson, Per, Olsson, O.,1988b. Investigation of a fracture zone, using the radar method. Phase 1, reference measurements with the radar equipment. SKB Progress Report AR 88-41, SKB, Stockholm, Sweden.

Andersson, Peter, Gustafsson, E., 1988. Investigation of flow distribution in a fracture zone, using the radar method. Phase 2, injection of saline water. SKB Progress Report AR 88-34, SKB, Stockholm, Sweden.

Andersson, Peter, Klockars, C-E., 1985. Hydrogeological investigations and tracer tests in a well-defined rock mass in the Stripa mine. SKB Technical Report TR 85-12, SKB; Stockholm, Sweden.

Archie, G. E., 1942. The electrical resistivity log as an aid in determining some reservoir characteristics. Trans. AIME, 146, 54-62.

Black, J., Holmes, D., Brightman, M., 1987. Crosshole investigations - Hydrogeological results and interpretation. Stripa Project TR 87-18, SKB, Stockholm, Sweden.

Brace, W. F., Orange, A. S., Madden, T. R., 1965. The effect of pressure on the electrical resistivity of water saturated crystalline rocks. Journal of Geophysical Research, 70 (22), 5669-5678.

Bourke, P.J., Durrance, E.M., Heath, M.J., Hodgkinson, D.P., 1985. Fracture hydrology relevant to radionuclide transport. Atomic Energy Research Establishment, AERE-R 11414, Harwell, England.

Carlsson, L., Olsson, T., 1985. Hydrogeological and hydrogeochemical investigations in boreholes -

Injection-recovery tests and interference tests. Stripa Project IR 85-09, SKB, Stockholm, Sweden.

Carlsson, L., Stejskal, V., Olsson, T., 1982. Core-logs of the subhorizontal boreholes N1 and E1. Stripa Project IR 82-04, SKB, Stockholm, Sweden.

Carlsten, S., Magnusson, K.-Å., Olsson, O., 1985. Crosshole investigations - Description of the small scale site. Stripa Project IR 85-05, SKB, Stockholm, Sweden.

Carlsten, S., Stråhle, A., 1985. Crosshole investigations - Compilation of core log data from F1-F6. Stripa Project IR 85-13, SKB, Stockholm, Sweden.

Gelhar, L., 1987. Applications of stochastic models to solute transport in fractured rocks. SKB Technical Report TR 87-05, SKB, Stockholm, Sweden.

Gustafsson, E., Klockars, C-E., 1981. Studies on groundwater transport in fractured crystalline rock under controlled conditions using non-radioactive tracers. SKB Technical Report TR 81-07, SKB, Stockholm, Sweden.

Ivansson, S., 1984. Crosshole investigations - Tomography and its application to crosshole seismic measurements. Stripa Project IR 84-08, SKB, Stockholm, Sweden.

Ivansson, S., Hammarström, M., Pihl, J., 1987. Tomographic calculations for synthetic data. Internal report, NAGRA, Baden, Switzerland.

Magnusson, K.-Å., Carlsten, S., Olsson, O., 1987. Crosshole investigations - Physical properties of core samples from borehole F1 and F2. Stripa Project TR 87-10, SKB, Stockholm, Sweden.

Moye, D.G., 1967. Drilling for foundation exploration. Civil Eng. Trans., Inst. Eng. Australia, 95-100.

Niva, B., Olsson, O., 1988a. Radar crosshole tomography at the Grimsel Test Site - Results from phase 2. Internal report, NAGRA, Baden, Switzerland.

Niva, B., Olsson, O., 1988b. Radar crosshole tomography at the Grimsel Test Site - Results from phase 3. Internal report, NAGRA, Baden, Switzerland.

Norton, D., Knapp,R., 1977. Transport phenomena in hydrothermal systems: the nature of porosity. Am. Journal of Science, Vol 277, 913-936.

Ogata, A., Banks, R., 1961. A solution of the differential equation of longitudinal dispersion in porous media. U S Geological Survey Prof. Paper 411-A, Washington.

Olsson, O., Jämtlid, A., 1984. Hydrogeological and hydrogeochemical investigations - Geophysical borehole measurements. Stripa Project IR 84-03, SKB, Stockholm, Sweden.

Olsson, O., Falk, L., Forslund, O., Lundmark, L., Sandberg, E., 1987. Crosshole investigations - Results from borehole radar investigations. Stripa Project TR 87-11, SKB, Stockholm, Sweden.

Olsson, O., Black, J. H., Cosma, C., Pihl, J., 1987. Crosshole investigations - Final report. Stripa Project TR 87-16, SKB, Stockholm, Sweden.

Olsson, O., Eriksson, J., Falk, F., Sandberg, E., 1988. Site characterization and validation - Borehole radar investigations, Stage I. Stripa Project IR 88-03, SKB, Stockholm, Sweden.

Sen, P. N., Scala, C., Cohen, M. H., 1981. A self-similar model for sedimentary rocks with application to the dielectric constant of fused glass beads. Geophysics, 46, 781-795.

Shen, L. C., Savre, W. C., Price, J. M. Ahtavale, K., 1985. Dielectric properties of reservoir rocks at ultra-high frequencies. Geophysics, 50, 692-704.

Sihvola, A. H., 1989. Self-consistency aspects of dielectric mixing theories. IEEE transactions on geoscience and remote sensing, 27, 403-415.

Snow, D.T., 1968. Rock fracture spacings, openings, and porosities. Journal of Soil Mech. Found. Div. ASCE, Vol 94, No SM 1.

Strack, O., in press. Groundwater mechanics.

Zuber, A., 1974. Theoretical possibilities of the two-well pulse method. Isotope Techniques in groundwater hydrology. Proc. Symp. IAEA, Vienna.

APPENDIX 1.	Radar reflectograms from Phase 3 measurements.
APPENDIX 2.	Radar difference reflectograms.
APPENDIX 3.	Residual slowness tomograms from Phase 3 measurements.
APPENDIX 4.	Residual attenuation tomograms from Phase 3 measurements.
APPENDIX 5.	Difference attenuation tomograms combined with tracer injection data.
APPENDIX 6.	Conductivity logs.
APPENDIX 7.	CAD-generated views of Zone C radar model and the interpreted saline tracer migration model as well as a combination of these two models.

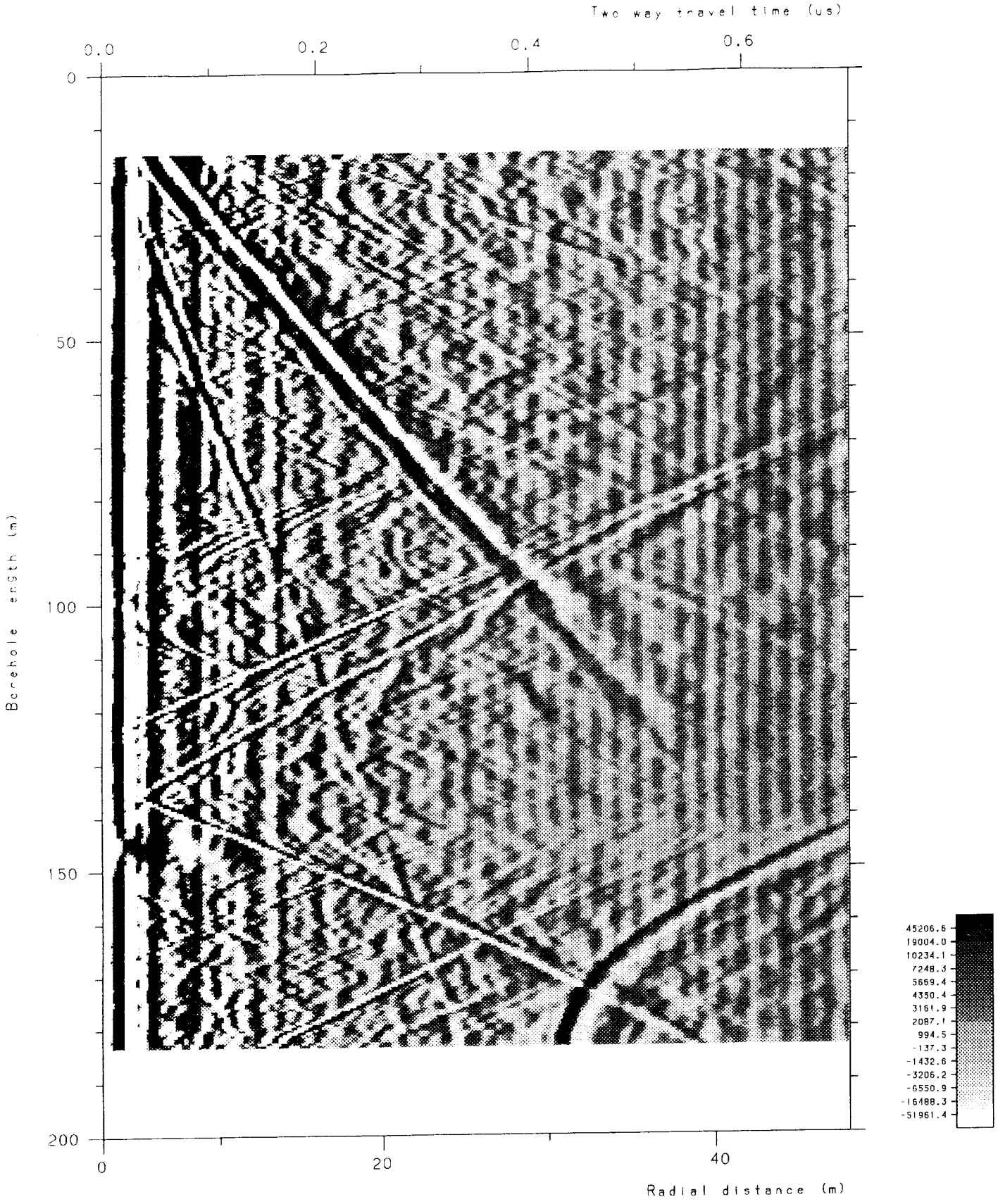

Radar map from single hole reflection survey in E1. 60 MHz antenna, deconvolution filtered data. Phase 3, during salt injection.

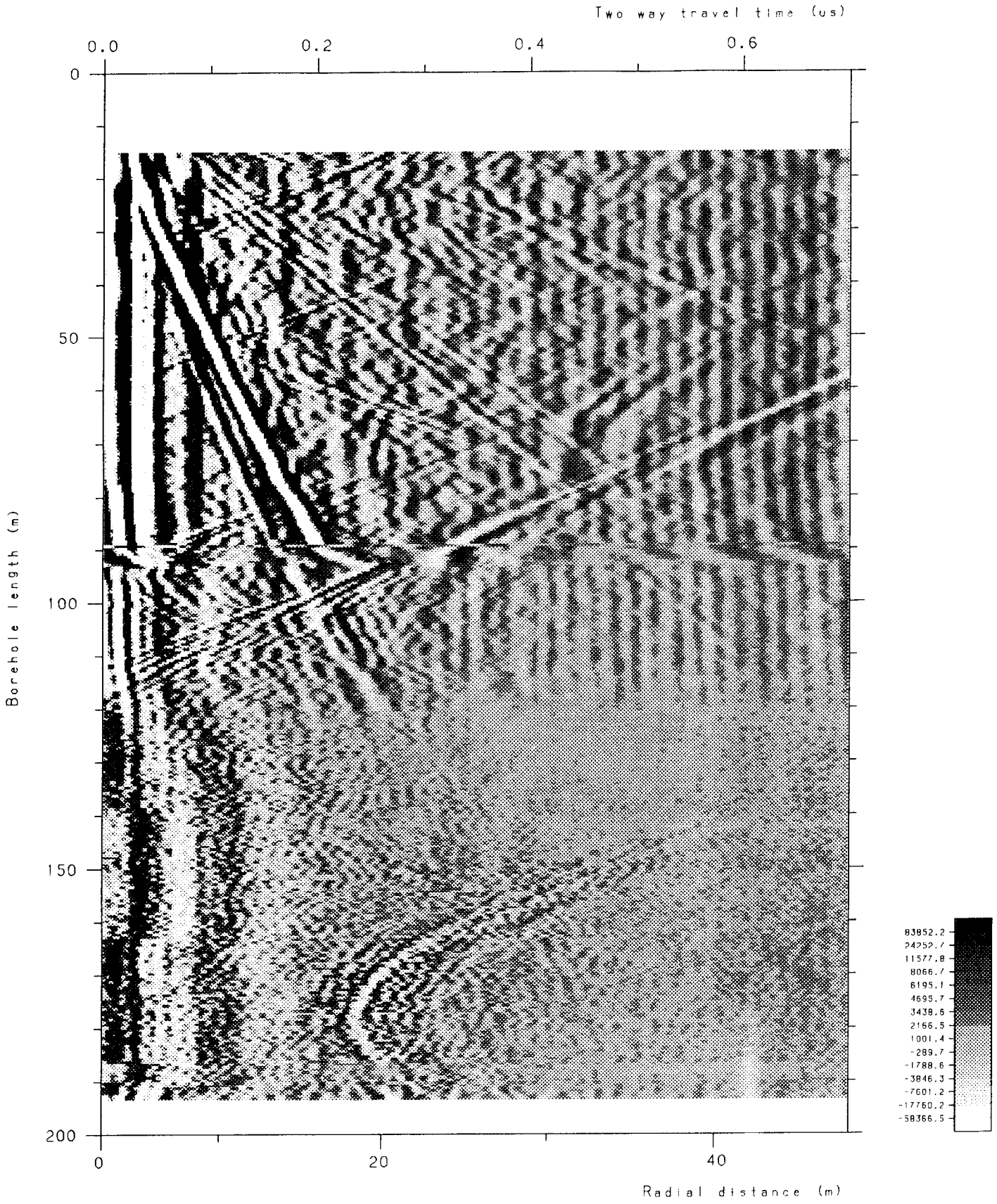

Radar map from single hole reflection survey in F1. 60 MHz antenna, deconvolution filtered data. Phase 3, during salt injection.

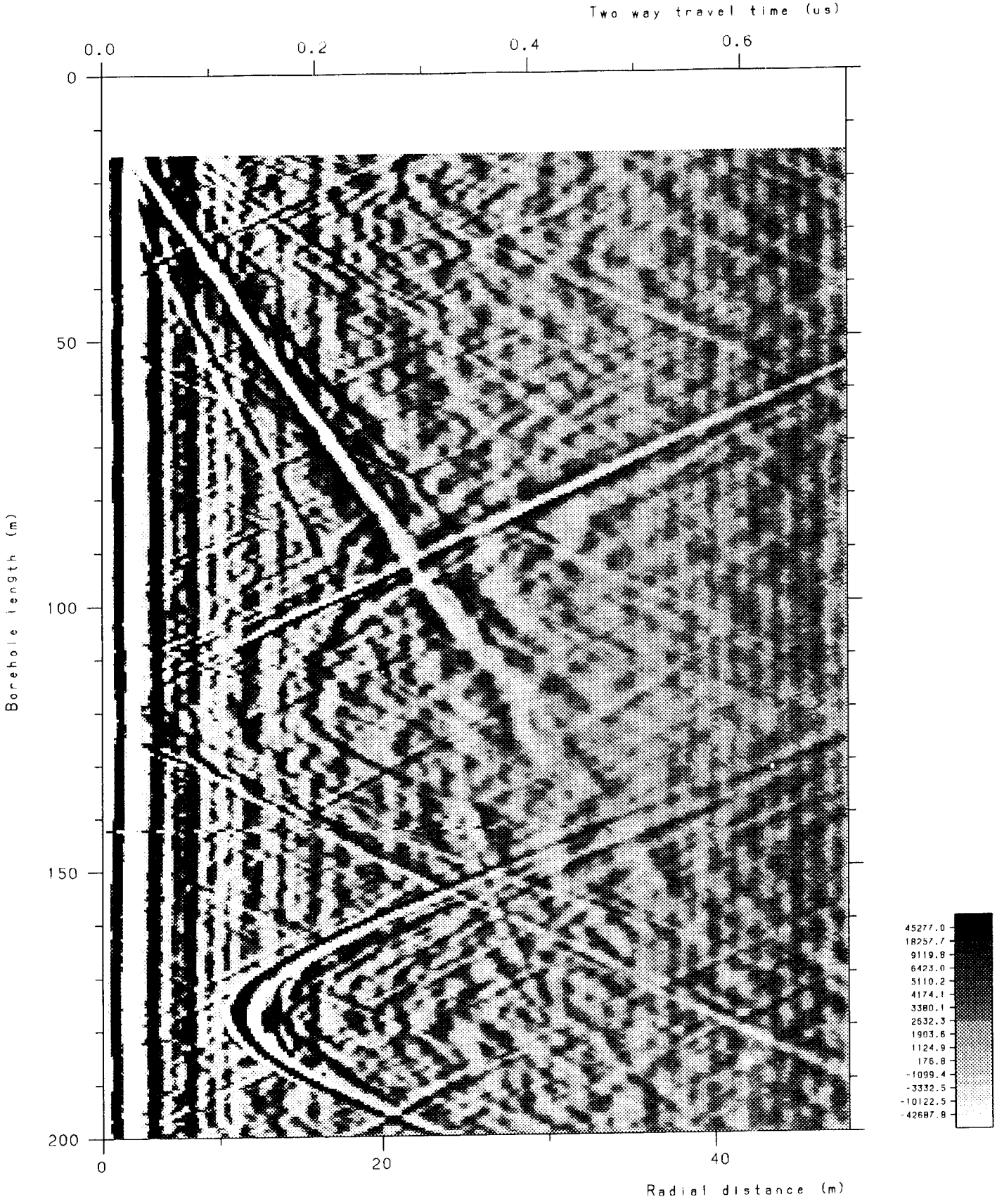

Radar map from single hole reflection survey in F2. 60 MHz antenna, deconvolution filtered data. Phase 3, during salt injection.

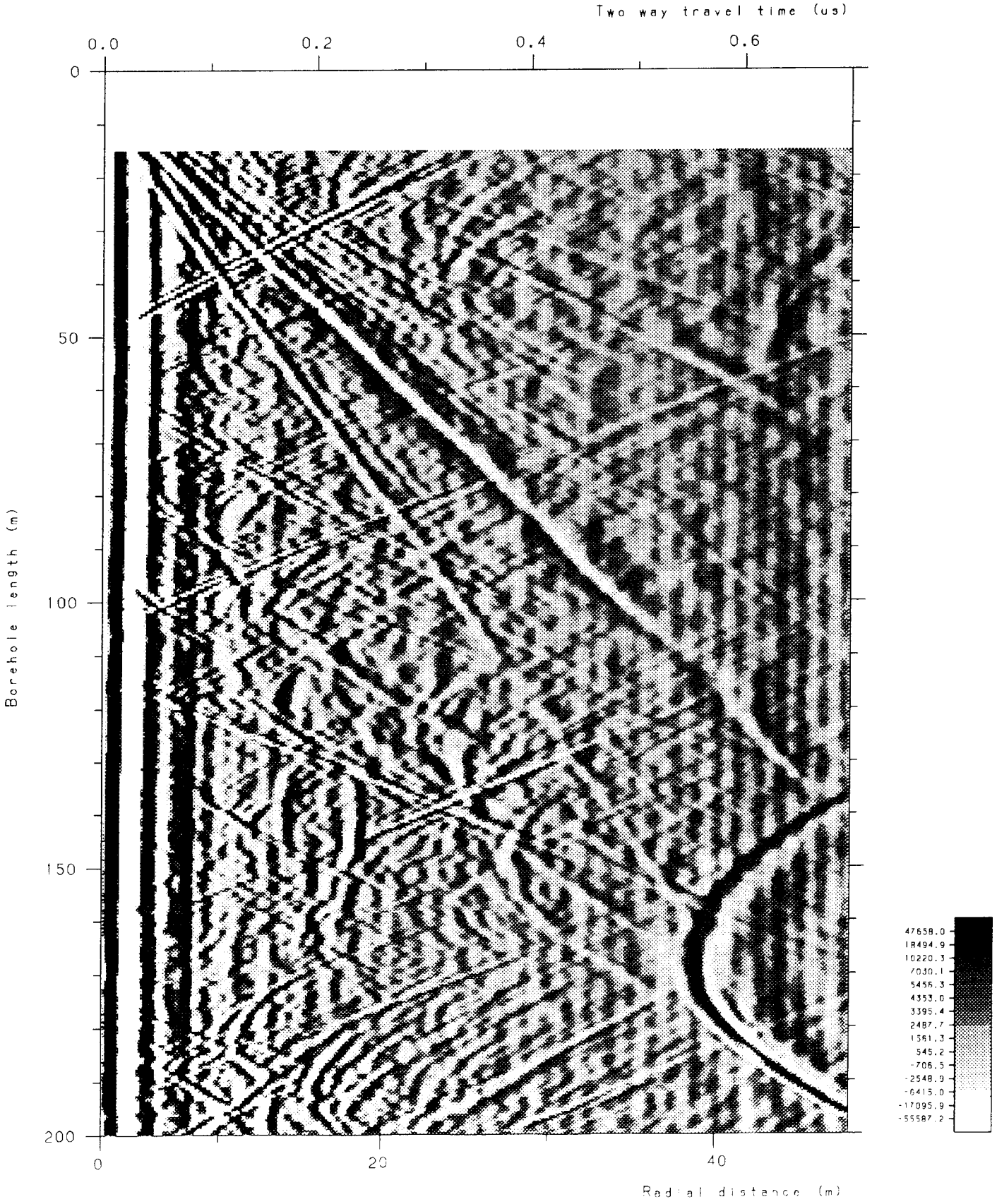

Radar map from single hole reflection survey in F4. 60 MHz antenna, deconvolution filtered data. Phase 3, during salt injection.

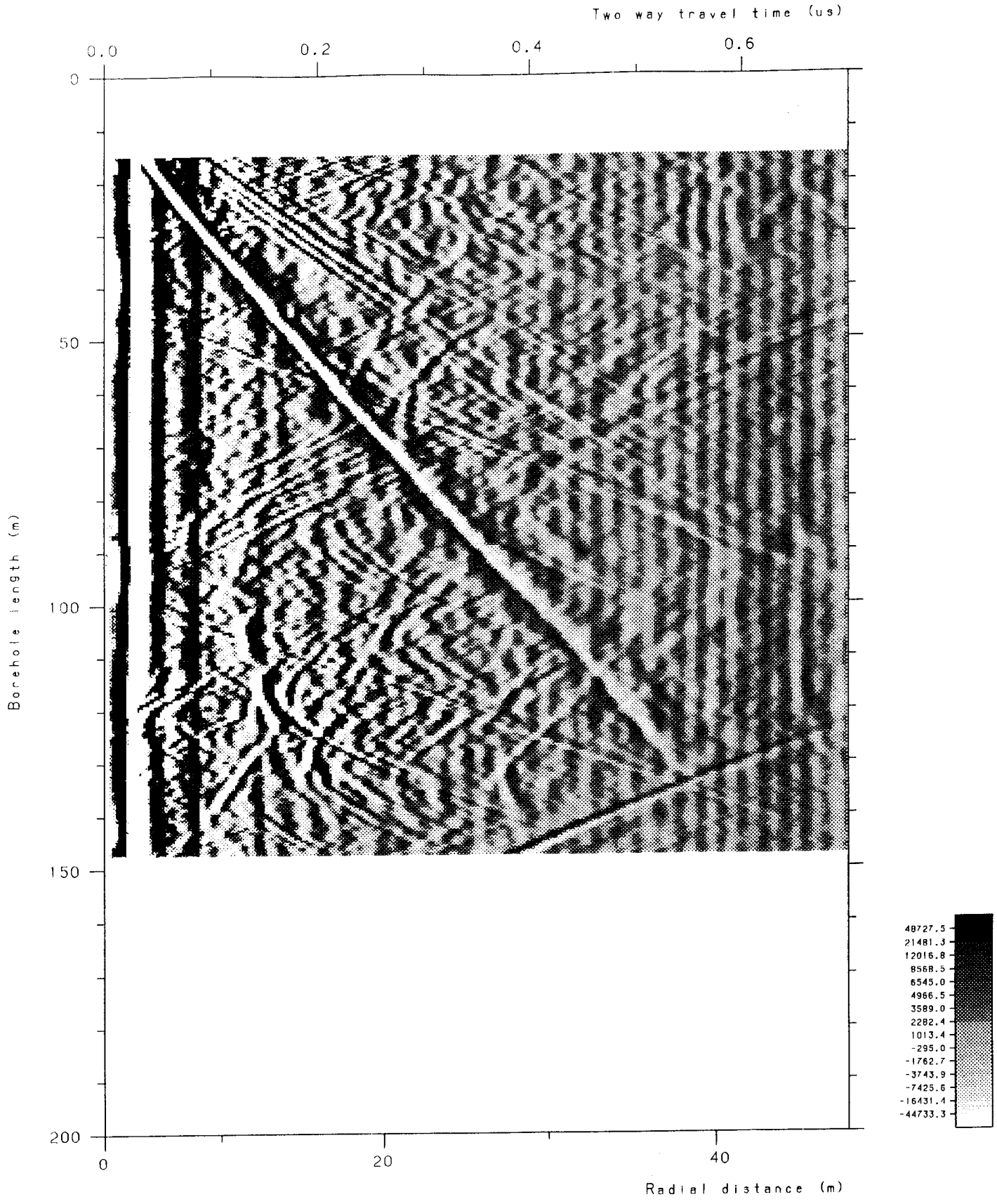

Radar map from single hole reflection survey in F5. 60 MHz antenna, deconvolution filtered data. Phase 3, during salt injection.

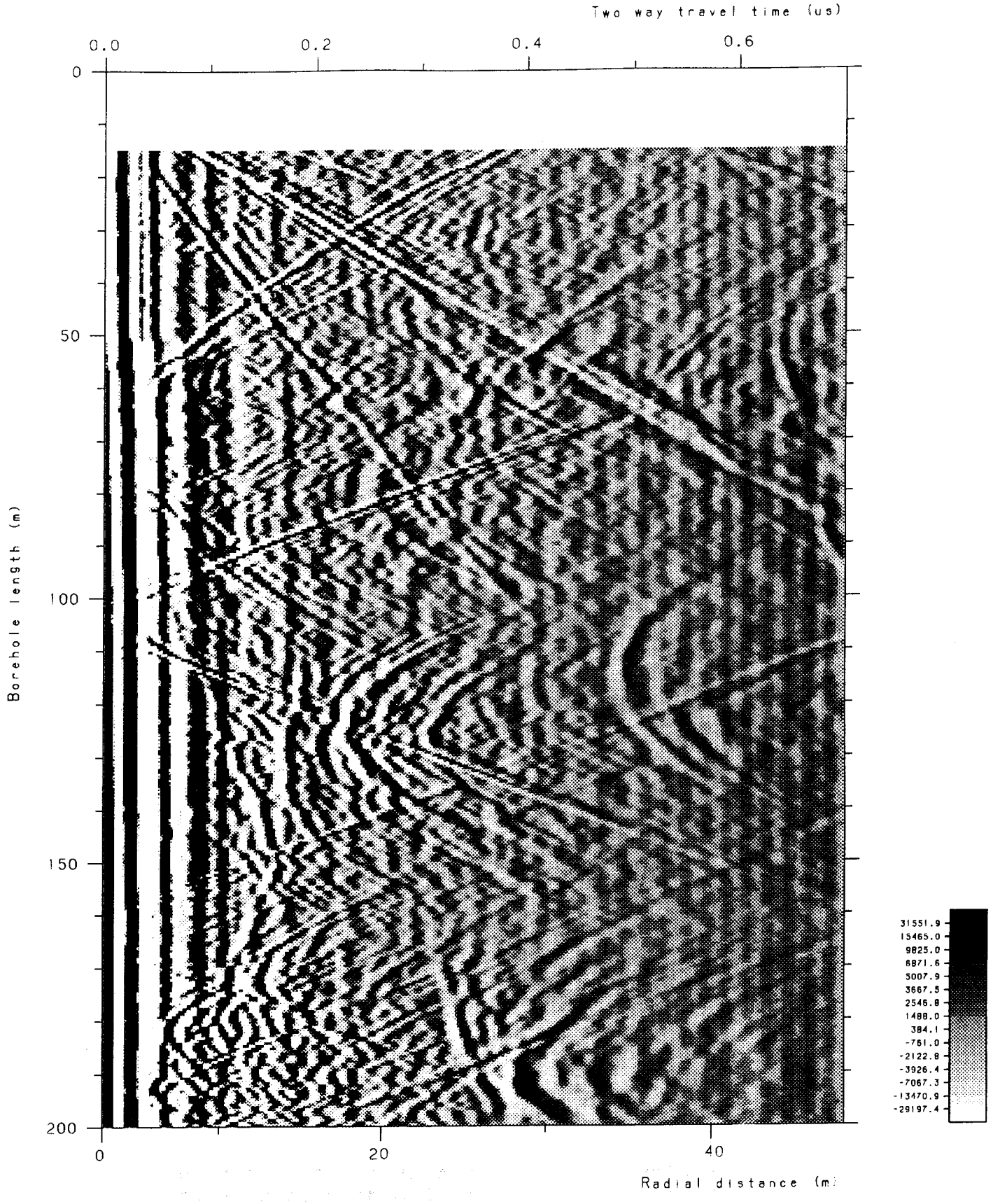

Radar map from single hole reflection survey in F6. 60 MHz antenna, deconvolution filtered data. Phase 3, during salt injection.

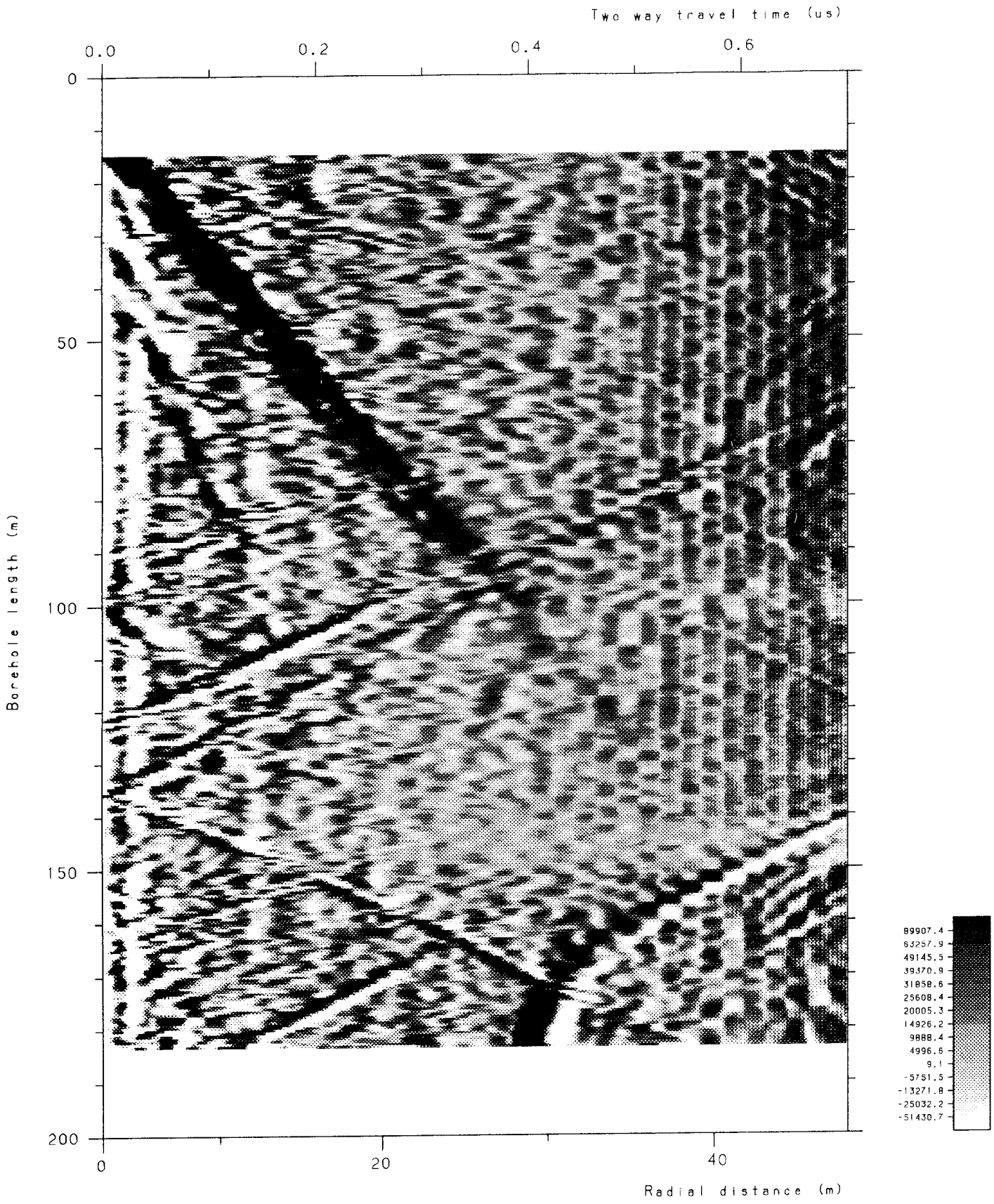

Difference radar reflectogram from two separate surveys in borehole E1, showing changes in the rock formation, due to injection of saline tracer. 60 MHz antenna, envelope filtered data.

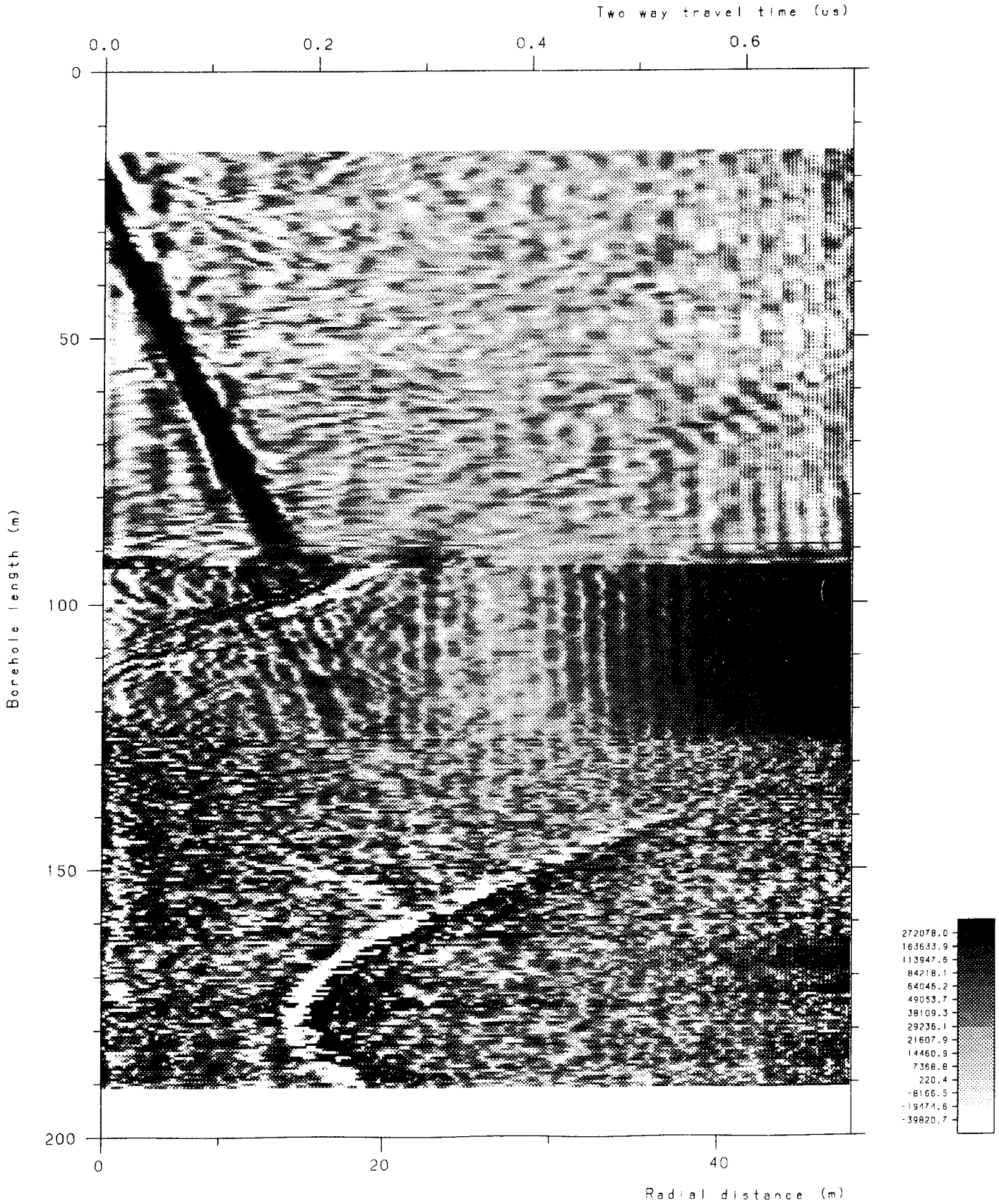

Difference radar reflectogram from two separate surveys in borehole F1, showing changes in the rock formation, due to injection of saline tracer. 60 MHz antenna, envelope filtered data.

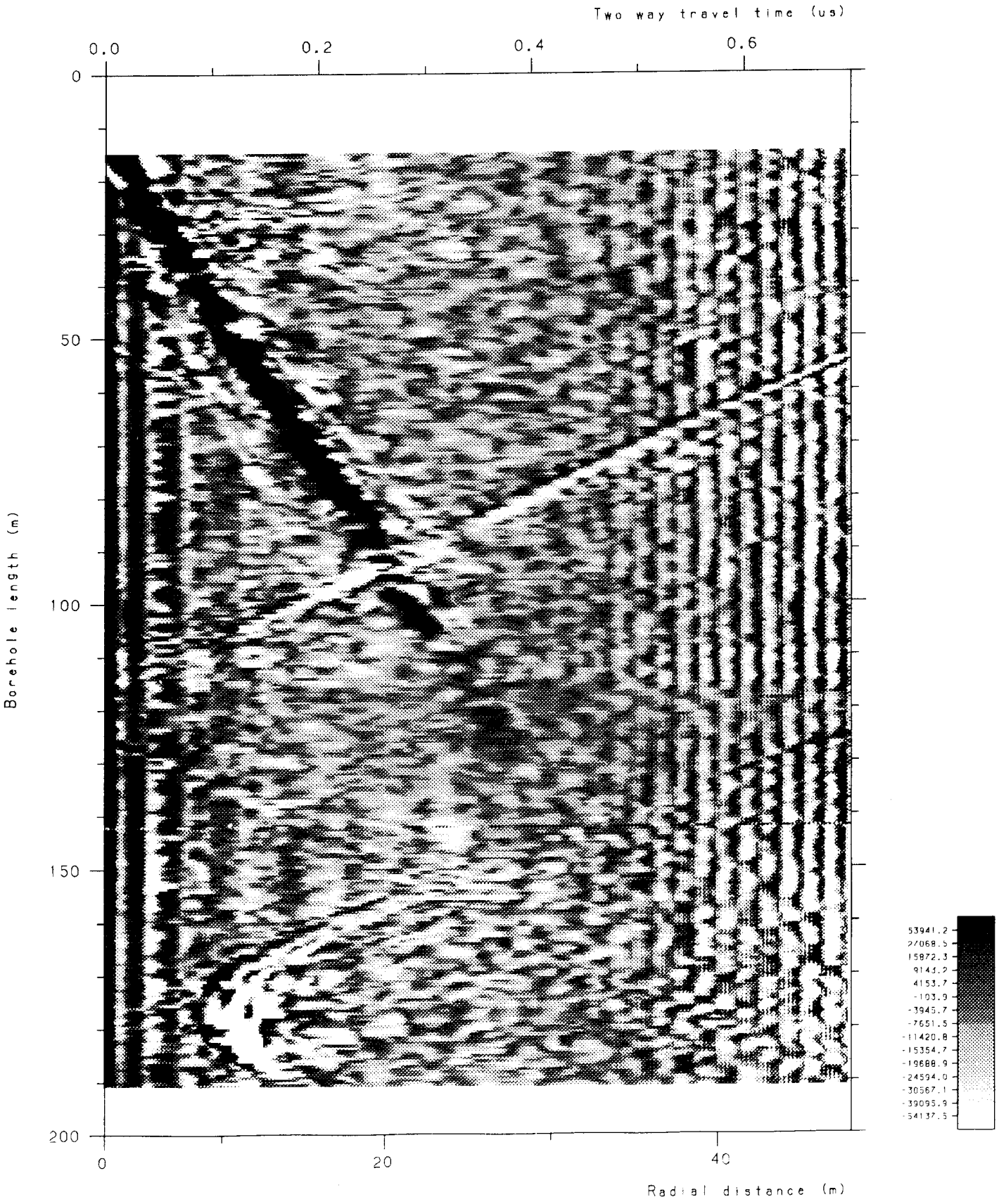

Difference radar reflectogram from two separate surveys in borehole F2, showing changes in the rock formation, due to injection of saline tracer. 60 MHz antenna, envelope filtered data.

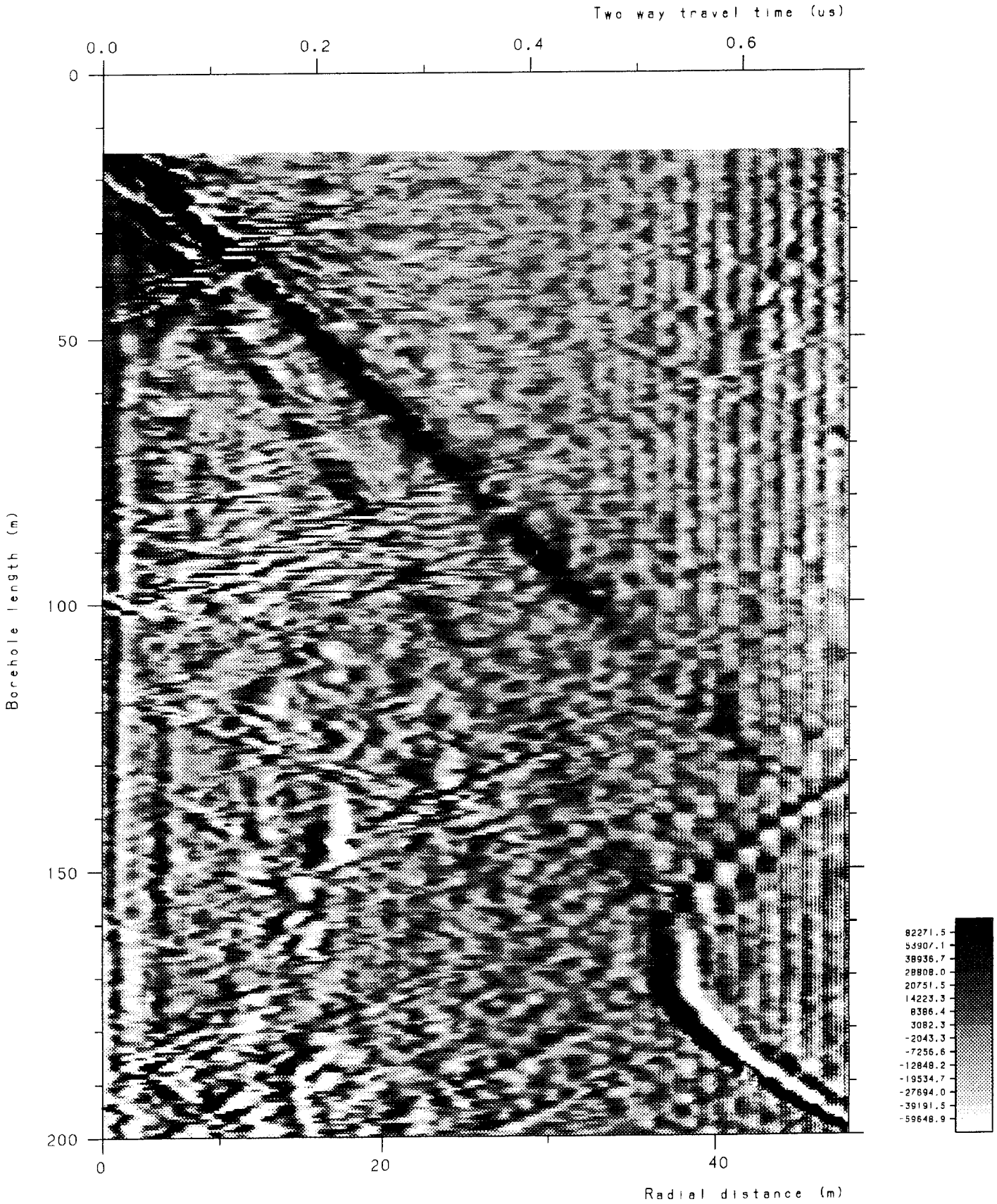

Difference radar reflectogram from two separate surveys in borehole F4, showing changes in the rock formation, due to injection of saline tracer. 60 MHz antenna, envelope filtered data.

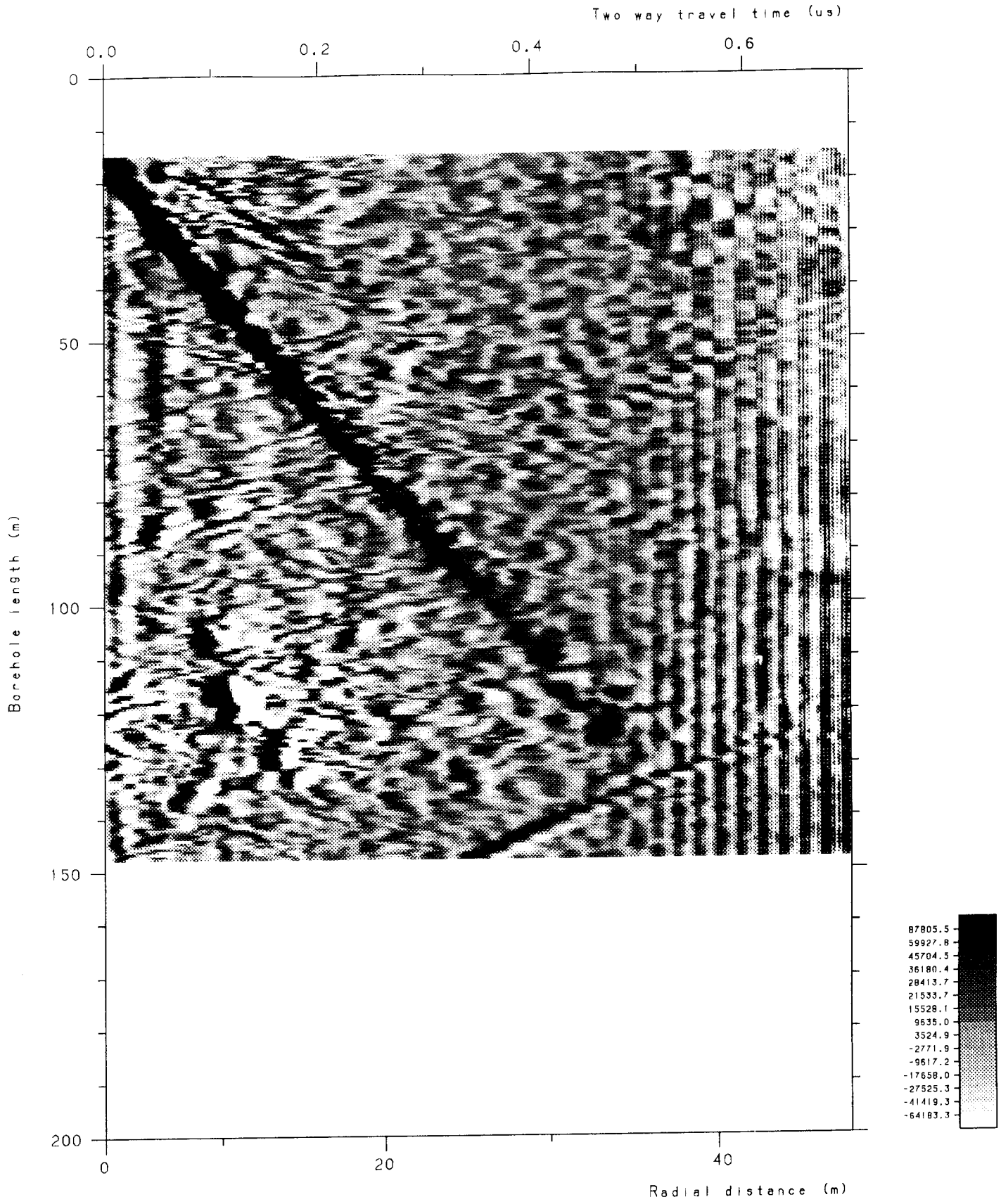

Difference radar reflectogram from two separate surveys in borehole F5, showing changes in the rock formation, due to injection of saline tracer. 60 MHz antenna, envelope filtered data.

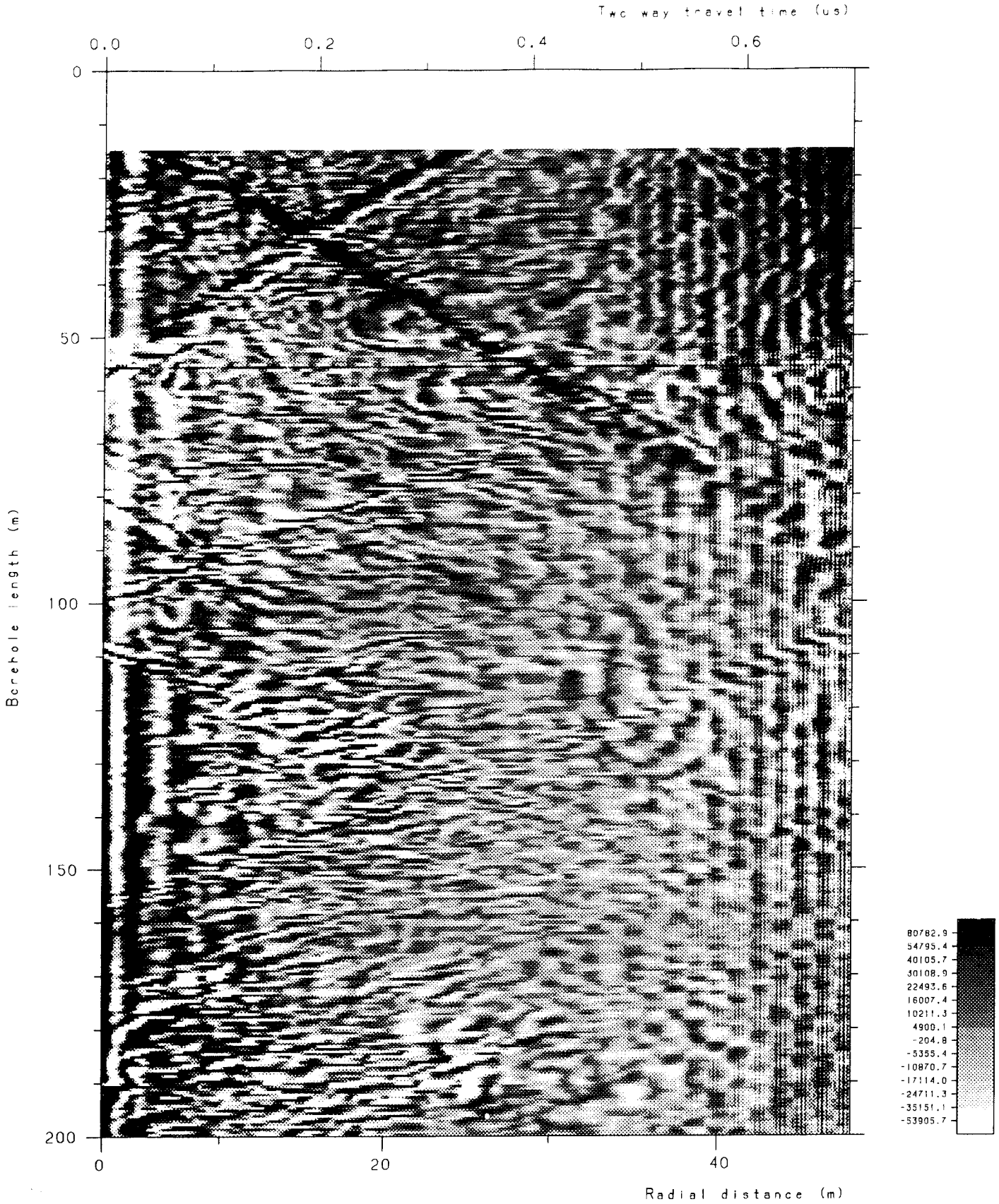

Difference radar reflectogram from two separate surveys in borehole F6, showing changes in the rock formation, due to injection of saline tracer. 60 MHz antenna, envelope filtered data.

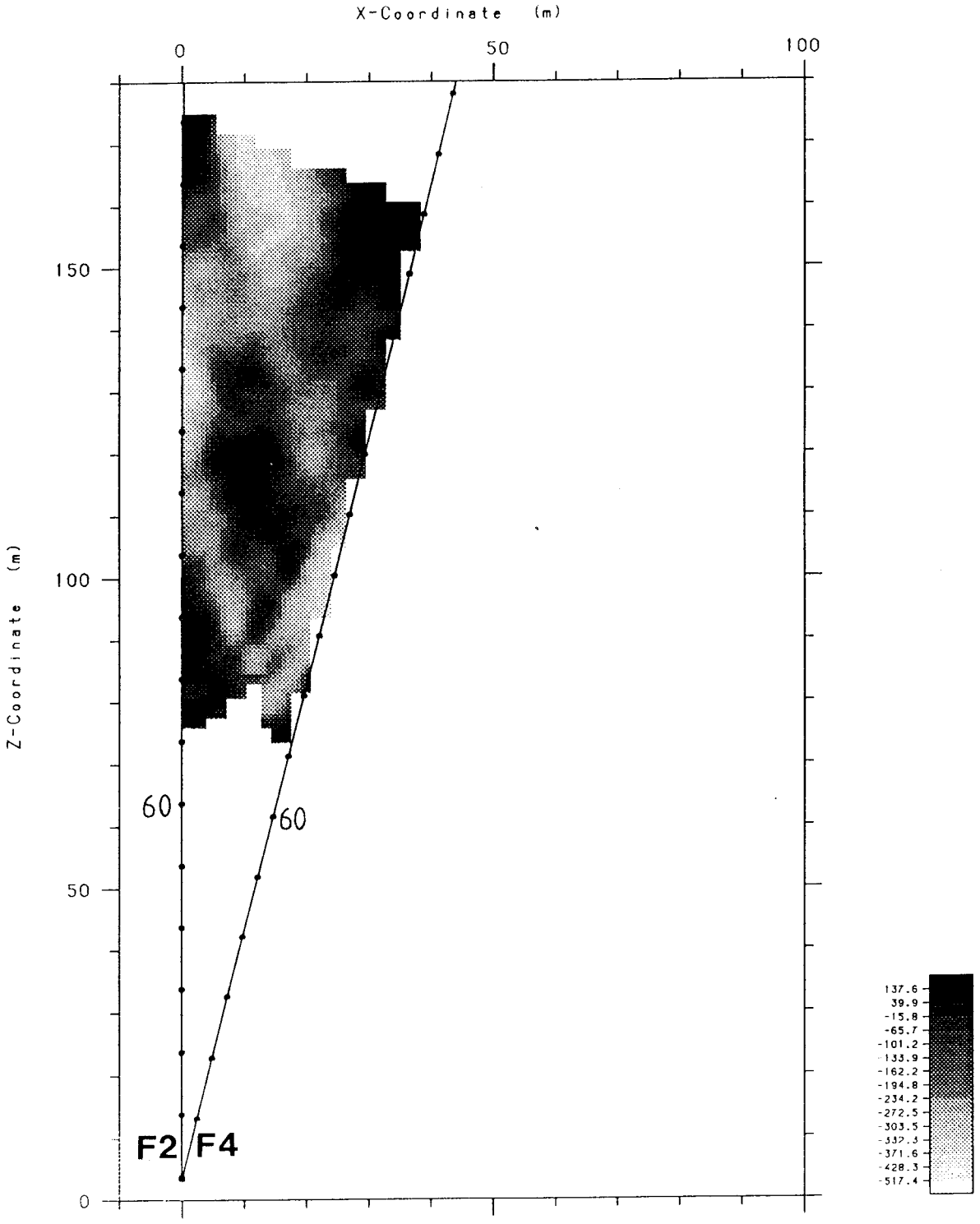

Residual slowness tomogram (ps/m) for the borehole section F2-F4 made with a center frequency of 60 MHz.

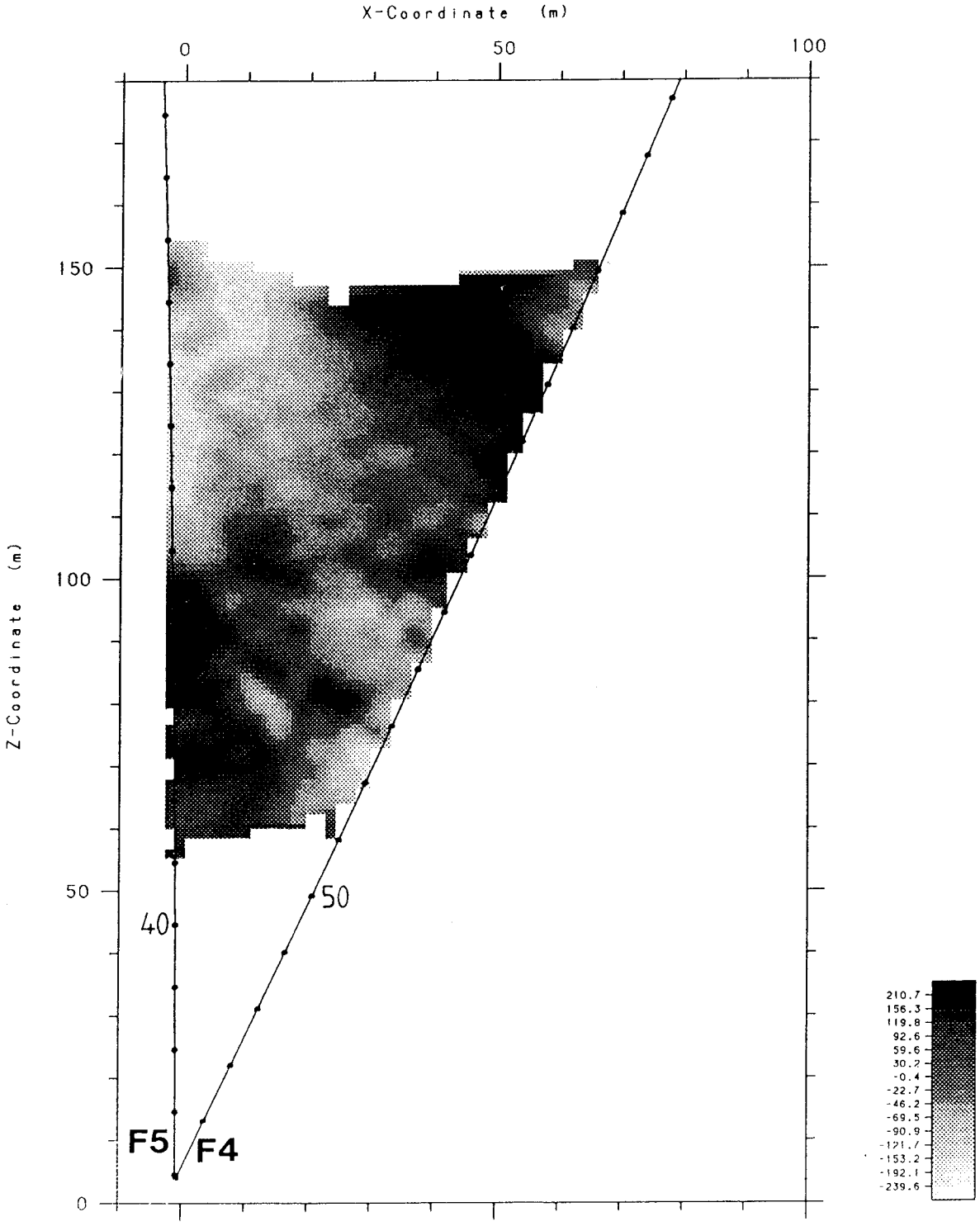

Residual slowness tomogram (ps/m) for the borehole section F5-F4 made with a center frequency of 60 MHz.

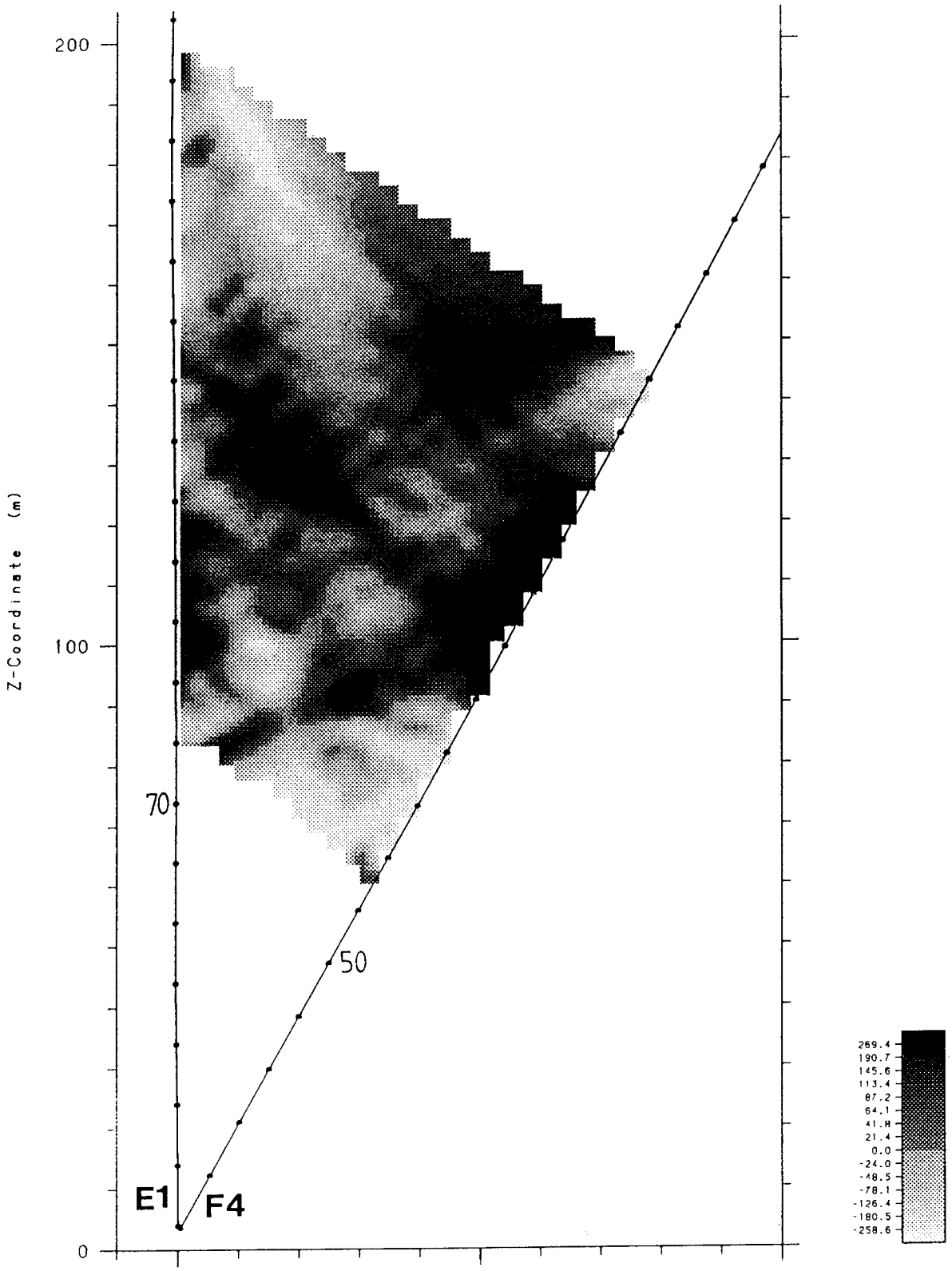

Residual slowness tomogram (ps/m) for the borehole section E1-F4 made with a center frequency of 60 MHz.

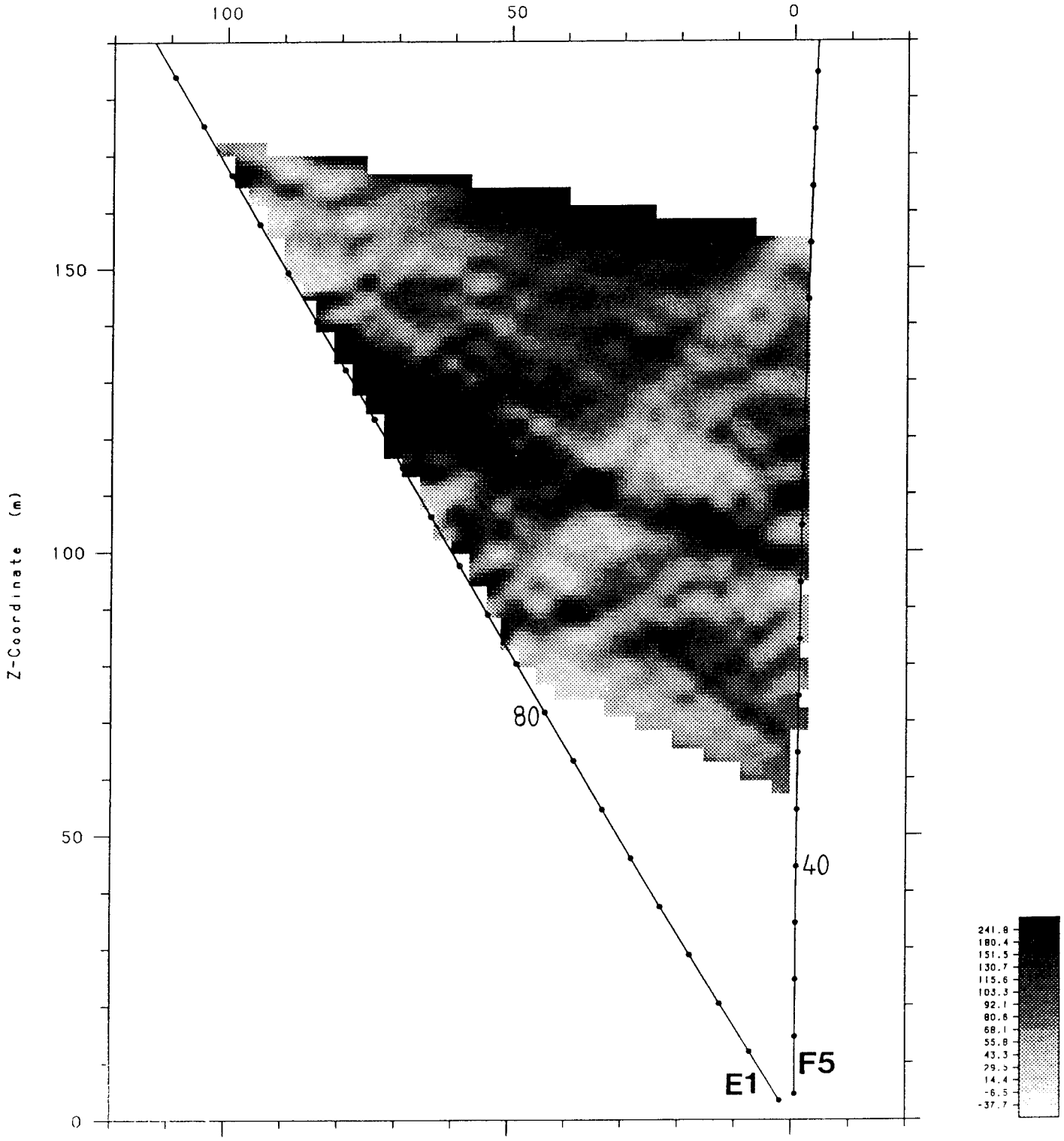

Residual slowness tomogram (ps/m) for the borehole section F5-E1 made with a center frequency of 60 MHz.

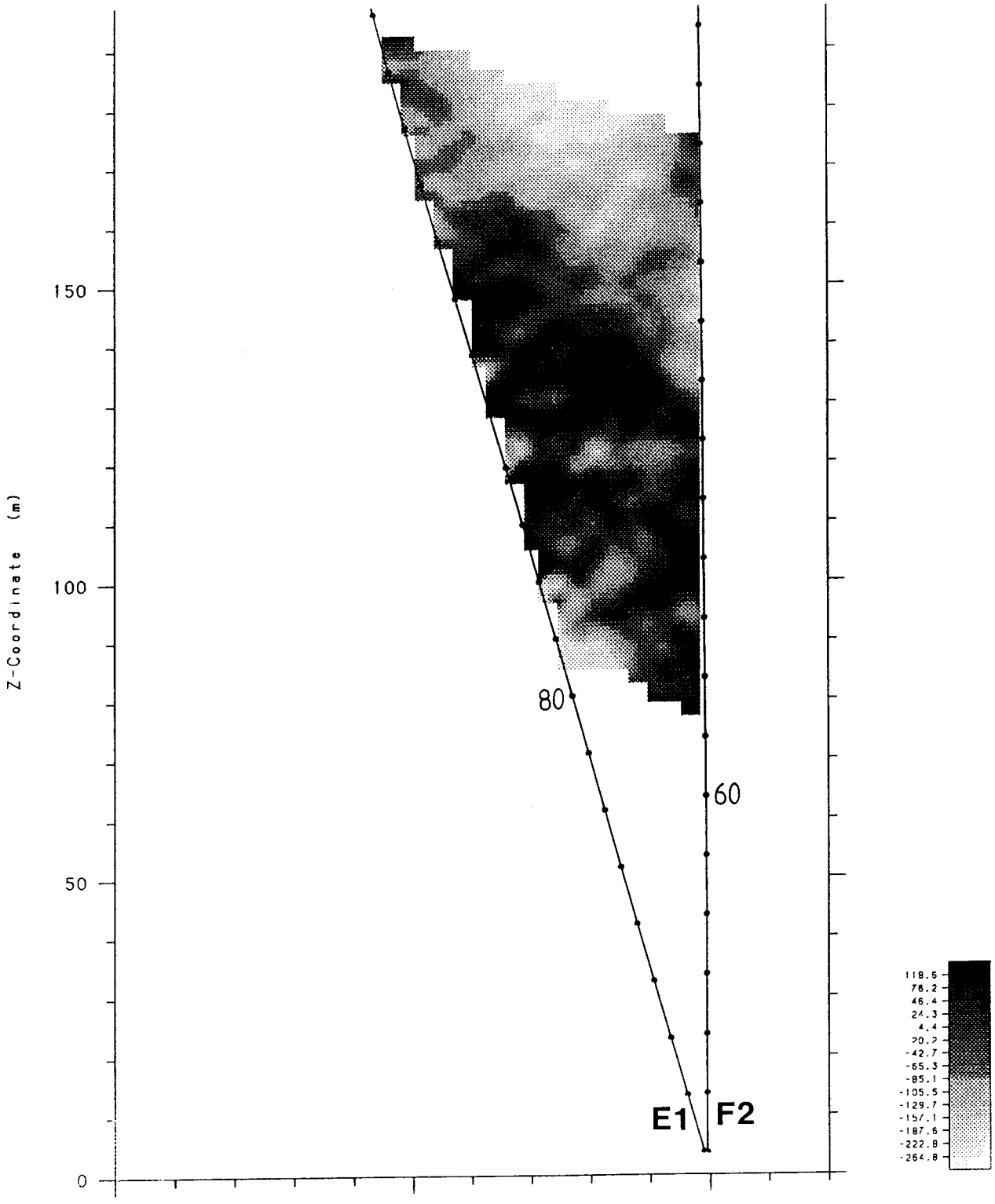

Residual slowness tomogram (ps/m) for the borehole section F2-E1 made with a center frequency of 60 MHz.

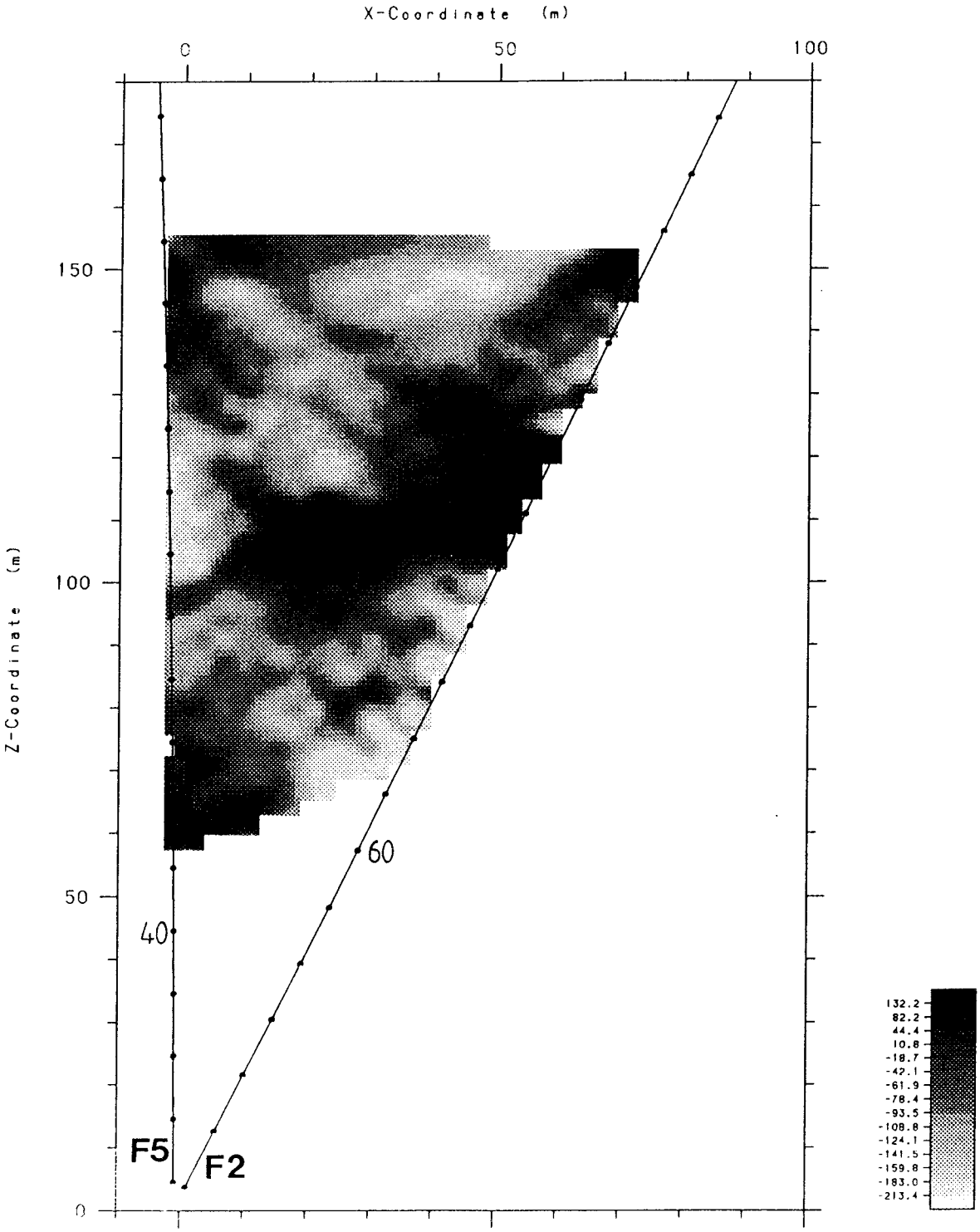

Residual slowness tomogram (ps/m) for the borehole section F5-F2 made with a center frequency of 60 MHz.

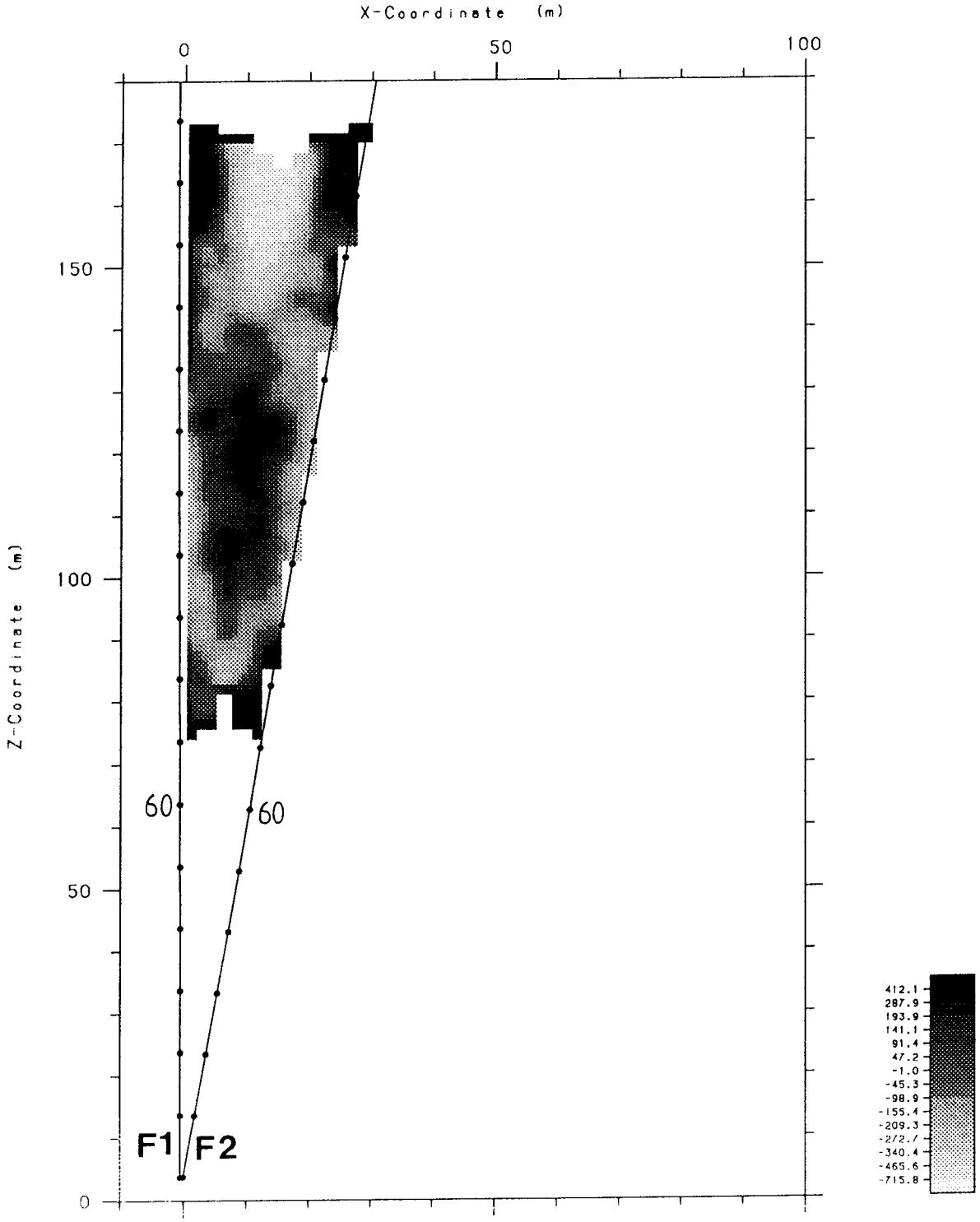

Residual slowness tomogram (ps/m) for the borehole section F1-F2 made with a center frequency of 60 MHz.

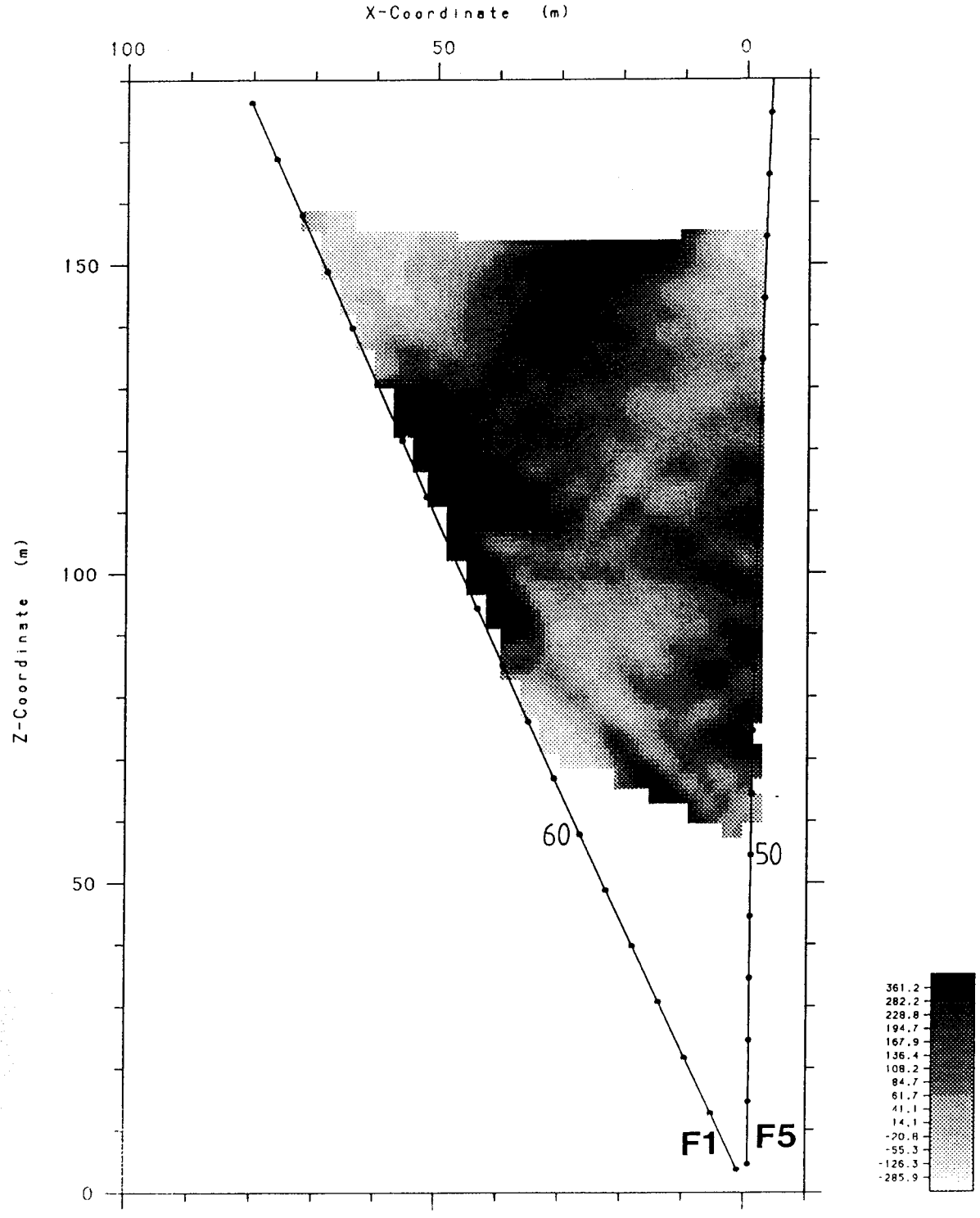

Residual slowness tomogram (ps/m) for the borehole section F5-F1 made with a center frequency of 60 MHz.

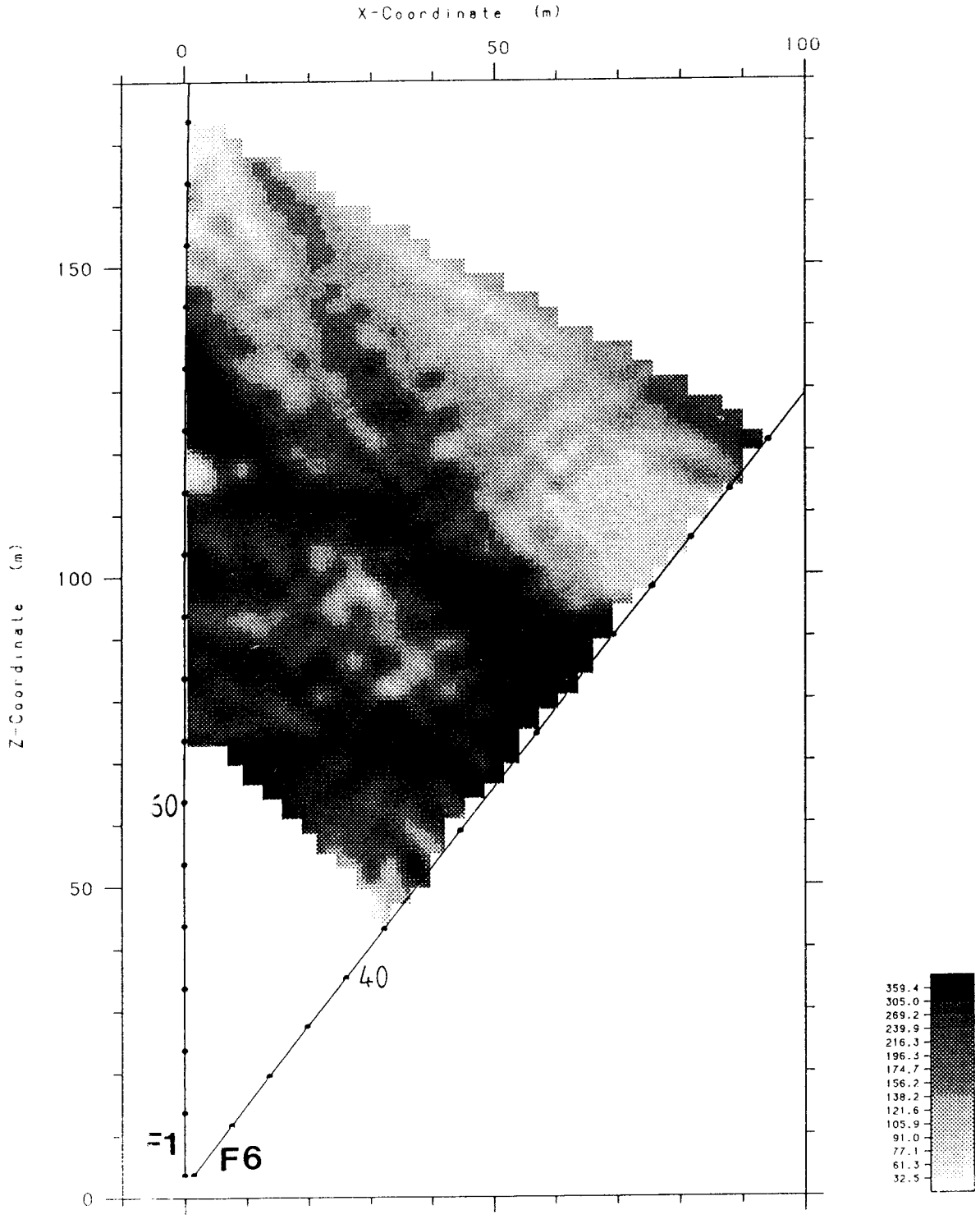

Residual slowness tomogram (ps/m) for the borehole section F1-F6 made with a center frequency of 60 MHz.

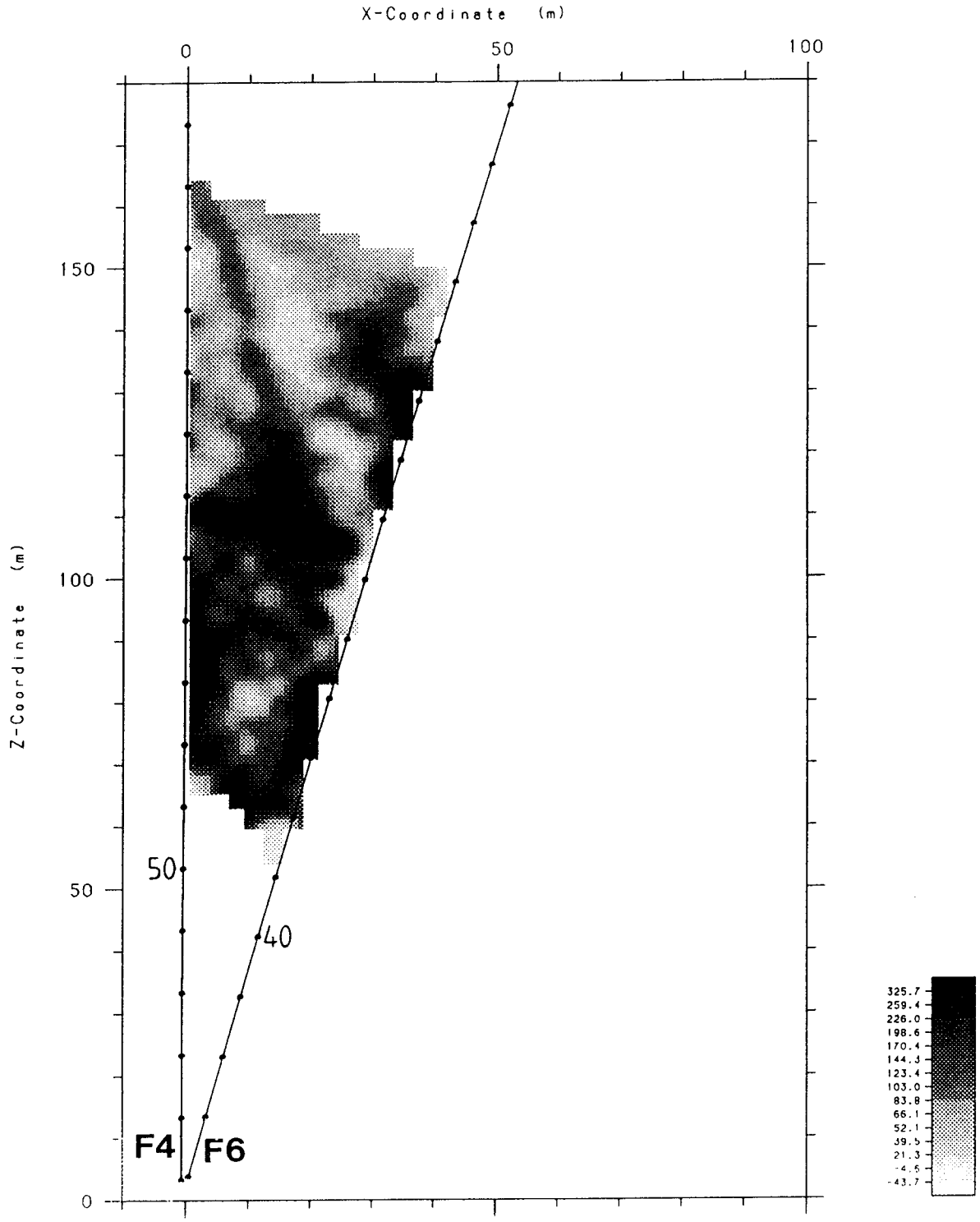

Residual slowness tomogram (ps/m) for the borehole section F4-F6 made with a center frequency of 60 MHz.

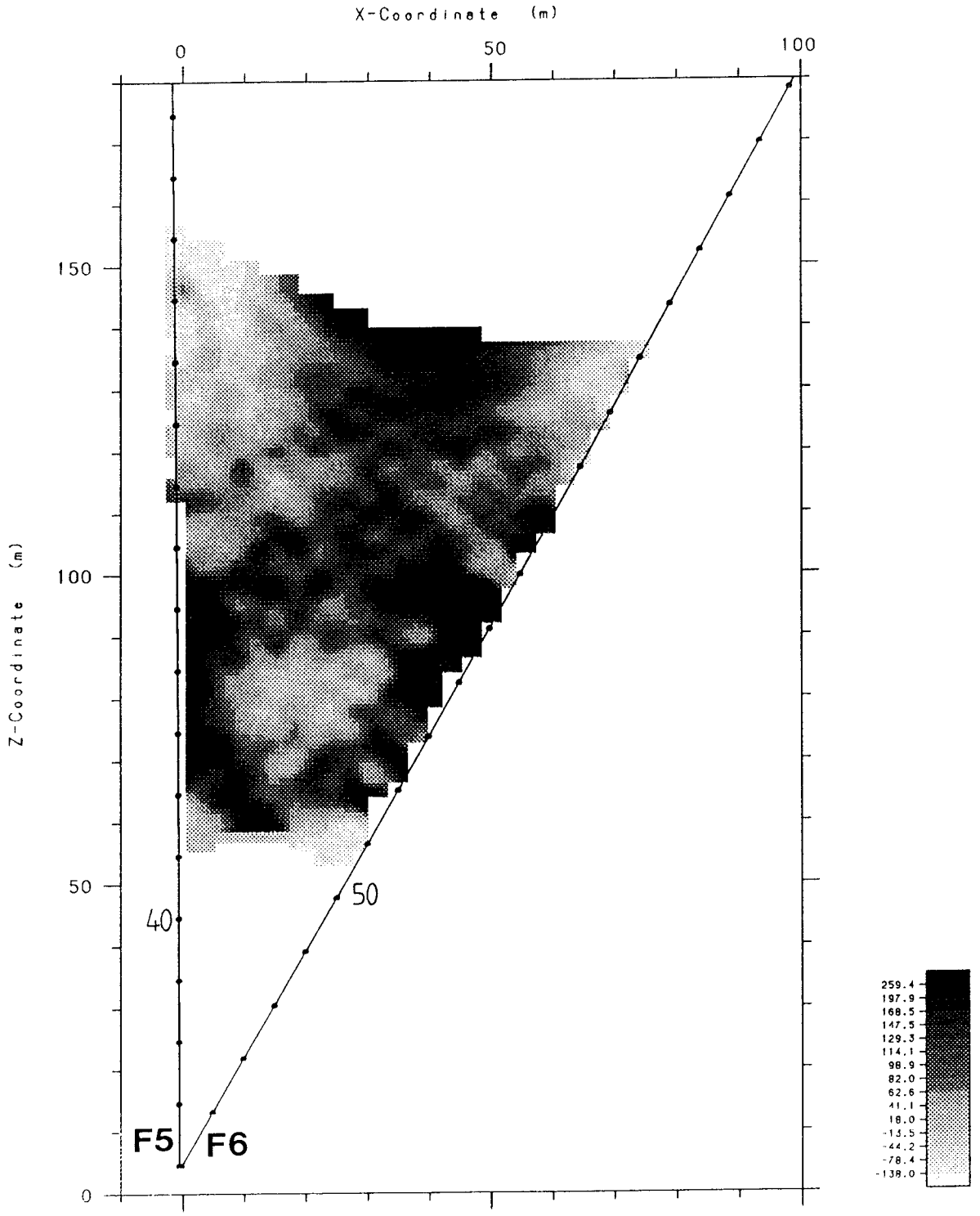

Residual slowness tomogram (ps/m) for the borehole section F5-F6 made with a center frequency of 60 MHz.

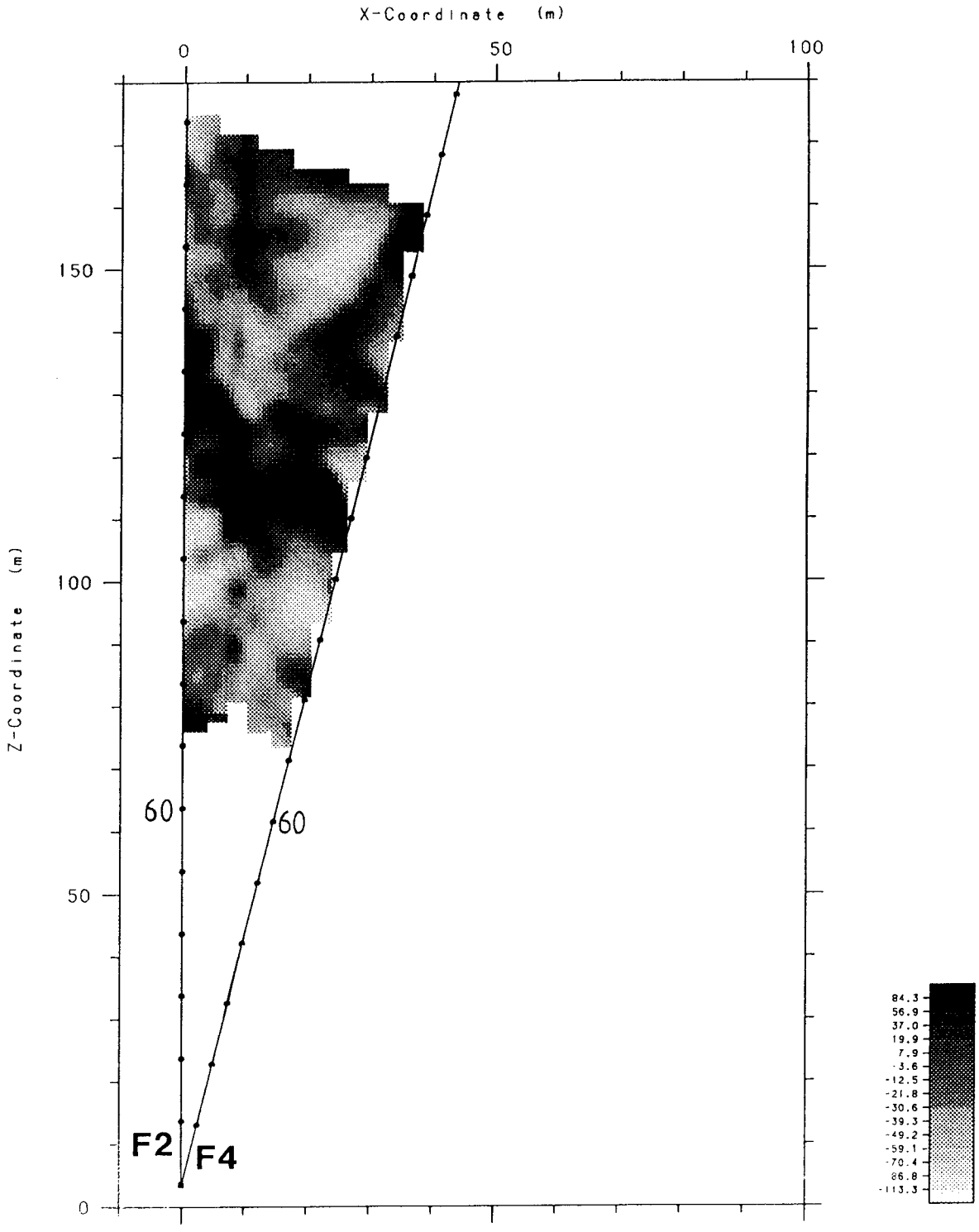

Residual attenuation tomogram (dB/km) for the borehole section F2-F4 made with a center frequency of 60 MHz.

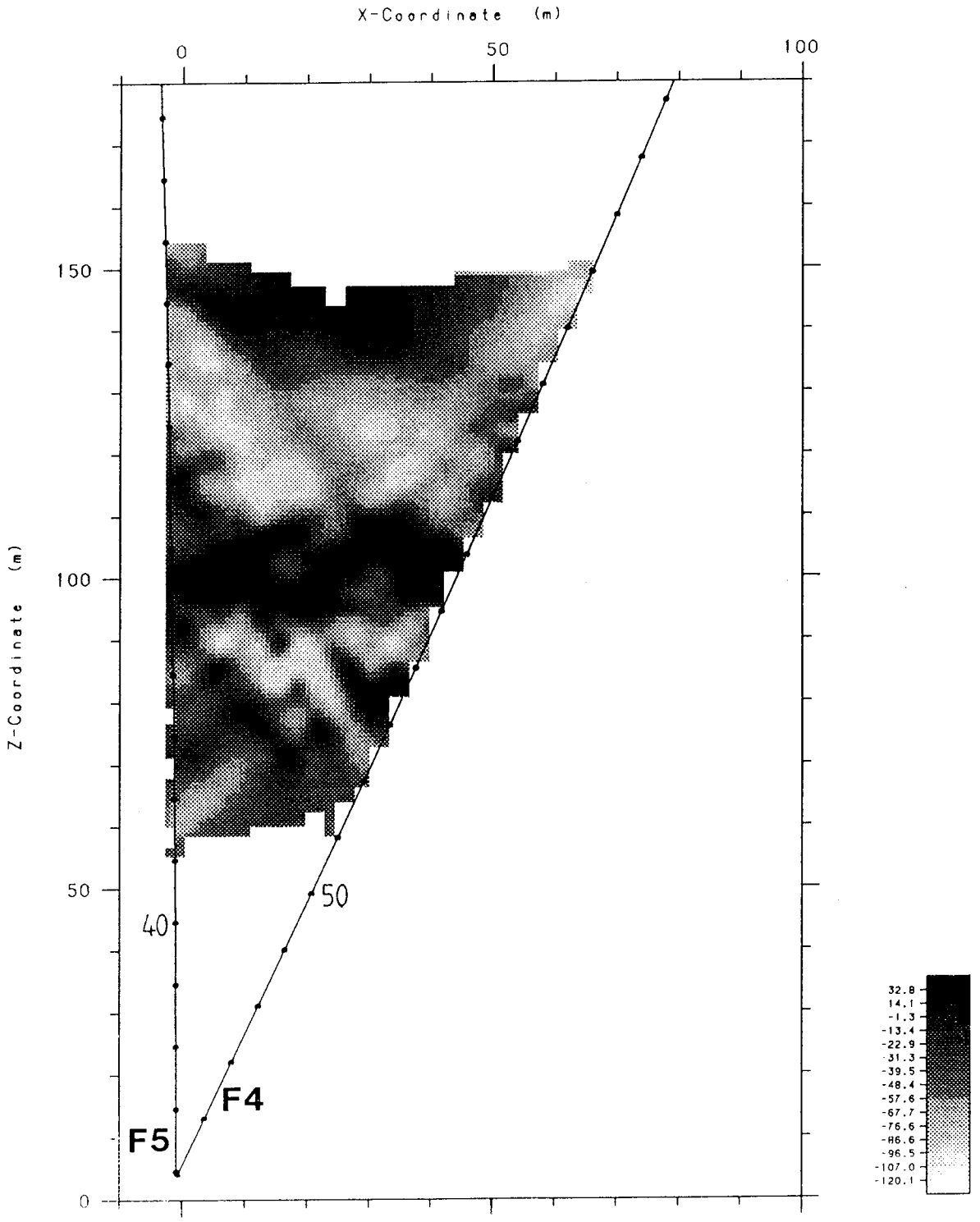

Residual attenuation tomogram (dB/km) for the borehole section F5-F4 made with a center frequency of 60 MHz.

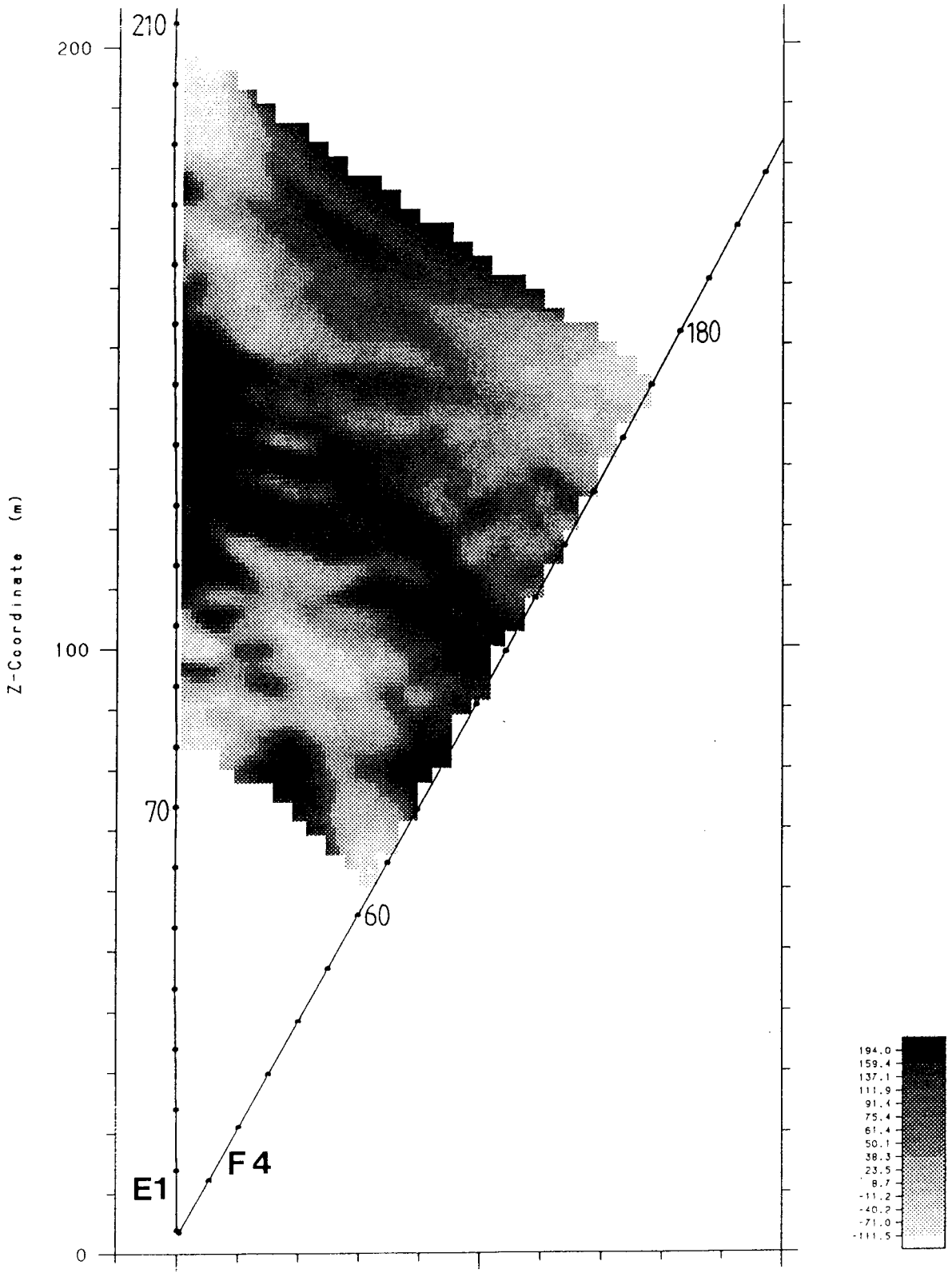

Residual attenuation tomogram (dB/km) for the borehole section E1-F4 made with a center frequency of 60 MHz.

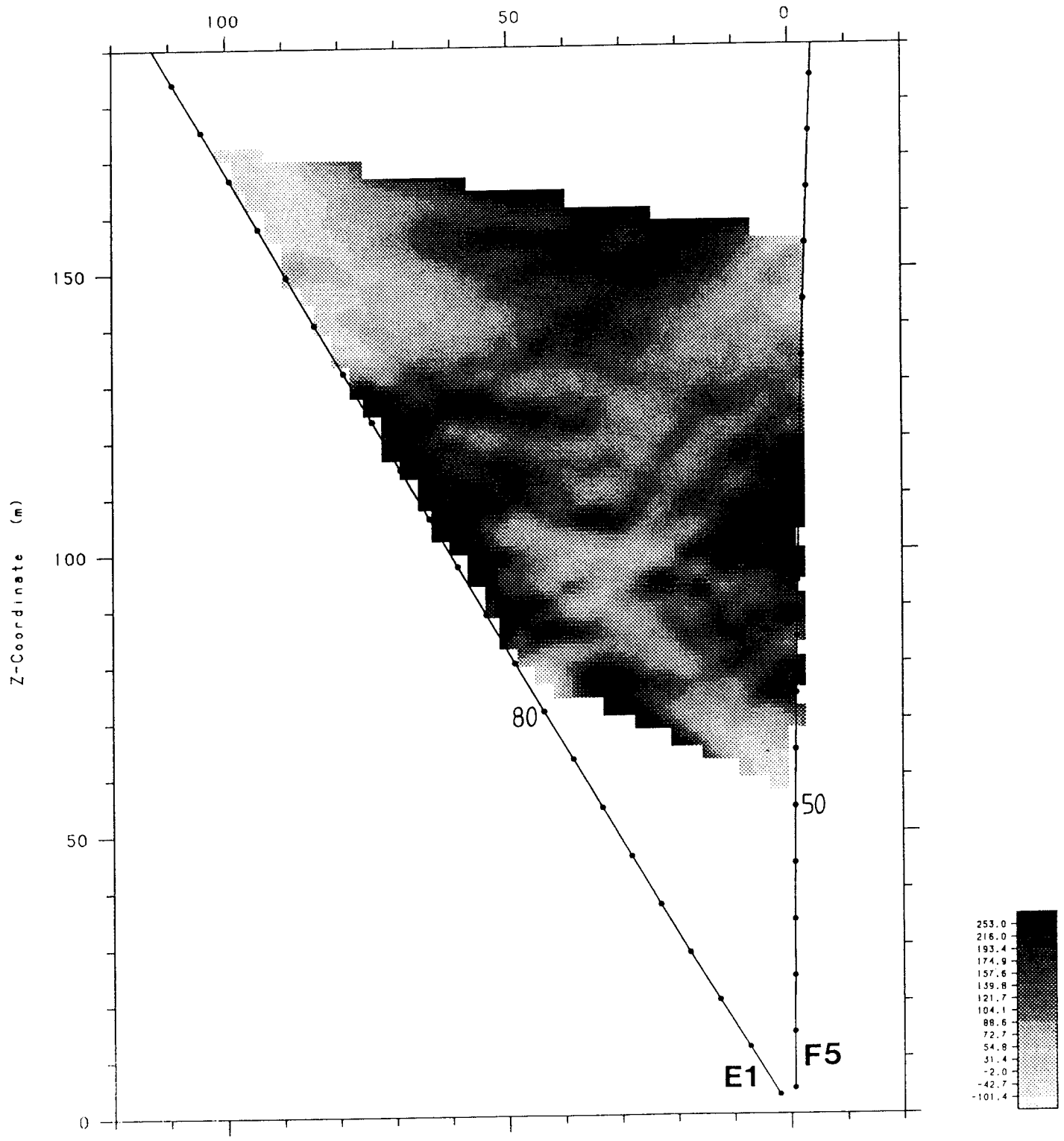

Residual attenuation tomogram (dB/km) for the borehole section F5-E1 made with a center frequency of 60 MHz.

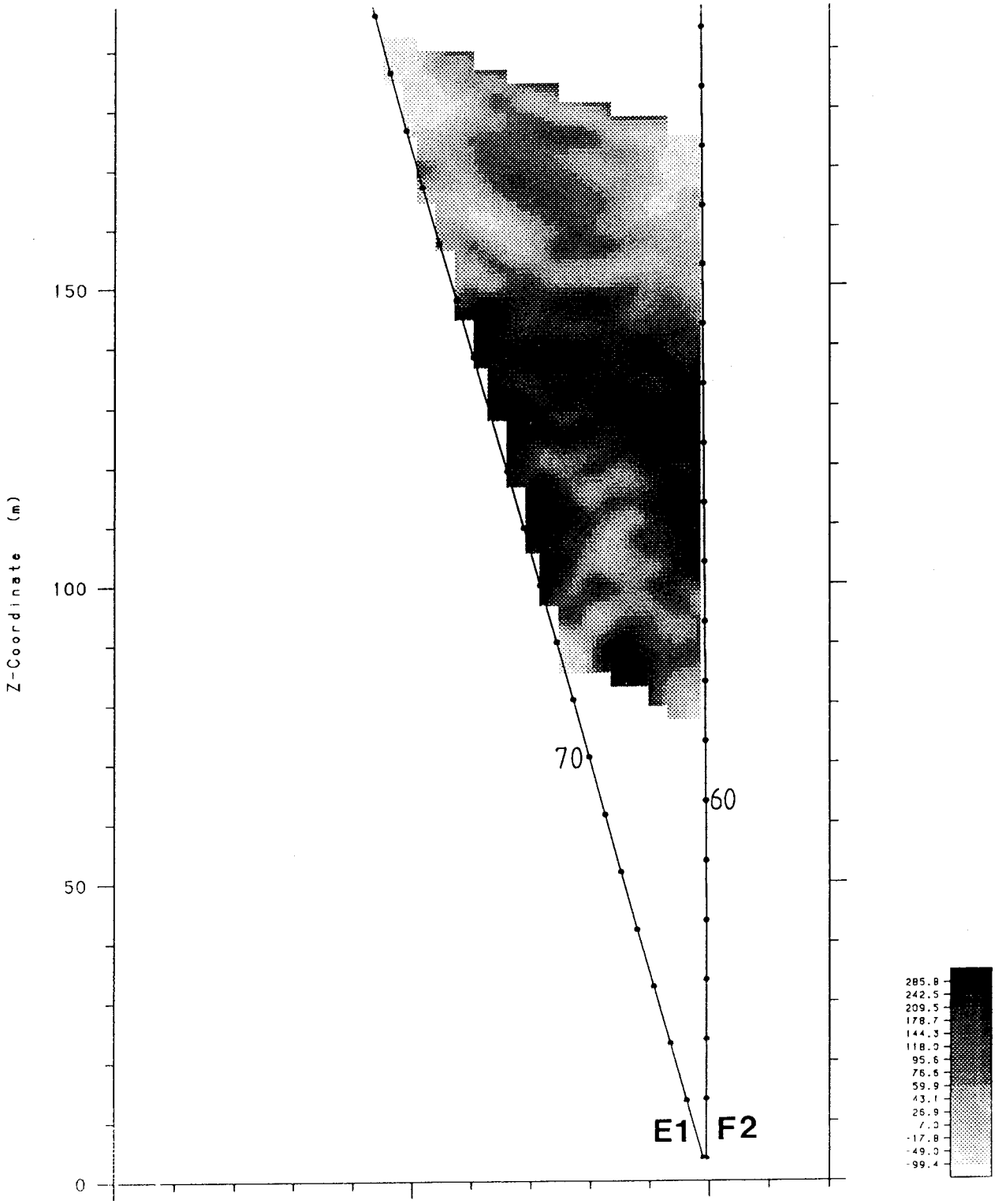

Residual attenuation tomogram (dB/km) for the borehole section F2-E1 made with a center frequency of 60 MHz.

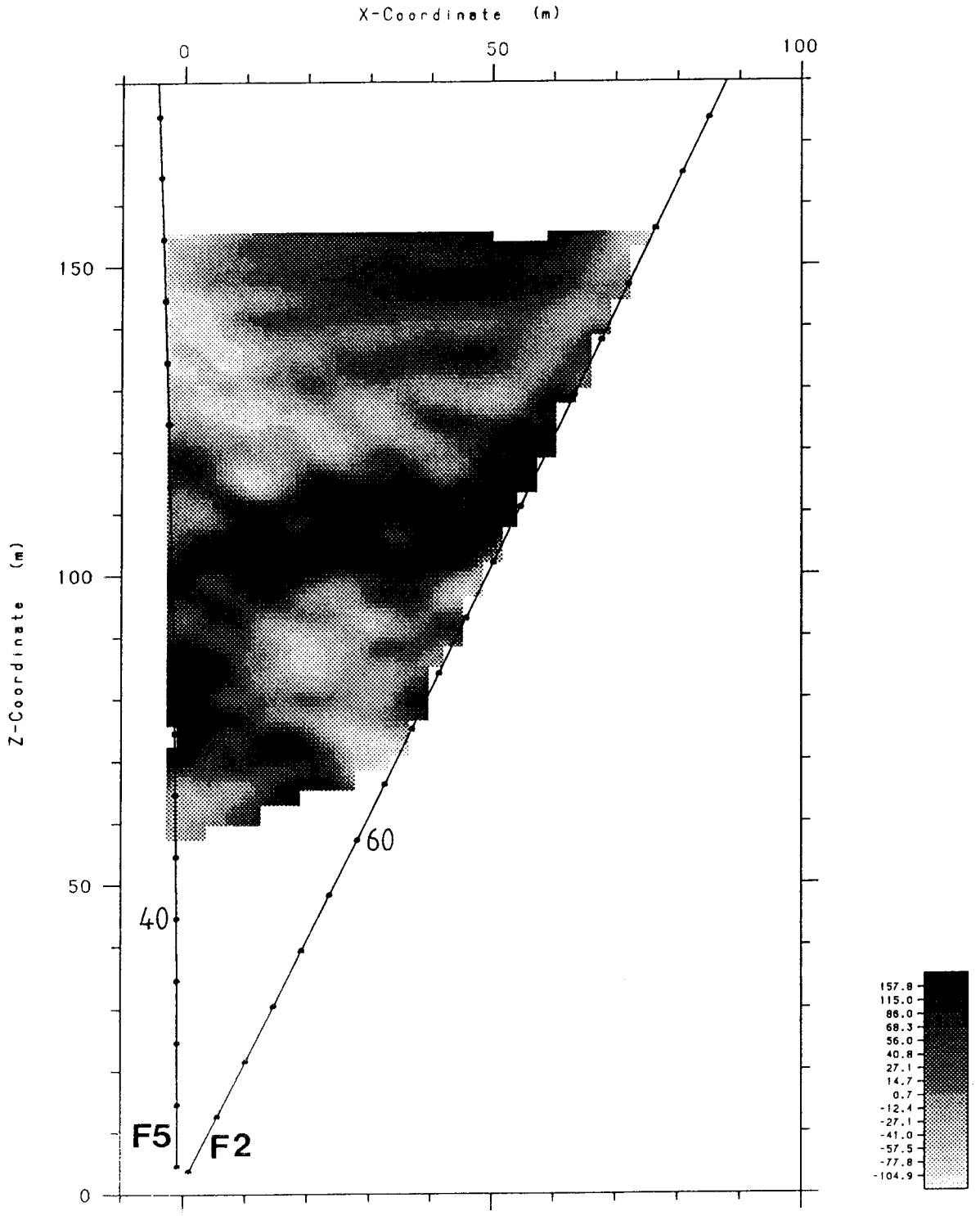

Residual attenuation tomogram (dB/km) for the borehole section F5-F2 made with a center frequency of 60 MHz.

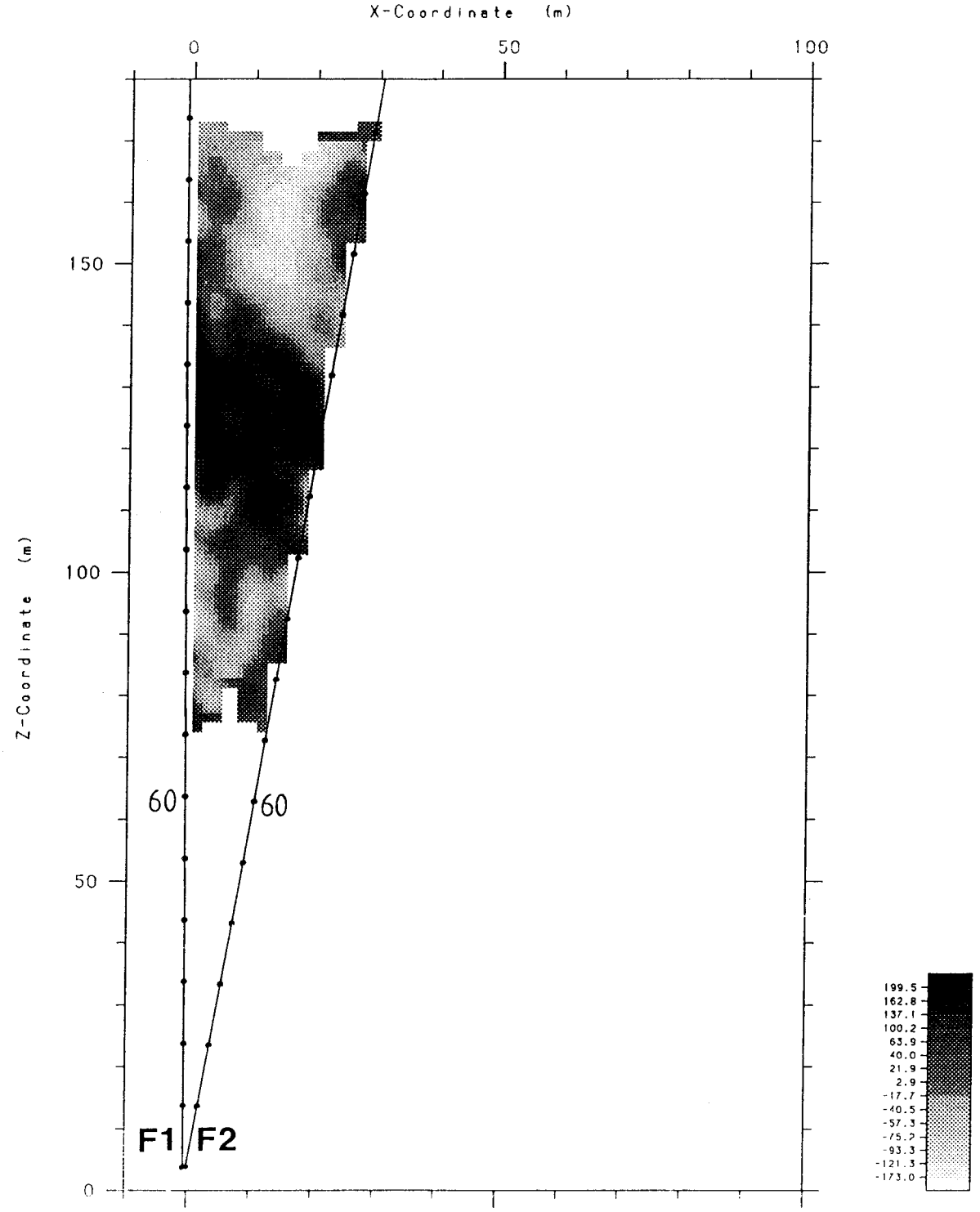

Residual attenuation tomogram (dB/km) for the borehole section F1-F2 made with a center frequency of 60 MHz.

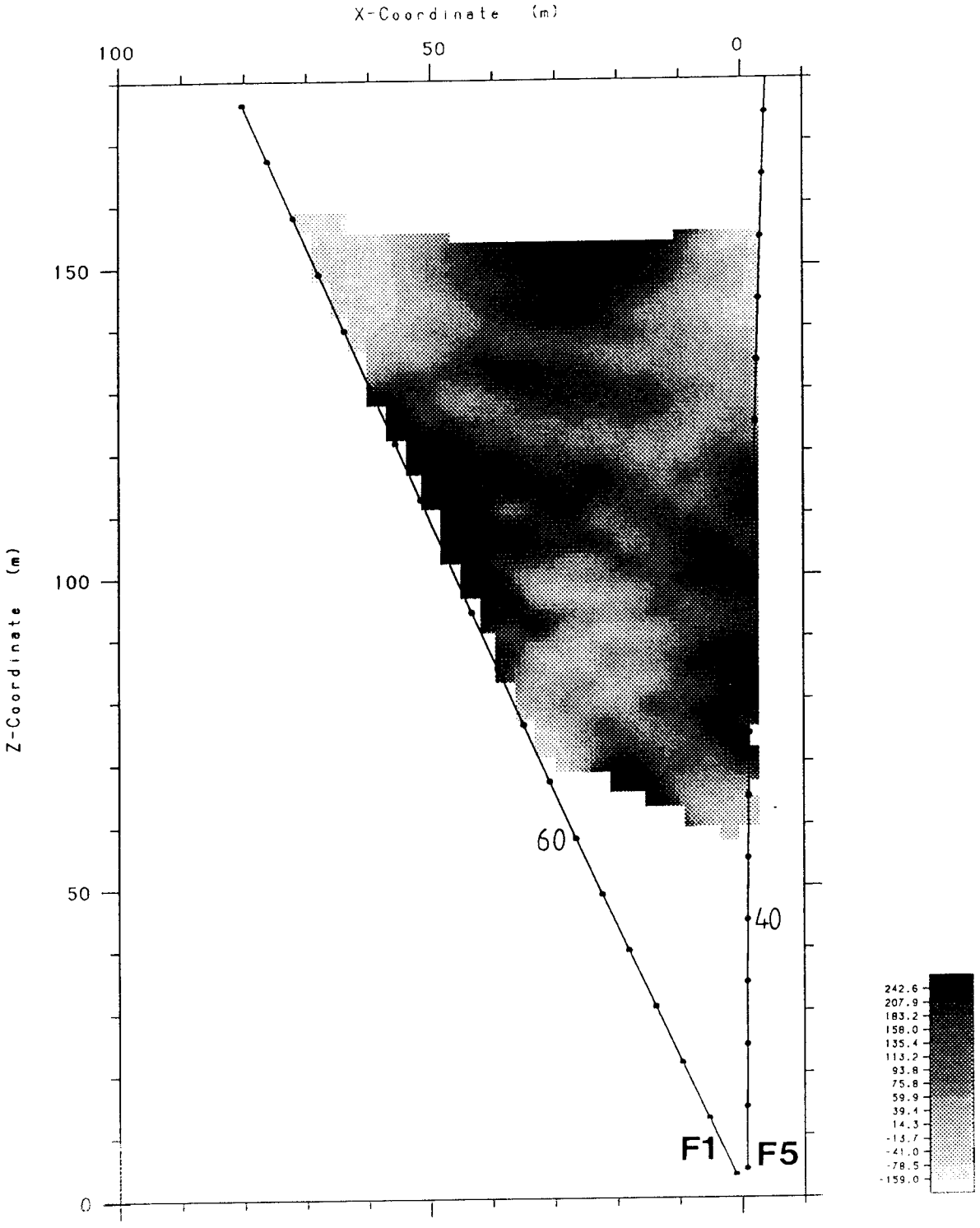

Residual attenuation tomogram (dB/km) for the borehole section F5-F1 made with a center frequency of 60 MHz.

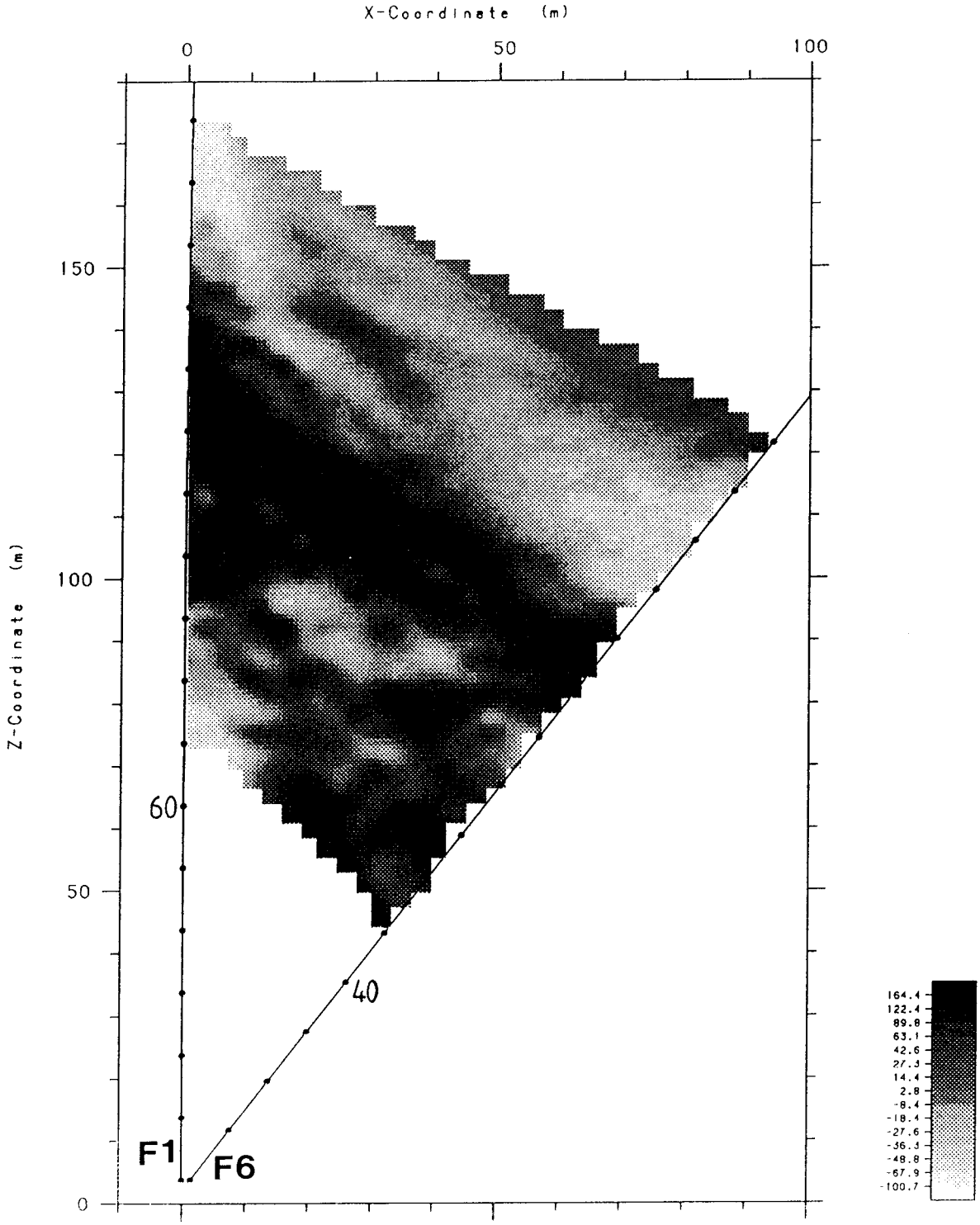

Residual attenuation tomogram (dB/km) for the borehole section F1-F6 made with a center frequency of 60 MHz.

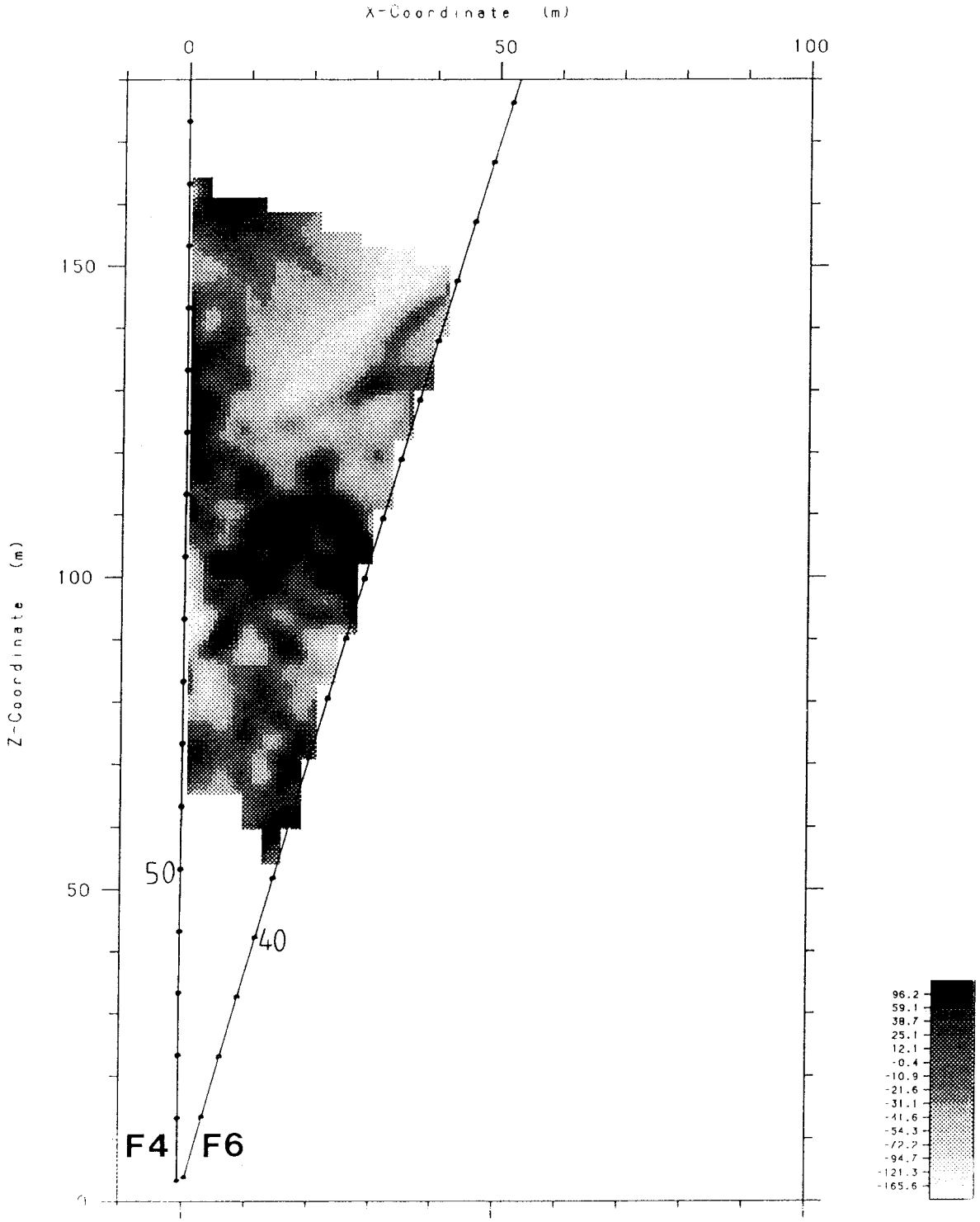

Residual attenuation tomogram (dB/km) for the borehole section F4-F6 made with a center frequency of 60 MHz.

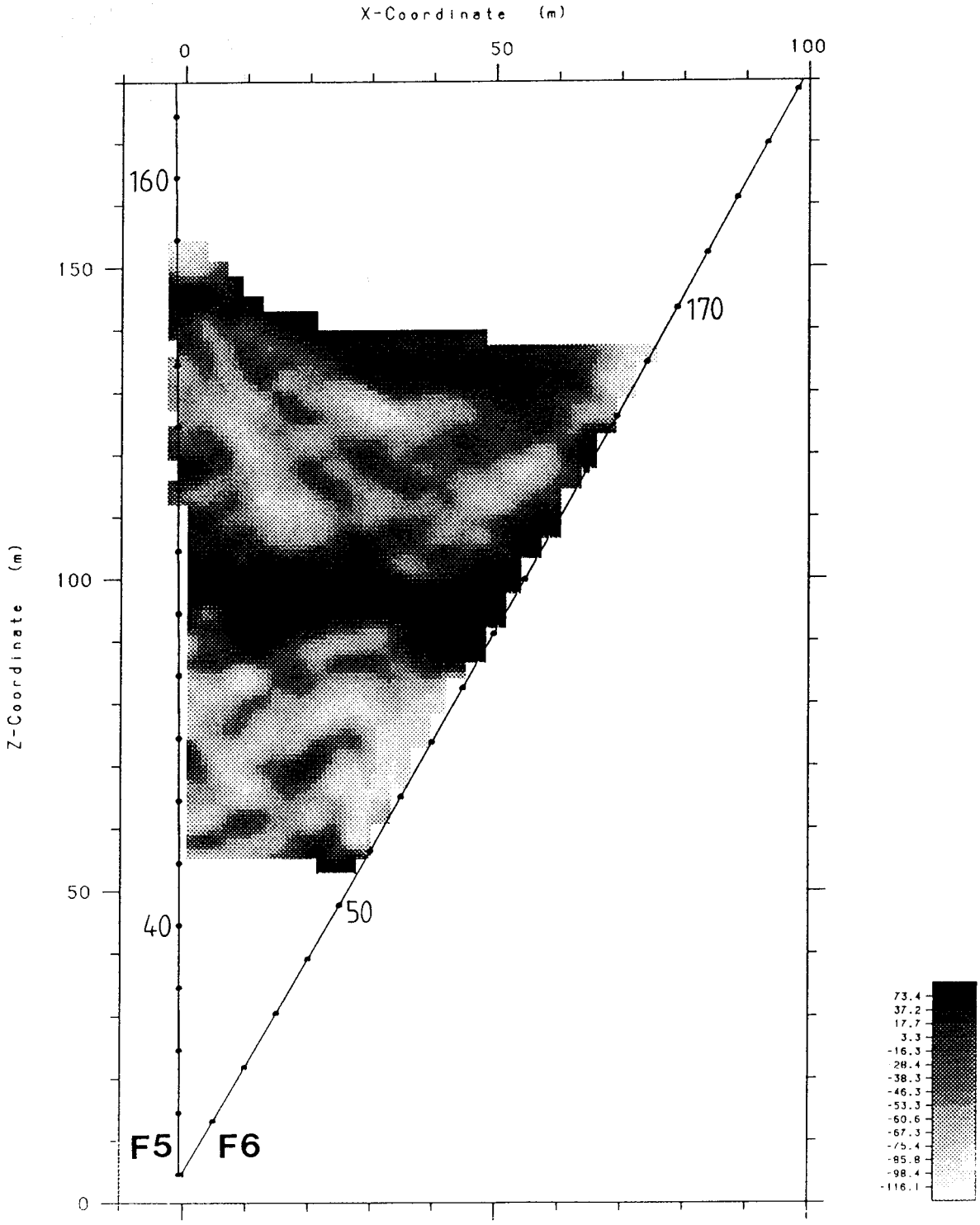

Residual attenuation tomogram (dB/km) for the borehole section F5-F6 made with a center frequency of 60 MHz.

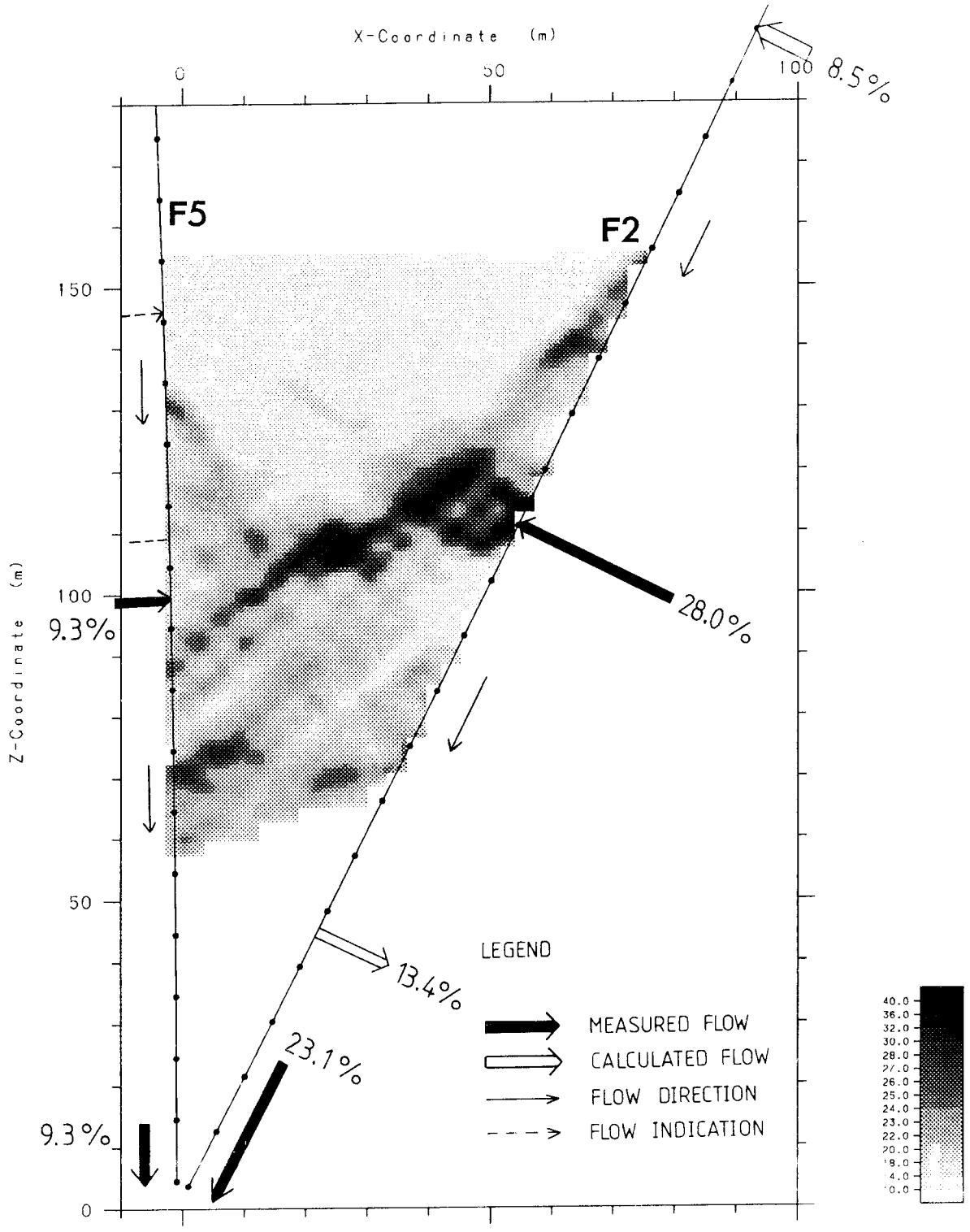

Difference tomogram for section F5F2 showing residual attenuation (dB/km) in the rock formation, due to injection of saline tracer. Location of tracer breakthrough and flow direction are marked with arrows. Numbers are referring to the recovery, R_f.

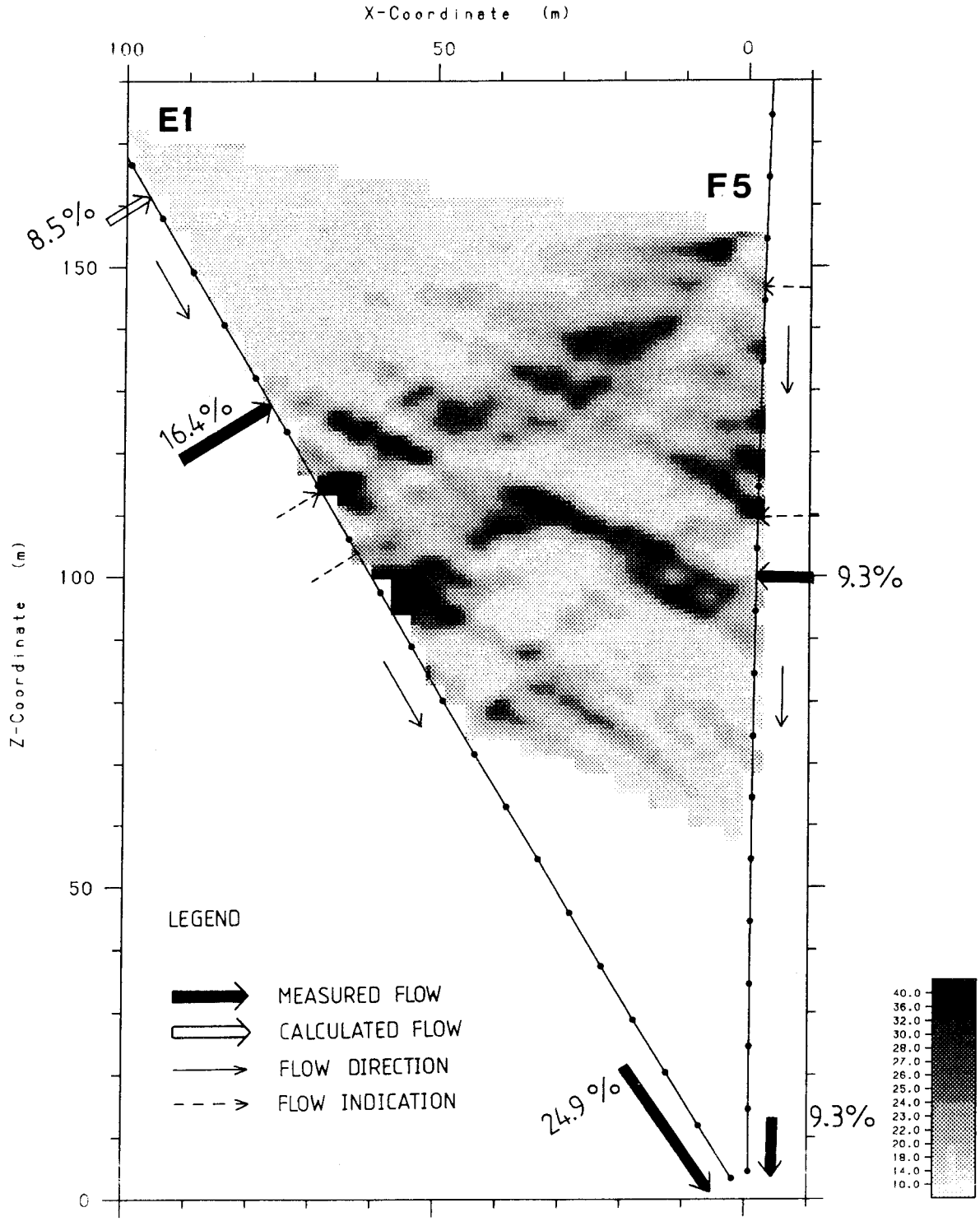

Difference tomogram for section F5E1 showing residual attenuation (dB/km) in the rock formation, due to injection of saline tracer. Location of tracer breakthrough and flow direction are marked with arrows. Numbers are referring to the recovery, R_f.

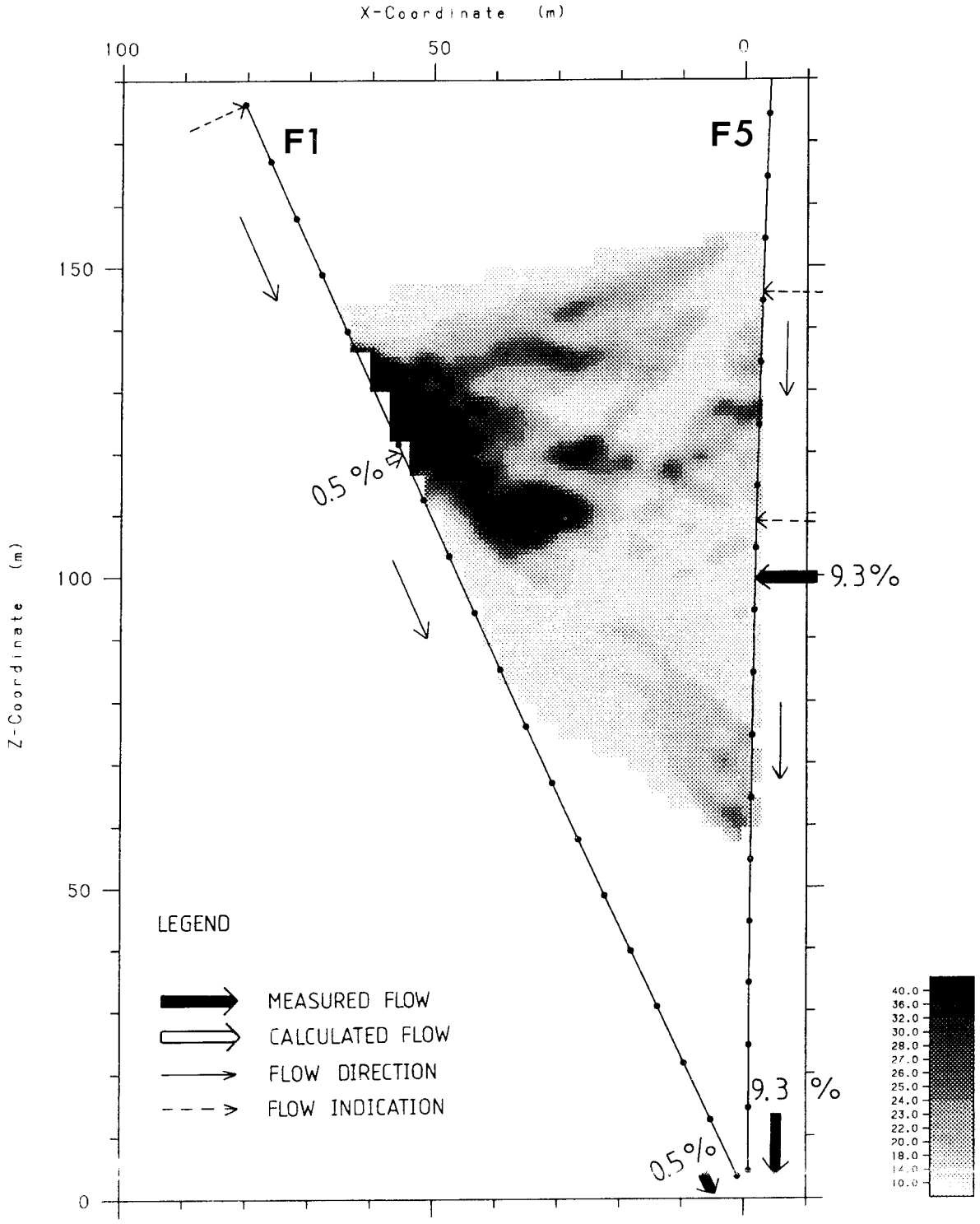

Difference tomogram for section F5F1 showing residual attenuation (dB/km) in the rock formation, due to injection of saline tracer. Location of tracer breakthrough and flow direction are marked with arrows. Numbers are referring to the recovery, R_f.

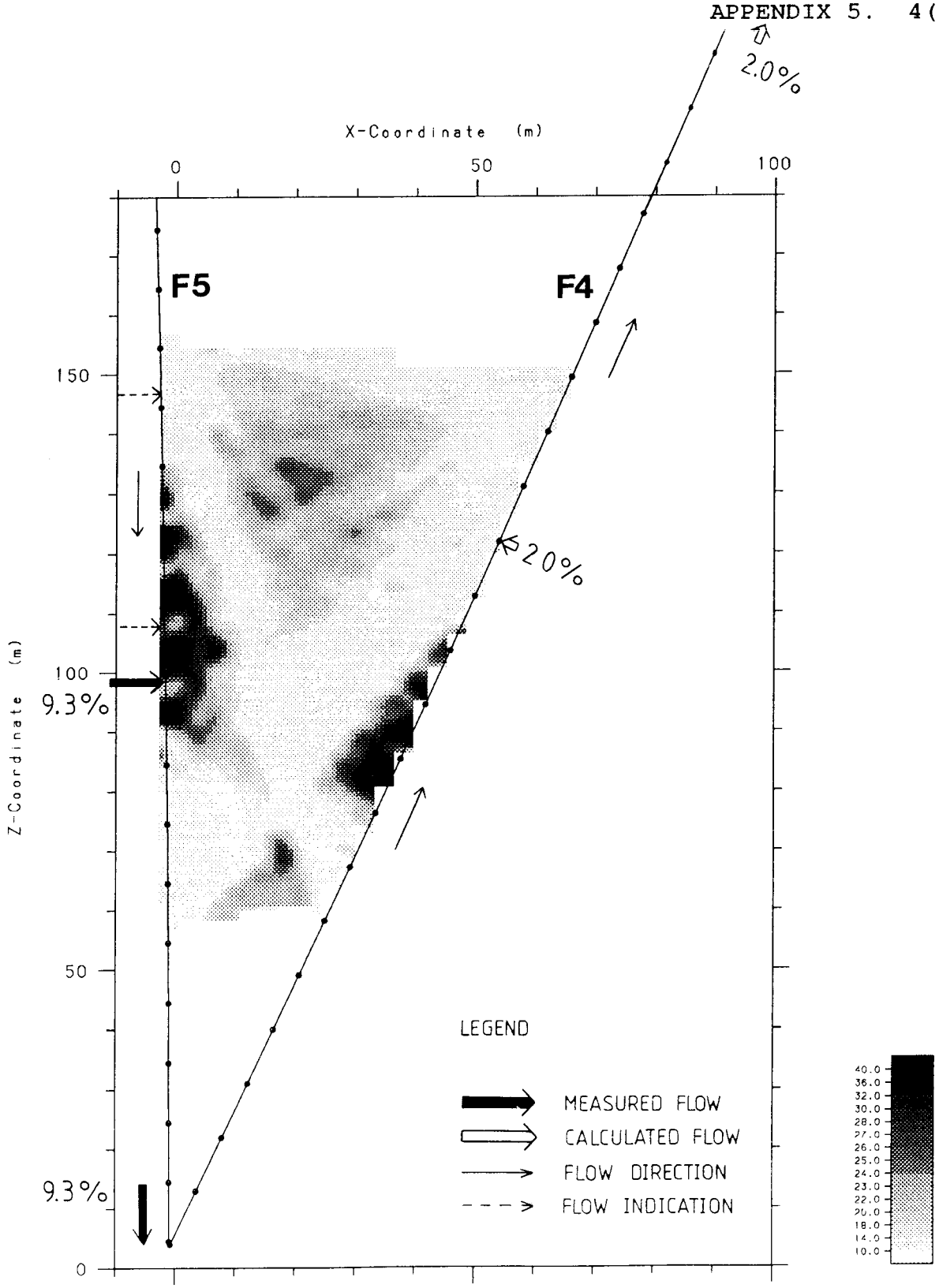

Difference tomogram for section F5F4 showing residual attenuation (dB/km) in the rock formation, due to injection of saline tracer. Location of tracer breakthrough and flow direction are marked with arrows. Numbers are referring to the recovery, R_f.

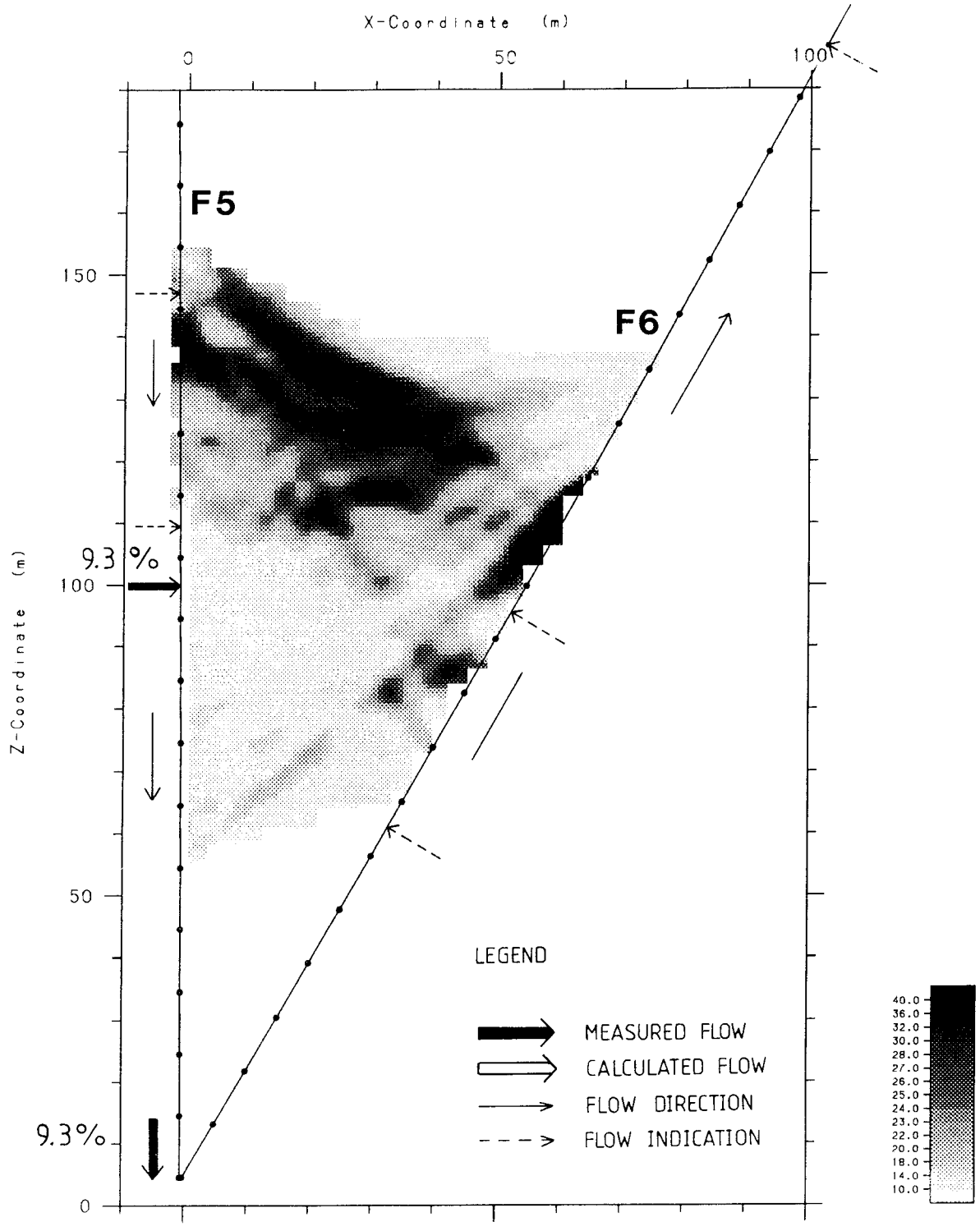

Difference tomogram for section F5F6 showing residual attenuation (dB/km) in the rock formation, due to injection of saline tracer. Location of tracer breakthrough and flow direction are marked with arrows. Numbers are referring to the recovery, R_f.

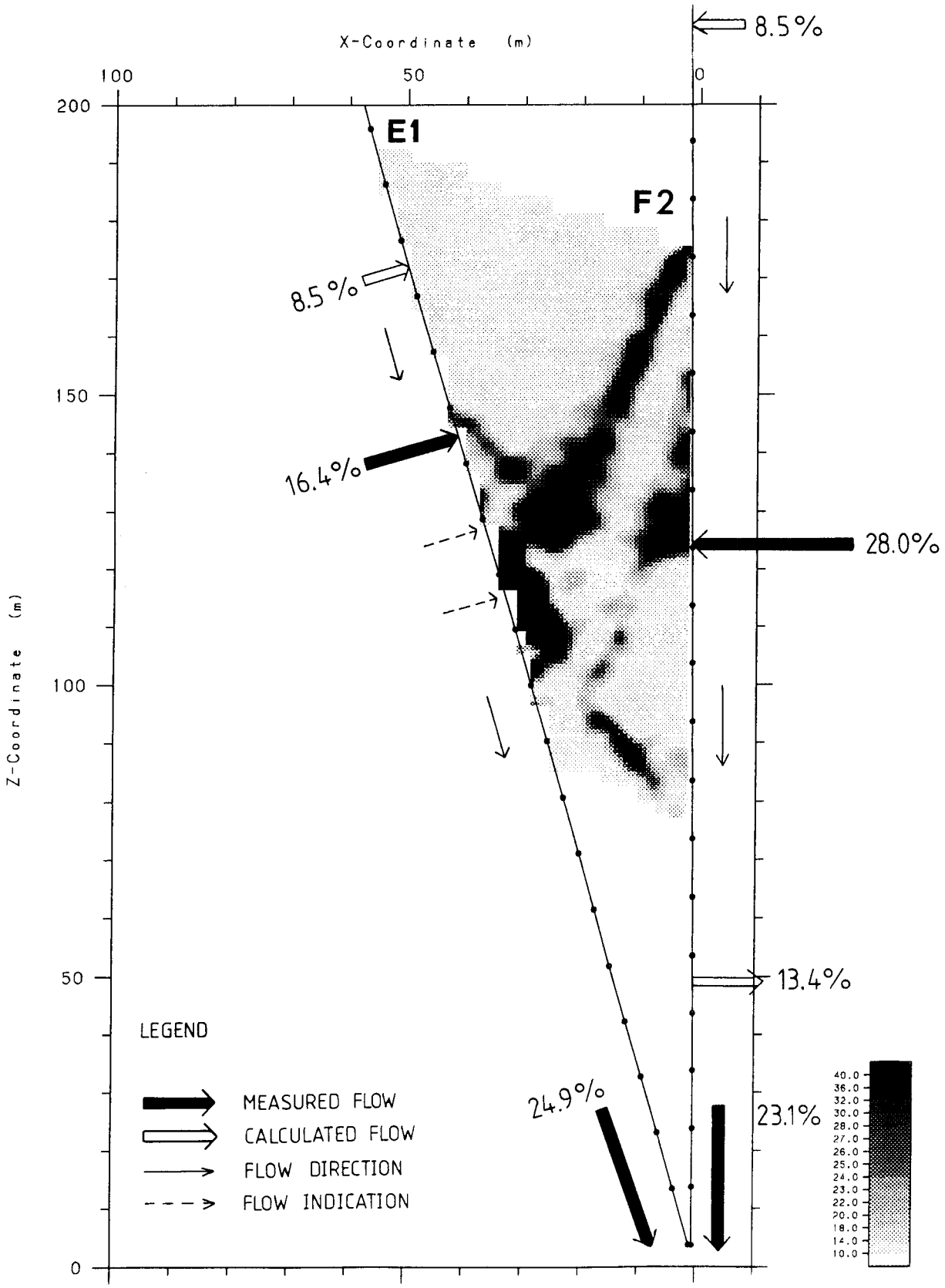

Difference tomogram for section F2E1 showing residual attenuation (dB/km) in the rock formation, due to injection of saline tracer. Location of tracer breakthrough and flow direction are marked with arrows. Numbers are referring to the recovery, R_f.

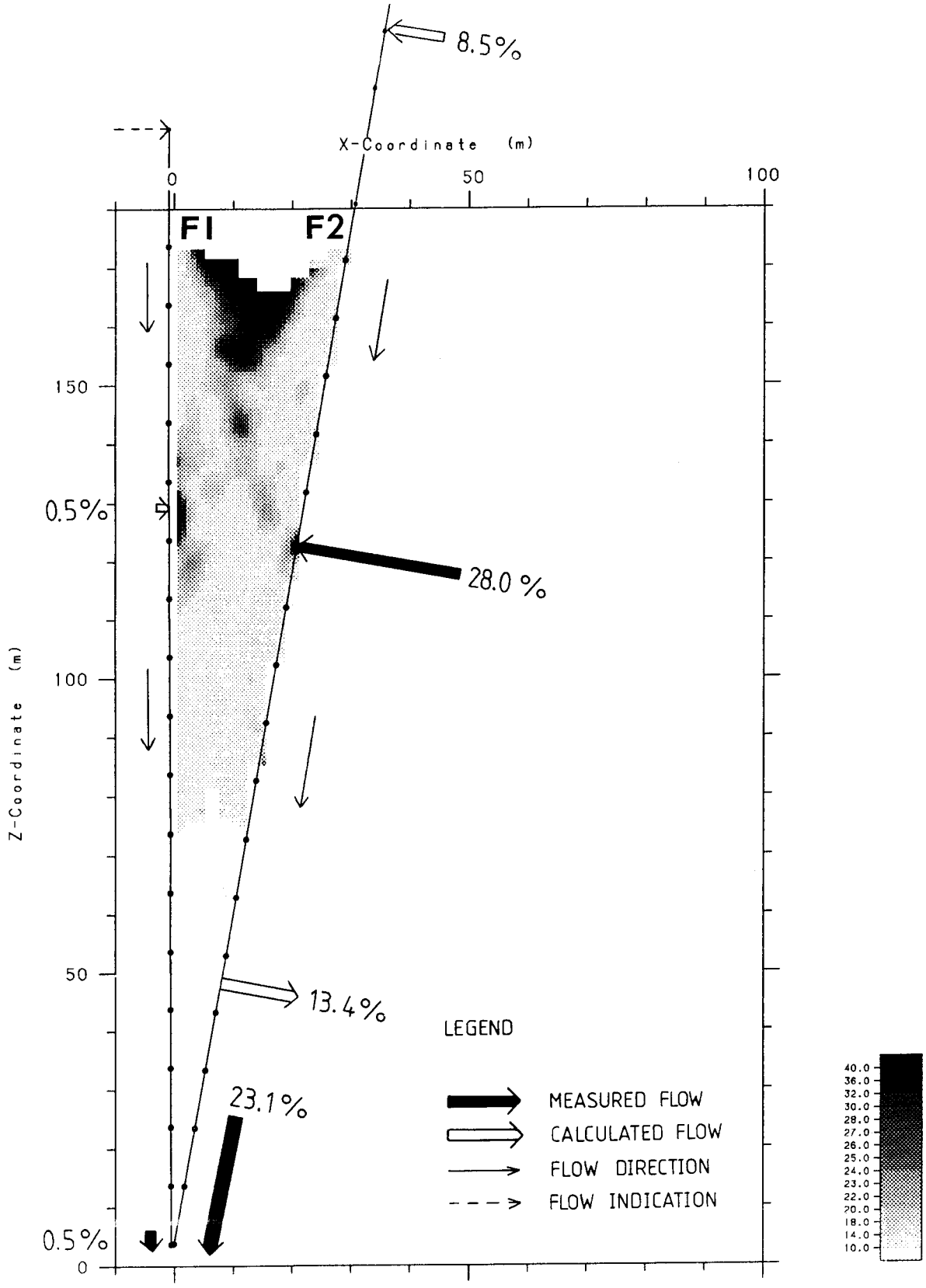

Difference tomogram for section F1F2 showing residual attenuation (dB/km) in the rock formation, due to injection of saline tracer. Location of tracer breakthrough and flow direction are marked with arrows. Numbers are referring to the recovery, R_f.

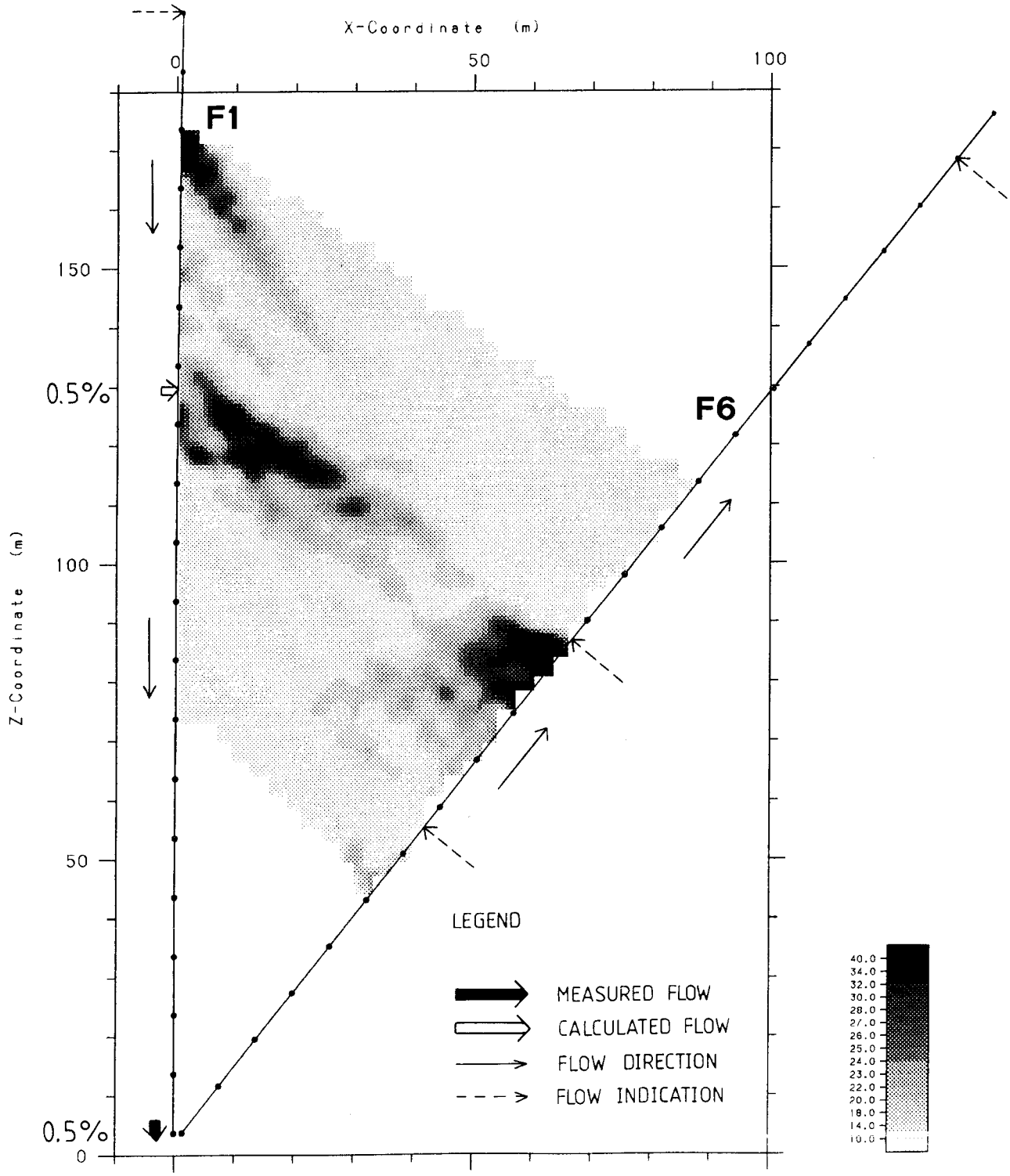

Difference tomogram for section F1F6 showing residual attenuation (dB/km) in the rock formation, due to injection of saline tracer. Location of tracer breakthrough and flow direction are marked with arrows. Numbers are referring to the recovery, R_f.

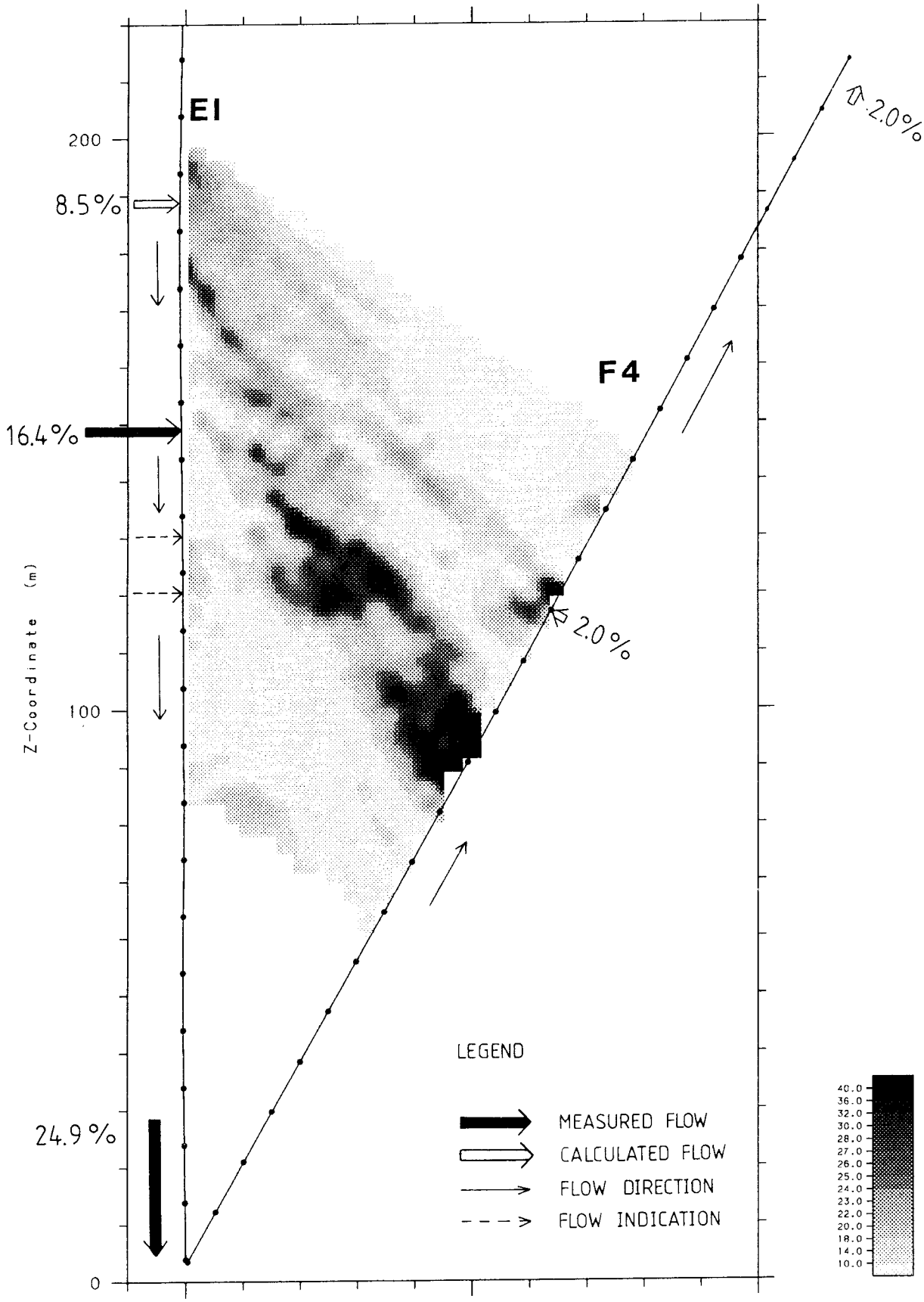

Difference tomogram for section E1F4 showing residual attenuation (dB/km) in the rock formation, due to injection of saline tracer. Location of tracer breakthrough and flow direction are marked with arrows. Numbers are referring to the recovery, R_f.

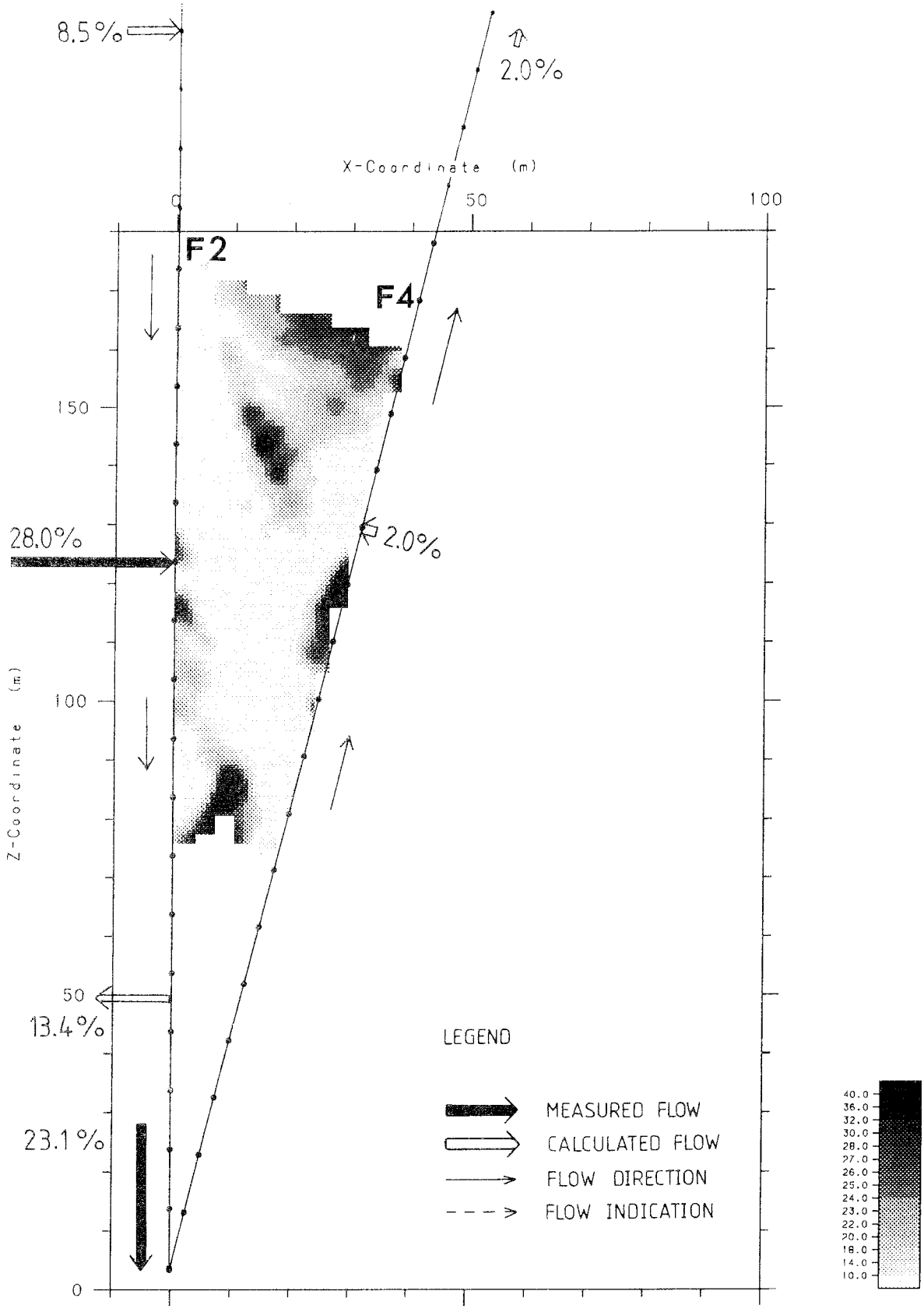

Difference tomogram for section F2F4 showing residual attenuation (dB/km) in the rock formation, due to injection of saline tracer. Location of tracer breakthrough and flow direction are marked with arrows. Numbers are referring to the recovery, R_f.

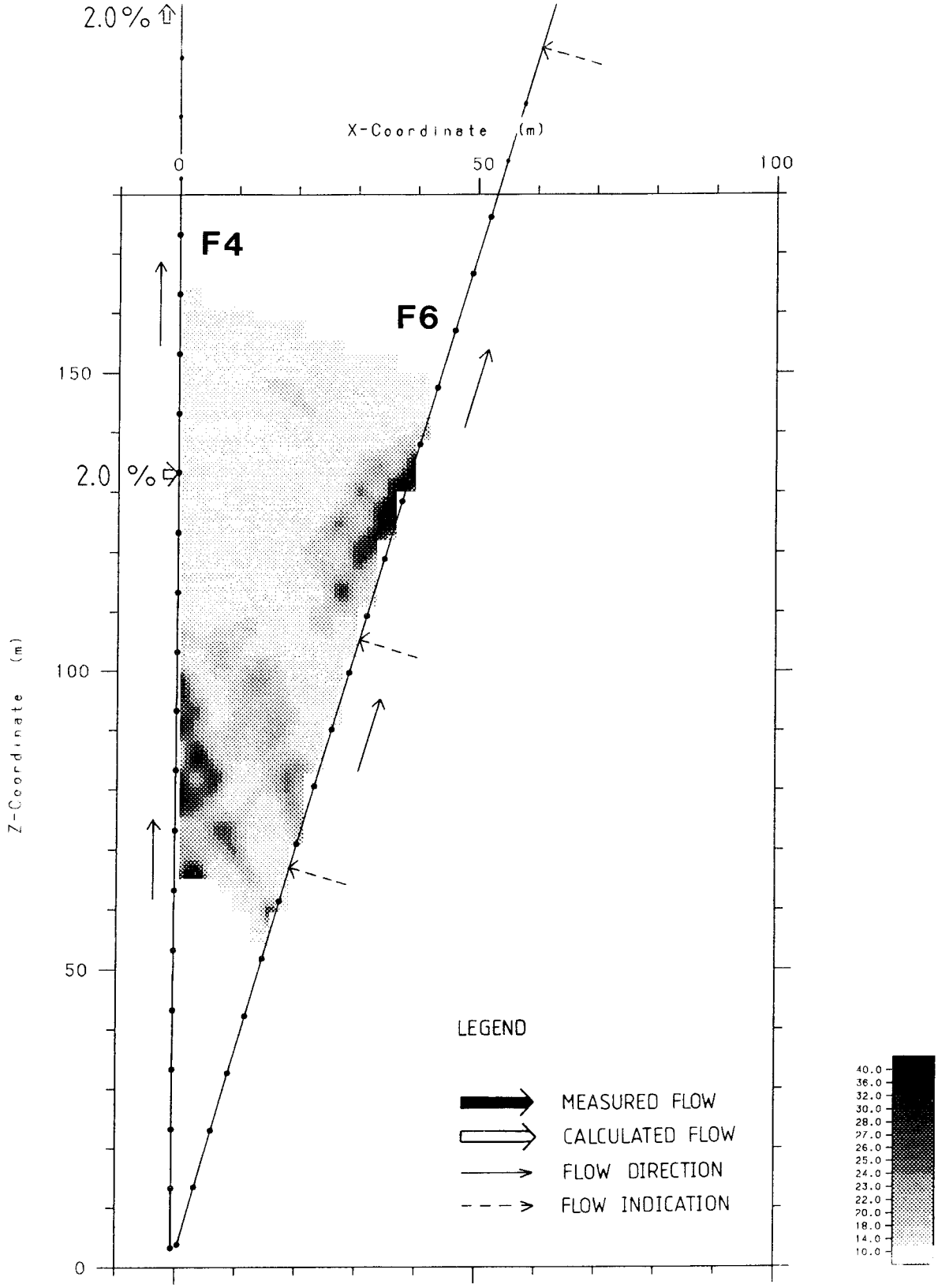

Difference tomogram for section F4F6 showing residual attenuation (dB/km) in the rock formation, due to injection of saline tracer. Location of tracer breakthrough and flow direction are marked with arrows. Numbers are referring to the recovery, R_f.

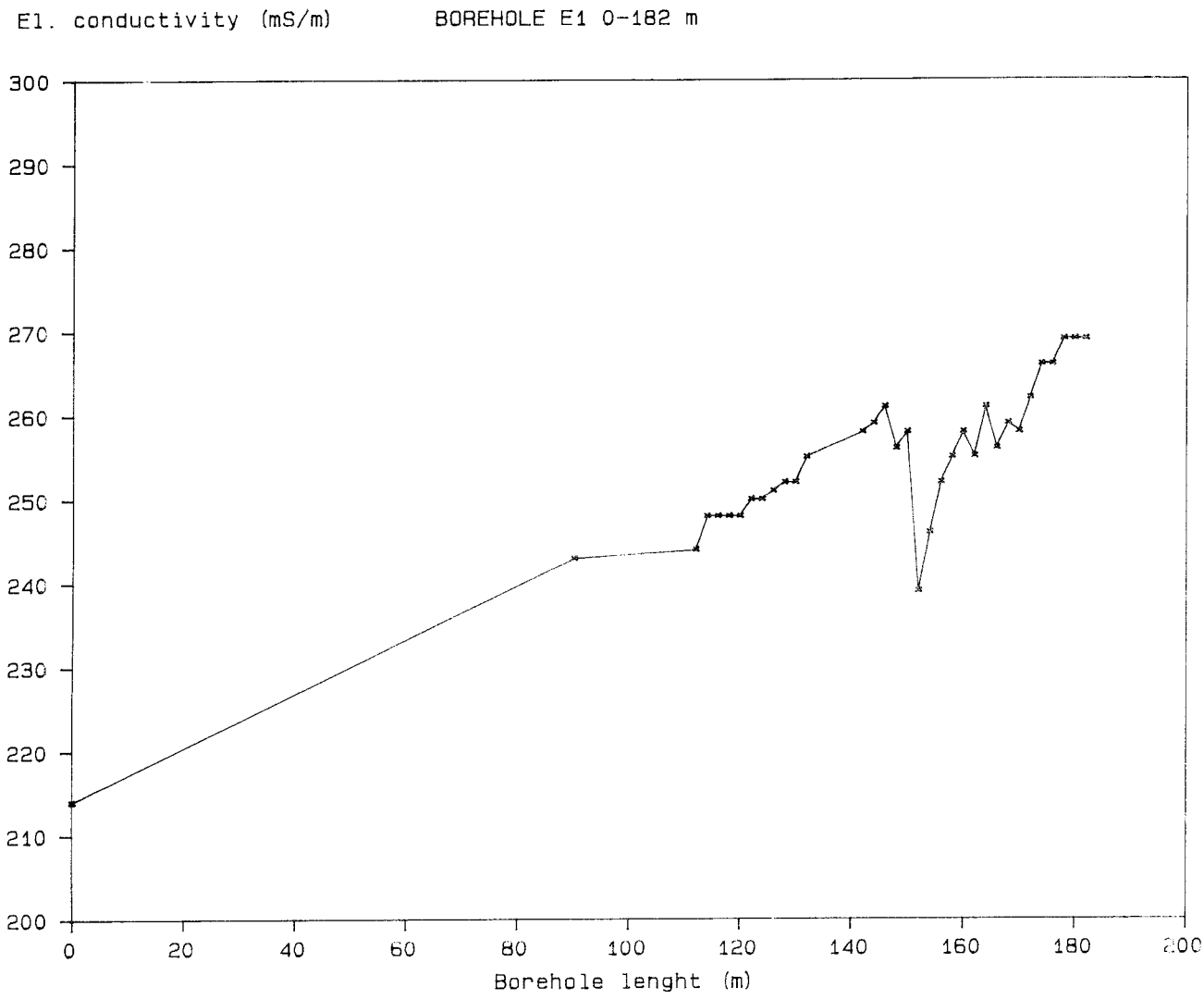

Electrical conductivity log, borehole E1; 0-182 meter.

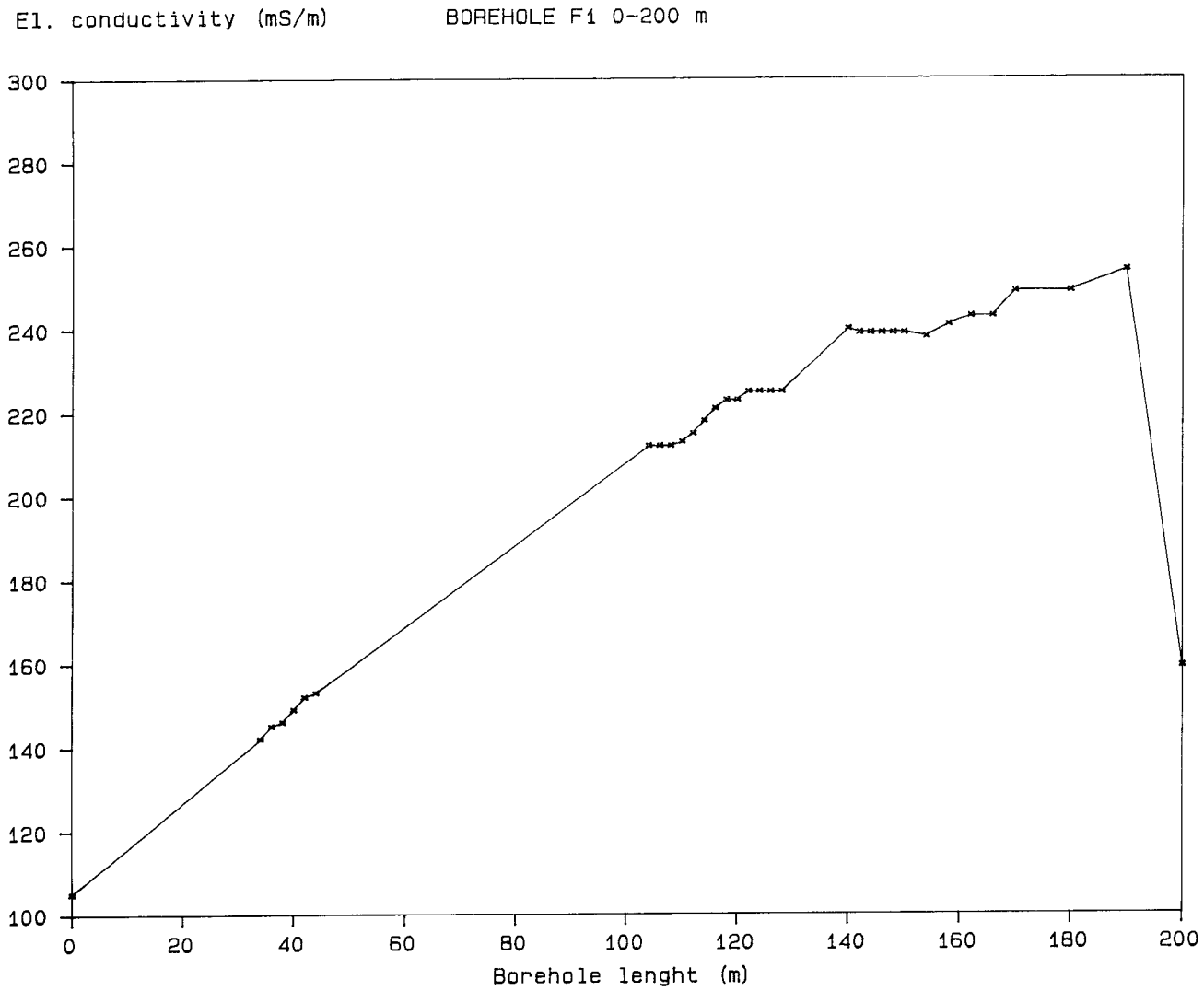

Electrical conductivity log, borehole F1; 0-200 meter.

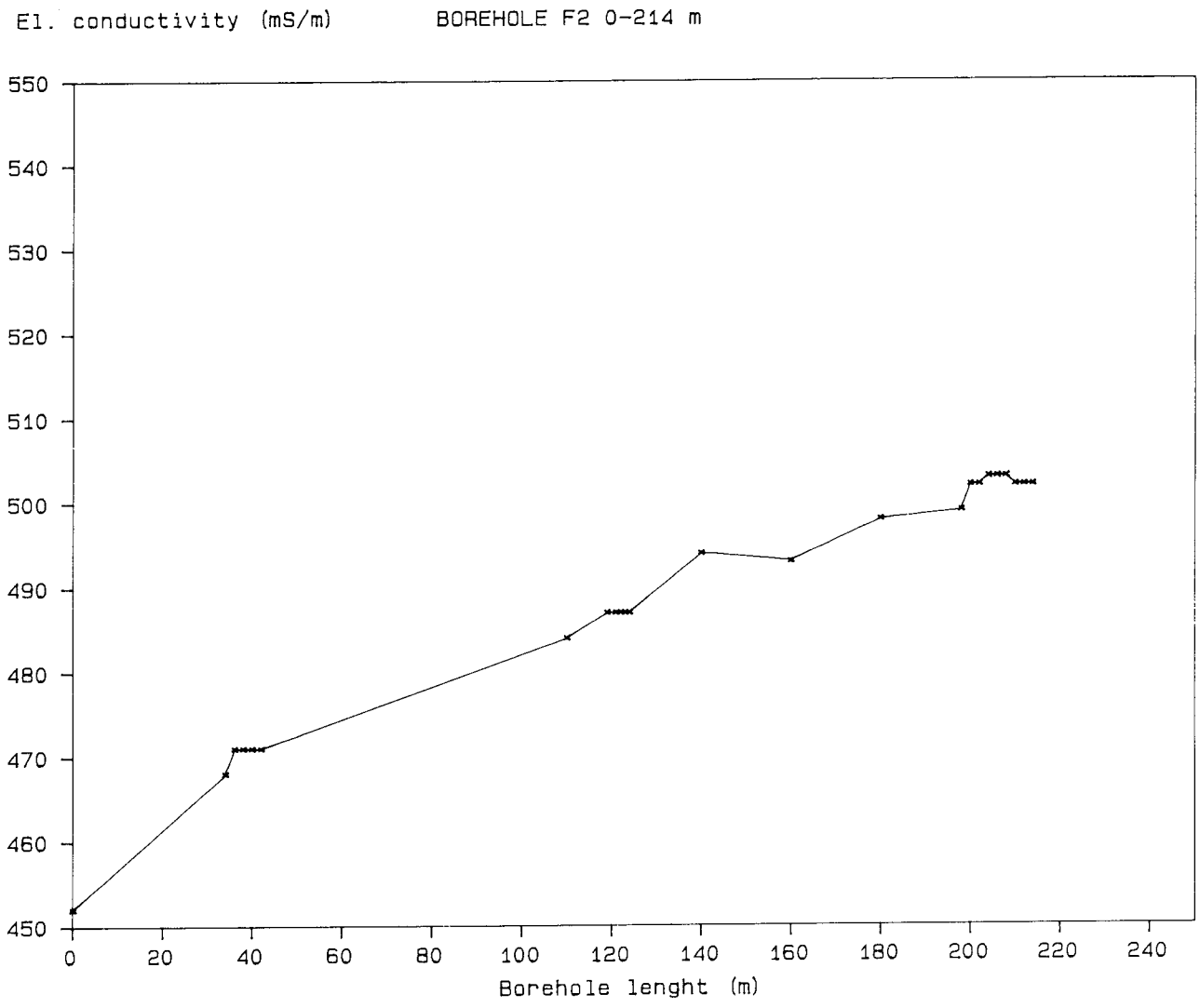

Electrical conductivity log, borehole F2; 0-214 meter.

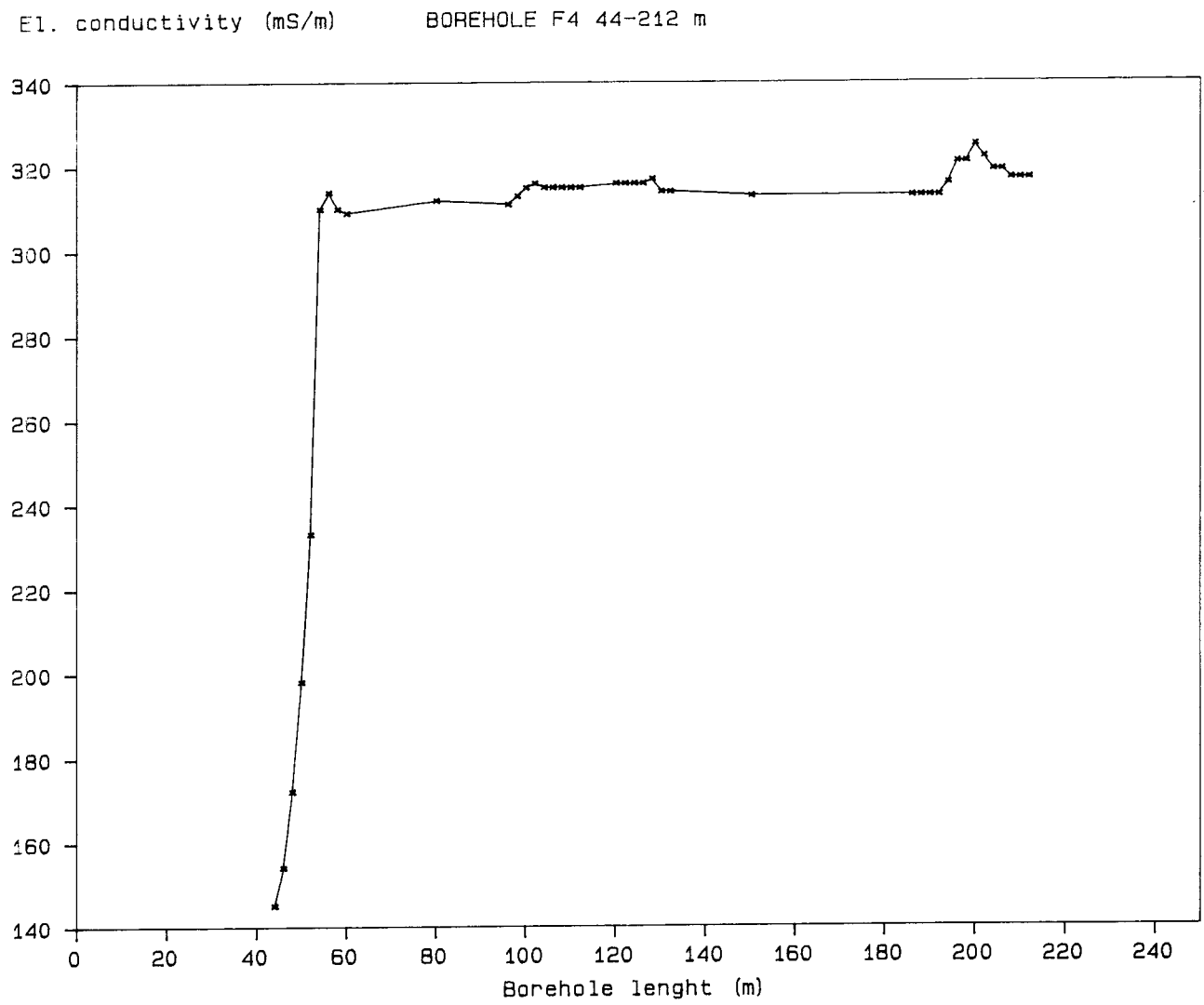

Electrical conductivity log, borehole F4; 44-212 meter.

List of SKB reports

Annual Reports

1977–78
TR 121
KBS Technical Reports 1 – 120.
Summaries. Stockholm, May 1979.

1979
TR 79–28
The KBS Annual Report 1979.
KBS Technical Reports 79-01 – 79-27.
Summaries. Stockholm, March 1980.

1980
TR 80–26
The KBS Annual Report 1980.
KBS Technical Reports 80-01 – 80-25.
Summaries. Stockholm, March 1981.

1981
TR 81–17
The KBS Annual Report 1981.
KBS Technical Reports 81-01 – 81-16.
Summaries. Stockholm, April 1982.

1982
TR 82–28
The KBS Annual Report 1982.
KBS Technical Reports 82-01 – 82-27.
Summaries. Stockholm, July 1983.

1983
TR 83–77
The KBS Annual Report 1983.
KBS Technical Reports 83-01 – 83-76
Summaries. Stockholm, June 1984.

1984
TR 85–01
Annual Research and Development Report 1984
Including Summaries of Technical Reports Issued during 1984. (Technical Reports 84-01– 84-19)
Stockholm June 1985.

1985
TR 85-20
Annual Research and Development Report 1985
Including Summaries of Technical Reports Issued during 1985. (Technical Reports 85-01-85-19)
Stockholm May 1986.

1986
TR 86-31
SKB Annual Report 1986
Including Summaries of Technical Reports Issued during 1986
Stockholm, May 1987

1987
TR 87-33
SKB Annual Report 1987
Including Summaries of Technical Reports Issued during 1987
Stockholm, May 1988

1988
TR 88-32
SKB Annual Report 1988
Including Summaries of Technical Reports Issued during 1988
Stockholm, May 1989

Technical Reports

1989
TR 89-01
Near-distance seismological monitoring of the Lansjärv neotectonic fault region Part II: 1988
Rutger Wahlström, Sven-Olof Linder, Conny Holmqvist, Hans-Edy Mårtensson
Seismological Department, Uppsala University, Uppsala
January 1989

TR 89-02
Description of background data in SKB database GEOTAB
Ebbe Eriksson, Stefan Sehlstedt
SGAB, Luleå
February 1989

TR 89-03
Characterization of the morphology, basement rock and tectonics in Sweden
Kennert Röshoff
August 1988

TR 89-04
SKB WP-Cave Project
Radionuclide release from the near-field in a WP-Cave repository
Maria Lindgren, Kristina Skagius
Kemakta Consultants Co, Stockholm
April 1989

TR 89-05
SKB WP-Cave Project
Transport of escaping radionuclides from the WP-Cave repository to the biosphere
Luis Moreno, Sue Arve, Ivars Neretnieks
Royal Institute of Technology, Stockholm
April 1989

TR 89-06
SKB WP-Cave Project
Individual radiation doses from nuclides contained in a WP-Cave repository for spent fuel
Sture Nordlinder, Ulla Bergström
Studsvik Nuclear, Studsvik
April 1989

TR 89-07
SKB WP-Cave Project
Some Notes on Technical Issues
Part 1: Temperature distribution in WP-Cave: when shafts are filled with sand/water mixtures
Stefan Björklund, Lennart Josefson
Division of Solid Mechanics, Chalmers University of Technology, Gothenburg, Sweden
Part 2: Gas and water transport from WP-Cave repository Luis Moreno, Ivars Neretnieks
Department of Chemical Engineering, Royal Institute of Technology, Stockholm, Sweden
Part 3: Transport of escaping nuclides from the WP-Cave repository to the biosphere. Influence of the hydraulic cage
Luis Moreno, Ivars Neretnieks
Department of Chemical Engineering, Royal Institute of Technology, Stockholm, Sweden
August 1989

TR 89-08
SKB WP-Cave Project
Thermally incuded convective motion in groundwater in the near field of the WP-Cave after filling and closure
Polydynamics Limited, Zürich
April 1989

TR 89-09
An evaluation of tracer tests performed at Studsvik
Luis Moreno[1], Ivars Neretnieks[1], Ove Landström[2]
[1] The Royal Institute of Technology, Department of Chemical Engineering, Stockholm
[2] Studsvik Nuclear, Nyköping
March 1989

TR 89-10
Copper produced from powder by HIP to encapsulate nuclear fuel elements
Lars B Ekbom, Sven Bogegård
Swedish National Defence Research Establishment
Materials department, Stockholm
February 1989

TR 89-11
Prediction of hydraulic conductivity and conductive fracture frequency by multivariate analysis of data from the Klipperås study site
Jan-Erik Andersson[1], Lennart Lindqvist[2]
[1] Swedish Geological Co, Uppsala
[2] EMX-system AB, Luleå
February 1988

TR 89-12
Hydraulic interference tests and tracer tests within the Brändan area, Finnsjön study site The Fracture Zone Project – Phase 3
Jan-Erik Andersson, Lennart Ekman, Erik Gustafsson, Rune Nordqvist, Sven Tirén
Swedish Geological Co, Division of Engineering Geology
June 1988

TR 89-13
Spent fuel
Dissolution and oxidation
An evaluation of literature data
Bernd Grambow
Hanh-Meitner-Institut, Berlin
March 1989

TR 89-14
The SKB spent fuel corrosion program Status report 1988
Lars O Werme[1], Roy S Forsyth[2]
[1] SKB, Stockholm
[2] Studsvik AB, Nyköping
May 1989

TR 89-15
Comparison between radar data and geophysical, geological and hydrological borehole parameters by multivariate analysis of data
Serje Carlsten, Lennart Lindqvist, Olle Olsson
Swedish Geological Company, Uppsala
March 1989

TR 89-16
Swedish Hard Rock Laboratory – Evaluation of 1988 year pre-investigations and description of the target area, the island of Äspö
Gunnar Gustafsson, Roy Stanfors, Peter Wikberg
June 1989

TR 89-17
Field instrumentation for hydrofracturing stress measurements
Documentation of the 1000 m hydrofracturing unit at Luleå University of Technology
Bjarni Bjarnason, Arne Torikka
August 1989

TR 89-18
Radar investigations at the Saltsjötunnel – predicitions and validation
Olle Olsson[1] and Kai Palmqvist[2]
[1] Abem AB, Uppsala, Sweden
[2] Bergab, Göteborg
June 1989

TR 89-19
Characterization of fracture zone 2, Finnsjön study-site
Editors: K. Ahlbom, J.A.T. Smellie, Swedish Geological Co, Uppsala
Part 1: Overview of the fracture zone project at Finnsjön, Sweden
K. Ahlbom and J.A.T. Smellie. Swedish Geological Company, Uppsala, Sweden.
Part 2: Geological setting and deformation history of a low angle fracture zone at Finnsjön, Sweden
Sven A. Tirén. Swedish Geological Company, Uppsala, Sweden.
Part 3: Hydraulic testing and modelling of a low-angle fracture zone at Finnsjön, Sweden
J-E. Andersson[1], L. Ekman[1], R. Nordqvist[1] and A. Winberg[2]
[1] Swedish Geological Company, Uppsala, Sweden
[2] Swedish Geological Company, Göteborg, Sweden
Part 4: Groundwater flow conditions in a low angle fracture zone at Finnsjön, Sweden
E. Gustafsson and P. Andersson. Swedish Geological Company, Uppsala, Sweden
Part 5: Hydrochemical investigations at Finnsjön, Sweden
J.A.T. Smellie[1] and P. Wikberg[2]
[1] Swedish Geological Company, Uppsala, Sweden
[2] Swedish Nuclear Fuel and Waste Management Company, Stockholm, Sweden
Part 6: Effects of gas-lift pumping on hydraulic borehole conditions at Finnsjön, Sweden
J-E- Andersson, P. Andersson and E. Gustafsson. Swedish Geological Company, Uppsala, Sweden
August 1989

TR 89-20
WP-Cave - Assessment of feasibility, safety and development potential
Swedish Nuclear Fuel and Waste Management Company, Stockholm, Sweden
September 1989

TR 89-21
Rock quality designation of the hydraulic properties in the near field of a final repository for spent nuclear fuel
Hans Carlsson[1], Leif Carlsson[1], Roland Pusch[2]
[1] Swedish Geological Co, SGAB, Gothenburg, Sweden
[2] Clay Technology AB, Lund, Sweden
June 1989

TR 89-22
Diffusion of Am, Pu, U, Np, Cs, I and Tc in compacted sand-bentonite mixture
Department of Nuclear Chemistry, Chalmers University of Technology, Gothenburg, Sweden
August 1989

TR 89-23
Deep ground water microbiology in Swedish granitic rock and it's relevance for radionuclide migration from a Swedish high level nuclear waste repository
Karsten Pedersen
University of Göteborg, Department of Marine microbiology, Gothenburg, Sweden
March 1989

TR 89-24
Some notes on diffusion of radionuclides through compacted clays
Trygve E Eriksen
Royal Institute of Technology, Department of Nuclear Chemistry, Stockholm, Sweden
May 1989

TR 89-25
Radionuclide sorption on crushed and intact granitic rock
Volume and surface effects
Trygve E Eriksen, Birgitta Locklund
Royal Institute of Technology, Department of Nuclear Chemistry, Stockholm, Sweden
May 1989

TR 89-26
Performance and safety analysis of WP-Cave concept
Kristina Skagius[1], Christer Svemar[2]
[1] Kemakta Konsult AB
[2] Swedish Nuclear Fuel and Waste Management Co
August 1989

TR-89-27
Post-excavation analysis of a revised hydraulic model of the Room 209 fracture, URL, Manitoba, Canada
A part of the joint AECL/SKB characterization of the 240 m level at the URL, Manitoba, Canada
Anders Winberg[1], Tin Chan[2], Peter Griffiths[2], Blair Nakka[2]
[1] Swedish Geological Co, Gothenburg, Sweden
[2] Computations & Analysis Section, Applied Geoscience Branch, Atomic Energy of Canada Limited, Pinawa, Manitoba, Canada
October 1989

TR 89-28
Earthquake mechanisms in Northern Sweden Oct 1987 — Apr 1988
Ragnar Slunga
October 1989

TR 89-29
Interim report on the settlement test in Stripa
Lennart Börgesson, Roland Pusch
Clay Technology AB, Lund
November 1989

TR 89-30
Seismic effects on bedrock and underground constructions. A literature survey of damage on constructions, changes in groundwater levels and flow, changes in chemistry in groundwater and gases
Kennert Röshoff
June 1989

TR 89-31
Interdisciplinary study of post-glacial faulting in the Lansjärv area Northern Sweden 1986–1988
Göran Bäckblom, Roy Stanfors (eds.)
December 1989

TR-89-32
Influence of various excavation techniques on the structure and physical properties of "near-field" rock around large boreholes
Roland Pusch
Clay Technology AB and Lund University of Technology and Natural Sciences, Lund
December 1989

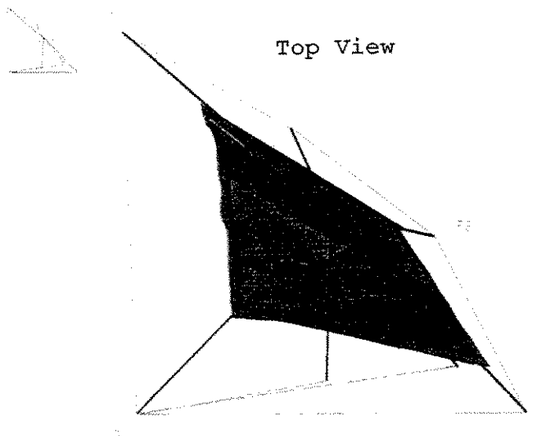

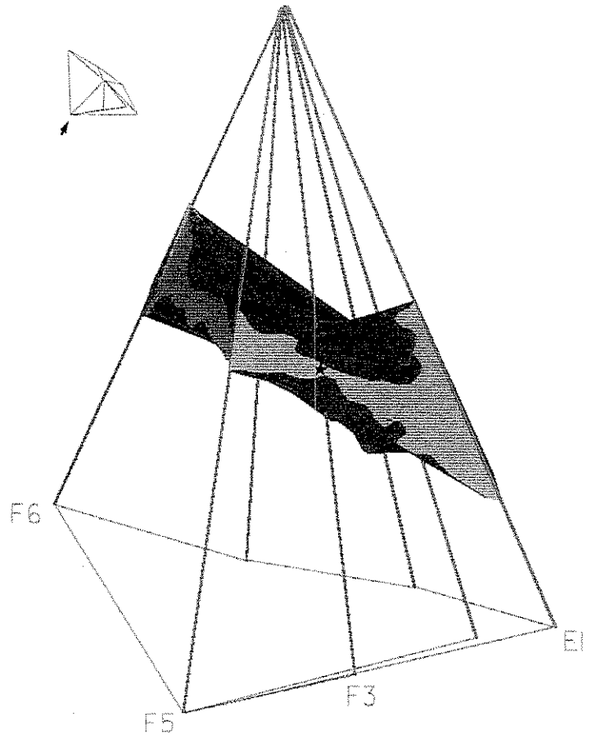

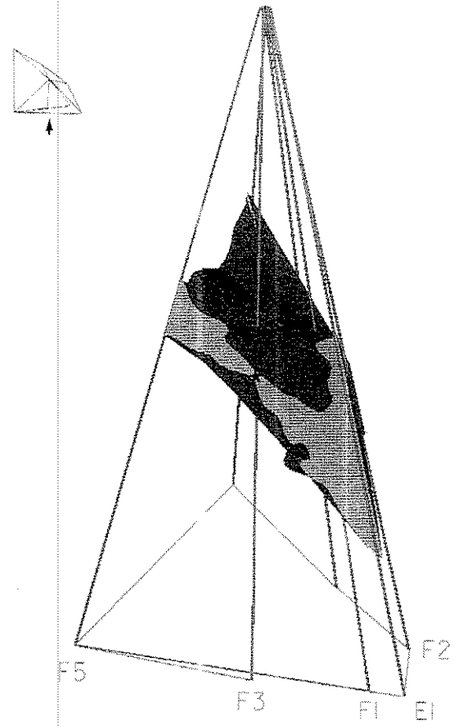

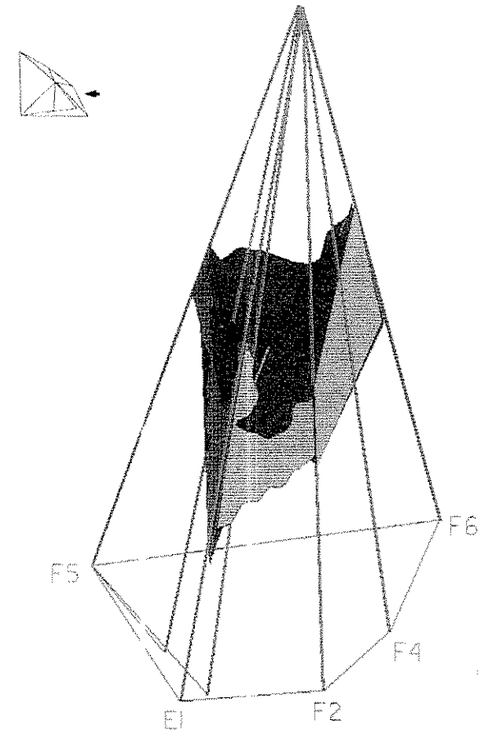

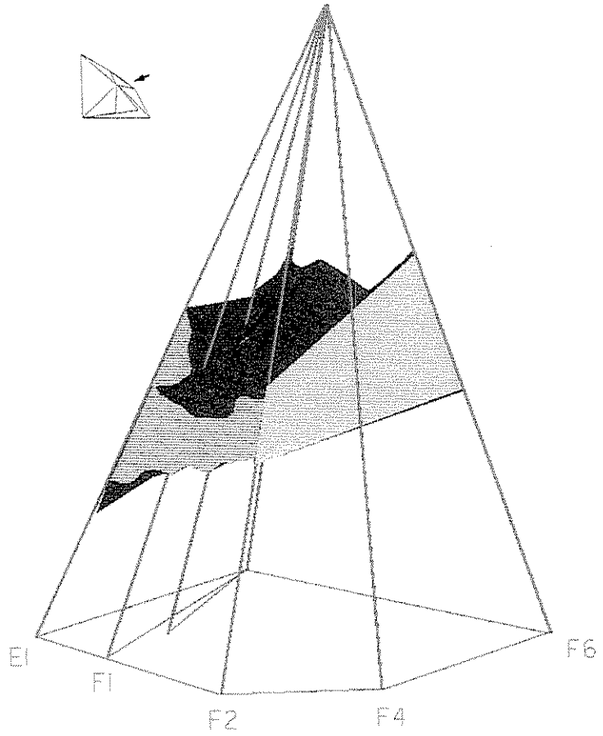

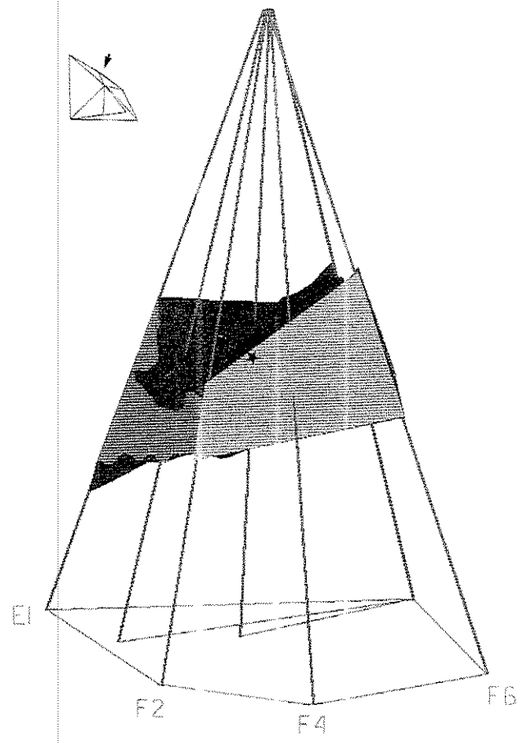

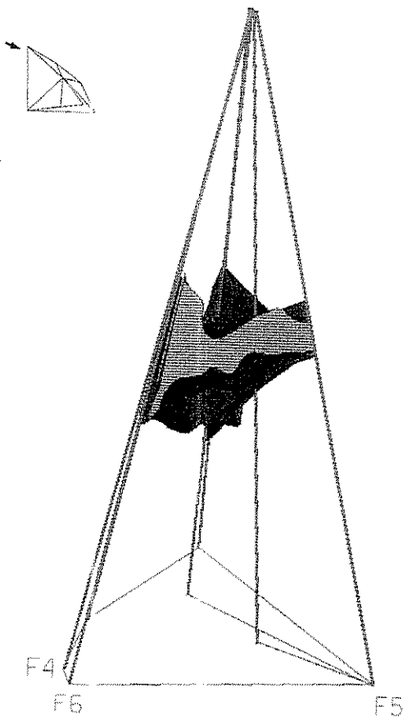

Appendix 7.1 The generalized model of the mapped Zone C model. The large width of zone 'C' between borehole F2 and F6, marked by a light blue colour, is an artifact caused by linear interpolation between tomographic sections and truncation. The lenghts of the plotted boreholes are 200 meter. Saline injection took place in section 103.0-118.5 m in borehole F3.

★ INJECTION POINT

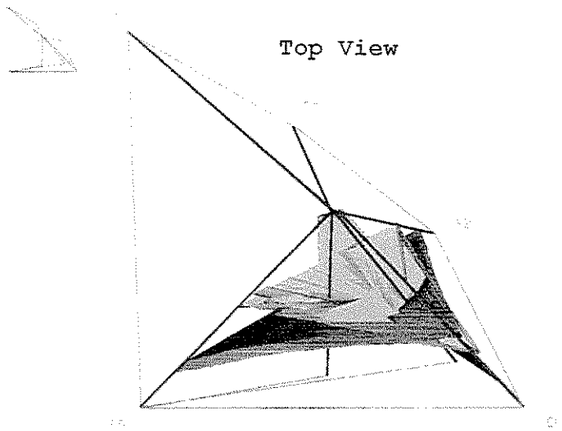

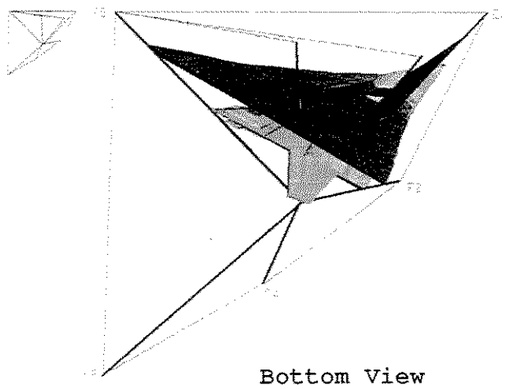

Bottom View

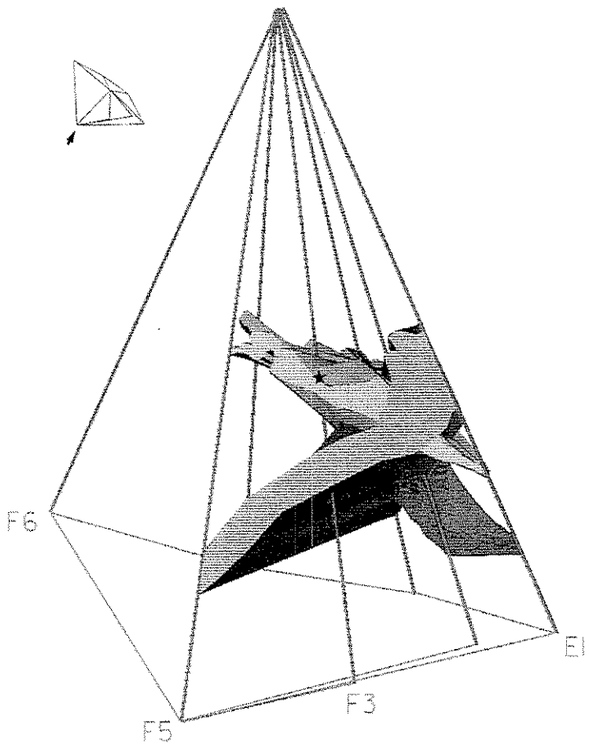

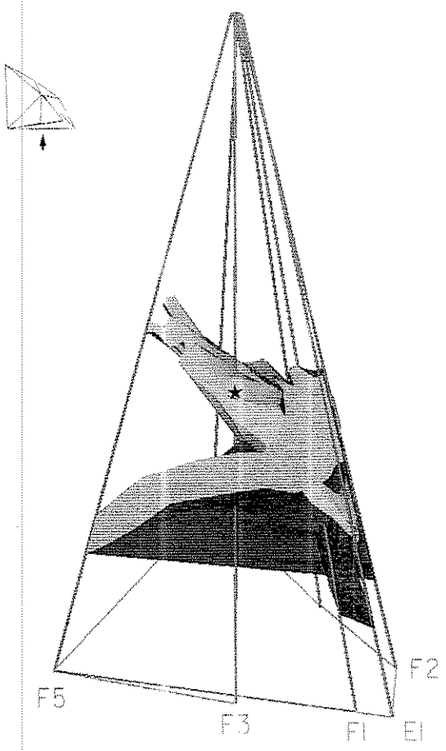

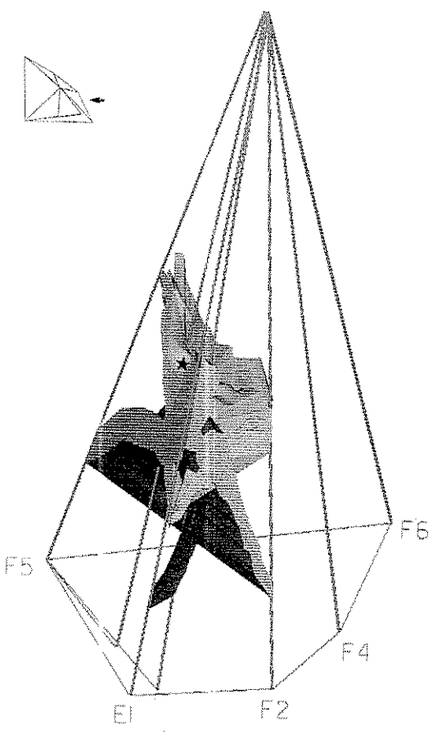

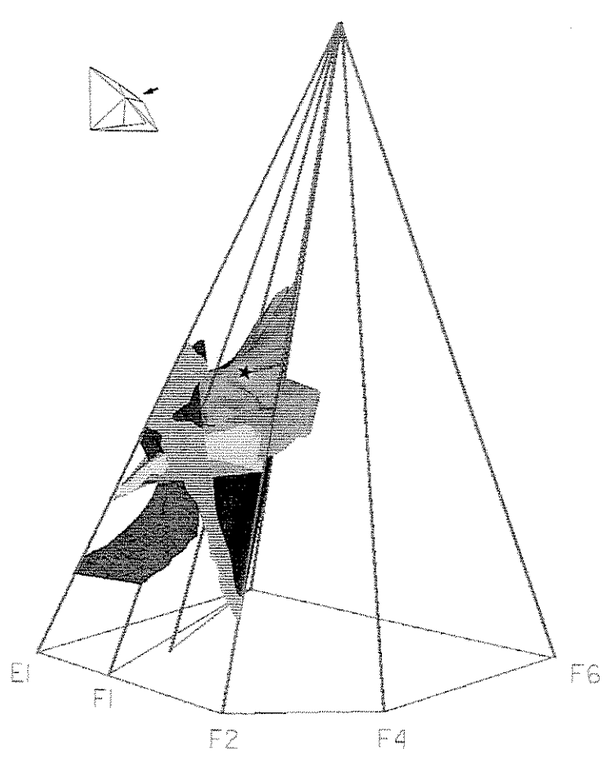

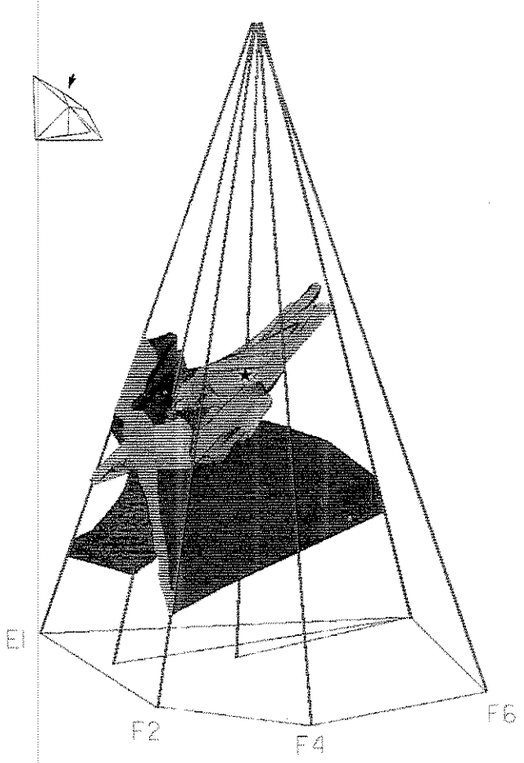

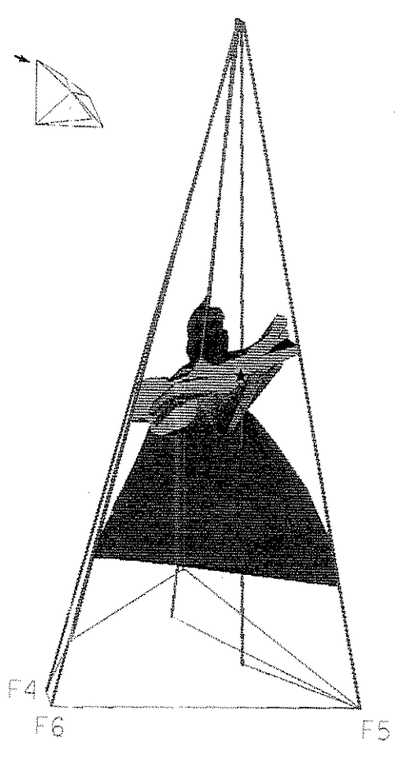

Appendix 7.2 The generalized model of the injected saline tracer distribution within the investigated volume. Yellow colour corresponds with Zone C, red corresponds with Zone X and green to Zone Y. The lenghts of the plotted boreholes are 200 meter. Saline injection took place in section 103.0-118.5 m in borehole F3.

★ INJECTION POINT

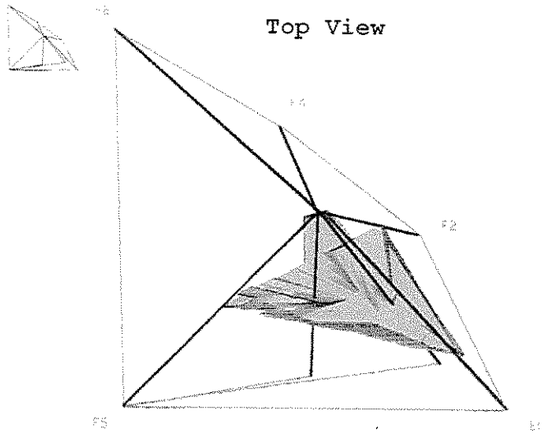

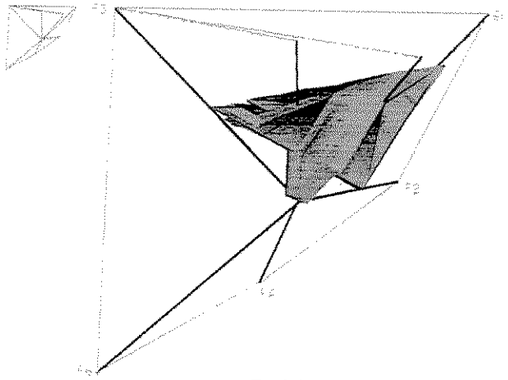

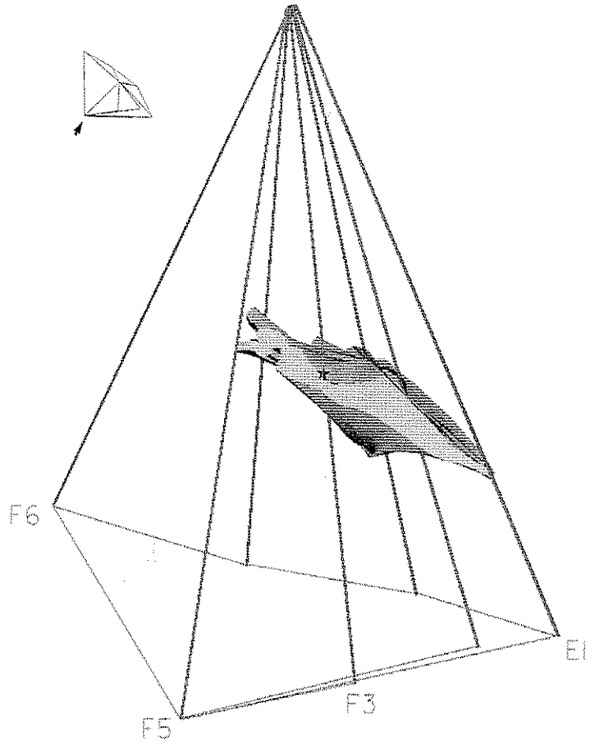

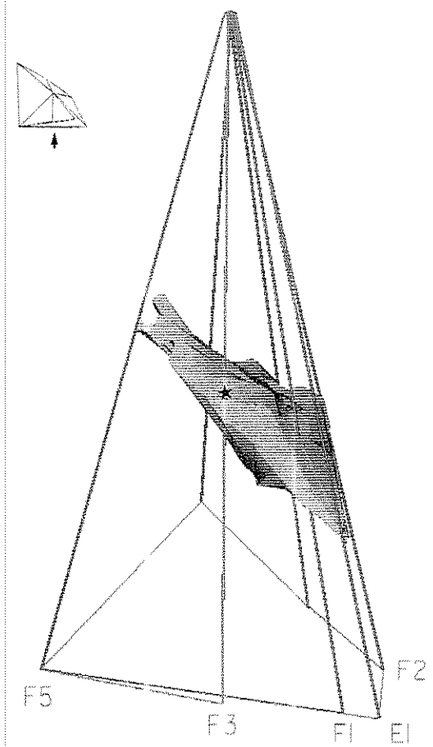

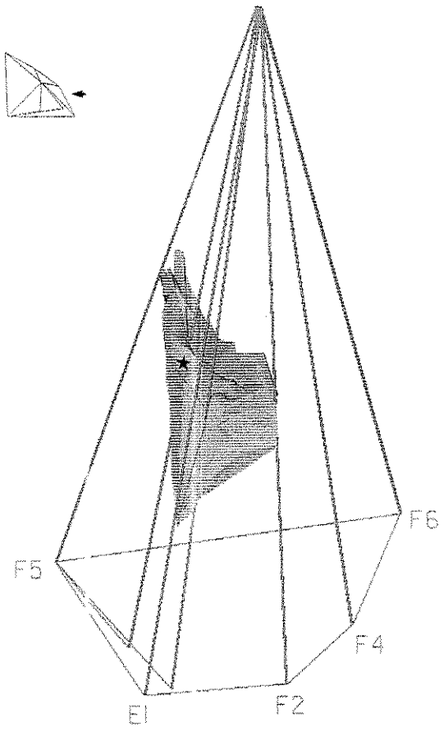

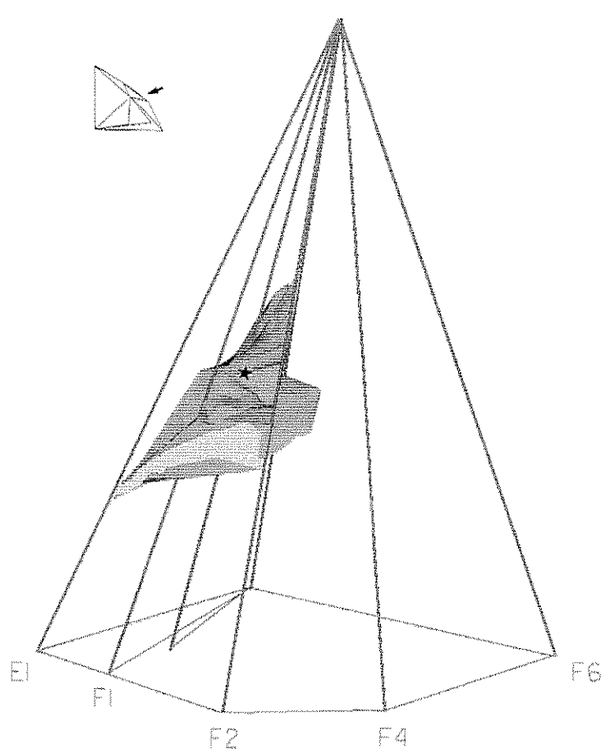

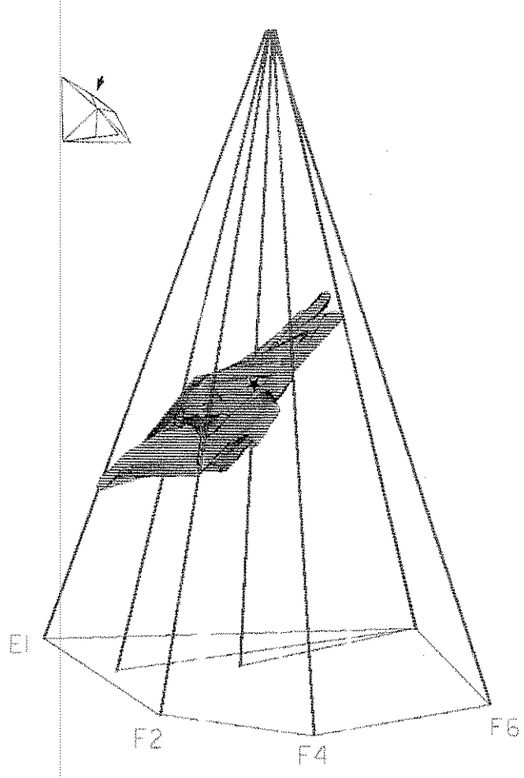

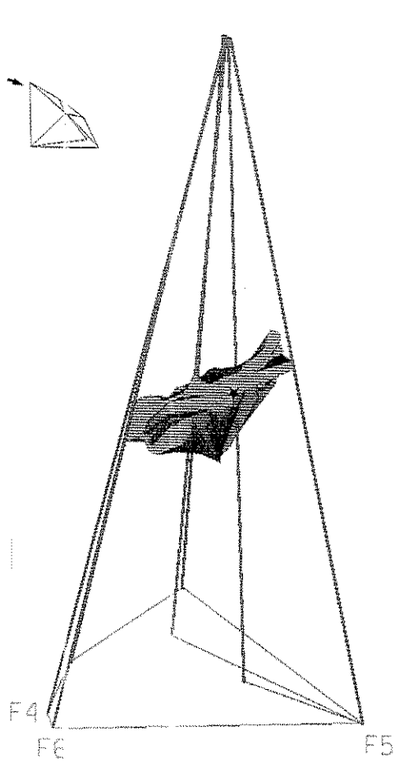

Appendix 7.3 The generalized model of the injected saline tracer distribution within Zone C. The lenghts of the plotted boreholes are 200 meter. Saline injection took place in section 103.0-118.5 m in borehole F3.

★ INJECTION POINT

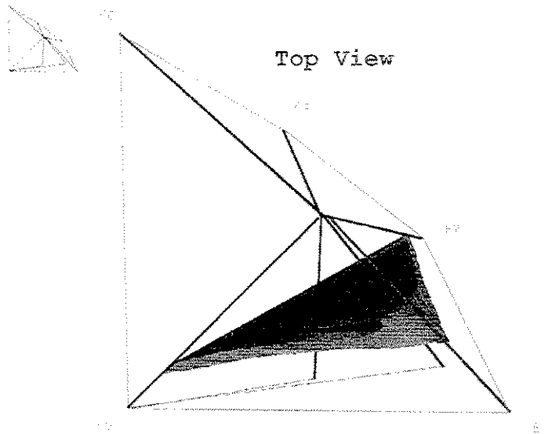

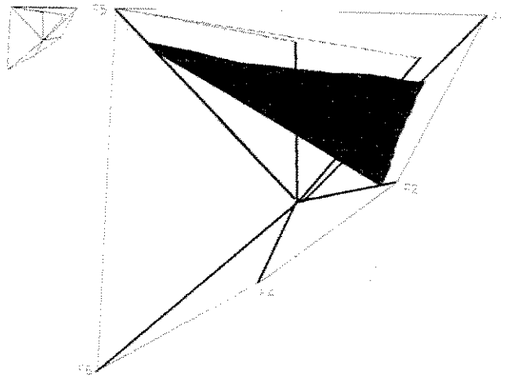

Bottom View

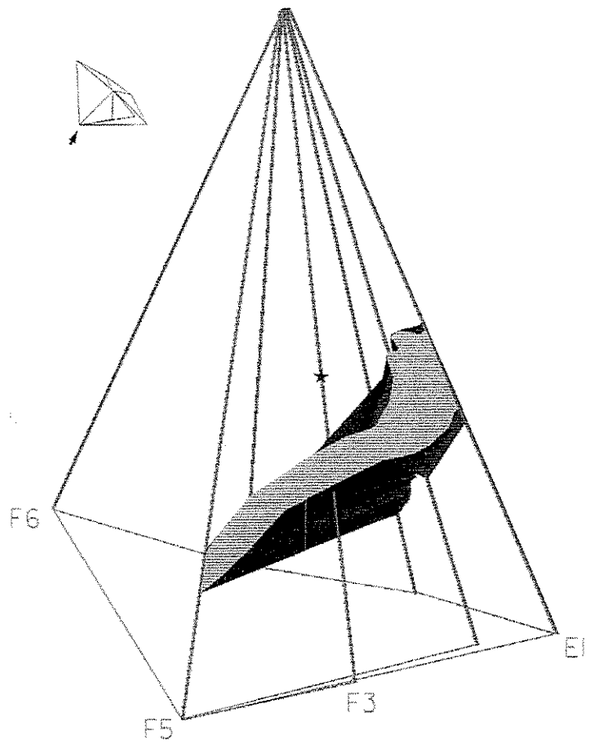

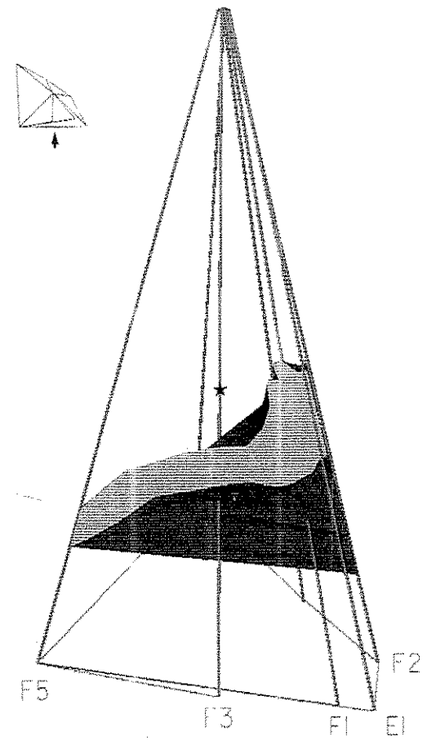

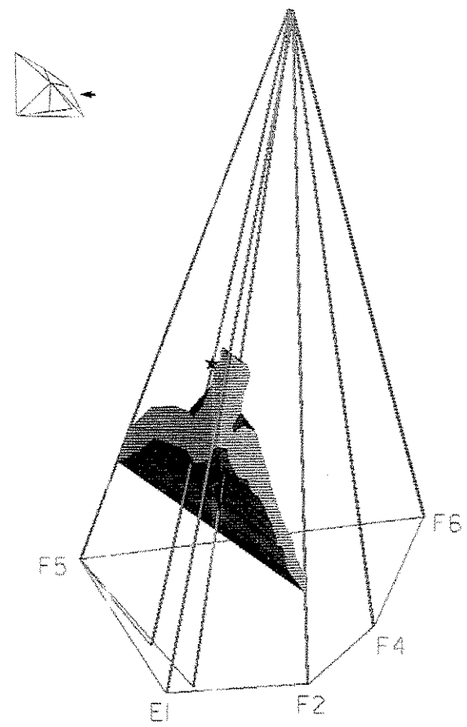

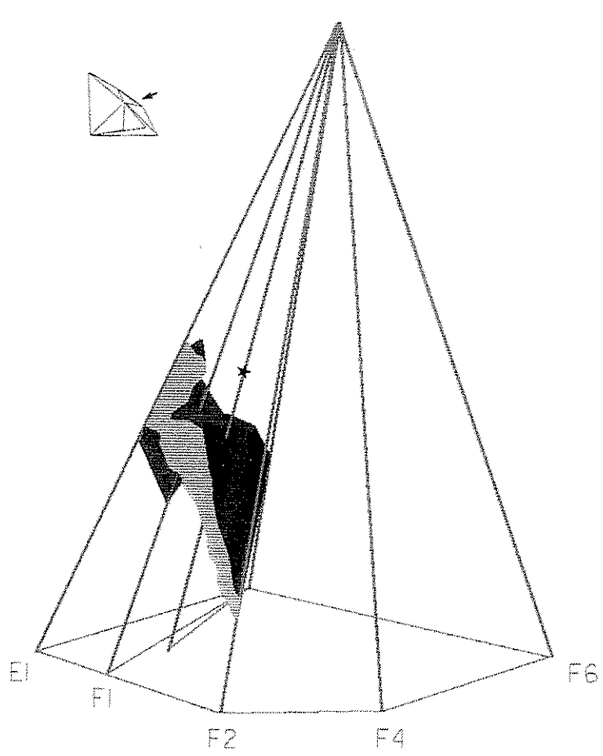

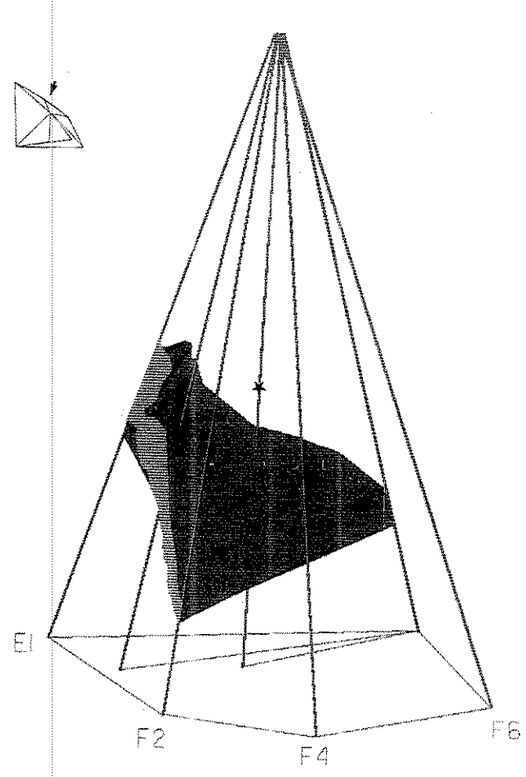

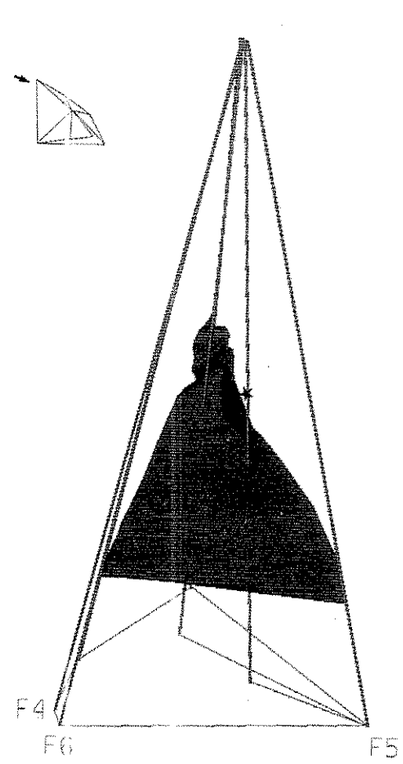

Appendix 7.4 The generalized model of the injected saline tracer distribution within Zone X. The lenghts of the plotted boreholes are 200 meter. Saline injection took place in section 103.0-118.5 m in borehole F3.

★ INJECTION POINT

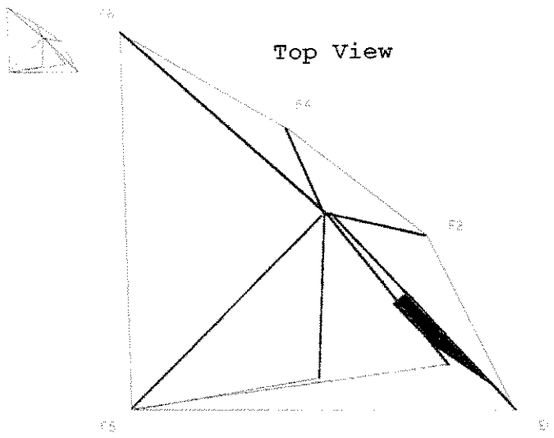

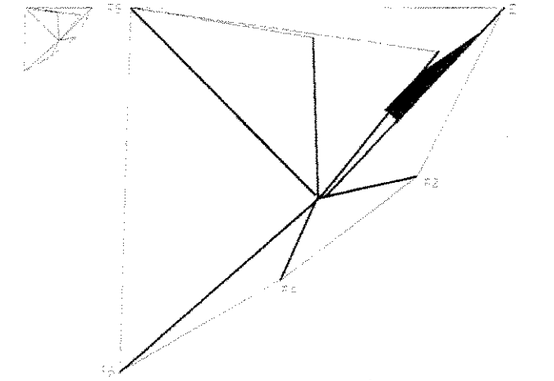

Bottom View

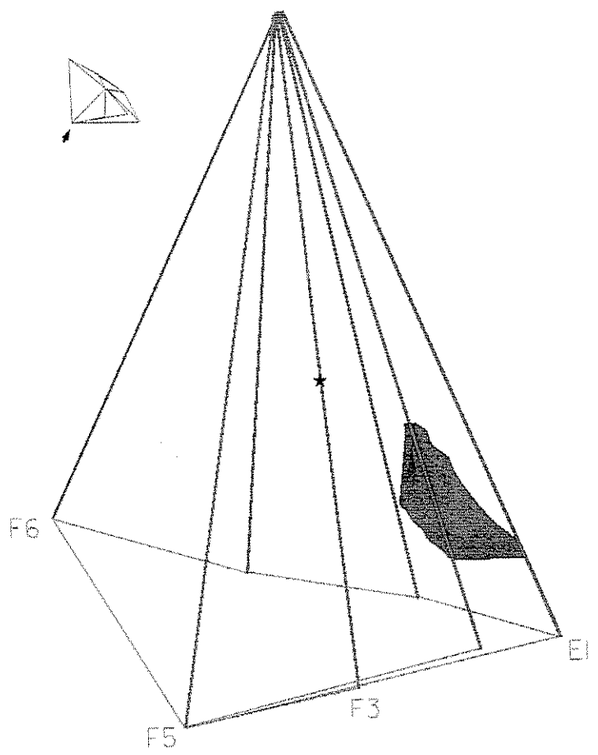

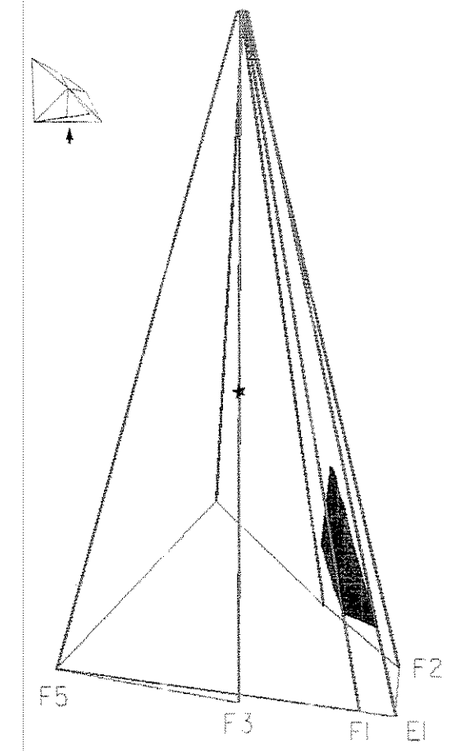

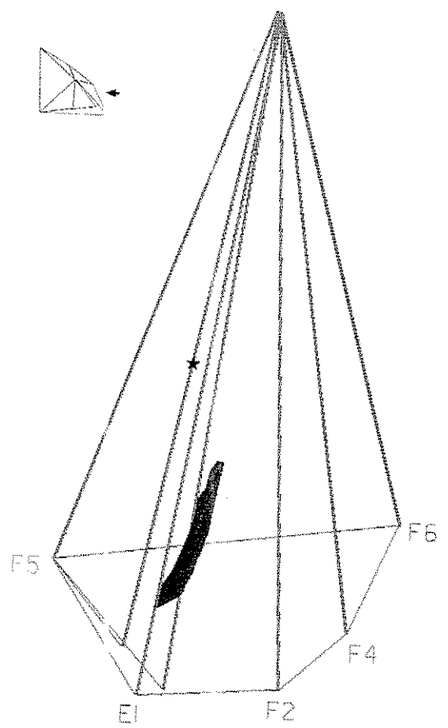

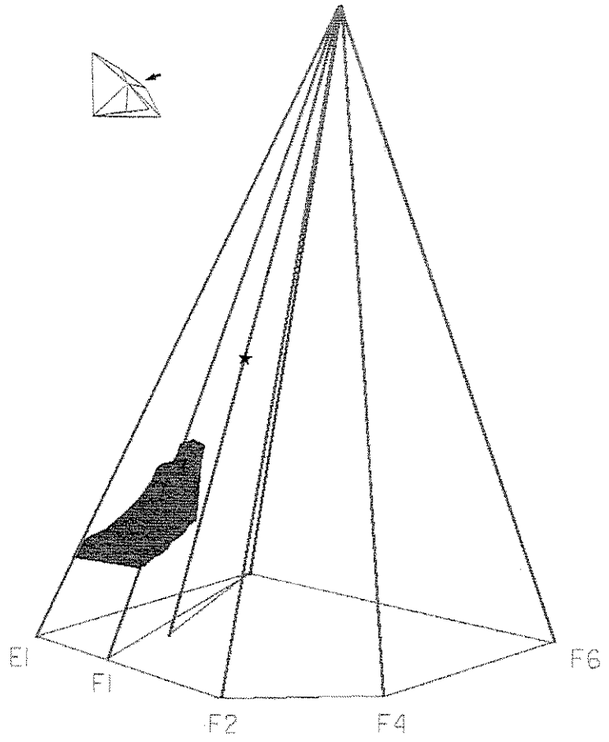

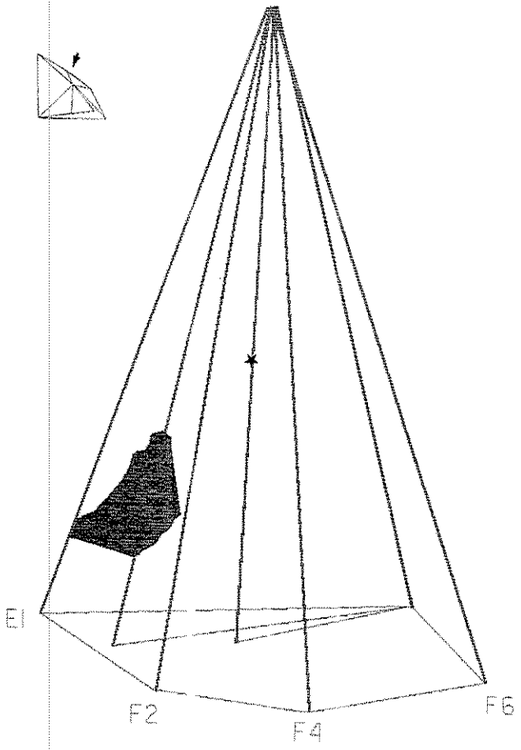

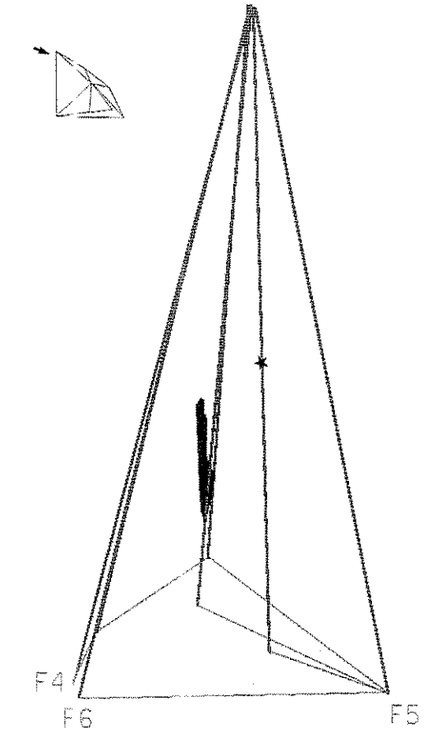

Appendix 7.5 The generalized model of the injected saline tracer distribution within Zone Y. The lenghts of the plotted boreholes are 200 meter. Saline injection took place in section 103.0-118.5 m in borehole F3.

★ INJECTION POINT

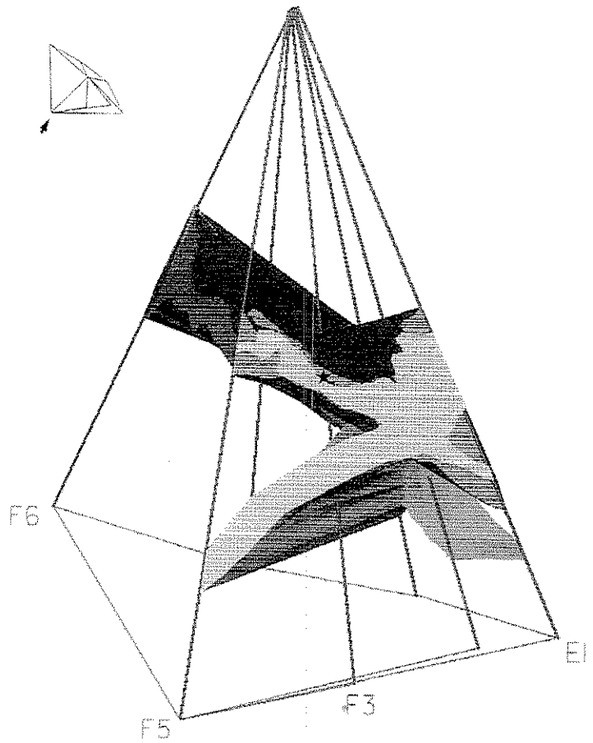

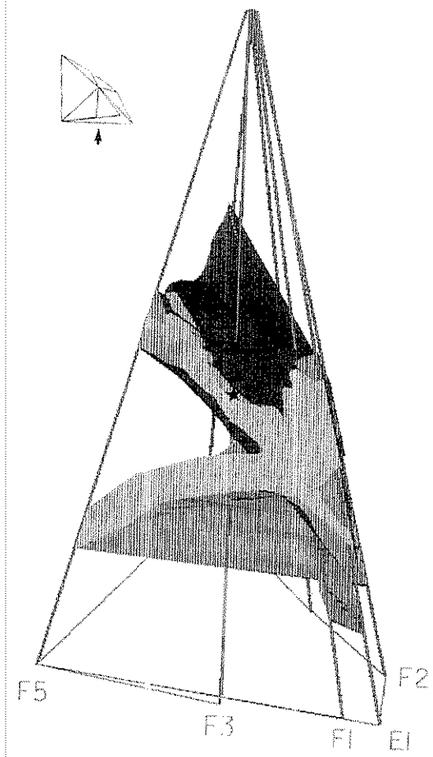

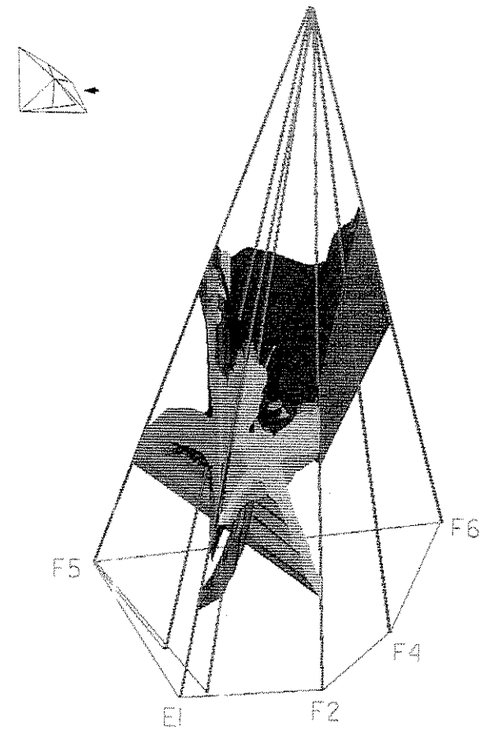

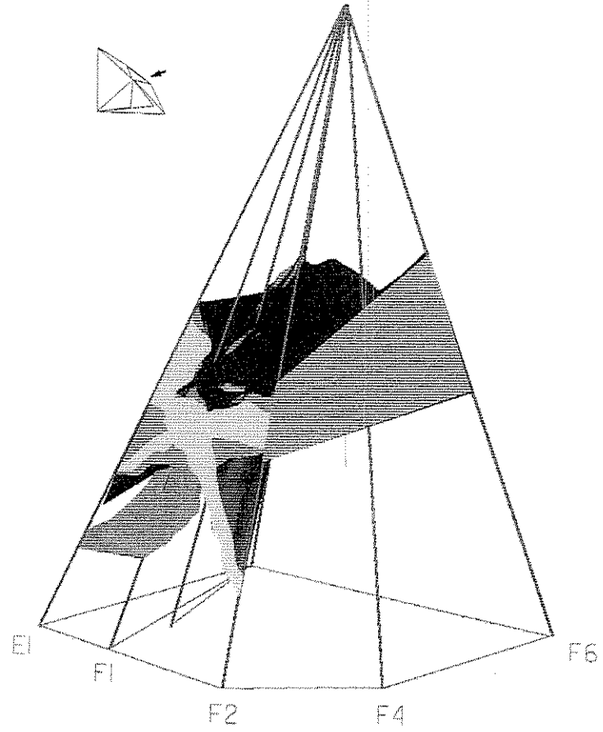

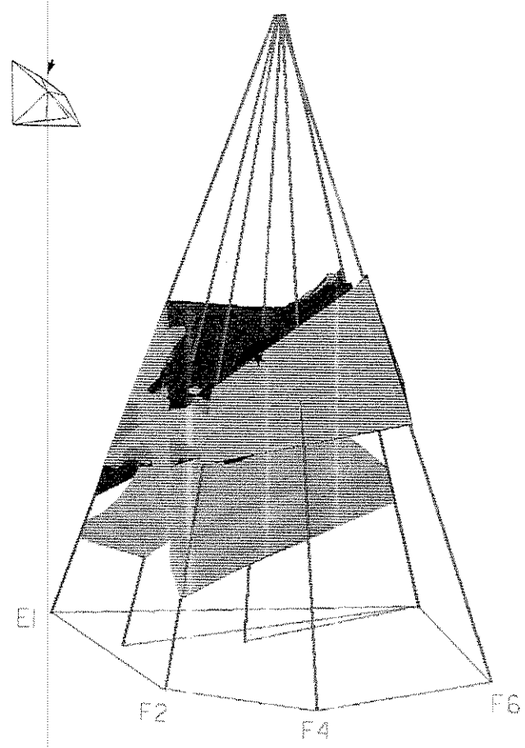

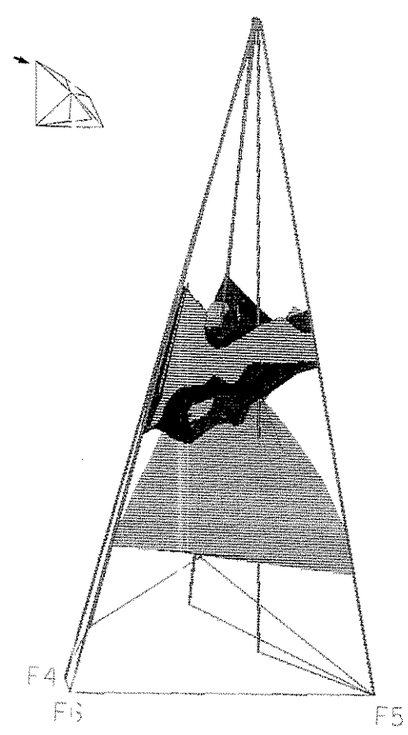

Appendix 7.6 The generalized model of the injected saline tracer distribution within the investigated volume in combination with the Zone C model. Yellow colour corresponds to the tracer distribution within the investigated rock volume. Red colour corresponds with the Zone C model. The lenghts of the plotted boreholes are 200 meter. Saline injection took place in section 103.0-118.5 m in borehole F3.

★ INJECTION POINT